THE UNIVERSITY
of EDINBURGH

Investigating the role of the non-canonical inflammasome in senescence

Irene Fernández-Duran

THE UNIVERSITY *of* EDINBURGH

Thesis submitted for the degree of Doctor of Philosophy

The University of Edinburgh

2019

Declaration

I declare that this thesis has been composed solely by myself and that it has not been submitted, in whole or in part, in any previous application for a degree. Except where states otherwise by reference or acknowledgment, the work presented is entirely my own.

Irene Fernández-Duran, April 2019

Acknowledgements

...el mejor de la vida es viajar y perder las teorías, perderlas todas...

— Enrique Vila-Matas

I would like to thank Dr Juan Carlos Acosta for giving me the opportunity to conduct my doctoral thesis in his laboratory. I would also like to thank the members of the JCA lab and, specially, Dr Núria Tarrats, Dr Andrea Quintanilla and Dr Fraser Miller for their experimental support in different stages of the work here presented. A special thanks to Maria Gomez, my desk-sharing friend for all your support in and out of the lab.

To all the amazing people I have had the opportunity to meet over these years, Ylenia, Sonsi, Itzi, Deborah, Marta V and all other friends, thank you for sharing moments together. Núria and Ainara, your strength and wisdom is inspiring.

Jordi, has estado ahí desde el primer hasta el último día, un trocito de esta tesis te pertenece.

A Mikel, gracias por nuestros momentos juntos en tu querida Edimburgo y por enseñarnos el Aberdeenshire y los delfines de las cinco en punto; espero que nuestros caminos se vuelvan a cruzar.

Gràcies Marta, per la teva lleial amistat que no té fronteres; d'entre totes les nostres aventures els darrers anys, sens dubte Cuba ens ha deixat records amb els que és impossible no somriure al recordar-los!

A mi padre, gracias por transmitirme genuina pasión por la ciencia. A mi hermana Sofía, ¡gracias por haberme visitado tantas veces! Seguiremos creando recuerdos imborrables allí donde estemos. Al resto de la familia, os agradezco haber pensado en mí todos estos años en los que no he estado tan cerca.

A la meva mare, gràcies per comprendre el meu esperit nòmade i per totes les vegades que has vingut a veure'm (i la maleta plena de menjar que portaves).

I a tu, Anna, gràcies per la teva paciència i pel teu suport en cada moment durant tots aquests anys; no és mesurable la felicitat de poder compartir el camí amb tu.

Abstract

Cellular senescence is a permanent proliferative arrest of cells triggered by several different stress mechanisms. Senescent cells display an inflammatory phenotype termed the senescence-associated secretory phenotype (SASP), being IL-1 signalling one of its key signalling pathways. Full-length IL-1β is cleaved into its mature active form by caspase-1, core enzymatic protein of a cytosolic platform called the canonical inflammasome. In contrast, caspase-4, central to the non-canonical inflammasome by analogy, can not cleave IL-1β although it can regulate canonical inflammasome activity. Moreover, research findings in recent years have revealed that inflammatory caspases (i. e. caspase-1 and caspase-4) are key mediators of a type of inflammatory cell death called pyroptosis. Although caspase-1 and 4 are crucial in inflammatory responses, the function of inflammatory caspases in senescence remained poorly studied. Thus, this research thesis was conducted to investigate the role of inflammatory caspases in oncogene-induced senescence (OIS). Caspase-4 expression was observed to be increased in RAS^{G12V}-induced senescence in human primary IMR90 fibroblasts. Depletion of caspase-4 in this model of OIS impacted on the inflammatory signature (including reduced expression of SASP members and regulation of IL-1β) as well as a partial bypass of the proliferation arrest. Activation of caspase-4 by intracellular lipopolysaccharide (LPS) induced not only cell death by pyroptosis but also a senescence phenotype in the fraction of cells surviving cell death. Finally, a protein-protein interaction study by a proximity biotinylation approach followed by mass spectrometry analysis was conducted to unravel potential interactors of inflammatory caspases in OIS. In all, this thesis describes a novel role for caspase-4 in senescence.

Lay summary

In case of a threat, the cells in our body can detect the danger and respond to it. For example, if a protein that can eventually lead to an oncogenic process activates, the cell is able to detect this event and activate a state of proliferative arrest called senescence that prevents further cell division. Senescence is not a unique response in cancer, but it also happens in many other contexts such as age-related diseases or developmental processes. Because senescence cells are implicated in multiple pathological events, their targeting is appealing to therapeutic intervention, and understanding its fundamental molecular processes might help identify novel clinical targets.

Senescent cells are distinctive from normal cells because, besides having stopped proliferating, they also exhibit inflammatory signals. These signals can have several different functions, some of which may be beneficial (such as promoting the neighbouring cells to become senescent) while others are detrimental (attracting immune system cells to kill and remove senescent cells) for senescence maintenance. Therefore, the senescence response as well as its derived inflammation is complex and needs of further investigation to be better understood. In this line, during my thesis I have studied a group of proteins called inflammatory caspases, that are involved in inflammatory processes. I have found a new role for these proteins in senescence in both the control of the production and secretion of inflammatory proteins as well as in the regulation of cell proliferation. As the inflammatory signature is a key feature of senescent cells, providing these new findings contributes to a better understanding of cellular senescence and may provide exploitable targets for therapeutic studies.

Table of Contents

List of Figures

List of Tables

List of Abbreviations

4OHT	4-hydroxytamoxifen
aa	Amino acid
AFC	7-Amino-4-trifluoromethylcoumarin
ANOVA	Analysis of Variance
APAF-1	Apoptosis protease-activating factor-1
ASC	Apoptosis-associated speck-like protein containing a CARD domain
ATP	Adenosine triphosphate
bp	Base pair
BrdU	5-bromo-2-deoxyuridine
CARD	Caspase activation and recruitment domain
CDK	Cyclin-dependent kinase
CDKI	Cyclin-dependent kinase inhibitor
CDKN1A	Cyclin-dependent kinase Inhibitor 1A
CDKN2A	Cyclin-dependent kinase Inhibitor 2A
CDKN2B	Cyclin-dependent kinase Inhibitor 2B
CDS	Coding DNA sequence
COP	CARD-only protein
CYCS	Cytochrome c
DAMP	Damage-associated molecular pattern
DAPI	4',6-diamidino-2-phenylindole
DEG	Differentially expressed gene
DIABLO	Direct inhibitor of apoptosis proteins (IAP) binding protein with low pI
DNA	Deoxyribonucleic acid

dsDNA	Double-strand DNA
DSS	Disuccinimidyl suberate
ELISA	Enzyme-linked immunosorbent assay
ER	Estrogen receptor
FBS	Fetal bovine serum
FC	Fold change
FDR q-val	False discovery rate q-value
FITC	Fluorescein isothiocyanate
GBP1	Guanylate-binding protein 1
GSDMD	Gasdermin-D
GSEA	Gene set enrichment analysis
GTP	Guanosine triphosphate
ICE	IL-1 converting enzyme
IL	Interleukin
IL-1R	Interleukine-1 receptor
LFQ	Label-free quantification
LPS	Lipopolysaccharide
MDP	Muramyl dipeptide
mRNA	Messenger RNA
MS	Mass Spectrometry
MSCV	Murine Stem Cell Virus
mtDNA	mitochondrial DNA
NES	Normalized enrichment score
NF-κB	Nuclear factor kappa-light-chain-enhancer of activated B cells
NTP	Non-targeting pool

OIS	Oncogene-induced senescence
PAMP	Pathogen-associated molecular pattern
PCA	Principal component analysis
PCR	Polymerase chain reaction
pRb	Retinoblastoma protein
PRRs	Pattern recognition receptors
QC	Quality control
RIN	RNA Integrity number
RNA	Ribonucleic acid
ROS	Reactive oxygen species
RT-qPCR	Reverse transcription-quantitative real time PCR
SA-β-galactosidase	Senescence-associated-β-galactosidase
SASP	Senescence-associated secretory phenotype
SDS-PAGE	Sodium dodecyl sulfate-polyacrylamide gel electrophoresis
shRNA	Short hairpin RNA
siNTP	Non-targeting pool siRNA
siRNA	Small interfering RNA
WT	Wild-type

Chapter 1 - Introduction

1.1 Cellular senescence

1.1.1 Definition and general aspects

Cellular senescence was first described by Leonard Hayflick in 1961, who observed that, after a certain number of passages in culture, human fibroblasts cease to divide thus entering a new non-proliferative state (1). Although the finding was not immediately accepted by the whole scientific community, the key importance of this restriction point, today called "Hayflick's limit", is now undeniable and has been thoroughly studied in many biology disciplines, from aging to cancer.

Currently, cellular senescence is defined as "a state of permanent cell cycle arrest in response to different damaging stimuli" (2). Diverse senescence activation mechanisms exist, highlighting the complexity behind the acquisition of the senescence phenotype. These mechanisms are reviewed later in this chapter.

The senescent phenotype is deeply heterogeneous and depends not only on the cause but also on the cellular and physiological context. Moreover, although there are some general phenotypical aspects which are commonly shared by most senescent cells, these are not exclusive of senescence (2, 3). Therefore, in the lack of a universal senescent marker, a combination of them is recommended to identify senescent cells (4). General aspects of senescent cells as well as some of the most widely used markers to identify them are reviewed next.

1.1.1.1 Morphological changes

In vitro, senescent cells are enlarged, flat and have an altered shape compared to their proliferating counterparts (Figure 1.1). However, this morphology, which is easily observed in dish-cultured cells, is not discerned *in vivo* (5).

1.1.1.2 Senescence-associated β-galactosidase activity

In 1995, Dimri *et al.* described a protocol to detect β-galactosidase activity at pH 6.0 that distinguished senescent cells from other phenotypes (6). The enhanced β-galactosidase activity observed in senescent cells is the result of an increased lysosomal content (7). Despite the assay also detects non-senescent cells such as those undergoing cell contact inhibition due to excessive cellular confluence (8), senescence-associated β-galactosidase (SA-β-galactosidase) activity detection remains the most widely used senescence biomarker to date (5) (Figure 1.1).

1.1.1.3 Cellular proliferation halt

One of the hallmarks of senescence is cellular proliferation halt, which can be measured using various techniques, being two of the most popular the quantification of 5-bromo-2-deoxyuridine (BrdU) incorporation and Ki-67 staining (9). Because BrdU is an analogue of thymidine, it is incorporated into newly synthesized DNA during the cell cycle S phase, thus BrdU labelling is used to identify proliferating cells (10) (Figure 1.1). Additionally, Ki-67 is an endogenous nuclear protein specifically expressed during mitosis (11). However, because both BrdU labelling and Ki-67 positive staining are proliferative markers, these assays also detect other non-proliferative states such as quiescence and therefore fail to be senescence-specific (12). In parallel, cell cycle arrest can also be monitored through the detection of increased levels of key cell cycle regulators such as p53, p21, p16 and p15, although, again, increased levels of these tumour suppressor genes are not indicators of cellular proliferation halt or senescence *per se* (5, 13).

1.1.1.4 Nuclear changes

Many changes occur in the nucleus of senescent cells. Senescence-associated heterochromatin foci (SAHF), which are dependent on the retinoblastoma protein (pRb) pathway, are chromatin rearrangements that result in dense aggregations visible upon 4′,6-diamidino-2-phenylindole (DAPI) staining (14) (Figure 1.1). Another event that takes place is the reduction of the levels of lamin B1, a constituent protein of the nuclear lamina (15). These and other structural changes in the nucleus result in epigenetic remodelling and consequent modulation of gene expression (3). Additional nuclear alterations that senescent cells can present include an increased number and size of promyelocytic (PML) nuclear bodies (16, 17) and the emergence of DNA segments with chromatin alterations (DNA-scars) (18).

1.1.1.5 The senescence-associated secretory phenotype

The collective production and secretion of inflammatory cytokines, chemokines and other factors by senescent cells is known as the senescence-associated secretory phenotype (SASP) (19, 20). The SASP has a key regulator role in senescence and will be reviewed later. It is important to note that, because the transcriptional activation of some SASP-associated genes leads to a logarithmic increase of the mRNA and protein levels of these factors, their detection is also useful in the identification of senescent cells (21) (Figure 1.1). However, these factors can also be present in many other inflammatory contexts and, conversely, not all senescent cells present a SASP. For instance, overexpression of the key senescence cyclin regulators CDKN1A or CDKN2A induces cell cycle arrest without SASP expression (22). Nonetheless, the SASP is a hallmark of senescence which is not present in other proliferative arrests such as quiescence.

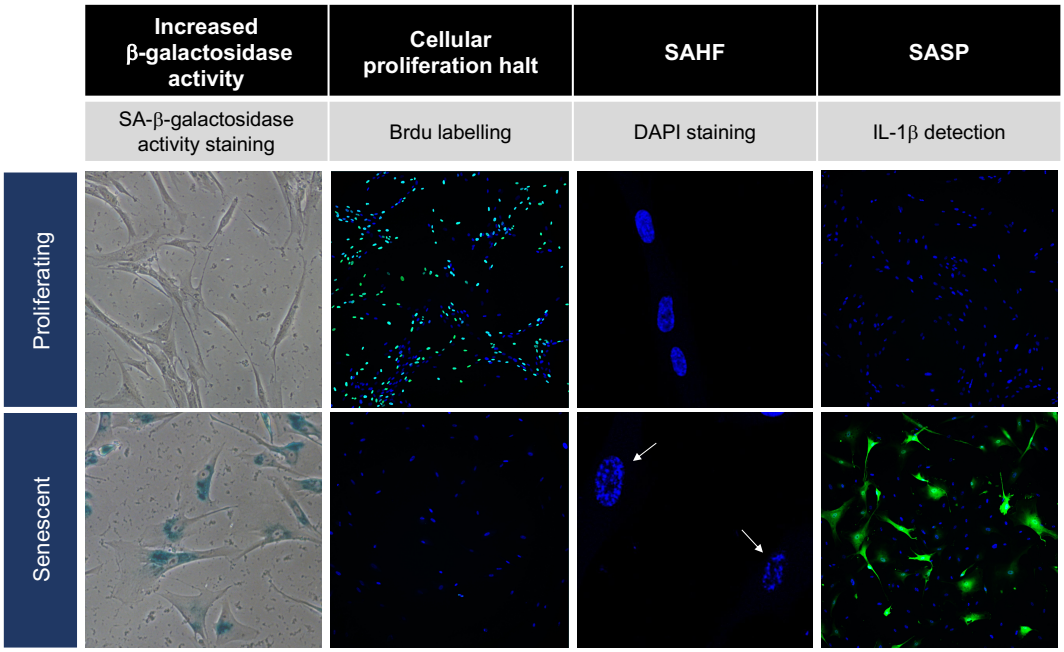

Figure 1.1 Identifying senescent cells

Because no universal senescence marker has been identified, a combination of techniques is used to detect senescent cells, some of which are shown in this figure. Proliferating (*top*) and oncogene-induced senescent (*bottom*) IMR90 human fibroblasts were stained to detect SA-β-galactosidase activity (*left*). Note as well that a distinctive morphology can be observed in senescent cells: these are more enlarged and have lost the elongated shape of proliferating fibroblasts. Using immunofluorescence microscopy, it is also possible to detect BrdU incorporation (anti-BrdU (FITC); DAPI), SAHF formation (DAPI) and IL-1β production (anti-IL-1β (FITC); DAPI), as shown in the figure from left to right. Arrows indicate SAHF.

1.1.1.6 Resistance to apoptosis

Resistance to apoptosis is a hallmark of senescent cells (23). Some stress inducers can trigger both apoptosis and senescence and, importantly, the mechanisms that determine which of these two responses is activated are not yet well understood (24). Nonetheless, senescent cells inhibit apoptosis through the upregulation of BCL-2 proteins (25) and inhibition of this protein family triggers apoptosis in senescent cells (26); these findings have been of critical importance in the development of senolytic agents, as later discussed.

1.1.1.7 Metabolism

Senescence is a metabolically highly active response. Increased AMP:ATP and ADP:ATP ratios due to augmented glycolysis in senescent cells are sensed by AMP-activated protein kinase (AMPK) (27). Activation of AMPK contributes to cell cycle arrest through two described mechanisms: [1] phosphorylation of p53 (28) and [2] inhibition of Hu antigen R (HuR)-dependent degradation of p21 and p16-coding mRNAs (29).

Importantly, mitochondrial mass is increased in senescent cells (30, 31) as a consequence of reduced mitophagy (32). Because mitochondria generate reactive oxygen species (ROS), accumulation of mitochondria has been linked to the increased levels of ROS found in senescent cells (33). In addition, mitochondrial dysfunction is commonly observed in senescent cells, independently of the triggering stimulus (33). Moreover, Correia-Melo *et al.* showed that depletion of mitochondria by E3 ligase Parkin-induced mitophagy prevents senescence, demonstrating the essential requirement of mitochondria for the induction and establishment of the senescent phenotype (34).

Many studies link autophagy perturbation and senescence and, specifically, increased macroautophagy has been broadly described in senescent cells (27). Induction of autophagy and autophagy malfunctioning have been shown to promote a senescence response (35, 36). Nonetheless, loss of autophagy has also been described to act as a pro-senescence mechanism through stabilization of the levels of the transcription factor GATA4 (37). One proposed explanation for this opposite role of autophagy in senescence is that general autophagy might promote cellular senescence whereas selective autophagy may inhibit it (38). In addition, in a recent study, García-Prat *et al.* showed that an autophagy-dependent mechanism prevents senescence in muscle stem cells and, impairment of this mechanism results in mitochondrial dysfunction and cellular senescence (39). Autophagy and its crosstalk with mitochondrial metabolism in senescence remains under discussion and active investigation (24).

Lipid content is also altered in cellular senescence. Because lipofuscin (fluorescent aggregates that contain lipids and highly oxidized proteins) accumulates in the cytoplasm of senescent cells (40), its detection is used to identify senescence by means of histochemical techniques such as Sudan Black B staining (41). Moreover, increased ROS can react with membrane lipids causing lipid peroxidation and the generation of free radical secondary messengers. Consequently, elevated lipid peroxidation and altered fatty acid catabolism result in metabolic alterations and changes in the lipid profile of senescent cells (42). In particular, ceramide levels are deregulated in senescent cells (43). Interestingly, a lipidomic study showed that the metabolic signature acquired by senescent cells may vary depending on the senescence-inducing stimulus (44).

1.1.2 Types of cellular senescence

The criteria used to distinguish between senescent phenotypes focuses on the origin, i.e. the stimulus that causes a particular senescence response (Figure 1.2).

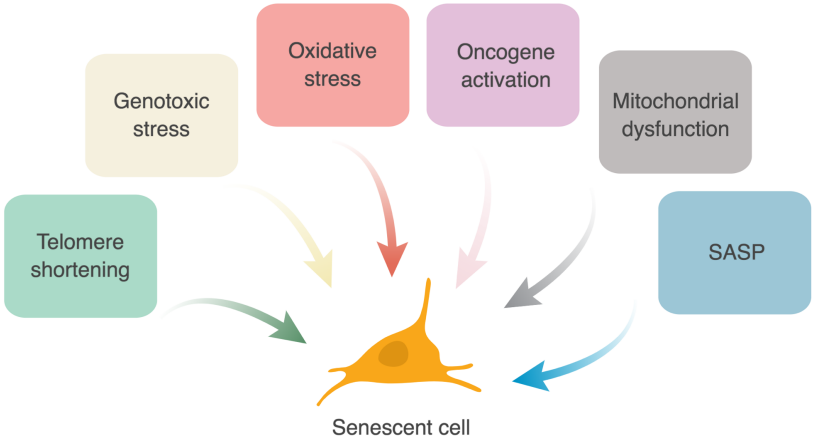

Figure 1.2 Schematic representation of several inducers of senescence
Various triggers can cause cellular senescence, some of which are outlined in this figure.

1.1.2.1 Replicative senescence

Cellular senescence as firstly described by Leonard Hayflick is nowadays termed replicative senescence and its cause is not strictly the passage of time but the number of rounds of DNA replication that have taken place (45).

Telomeres are short DNA repeats found at the end of chromosomes that shorten at each DNA replication round. Historically, although telomeres were described as early as in the 1940s (46), it was not until the late 1980s that scientists observed different telomere lengths among different cell types (47) and shorter telomere lengths in senescent cells (48). Finally, in 1998, Bodnar *et al.* ectopically expressed telomerase (the enzyme responsible for telomere maintenance) in telomerase-deficient cell lines; as a consequence, telomerase-expressing cells continued to proliferate while the control telomerase-deficient cells underwent senescence, proving that telomere shortening is the main event leading to replicative senescence (49). Mechanistically, telomere uncapping activates the DNA damage response (DDR) which in turn promotes senescence induction.

1.1.2.2 Genotoxic stress-induced senescence

Damaged DNA in non-telomeric sites can also lead to a senescence response (50). Unrepaired DNA breaks caused by gamma radiation induce a potent senescence response (51). Non-ionizing radiation, such as ultraviolet (UV) rays, can also activate cellular senescence (52).

Small molecule compounds including chemotherapy drugs such as etoposide (a DNA topoisomerase inhibitor), bleomycin (a DNA break inducer) or cisplatin (a DNA alkylating agent) also inflict DNA damage-induced senescence (53). Of note, many DNA damaging agents trigger an apoptotic response at high doses but the induction of senescence after sublethal administration (2).

1.1.2.3 Oxidative stress-induced senescence

Reactive oxygen species (ROS) can trigger a senescence response by causing DNA damage (54, 55). ROS have also been shown to play a role in the establishment and maintenance of DNA damage-induced senescence through a p21-mediated positive feedback loop (56). ROS production is also increased in replicative senescence (30) and oncogene-induced senescence (OIS) (31, 57). Although addition of antioxidants has been shown to delay or prevent senescence onset in some contexts (57-59), the mechanisms of ROS as initiators and effectors of senescence programs remain to be further investigated (4, 60). *In vitro*, sublethal hydrogen peroxide (H_2O_2) treatment is widely used to induce senescence by oxidative stress (61).

1.1.2.4 Oncogene-induced senescence

Activation of more than 50 oncogenes can lead to a senescence response, known as oncogene-induced senescence (OIS) (62). The first observation of OIS was described by Serrano *et al.* after expression of oncogenic H-RAS^{G12V} in human fibroblasts (63). In contrast to replicative senescence, expression of telomerase does not hinder OIS (64). Genetic alterations leading to OIS include gain of function mutations (RAS, BRAF, AKT), gene amplification and gene overexpression (65). Activation of OIS prompts the engagement of different signalling pathways depending on the activated oncogene and cell type. Frequently, an initial hyper-replication phase induces DNA damage and increased ROS production that initiate positive feedback loops and will maintain OIS (5, 66, 67). Metabolic reprogramming also plays a key role in OIS; for instance, Kaplon *et al.* showed that activation of pyruvate dehydrogenase (PDH) by phosphorylation is indispensable for the development of OIS (68). Evidence for *in vivo* OIS has been widely reported (65). OIS has been proposed to be both a preventing and promoting mechanism of tumour progression (69).

H-Ras, K-Ras and N-Ras are proto-oncogenic Ras proteins (a small family of GTPases) that have been used as prototypes in the study of the mechanisms triggered by OIS (70). Point mutations (generally located in amino acids 12, 13 or 61) in alleles of these Ras isoforms are commonly found in human cancers and render constitutive active

oncogenic Ras proteins with enhanced guanosine triphosphate (GTP) binding affinity that alters the downstream signalling effector pathways (71, 72). Mechanistically, oncogenic Ras triggers senescence by activating the DNA damage response, leading to signalling transduction events through the p53/p21 axis, as well as activation of the INK4/ARF locus (73). In this thesis, overexpression of H-RAS^{G12V} in human fibroblasts is used as a model of OIS.

Likewise, loss of a tumour suppressor can also induce senescence (62). In this context, the phosphatase and tensin homolog (PTEN) inactivation is the best characterized activation mechanism: loss of the tumour suppressor PTEN induces a cellular senescence response *in vivo* through activation of PI3K/Akt/mTOR signalling (74, 75).

1.1.2.5 Mitochondrial dysfunction-associated senescence

Recently, a distinct senescence response due to mitochondrial dysfunction, and thereby termed mitochondrial dysfunction-associated senescence (MiDAS), was described (76). In contrast to other senescent phenotypes, cells undergoing MiDAS display a mild SASP with no activation of IL-1 signalling. The authors also described that the mechanism behind MiDAS activation is independent of ROS and DNA damage and relies on a NAD-AMPK-p53-dependent signalling pathway.

1.1.2.6 Paracrine senescence

The soluble factors secreted by senescent cells can reinforce senescence in an autocrine manner by promoting positive feedback-loops. Mechanistically, autocrine senescence has been proved by showing no cellular growth arrest upon inhibition of IL-6R, IGFBP7 or CXCR2 (77-79). Moreover, a senescent cell can also induce senescence in a neighbour non-senescent cell: a phenomenon known as paracrine senescence. The SASP mediates non-cell autonomous senescence through transforming growth factor-β (TGF-β) and IL-1 signalling (80, 81). Besides the SASP, senescent cells interact with surrounding cells in other ways including NOTCH signalling (82), production of ROS (83), cytoplasmic bridges (84) and exosome trafficking (85).

1.1.3 The signalling pathways behind cellular senescence

Cellular senescence entails a highly complex and dynamic network of interacting molecular pathways. Next, key signalling pathways and their roles in cellular senescence are summarized.

1.1.3.1 The DNA damage response

When the DDR is activated, DNA damage sensor proteins at DNA damage foci recruit the Ataxia-telangiectasia-mutated (ATM) and ataxia telangiectasia and Rad3-related (ATR) kinases. ATM and ATR then phosphorylate the downstream signalling checkpoint kinases 1 (CHK1) and 2 (CHK2) causing [1] inhibition of CDC25 phosphatases and [2] p53 phosphorylation and stabilization; thus limiting cellular proliferation (86) (Figure 1.3). The DDR does not only induce senescence; besides cell cycle arrest, it can also activate other programs, such as those related to DNA repair or apoptosis, depending on the context (87).

1.1.3.2 p53 and p21

The tumour suppressor p53 is also stabilized in senescence by ARF (encoded in the INK4/ARF locus); ARF inhibits MDM2, a p53-degrading protein (88, 89). P53 stabilization results in increased expression of its downstream effector, the cyclin-dependent kinase interacting protein (CIP) p21, also known as p21 or $p21^{CIP}$ (90) (Figure 1.3). P21 is a cyclin-dependent kinase inhibitor (CDKI). In addition to p53-dependent signalling, p21 can be regulated in senescence by other transcriptional, post-transcriptional and post-translational mechanisms including RNA binding proteins, binding of miRNAs, phosphorylation and proteosomal degradation (2).

1.1.3.3 INK4/ARF locus

The INK4/ARF locus contains the tumour suppressors genes CDKN2A and CDKN2B. CDKN2A encodes two transcripts which are translated into the functionally different proteins p16 (also known as $p16^{INK4a}$) and ARF (also known as $p14^{ARF}$) whereas CDKN2B

encodes p15 (also known as $p15^{INK4b}$) (88). In senescence, the loss of Polycomb-mediated silencing mechanisms in this locus leads to increased expression of its encoded genes (24). Functionally, ARF stabilizes p53 (as explained previously) whereas p16 and p15 are CDKIs (Figure 1.3). It has been suggested that p16 activation may be key for the establishment of irreversible senescence in human cells (91).

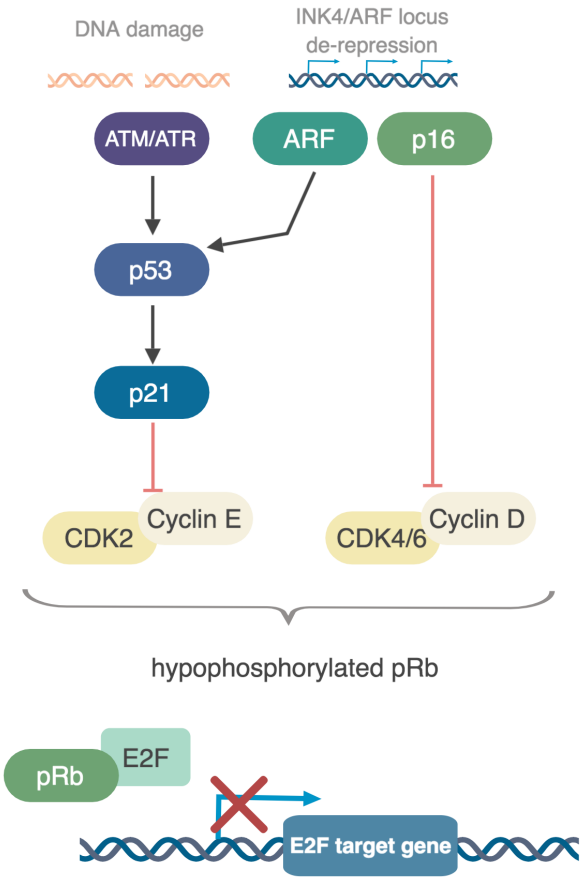

Figure 1.3 Key signalling pathways controlling cell cycle arrest in senescence

DNA damage sensing activates p53 and its downstream cell cycle regulator p21. Epigenetic remodelling of the INK4/ARF locus facilitates the transcription of its encoded genes. Both p53/p21 and p16 pathways converge in preventing pRb phosphorylation by inhibiting the formation of CDK-cyclin complexes. Consequently, hypophosphorylated pRb sequesters the transcription factor E2F and inhibits the transcription of its target genes, which are necessary for cell cycle progression.

1.1.3.4 Regulation of pRb phosphorylation and E2F targets expression

CDKIs play a key role in senescence by inhibiting the formation of CDK-cyclin complexes. P21 inhibits the activity of CDK2-cyclin E complexes whereas p15 and p16 inhibit the formation of CDk4/CDK6-cyclin D complexes (92). In proliferating cells, these complexes phosphorylate pRb which dissociates from the transcription factor E2F, allowing the transcriptional activation of essential genes for proliferation. In senescent cells, hypophosphorylated pRb prevents E2F from activating the expression of its target genes, thus halting cell cycle progression (5) (Figure 1.3).

1.1.3.5 The senescence-associated secretory phenotype (SASP)

The production and secretion from senescent cells of a myriad of soluble and insoluble factors, including cytokines (IL-1α, IL-1β, IL-6), chemokines (IL-8, GROα), proteases (MMP-1, MMP-3) and growth factors, is known as the SASP (19, 20, 93). The composition of the SASP and its function depends on the senescence stimulus, cell type, genetic status and neighbouring environment; however, it frequently includes a potent subset of proinflammatory molecules (24). Classically proposed as a strictly downstream mechanism of the DDR (94, 95), the SASP can also be activated by DDR-independent mechanisms, such as p38/MAPK signalling (96) and the cGAS/STING pathway (97-99) (Figure 1.4).

During infection, trigger detection by innate immune receptors is key in inducing cellular inflammatory responses that include the activation of transcriptional proinflammatory programs. These pathways are also activated and play master roles during sterile inflammation. Recently, a noteworthy mechanistic connection between an innate immune sensor system and the SASP has been made: cytosolic chromatin fragments in senescent cells activate the cGAS-STING DNA sensing innate immune pathway which in turn controls the transcription of SASP factors (97-99). Because innate immunity is crucial in the interplay between danger sensing and the inflammatory response, it is tempting to speculate that other innate immune pathways may be implicated in SASP activation during senescence.

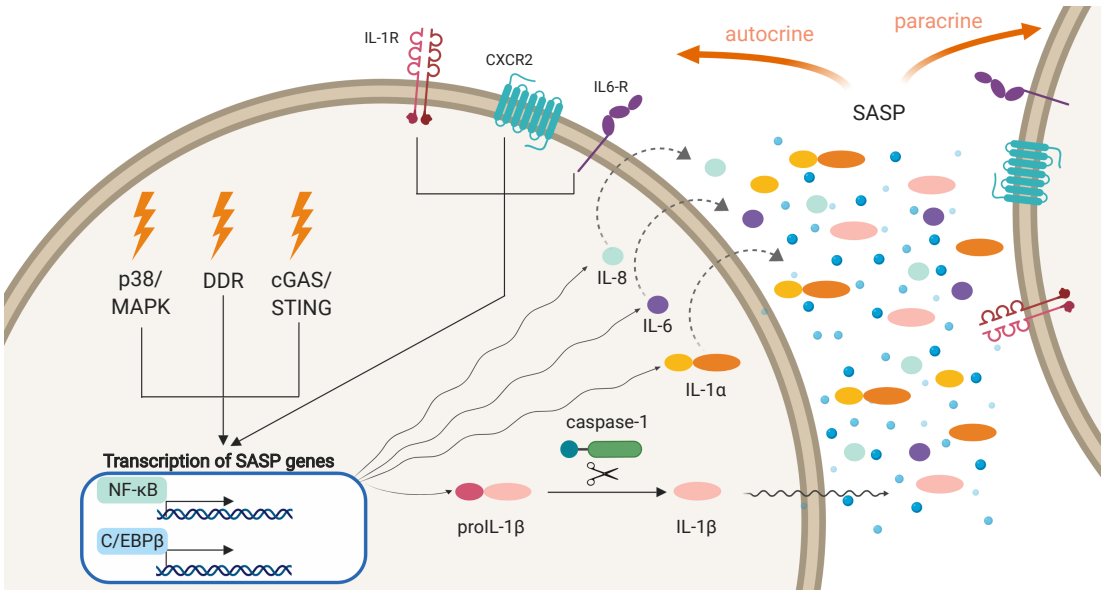

Figure 1.4 Key SASP signalling events

Stress inducers activate the p38/MAPK, DDR and cGAS/STING pathways, leading to the transcription of NF-κB and C/EBPβ target genes. SASP genes, such as IL8, IL6, IL1A and IL1B, are translated into SASP factors which are secreted to the extracellular space. There, SASP factors reinforce autocrine senescence and promote paracrine senescence among other functions as described in the main text.

Many functions have been attributed to the SASP (Figure 1.5), with beneficial or detrimental consequences depending on the (patho)physiological context. Some of these biological functions and effects are summarized below:

1. **Reinforcement of autocrine senescence**

   In OIS, positive feedback loops mediated by IL-6R, IGFBP7 or the IL-8 receptor CXCLR2 (77-79) have been shown to control cell cycle arrest in an autocrine fashion. Moreover, senescence-associated IL-6 and IL-8, which reinforce senescence through positive feedback loops that sustain NF-kB and C/EBPβ-dependent transcriptional activation, are upstream regulated by cell-surface bound IL-1α (100).

2. **Paracrine senescence**

   Secreted SASP factors can induce senescence in surrounding non-senescent cells through the TGF-β and IL-1 signalling pathways (80, 81). Whereas TGF-β mainly

regulates paracrine senescence (through the induction of the NADPH-oxidase NOX4 in neighbouring cells), IL-1 signalling controls both autocrine and paracrine senescence.

3. **Promotion of tumorigenesis**

   In contrast to the two above mentioned functions, paradoxically, the SASP can also promote cellular proliferation of surrounding cells, tumour growth, epithelial-to-mesenchymal transition and invasion in tumorigenic contexts (19, 101-104).

4. **Recruitment of immune cells**

   SASP-mediated recruitment of innate (NK cells, macrophages) and adaptive (T cells) immune cells contributes to beneficial tumour immunosurveillance as shown in *in vivo* studies (105-107). However, adverse tumorigenic effects of SASP-recruited immunosuppressive myeloid cells have also been recently described (108-110).

5. **Promotion of angiogenesis**

   Senescent conditioned medium containing the SASP vascular endothelial growth factor (VEGF) stimulates the proliferation and invasion of endothelial cells (111). In a pathological context, detrimental SASP-induced neovascularization has been described in tumorigenesis as well as in retinopathy (112, 113).

6. **Tissue homeostasis**

   SASP factors acutely secreted by senescent fibroblasts, such as CCN1 or PGDF-AA, remodel the extracellular matrix during optimal wound healing (114, 115). The SASP is also implicated in restricting fibrotic responses (116, 117). In addition, IL-6 signalling from senescent cells facilitates *in vivo* cellular reprogramming after tissue damage (118). Moreover, acute SASP production may also contribute to tissue regeneration by promoting stemness (119). Nonetheless, remodelling of the extracellular matrix by secreted matrix metalloproteinases (MMPs) can also have deleterious effects in age-related diseases (120, 121).

7. **Chronic inflammation**

   The SASP has been associated with low-level inflammation accumulating in aged tissues, a phenomenon also known as *inflammaging* (122). However, the specific contribution of the SASP to the detrimental effects of increased senescence in aged tissues remains to be better understood (24).

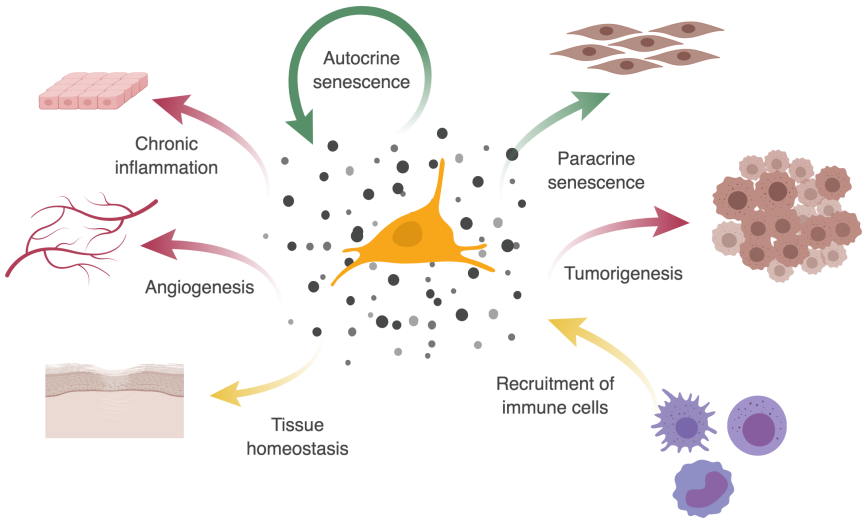

Figure 1.5 Functions and effects of the SASP

The SASP can exert a plethora of distinct functions and effects. Green and red arrows symbolize functions for which mainly beneficial or detrimental effects have been suggested, respectively. A yellow arrow is used when both positive and negative consequences have been proposed.

Because of its many potential roles, the SASP is tightly controlled. Activation of the transcription factors NF-kB and CCAAT/enhancer-binding protein-β (C/EBPβ) boosts the transcription of SASP factors (78, 123). Epigenetic mechanisms such as fading of repressive marks, chromatin rearrangements and histone variants also regulate the transcription of SASP factors (2). Moreover, a recent study has shown a regulatory mechanism involving alternative splicing: the splicing factor PTBP1 is necessary for exon skipping during pre-mRNA processing of key genes involved in intracellular trafficking, one of which, the Exocyst complex component 7 (EXOC7), controls a particular subset of proinflammatory cytokines of the SASP (124). At the post-transcriptional level, the mechanistic target of rapamycin (mTOR) controls the translation of SASP factors (125-127).

Importantly, post-translational mechanisms also maintain, tune and amplify the inflammatory signalling. IL-1 signalling is a master regulator of the SASP: IL-1α depletion reduces NF-kB and C/EBPβ activity (100) whereas blockage of the Interleukin-1 receptor (IL-1R) or the inflammasome activity, essential for IL-1β

processing, blunts the SASP (80). Moreover, dynamic NOTCH1 activity can act as a switching mechanism between a TGF-β secretome in earlier stages of senescence and a subsequent C/EBPβ-mediated SASP (82). Release to the extracellular space of some SASP factors depends on effective intracellular trafficking by specific proteins, such as the sheddase ADAM17 (128, 129), as well as exosome secretion (85, 130). In all, the complex multi-level elements of SASP regulation reflect its heterogeneous composition and function.

1.1.4 Pathophysiology of cellular senescence

Occurring cellular senescence has been described in a wide variety of physiological contexts, from embryonic development to disease (5). In particular, the role of cellular senescence has been and still is widely studied in cancer, ageing and age-related diseases, including cardiovascular diseases, metabolic diseases (such as type 2 diabetes) and other diseases that resemble or are linked to premature aging (chronic obstructive pulmonary disease (COPD), progeria). This subheading includes a summary of the key findings and current developments in cancer and ageing.

1.1.4.1 The dual role of senescence in cancer

Detection of senescence in pre-malignant human and mice tumours but not in their corresponding more advanced stages suggested a tumour suppressor role for senescence in cancer (74, 131-134). Genetic suppression of modulators of senescence concomitant to an oncogenic stress enhances tumour malignancy and accelerates progression, confirming a tumour suppressor role for senescence (74, 134). Mechanistically, activation of key tumour suppressors (such as p53 or 16) due to increased oncogenic signalling leads to the activation of a senescence response and consequent proliferation arrest (131). Mutations in these tumour suppressor genes, a common event in progressing human malignant tumours, block senescence-induced cell cycle arrest in favour of tumour progression (135). Noteworthy, reactivation of p53 in some mouse models of *in vivo* tumorigenesis leads to tumour regression and/or tumour clearance (105, 136). It has been proposed that, although p53 can mediate both

apoptotic and senescent responses, its role as a tumour suppressor depends on its ability to prevent cellular proliferation rather than its apoptotic function (137). The SASP also promotes anti-tumorigenic proliferation arrest by reinforcing autocrine senescence and promoting paracrine senescence (77-79).

Besides its intrinsic ability to halt proliferation, senescence can also exert a protective role in cancer by triggering the immune response through the SASP (138). Xue *et al.* described for the first time clearance of tumour senescent cells by recruitment of innate immune cells (neutrophils, macrophages and NK cells) to established H-RAS^{G12V} liver carcinomas (105). In mice with an intact adaptive immune system, this beneficial immunosurveillance program was conducted by $CD4^+$ T lymphocytes and macrophages recruited to N-RAS^{G12V} pre-malignant senescent hepatocytes (106). SASP-mediated immunosurveillance, which results in the clearance of cells in the tumour microenvironment to limit tumorigenic progression, has thenceforth been confirmed in a number of *in vivo* studies (107).

Despite abundant literature supporting a tumour suppressor role for senescence, there is also evidence that senescence can promote tumorigenesis (139). Indeed, several studies indicate that the SASP promotes cancerous invasiveness (94, 101), angiogenesis (111) and cellular proliferation (140), growth (103, 141) and dedifferentiation (102). Moreover, SASP-mediated recruitment of an immunosuppressive set of myeloid immune cells can cause an immunotolerant tumour environment that promotes tumour growth (108-110). In this scenario, one proposed hypothesis is that the SASP might prevent tumorigenesis in a p53-intact context but promote malignancy if p53 signalling is impaired, i.e., the SASP might be protective in pre-malignant lesions but pro-tumorigenic in advanced tumours (110, 138, 142).

In summary, the beneficial or detrimental role of senescence in cancer and, in particular, of the SASP, varies depending on the tissue, state of progression, immune landscape, genetic alterations and other characteristics of the tumour. Hence potential interventions exploiting/inhibiting senescence or/and the SASP are under investigation in cancer therapeutics.

1.1.4.2 Ageing and age-related pathologies

Accumulation of senescent cells during ageing, either by an accelerated increase in their presence or by malfunctioning of their clearance mechanisms, has been linked to organismal tissue decline (143, 144). Several senescent markers are progressively detected at higher levels in some aged tissues (145); among these, p16 has received much attention (146). In particular, a key study using an *in vivo* mouse model of progeria, a disease that mimics accelerated aging, showed that selective depletion of p16-expressing cells ameliorates some ageing–related disorders of the phenotype (147). The authors used the same smart genetic approach, a drug-inducible apoptotic fusion protein under the p16 promoter, to later validate the beneficial effects of killing p16-expressings cells during natural ageing in mice (148).

Not all studies link senescence in ageing to detrimental effects. In fact, some studies show that increased levels of some tumour-suppressor genes can be protective during ageing and enhance lifespan (149, 150). A suggested explanation to our current knowledge is based on the concept of "antagonistic pleiotropy" (151): the acute presence of senescent cells promotes beneficial tissue homeostasis whereas chronic, persistent senescence weakens the tissue and increases its vulnerability to age-related disorders (144).

Aged tissues present increased chronic low-inflammation levels, a circumstance that has been named *inflammaging* and is majorly linked with deleterious effects (122). It is thought that, because of its nature, the SASP may be key to *inflammaging*. Indeed, clearance of senescence cells in some aged tissues reduces inflammation (121, 148, 152). Moreover, some of the SASP factors have been functionally associated with age-related disorders (146) and targeted clearance of high-SASP senescent cells ameliorates kidney function in a fast-aging mice model (152). Inhibition of mTOR, which can promote the mRNA translation of many SASP factors, increases lifespan in mice (153). However, how the SASP might contribute to *inflammaging* remains mechanistically ill-defined (146).

1.1.4.3 Therapeutic implications of cellular senescence

Because senescence can have beneficial and detrimental effects depending on the context, both pro-senescence and anti-senescence therapeutic approaches haven been explored.

On the subject of pro-senescence strategical approaches, the term therapy-induced senescence (TIS) was coined to refer to the use of chemotherapeutical drugs to induce senescence and promote its potential beneficial tumour suppressor effect in cancer targeting (73, 154). For example, the FDA-approved drug for breast cancer treatment palbociclib induces senescence by inhibiting CDK4/CDK6 (155-157). Not all studies convey in the idea that promoting cellular senescence prevents tumour progression; in fact, although the SASP has been shown to enhance tumour chemosensitivity (158), senescence has also been associated with worse clinical outcome after chemotherapy, including increased tumour relapse (159, 160).

On the other hand, two anti-senescence therapeutic approaches have been taken: [1] to attack a particular aspect of senescent cells (such as the SASP) and [2] to deplete senescent cells. Noteworthy, the recent advances in the development of senolytics have been of great importance for the later strategy.

Although selective depletion of the SASP has been proposed as a mechanism to inhibit particular negative effects in some contexts such as ageing and OIS (161), targeting the SASP remains complex because of its numerous functions and therefore potential off-target effects (162). To limit the later, specific SASP inhibitors that target particular SASP subsets have been investigated (163). For instance, rapamycin, an mTOR inhibitor, is a potent suppressor of the IL-1 arm (125, 126). Other evaluated SASP-targeted strategies include NF-κB inhibitors, including glucocorticoids and metformin (164, 165), as well as the use of specific antibodies targeting selected secreted factors such as IL-6 (166). Nevertheless, a better understanding of the regulation and functions of the SASP is necessary for the identification of novel targets and development of therapeutic strategies with limited off-target effects (142, 146).

As earlier mentioned, resistance to apoptosis is a hallmark of senescent cells. This apparent obstacle for their elimination has turned out to be its "Achilles' Heel" as a number of compounds targeting the upregulated anti-apoptotic pathways have proven to specifically eliminate senescent cells (26, 167). Among these senolytic drugs, BCL-2 family inhibitors have shown promising results both *in vitro* and *in vivo* in age-related disorders (167, 168). Treatment with senolytics can also inhibit tumour formation and metastatic spread (148, 159). In addition, to limit potential off-target effects, a combined strategy of chemotherapy followed by senolytics has been proposed (169, 170). Interestingly, a recent study has shown that senolytic strategies with already approved FDA-drugs can improve aging phenotypes in mice (171). Introducing a different targeted approach, Muñoz-Espín and colleagues showed that drugs with no preference for senescent cells could be specifically delivered to these cells by encapsulating the compounds with galacto-oligosaccharides; consequently, the content of these nanoparticles is distinctively released in senescent cells due to their increased lysosomal activity (172). In all, it is clear that numerous efforts are currently being made towards exploiting senescence targeting for its potential therapeutic benefits.

1.2 Inflammatory caspases

1.2.1 Caspase definition and general aspects

To group the family of phylogenetically related proteins with endoprotease activity relying on [1] an own catalytic cysteine residue and [2] an aspartic acid residue on the substrate's cleavage motif, the term caspase, i.e. cysteine-dependant aspartate-directed protease, was proposed in 1996 (173).

1.2.1.1 Classification and function of caspases

Caspases are classically divided in two major groups: those related to inflammation (caspase-1, -4, -5, -11 and -12) and those related to apoptosis (caspase-2, -3, -6, -7, -8, -9 and -10) (Table 1.1) (174-176). Apoptotic caspases are further subdivided into initiators, which interact with upstream molecules, or effectors, i.e. downstream of the initiator caspases. Among apoptotic initiator caspases, caspase-8 mediates the extrinsic pathway of apoptosis (due to extracellular perturbation sensing) whereas caspase-9 mediates the intrinsic pathway of apoptosis (due to extra or intracellular stress); both active caspase-8 or caspase-9 can cleave and activate the effector caspases-3, 6 and 7 (177). Caspase-14 does not belong to any of the aforementioned groups and has a unique role in keratinocyte differentiation (178). This simplistic classification clashes with the real functions of caspases as caspases from both groups have been described to be involved in processes initially only attributed to the other subgroup (179-182).

In terms of structure, caspases have an N-terminal pro-domain, generally involved in binding with signalling molecules, and a C-terminal proteolytic domain, where the active site lies (i.e. the catalytic cysteine residue). All inflammatory and some initiator apoptotic caspases have a caspase activation and recruitment domain (CARD) within the pro-domain. Beyond caspases, other key inflammatory and apoptotic proteins bear a CARD domain; in fact, CARD-CARD domain interactions among caspases and with other adaptor proteins are an essential part of multimeric assembly and signal transduction (183). Caspases with no CARD domain have either a death effector domain (DED) or no pro-domain (Table 1.1).

Caspase	Type	Organism	Structure
1	Inflammatory	M, H	
2	Apoptotic (Initiator)	M, H	
3	Apoptotic (Effector)	M, H	
4	Inflammatory	H	
5	Inflammatory	H	
6	Apoptotic (Effector)	M, H	
7	Apoptotic (Effector)	M, H	
8	Apoptotic (Initiator)	M, H	
9	Apoptotic (Initiator)	M, H	
10	Apoptotic (Initiator)	H	
11	Inflammatory	M	
12	Inflammatory	M, H	
14	Cell differentiation	M, H	

Table 1.1 Classification of caspases

Caspases classified according to their role and host. A schematic representation of each structure is also shown. M: gene present in mice, H: gene present in humans.

Originally, mammalian caspases were identified as proteases whose function depends on the ability to cleave themselves, other caspases or other substrates (184, 185). In fact, most caspases are synthetized as full-length zymogens, and are active after dimerization and/or self-cleavage by auto-processing or external cutting by other proteases (186, 187). Cleavage after the pro-domain and within the catalytic domain (in the inter-subunit linker) leads to the generation of shorter active caspase forms that, in general, correspond to a large subunit and a small subunit, also known as p20 and p10 respectively due to their molecular sizes (188). These subunits frequently dimerize to

form active catalytic tetramers (189). However, many studies challenge these general observations by evidencing that [1] not all caspase functions depend on their catalytic activity (190, 191) and [2] dimerization but not processing, i.e. self-cleavage, is essential for activation of non-executioner caspases (192-196).

Nonetheless, catalytic activities remain the best well-defined caspase functions at the mechanistic level. On one hand, a highly conserved cysteine residue is found in the active site of all caspases (188). On the other hand, all their substrates contain a caspase cleavage amino acid sequence (P4-P3-P2-P1-P1'-P2'-P3'-P4', where each P is an amino acid and the cleavage takes place between P1 and P1') that bears an aspartic acid (D) in the P1 position (197). Using *in vitro* approaches based on positional scanning synthetic combinatorial libraries, optimal amino acid identity for P4, P3 and P2 positions were described for each caspase (198, 199). Subsequently, the initial cleavage motifs have been confirmed or corrected using more advanced technologies (200-203); table 1.2 describes the optimal peptide P4-P3-P2-P1 cleavage sequences agreed for inflammatory caspases.

Some caspases have hundreds of identified substrates whereas others are known to cleave only one specific protein (197). Identifying caspase substrates presents several caveats: [1] caspases are known to be promiscuous, with overlapping substrate specificities; [2] predicted optimal cleavage motifs are sometimes distant from actual cleavage events, for instance, the optimal substrate cleavage sequence described for caspase-1 is WEHD (P4-P3-P2-P1) but caspase-1 cleaves human proIL-1β after YVHD (204) and gasdermin-D after FLTD (205); [3] substrate identification based on linear peptide sequence does not account for secondary structures, which limit caspase accessibility to their substrates, and [4] *in vivo* intracellular concentration and [5] catalytic efficiency, i.e. rate of substrate cleavage, can differ in logarithmic folds between caspases (200, 201, 206-208). As a result, *in vitro* biochemical assays may not reflect the biological relevance / implications of caspases in a cellular context. Taking into consideration all the above mentioned concerns, it is also important to note that reagents based on optimal cleavage peptide sequences lack specificity and, therefore, their use is not reliable to target one specific caspase in whole cells either for their study or therapeutic targeting.

Caspase	Optimal peptide sequence P4-P3-P2-P1	Number of identified substrates	Key substrates with well-defined roles
1	WEHD	50-100	IL-1β, GSDMD, cGAS
4	(W/L)EHD, LEVD	1-5	GSDMD, cGAS
5	(W/L)EHD	1-5	GSDMD, cGAS

Table 1.2 Substrate specificity of inflammatory caspases

Predicted optimal cleavage peptide sequences for caspase-1, -4 and -5 activity are described. The number of identified substrates for each caspase is based on the most recent degradomics and functional studies (182, 201, 209). GSDMD: gasdermin-D; cGAS: cyclic GMP-AMP synthase.

1.2.1.2 Inflammatory caspases

Mammalian inflammatory caspases include caspase-1, -4, -5, -11 and -12. Interestingly, all inflammatory caspase genes cluster in the same region, located in chromosome 11 in humans or chromosome 9 in mice (210) (Figure 1.6). In fact, scientists that engineered the two initial CASP1 knockout mouse models by homologous recombination were unaware that the embryonic stem cells that they used to generate the mice belonged to a strain harbouring a CASP11 germline mutation that results in no caspase-11 protein expression; thus, the contribution of caspase-11 in these original studies was neglected (211, 212). Once researchers became aware of this fact (213), they also realized that segregation of the two genes and hence generation of single CASP1 knockout mice through thorough backcrossing was extremely unlikely because CASP1 and CASP11 genes are only separated by around 1500 bp. The development of more efficient gene targeting techniques has enormously contributed to accurately generate single CASP1 or CASP11 knockout models and revisit and reassess the previously overlooked function of caspase-11 (213-215).

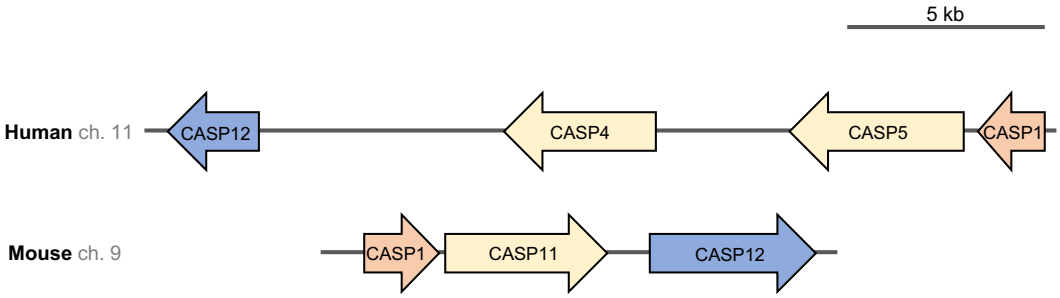

Figure 1.6 Genomic location of inflammatory caspase genes

Chromosomal organization of human (above) and mouse (below) inflammatory caspase genes. The schematically represented regions also encode other elements which have not been added for additional clarity. Of note, in humans this region also encodes a caspase pseudogene and several CARD-only protein (COPs).

Caspase-1 was the first ever identified caspase and was originally named IL-1 converting enzyme (ICE) under the observation of its ability to cleave inactive full-length proIL-1β into an active short fragment (184, 185). The function of caspase-1 will be described in section *1.2.2 The canonical inflammasome*.

Caspase-4 and -5 are the human orthologues of murine caspase-11 presumably as a consequence of a gene duplication event relatively recent in evolutionary terms (210) (Figure 1.6). However, caspase-4 and caspase-5 are not redundant: they are expressed in different tissues and each has distinctive functions. In fact, caspase-4 is expressed ubiquitously, in a similar fashion to caspase-1, whereas the detection of caspase-5 is limited to a restricted subset of myeloid cells; therefore, it has been suggested that caspase-4 has broader functions than caspase-5, the later having a functional role confined to restricted lineages (175, 216) (Figure 1.7). Moreover, functional observations on caspase-11 are not always translated to caspase-4 or/and -5 and vice versa, suggesting species-specific roles (217, 218). Caspase-4 and -5 will be further examined in section *1.2.3 The non-canonical inflammasome*.

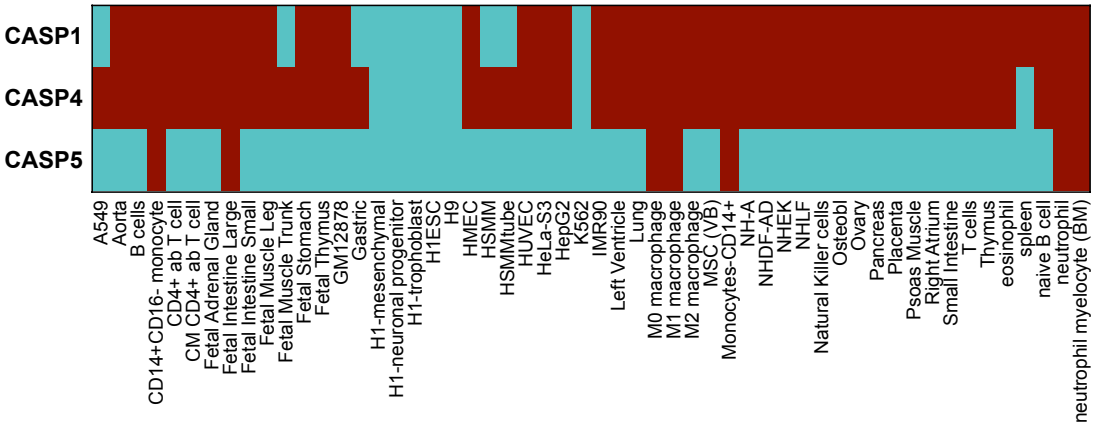

Figure 1.7 Expression of inflammatory caspases in human cells and tissues

Differential analysis of caspase expression in various tissues and cell types reveals a distinctive expression pattern for caspase-1, -4 and -5. Data were obtained from the *ensembl.org* website: using the Ensembl regulatory build resources, CASP1, CASP4 and CASP5 promoter activity (active: red; inactive: blue) were predicted based on the epigenetic signatures around these promoters obtained from curated publicly available datasets, including the ENCODE project (219).

Finally, the role of caspase-12 is poorly understood. Besides cleaving itself, and thus exerting an auto-processing role, no other substrates have been identified (220). Studies in mice proposing that caspase-12 is a negative regulator of caspase-1 have been contradicted and no clear function has been yet proposed for murine caspase-12 (221, 222). Moreover, in humans, a frameshift mutation in the CASP12 gene anticipates a stop codon and generates a truncated caspase-12 with no proteolytic domain (223). In less than 1% of humans, an additional single nucleotide polymorphism reverts the premature stop codon allowing transcription of the full gene; however, the proteolytic domain of this protein is also catalytic inactive due to further mutations (224). Although some studies have investigated whether human CASP12 and its mutated variants can be linked to inflammatory disease susceptibility, weak associations have been reported and no physiological relevance of either truncated or full-length human caspase-12 has been yet described (175, 221, 225-228). Given that human caspase-12 has a highly limited expression profile and its acquired host-specific mutations question its functionality, caspase-12 has not been approached during this thesis.

1.2.2 The canonical inflammasome

Inflammasomes are multimeric protein cytosolic complexes that serve as platforms for the recruitment and activation of inflammatory caspases and subsequent processing of their substrates (229). Their main role is to integrate external and internal stimuli into innate immune responses. Inflammatory caspases are the core enzymatic units of inflammasomes; hence inflammasomes are divided into two subtypes: [1] canonical and [2] non-canonical, depending on the presence of caspase-1 or caspase-4/-5/-11 respectively.

1.2.2.1 Canonical inflammasomes: types and functions

The principal function of canonical inflammasomes is to channel the recognition of a stimulus into an inflammatory response through caspase-1-mediated activation of IL-1β (230). Although inflammasomes have been extensively studied since their discovery fifteen years ago (229), there is a lack of consensus regarding their dynamics, including their activation and regulation (192). This fact might be explained by the abundance and complexity of mechanisms described, highlighting the versatility of the inflammasome in integrating immune responses. In this sub-section, a brief summary of the molecular mechanisms involved in canonical inflammasome activation, function and regulation is presented.

Inflammasome activation is initiated when exogenous or self-originated molecules, termed pathogen-associated molecular patterns (PAMPs) or damage-associated molecular patterns (DAMPs) respectively, are detected by cytosolic pattern recognition receptors (PRRs) (231). Examples of PAMPs include microbial nucleic acids and secretion systems or cell wall components. In contrast, DAMPs are molecules, such as uric acid crystals, ATP or heat-shock proteins, derived from the host and, therefore, can mediate inflammasome activation also during sterile inflammation (232). Besides recognizing PAMPs and DAMPs, PRRs can also detect the loss of cellular homeostasis (for instance, altered production of ROS); these broader processes were recently denominated 'homeostasis-altering molecular processes' (HAMPs) (233).

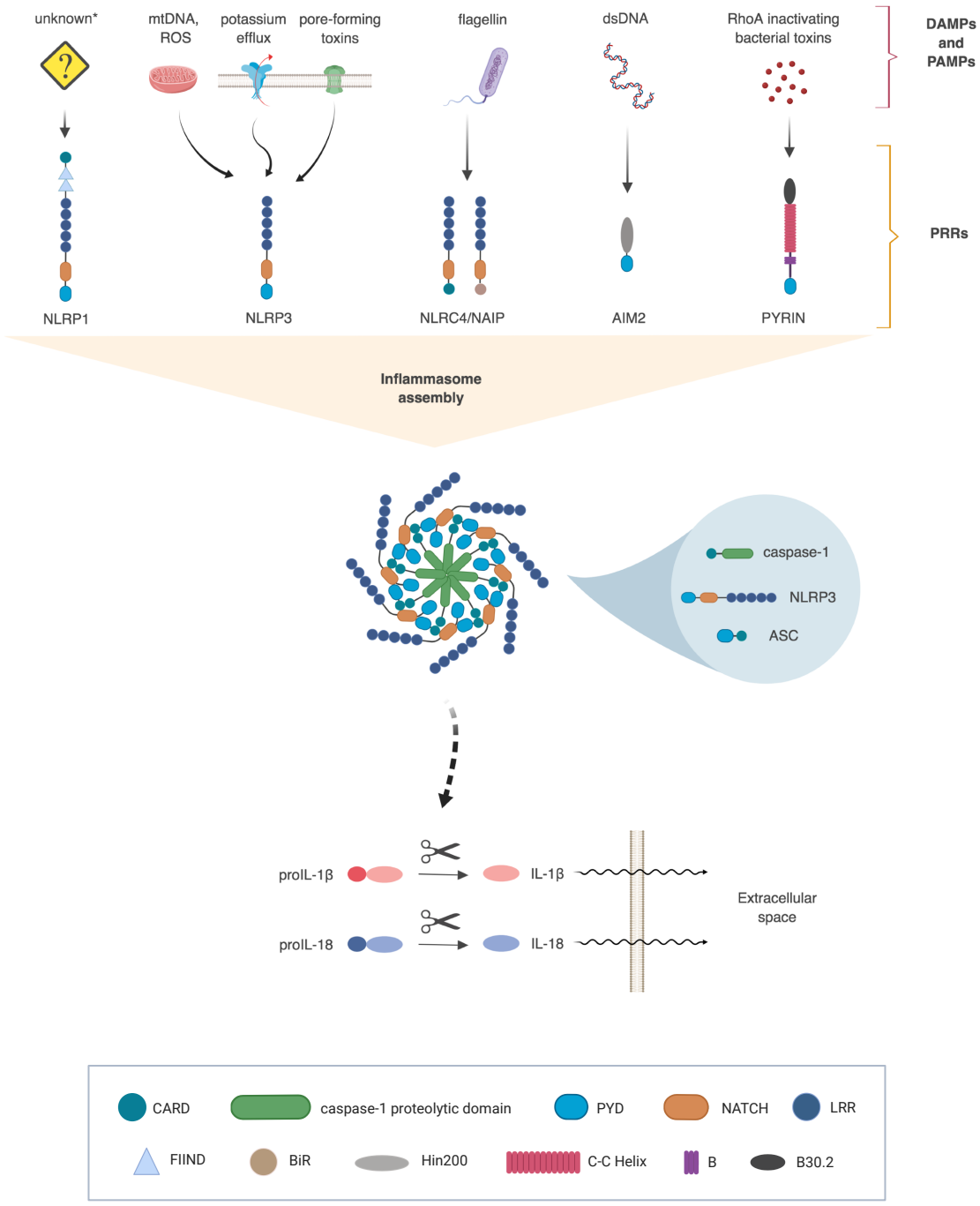

Figure 1.8 Canonical inflammasomes integrate innate immune sensing mechanisms to activate IL-1β and other cytokines

The schematic representation of canonical inflammasome assembly reflects its general mechanistic pattern: [1] a DAMP or PAMP is recognised either directly or indirectly by a specific PRR; [2] the different sensing mechanisms converge in the formation of a multimeric cytosolic platform that recruits caspase-1 through homotypic interactions with its CARD domain (depicted as dark green circles); the prototypical NLRP3 inflammasome is shown as an example;

[3] the final canonical inflammasome activates cytokines such as IL-1β or IL-18. NLRP1, NLRP3 and NLRC4 are all NLR proteins. *The NLRP1 receptor senses the anthrax lethal factor in mice; however, its ligand in humans remains unknown, although well-characterized single mucleotide polymorphism (SNP) mutations of its gene are associated with some auto-inflammatory diseases (234). mtDNA: mitochondrial DNA, dsDNA: double-strand DNA.

Some of the best studied PRRs are: the nucleotide-binding oligomerization domain (NOD) leucine-rich repeat (LRR) containing receptors (NLRs), the absent in melanoma 2 receptor (AIM-2) and the pyrin receptor (234, 235). Each of these PRRs specifically can detect one or several danger molecules or ligands and in turn interacts with specific mediator/adaptor proteins to activate the assembly of the inflammasome. Some of the better characterized sensing mechanisms including the respective PRRs involved are depicted in Figure 1.8.

Independently of the upstream activation signal, most PRRs oligomerize (through homo-domain protein-protein contacts) and generate nucleating surfaces where further interactions occur with other mediating proteins, such as the key apoptosis-associated speck-like protein containing a CARD domain (ASC) (235). Recruited ASC proteins also oligomerize through their homotypic domains and polymerize into linear filaments which, in turn, aggregate into macromolecular specks, contributing to the signal's amplification (236). Finally, ASC recruits caspase-1 through the interaction of their CARD domains. Subsequent local accumulation of caspase-1 facilitates its dimerization, indispensable for caspase-1 activation, the key objective of canonical inflammasome assembly (175, 192, 237).

It is widely accepted that active IL-1β-cleaving caspase-1 is found as a tetramer consisting of two p20 and two p10 subunits (p20/p10) (188). However, Boucher *et al.* have recently challenged this model and described that, in fact, active caspase-1 is found in either dimerized p45 (full-length) or p33/p10 tetramers, where p33 is a fragments that corresponds to the CARD domain plus the p20 subunit. Interestingly, these authors also propose that the p33/p10 processing into p20/p10 (the original described active conformation) is actually a mechanism of de-activation which renders caspase-1

inactive (192). Nevertheless, active caspase-1 located at the inflammasome site processes several precursor pro-inflammatory interleukins, such as IL-1β and IL-18, into their active secreted forms (204).

In summary, inflammasome assembly results in the activation of pro-inflammatory cytokines, amongst which, the master signalling cytokine IL-1β. IL-1β, which lacks a signal secretion sequence, is released from cells through a not yet fully understood unconventional secretion pathway (238). Once released, IL-1β binds to the extracellular side of the transmembrane protein type 1 IL-1 receptor (IL-1R1). Although they only share a 26 % amino acid homology (239), IL-1β and IL-1α have very similar secondary structures and share biological functions such as binding to IL-1R1 in its extracellular domain. In contrast to IL-1β, IL-1α [1] is not cleaved by caspase-1 (but by extracellular proteases which are not related to the inflammasome), [2] is an active molecule in its precursor form (although less bioactive than cleaved) and [3] it is a "dual-function cytokine": acts both as a transcription factor in the nucleus (where it can induce the expression of IL-8, for instance) and a signalling molecule secreted or bound to the extracellular membrane (240, 241). Although IL-1α is not processed by caspase-1, in the absence of caspase-1 IL-1α production is greatly reduced, suggesting that IL-1β controls Il-1α expression (211).

Binding of extracellular IL-1β or IL-1α to the IL-1R1 induces a conformational change in IL-1R1, and consequent interaction with the also transmembrane protein IL-1R3, with whom shares structural domains (240). Then MyD88 binds to the intracellular components of the heterodimer IL-1R1 / IL-1R3 and activates a strong proinflammatory signalling cascade that culminates with the activation of NF-kB. Therefore, IL-1 signalling amplifies a robust proinflammatory response by potentiating an autocrine positive feedback loop as well as paracrine activation.

Although IL-1α is constitutively expressed in many cell types whereas IL-1β expression is generally induced in response to a trigger, their biological functions are similar and key in promoting local and systemic inflammation (242). Besides being active signalling molecules in both innate and adaptive immunity, IL-1α and IL-1β are also signal transducers in non-immune cells (243). Proinflammatory processes directly or

indirectly mediated by IL-1 include: recruitment of immune cells to local sites of inflammation, partly due to the induction of the expression of adhesion molecules on endothelial cells; fever, caused by circulating IL-1β reaching the brain; and regulation of T cell polarization, for instance, by co-induction of IL-17 production (244-246).

Because overproduction of activated IL-1β can have detrimental effects (204), caspase-1 activity is tightly regulated. For example, in some cases, canonical inflammasome activation is regulated by a two-step mechanism. A first signal, also called priming, is required to boost the expression of the involved players and increase the pool of available proteins in the cytoplasm, such as proIL-1β or inflammasome components. This process is generally activated by transmembrane PRRs, such as the toll-like receptors (TLR), and results in the transcriptional activation of genes controlled by NF-κB. In these cases, the priming is followed by a second signal which induces the assembly of the inflammasome (231) (Figure 1.9).

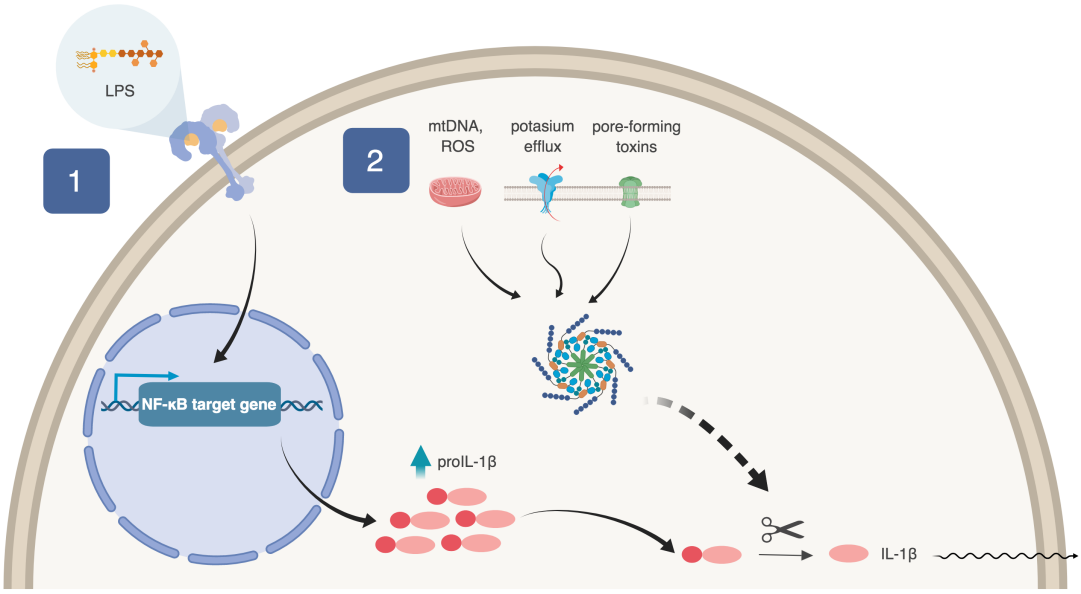

Figure 1.9 A two-step process regulates the activation of some inflammasomes
Priming (1) through PRRs activates the transcription of NF-κB target genes; in this diagram the recognition of extracellular lipopolysaccharide (LPS) by TLR-4 is depicted as an example. A second signal (2) contributes to the assembly of the canonical inflammasome. Activated caspase-1 can then process translated proIL-1β into its mature form.

Moreover, inflammasome activity is also intensively regulated, both positively and negatively, by other mechanisms, such as the interplay with autophagy, post-translational modifications (such as phosphorylation) of inflammasome components, and interaction with CARD-only proteins (COPs) and Pyrin-only proteins (POPs) (231, 234, 235, 247). Intriguingly, COPs and POPs encode genes that are present in humans and some primates but absent in mice, suggesting a further host specific difference in caspase-related mechanisms (248).

1.2.2.2 The canonical inflammasome and IL-1 signalling in disease

Although inflammasomes are crucial in the host's defence against infection, sterile immunity and general homeostasis, their dysregulation is linked to several diseases (249). A reason for this is that IL-1β overproduction is highly detrimental and can preclude its beneficial effects; hence IL-1β production is strictly controlled. Uncontrolled excessive IL-1β production drives inflammatory syndromes. In fact, mutations in inflammasome components, such as the PRRs, are the established cause of some autoinflammatory diseases (230, 250-252). For instance, in patients with cryopyrin-associated periodic syndromes (CAPS), the origin of the hereditary disease has been identified as gain-of-function mutations in the NRLP3 gene that render hyperactivation of NLRP3 inflammasome activity. CAPS and other autoinflammatory diseases are now effectively treated by FDA-approved IL-1 blocking agents, such as IL-1R1 pharmacological inhibitors or anti-IL-1β monoclonal antibodies (253-255).

Besides its prominent role in autoinflammatory syndromes, acute or low-chronic IL-1 due to aberrant inflammasome activation is also observed in other diseases with an inflammatory component, such as type 2 diabetes, rheumatoid arthritis or cardiovascular disease (246, 256, 257). Of interest, senescence has been associated with many of these sterile inflammatory diseases. Recent and on-going clinical trials are evaluating the outcome of therapeutic IL-1 blockade in these contexts: in general, when IL-1 is central to the aetiology of the disease, IL-1 blockade is efficient; otherwise, the benefits of this type of intervention are more controversial (258).

In cancer research, both beneficial and detrimental functions have been attributed to IL-1 signalling: on the one hand, IL-1 mediates the induction of antitumour adaptive immune responses; on the other hand, tumour angiogenesis, induction of an immunosuppressed environment and chronic inflammation are mechanisms by which IL-1 contributes to tumour progression and metastasis (259-261). Studies using mouse models have tried to further elucidate the role of the inflammasome proteins in cancer (262). For instance, in a murine model of colitis-associated colorectal cancer, depletion of some specific inflammasome components, including caspase-1, enhances tumorigenesis, suggesting a protective role for the inflammasome (263). In contrast, some other studies have shown that caspase-1 knock-out mice are less susceptible to specific models of skin and breast cancer (263). Except for the few cases in which mutations in an inflammasome component have been functionally linked to cancer susceptibility (252, 264), there is no universal mechanism of action for the inflammasome in cancer but the existence of different activated inflammasome pathways, and the outcome of their signalling depends on the cell type, tissue and cancer stage among other factors (265). It is clear that an improvement in our current knowledge regarding the molecular mechanisms that involve the inflammasomes would be beneficial for the design of tailored therapeutic strategies (262, 263).

Clinically, high IL1B mRNA expression has been associated with poor prognosis in some tumours (261). A recent study, emerging from a clinical trial with more than 10.000 enrolled patients and originally designed to evaluate the outcome of anti-IL-1β treatment in high risk atherosclerosis patients, found that administration of an anti-IL-1β antibody reduces lung cancer incidence and mortality (266). The underlying mechanism that supports these results is still to be characterized, but it is thought that IL-1β blockade might have inhibited tumour progression and induced its clearance (267). IL-1 targeting clinical trials for the treatment of multiple myeloma and advanced colorectal cancer have shown promising results (258, 268). Moreover, IL-1β production is commonly observed after administration of some chemotherapy drugs; however, although combined IL-1 blockade and chemotherapy has been proposed, preclinical studies in mice show controversial results (259, 261). IL-1 blockade is also under investigation to treat cytokine release syndrome (CRS), the most prevalent secondary effect of the innovative chimeric antigen receptor (CAR) T cell oncotherapy (269).

Overall, because inflammation, and in particular IL-1 signalling, is linked to many conditions, from autoinflammatory disorders to cancer, its targeting is of therapeutic interest. Although IL-1 blockade is approved for the treatment of some diseases (mainly those where IL-1 is clearly linked to the aetiology of the disease), the clinical benefit of IL-1 inhibition remains unclear for others (258). A better understanding of the context-specific molecular complexity of IL-1 signalling, including the inflammasome, is essential to [1] assess the specific contribution of IL-1 signalling in distinct phenotypes and [2] identify potential selective novel therapeutic targets for each scenario (235, 253).

1.2.3 The non-canonical inflammasome

1.2.3.1 The non-canonical inflammasome: description

Caspase-4 and -5, principal constituents of the non-canonical inflammasome, interplay with the canonical inflammasome during inflammatory responses (175). Although caspase-4 and -5 have an almost imperceptible ability to cleave proIL-1β *in vitro* compared to caspase-1 (270), absence of caspase-4 or -5 limits NLRP3 inflammasome-mediated IL-1β processing and release in response to microbial infections (218, 271-275), suggesting a role for caspase-4 and -5 as upstream regulators of the canonical inflammasome. Moreover, when co-overexpressed, direct interaction between caspase-1 and caspase-4 or -5 has also been reported (229, 271, 272). This has contributed to the hypothesis that a physical interaction between caspase-1 and caspase-4/-5 is required; however, the exact mechanism by which the non-canonical inflammasome exerts control over caspase-1-dependent IL-1β processing remains unclear. In mice, caspase-1 activity is regulated by caspase-11 (213, 276, 277). Besides regulating IL-1β processing and secretion, caspase-4 and -5 can also regulate the cellular release of other proteins, including IL-1α (218, 273).

Nonetheless, caspase-4, -5, and their murine counterpart caspase-11, have gained much relevance since the discovery over the last years of their functional role as key mediators in an inflammatory type of cell death termed pyroptosis. Pyroptosis is a type of

regulated cell death with distinctive morphology, caused by the formation of pores in the plasma membrane, and linked to innate immunity mechanisms (177). Although pyroptosis was identified as a distinct type of cell death more than 15 years ago (278), recent developments in its research have led to a much better understanding of its mechanism and biological relevance.

An initial ground-breaking study revisiting the function of caspase-11 (see section *1.2.1.2 Inflammatory caspases*) reported that, when challenged with a lethal LPS dose, caspase-11 deficient mice showed a significant increased survival rate compared to wild-type or caspase-1 knock-out mice (213). Subsequent independent studies revealed that resistance to LPS challenge was mediated by caspase-4 in humans (272). In 2013, two research groups described an exciting novel finding: LPS-induced lethality depends on intracellular LPS recognition by the non-canonical inflammasome (279, 280), in contrast to the previous thought that this pathway was activated by extracellular sensing of LPS by TLR4 (281).

Importantly, a further key study described that the lipid A of cytosolic LPS directly binds to the CARD domain of caspase-4, -5 or -11 (193); hence caspase-4, -5, -11 are PRRs themselves, unlike caspase-1. Binding of LPS induces oligomerization of caspase-4 or -11, indispensable for its catalytic activation (193) (Figure 1.10). Although caspase-5 also binds LPS *in vitro*, the authors observed that the loss of cell viability following LPS transfection in human cell lines (including epithelial cells and keratinocytes) was exclusively dependent on the presence of endogenous caspase-4 (193). In a different study, caspase-5 did not mediate cell death or IL-1β production in response to LPS transfection; however, caspase-5 was required for the death of human macrophages following infection with *Salmonella typhimurium* (274). Altogether, these and other studies (272, 275) suggest that caspase-5 does not participate in engaging pyroptosis after intracellular LPS transfection challenge but might be an essential part of the pyroptotic response to specific pathogens in limited subsets of cells of the immune system (282).

Following the seminal findings by Shi *et al.* (193), three studies reported the downstream mechanism by which activation of caspase-4, -5 or -11 leads to pyroptosis: inflammatory caspases cleave gasdermin-D into two fragments and the liberated N-terminal domain is the executioner of pyroptosis (283-285). After cleavage, the unleashed N-terminal domain of gasdermin-D binds to specific membrane lipids and forms lytic pores in the cell membrane, ultimately causing cell death (286-290).

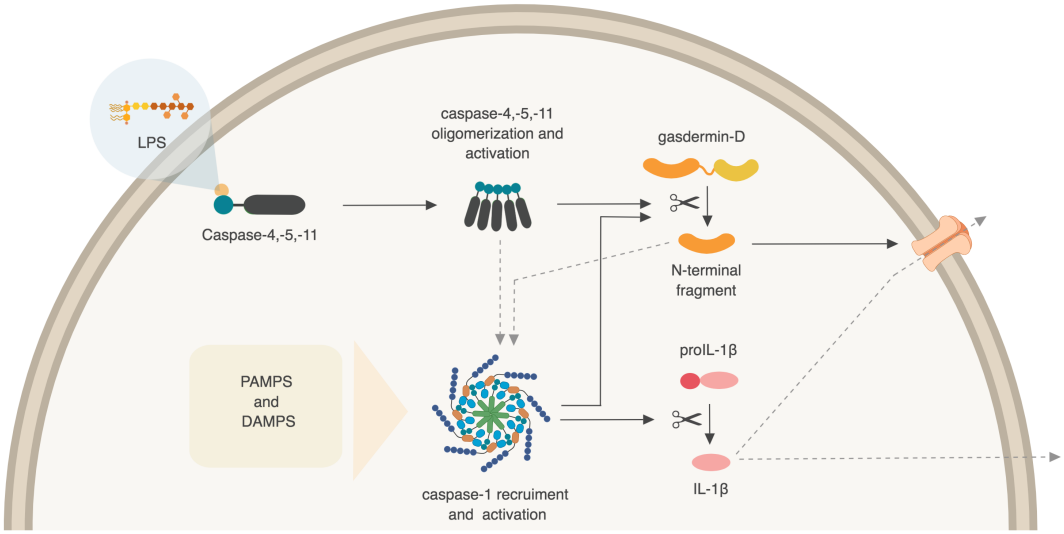

Figure 1.10 The roles of canonical and non-canonical inflammasome activation in IL-1 signalling

LPS binding to the CARD domain of caspase-4, -5 or-11 induces their oligomerization, activation and gasdermin-D cleavage. The liberated N-terminal fragment of gasdermin-D translocates to the plasma membrane, where it forms pores that can cause pyroptotic cell death. Activated caspase-1, due to the assembly of the canonical inflammasome, can also cleave gasdermin-D. The prototypical NLRP3 canonical inflammasome is depicted. Dashed lines represent processes which remain unclear: how the non-canonical inflammasome, both through and independently of gasdermin-D, activates the canonical inflammasome, and how IL-1β is released from cells.

Release of IL-1β into the extracellular space during cell death is a hallmark of pyroptosis (282, 291). Lack of gasdermin-D blocks IL-1β secretion in response to canonical inflammasome activation by diverse stimuli (283-285). In fact, it has been proposed that, besides mediating pyroptosis, transmembrane gasdermin-D pores also function as channels through which IL-1β is released (292, 293). IL-1β secretion can happen before pyroptosis or even in the absence of pyroptosis (294-298), which might be explained by a gradual concentration or a smaller number of gasdermin-D pores in the plasma membrane, respectively (299). Overall, the mechanisms that facilitate IL-1β secretion during pyroptosis, including the strict requirement for gasdermin-D pores, remain obscure. At a different IL-1 regulating level, it has also been suggested that the potassium efflux generated by gasdermin-D pores in the cell membrane might mechanistically explain how the non-canonical inflammasome can activate the NLRP3 canonical inflammasome (281).

Importantly, gasdermin-D is also cleaved by active caspase-1 and hence pyroptosis is not an exclusive function of the non-canonical inflammasome (205, 283-285). However, there are several differences regarding how the canonical and the non-canonical inflammasome induce pyroptosis. Of note, whereas caspase-1 activation depends on the previous assembly of the canonical inflammasome (and therefore the recruitment of mediator proteins), caspase-4 activation is prompted by the direct binding to its ligand. Nonetheless, whereas caspase-4,-5 and -11 trigger pyroptosis exclusively through gasdermin-D cleavage, caspase-1 activation can induce a different slower type of pyroptosis in the absence of gasdermin-D, suggesting a gasdermin-D independent pyroptotic mechanism downstream of caspase-1 activation (281, 284). A potential explanation to this evidence is that, in contrast to caspase-1, caspase-11 shows a much more limited substrate specificity (208). Finally, both the cell type and the specific trigger greatly influence whether gasdermin-D is cleaved by caspase-1, -4 or -5 (or a synergistic combination of more than one of them) and its outcome (cell death, IL-1β release or both).

Although most attention has focused on LPS, at least one endogenous lipid species can bind caspase-4 and -11: the oxidized phospholipid oxPAPC (oxidized 1-palmitoyl-2-arachidonyl-*sn*-glycero-3-phosphocoline). In contrast to LPS, oxPAPC binds to the

caspase's catalytic domain instead of the CARD (300). Paradoxically, oxPAPC has opposing roles regarding IL-1 secretion. On the one hand, oxPAPC binds caspase-11 specifically in dendritic cells and induces the release of IL-1β in the absence of pyroptotic cell death (300). On the other hand, oxPAPC blocks IL-1β release and pyroptosis in macrophages by preventing LPS binding to caspase-4 or -11 (301).

Besides regulating IL-1β cleavage indirectly and cleaving gasdermin-D, other biological functions have been attributed to caspase-4, -5, -11. For instance, caspase-11 interacts via its CARD domain with the actin-interacting protein 1 (AIP1) promoting cofilin-mediated depolymerisation (302). Furthermore, a role for caspase-4 in endoplasmatic reticulum-stress cell death has also been proposed (303, 304). Nonetheless, these and other caspase-4, -5, -11 biological functions remain to be further elucidated, especially in non-infectious settings.

1.2.3.2 The non-canonical inflammasome in health and disease

The non-canonical inflammasome plays a role in antimicrobial defence, particularly against Gram-negative bacteria as caspase-4, -5 and 11 directly sense LPS (305). Intracellular LPS activates caspase-4, -5 or 11, which in turn can, through gasdermin-D dependent and independent mechanisms, [1] stimulate the canonical inflammasome (and thus induce IL-1β cleavage) and [2] mediate IL-1β release, altogether promoting a pro-inflammatory response (281).

Moreover, caspase-4, -5 and -11, as well as caspase-1, can induce pyroptosis, eliminating the intracellular pathogen's replicative niche and allowing their release and exposure to immune antimicrobial clearance (299, 306). However, excessive pyroptosis activation can lead to unresolved damaged and eventual lethal sepsis. In mice models, caspase-11 or gasdermin-D deletion confers protection to endotoxic shock (213, 284). Therefore, gasdermin-D inhibitors are being developed and tested for the treatment of sepsis (307, 308).

Although caspase-4, -5 and -11 have been much less investigated than caspase-1, these caspases have also been associated to sterile damage. For instance, caspase-4 and -11 have been linked to the pathogenesis of some neurological disorders, such as multiple sclerosis or Alzheimer's disease (309, 310). Nonetheless, how caspase-4, -5 or -11 mechanistically function in these diseases is unclear.

In particular, whether the non-canonical inflammasome has a role in cancer has also been poorly investigated. Caspase-11 contributes to the intestinal homeostasis protecting against colitis-associated colorectal cancer (311, 312). In humans, CASP4 downregulated expression as well as infrequent loss-of function mutations have been described in some specific tumours, suggesting CASP4 is a tumour-suppressor gene (313, 314). Nonetheless, caspase-4 has also been positively correlated with malignancy: increased caspase-4 levels within intestinal epithelial cells or serum have been proposed as potential biomarkers for the diagnosis of colorectal and non-small cell lung cancer, respectively (315, 316). In all the aforementioned cancer-related studies, whether CASP4's association with a protective or malignant role was mechanistically related to IL-1β regulation was unexplored.

The role of pyroptosis in tumorigenesis has not yet been investigated (263). Interestingly, Val-boroPro, a potential anticancer agent that has reached Phase III trials, induces pyroptosis by indirectly activating caspase-1-dependent gasdermin-D (317, 318). Moreover, Wang et al. have recently described that chemotherapy drugs induce caspase-3 activation and cleavage of gasdermin-E, suggesting key roles for pyroptosis and the gasdermin family beyond inflammatory caspases (319).

1.3 Rationale, hypothesis and aims

The role of the SASP remains controversial in cancer and mechanistically ill-defined in ageing, two of the key pathophysiological contexts where senescence has been extensively investigated. Moreover, recent evidence proposes that different triggers might induce distinctive SASP subsets with concrete functions. Nonetheless, the SASP has started to arise interest as a potential therapeutic target in disease. Altogether, a better understanding of the molecular machinery scaffolding the SASP complexity is needed.

The canonical inflammasome is critical to the essence of the SASP (80). On the other hand, innate immunity research has unveiled an unexpected crucial role for the non-canonical inflammasome. Thus, we hypothesize that investigating caspase-4 may not only evidence and unreported role for the non-canonical inflammasome in senescence but also reveal functions that might be relevant beyond the senescence field.

In this line, and given the previous published evidence, several questions arise:

- Does the non-canonical inflammasome regulate the SASP in senescence?
- Does gasdermin-D have a functional role in senescence?
- Do inflammasomes have a broader role in senescence beyond cytokine regulation?
- What are the mechanisms by which inflammatory caspases might be activated in senescence?

Overall, this thesis aims to better understand the roles of inflammatory caspases in oncogene-induced senescence and, particularly, to explore, for the first time, the role of caspase-4 in cellular senescence.

Chapter 2 - Materials and methods

2.1 Reagents

Routinely used solutions were obtained from the in-house MRC Human Genetics Unit technical facilities:

Solution	Composition
Phosphate-buffered saline (PBS)	Dulbecco's tablets + dH2O
Tris-buffered saline (TBS)	25 mM Tris-HCl + 137 mM NaCl + 2.7 mM KCl, pH7.4
TBS-Tweem (TBS-T)	TBS + 0.05% Tween 20
Tris-acetate EDTA (TAE)	40 mM Tris, 0.1% glacial acetic acid, 1 mM EDTA
Immunofluorescence blocking buffer	PBS + 1% Bovine Serum Albumin + 0.2% Fish Gelatin
L-Agar	10 g/L tryptone, 5 g/L yeast extract, 10 g/L NaCl and 15 g/L agar
L-Broth	10 g/L tryptone, 5 g/L yeast extract, 10 g/L NaCl and 1 g/L glucose

Table 2.1 Regularly used solutions

All other reagents were purchased from the indicated suppliers.

2.2 Cell culture

2.2.1 Cell lines and maintenance

IMR90 and 293T cell lines were obtained from ATCC. All cells were routinely maintained in Dulbecco's Modified Eagle's Medium (DMEM) (Sigma, D5796),

supplemented with 10% Fetal Bovine Serum (FBS) (ThermoFisher, SV30180.03) and 1% antibiotic-antimycotic (ThermoFisher, 15240062), referred as standard media.

To induced oncogene-induced senescence, an inducible 4-hydroxy-tamoxifen (4-OHT) RAS^{G12V} in IMR90 cells model was used (320). For a detailed explanation of this system, see section 3.1.2. ER:STOP and ER:RAS cells were produced, expanded and froze by Dr Juan-Carlos Acosta. For the experiments included in this thesis, IMR90 ER:STOP and ER:RAS were thawed as routinely and maintained in standard media supplemented with geneticin (ThermoFisher, 10131-027) at a 200 µg/ml final concentration. For induction of senescence, cells were cultured with standard media supplemented with 200 µg/ml geneticin and 100 nM 4-hydroxytamoxifen (4OHT; Sigma, H7904).

All cell lines were incubated at 37°C with 5% CO_2 and tested for mycoplasma on a regular basis. Cells were cultured in 100 mm diameter round dishes as well as 6-well, 24-well and 96-well plates (Sigma, 430167, 657160, 662160 and 167008, respectively). To further subculture, per each 100 mm diameter dish cells were detached by washing once the attached monolayer with 3 mL of PBS before adding 1.5 mL of trypsin (ThermoFisher, 25300-054) for 5 min at 37 ºC. 8.5 mL of standard media was added to fully detached cells and these were pelleted by centrifugation at 1000 rpm for 5 min. The supernatant was discarded and 4 mL of standard media were added to the cells. After careful resuspension, 1 mL was transferred to each new dish already containing 9 mL of fresh standard media (split 1:4). Volumes were scaled down appropriately for smaller culture sizes.

2.2.2 Cell counting and viability

To determine cell concentration of cultures, after detached cells were collected by centrifugation, 50 uL of cells resuspended in standard media were added to 350 uL of Muse Count & Viability Reagent (Merck Millipore, MCH100102). After a 5 min incubation, cells were counted using the Muse Cell Analyzer (Merck Millipore), following manufacturer's instructions.

To determine cell viability, culture supernatants and attached cells were pooled together before centrifugation at 1000 rpm for 5 min. Pellets were resuspended in 50 uL of Muse Count & Viability Reagent (Merck Millipore, MCH100102) and further diluted 1:4. After a 5 min incubation, cells were counted using the Muse Cell Analyzer (Merck Millipore), following manufacturer's instructions. The Muse Count & Viability Reagent contains two dyes with differential permeability, one of which stains all cells whereas the other stains only nucleated (i.e. alive) cells. This system allows both the quantification and viability determination of the cell culture.

2.2.3 Freezing and thawing of cells

To freeze cells, cells were detached as explained in section 2.2.1. After centrifugation, the supernatant was discarded and cells were resuspended in 1 mL of 50% DMEM, 40% FBS, 10% DMSO per each 100 mm diameter dish, transferred to a cryogenic vial (Sigma, V7634), directly placed on dry ice and stored at -80 ºC. Cell stocks were stored in liquid nitrogen.

To thaw cells, frozen cryogenic vials were incubated 1-2 min in a pre-warmed 37 ºC water bath. The vial content was then transferred to a 15 mL tube containing 9 mL of media. Cells were pelleted by centrifugation at 1000 rpm 5 min and further resuspended in 1 mL of standard media before transferring to a 100 mm diameter dish containing 9 mL of fresh standard media.

2.2.4 Cell harvest

Cells were detached as explained in section 2.2.1. After centrifugation, pelleted cells were wash once with cold PBS and centrifuged 3 min at 3600 rpm in a bench-top centrifuge at 4 ºC. PBS was carefully removed and, if pellets were not immediately used, dried pellets were frozen at -80 ºC until further use.

2.2.5 Treatments

Pam2CSk4 (Tocris, 4637), Pam3CSK4 (Tocris, 4633), ultrapure lipopolysaccharide (LPS) from *E. coli* 111:B4 (Invovigen, tlrl-3pelps) and muramyldipeptide (MDP) (Tocris, tlrl-mdp) were reconstituted following manufacturer's instructions and stored at -20 ºC. Stock solutions were further diluted as needed for final concentration use on the day of the experiment. For inflammasome priming experiments, media was removed from cells and substituted with standard media supplemented with Pam2CSK4, Pam3CSk4, LPS and MDP at a final concentration of 0.05, 0.5, 1 and 1 µg/ml, respectively. For transfection experiments, LPS and MDP were used as explained in subheading 2.5.

2.3 Production of stable cell lines

2.3.1 Production of retroviral particles and infection of target cells

All viral work was performed using Category 2 cell culture facilities and good practices. The 293T packaging cell line was routinely used to produce both retroviral and lentiviral particles to stable infect IMR90. Common steps shared among both protocols are shown in figure 2.1.

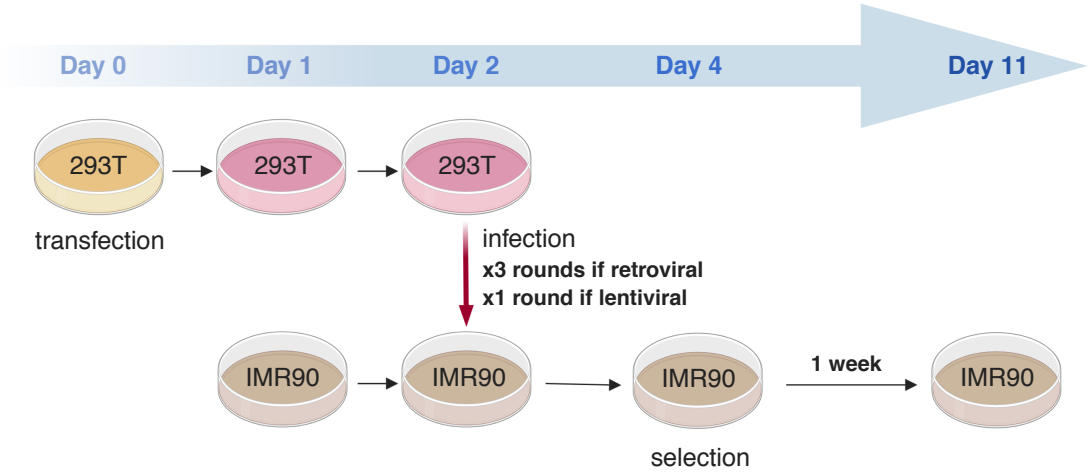

Figure 2.1 Stable cell line generation using retroviral or lentiviral particles
Schematic diagram showing the common steps of the protocols used to establish stable IMR90 cell lines using retroviral or lentiviral particles. The protocols are further detailed in the main text.

To stably overexpress or knockdown the expression of genes of interest, IMR90 cells were infected using retroviral particles. On the day prior to transfection, 293T cells were split 1:4 to achieve 85% cell confluency at the moment of transfection. On day 0, to co-transfect the required vectors into 293T cells, 2,5 µg of pCMV-VSVG, 7,5 µg of pUMVC3-gag-pol and 20 µg of the chosen plasmid were vortexed and incubated 10 min at room temperature in 0.5 mL of DMEM (Sigma, D5796) per each 10 cm dish to be transfected. During incubation, a separate mastermix containing polyethyleneimine (PEI) (Alfa Aesar, 43896) was prepared by adding 75 µl PEI (1 mg/mL stock concentration) to 425 uL of DMEM per each dish to be transfected. 0.5 mL of PEI mastermix vortexed solution were added to each tube containing the plasmids to be co-transfected. Each tube containing the transfection mix was gently vortexed and incubated 10 min at room temperature. Each transfection mix was carefully added drop by drop on each dish containing 293T. The following day (day 1), media was changed to all dishes. To check for transfection efficiency, a control dish was routinely transfected with a GFP-expressing plasmid. On day 1, IMR90s cells to be infected the next day were split 1:4.

On day 2, infections were performed. To perform infections, each viral supernatant was filtered using a 0,45 µm pore size filter (ThermoFisher, 15216869) into a 15 mL sterile Falcon tube. Each filtered media was complemented with polybrene (Sigma, H9268) to a final concentration of 4 µg/mL. Media on IMR90s was then substituted with the retroviral-containing supernatant and 6 mL of fresh standard media were added to the 293Ts cells. Infections were performed again, using the same procedure, 3 and 6 h after the first round. During the second and third rounds, filtered retroviral supernatants supplemented with polybrene were added to IMR90 cells without prior removal of media. 9 h after the first infection, supernatants on IMR90 cells were carefully aspirated and fresh standard media was added.

On day 4, infection efficiency was checked in IMR90 cells infected with a GFP-expressing plasmid. On day 4, cells were split 1:3 and cultured in standard media supplemented with 1µg/mL puromycin (ThermoFisher, A11138). A control dish was infected with a non-containing selection marker vector. Media was changed every 2-3 days with fresh standard media supplemented with the selection agent for over a week or until nor more dead cells were observed before further experimental set-up.

2.3.2 Production of lentiviral particles and infection of target cells

To stably knockdown the expression of genes of interest, IMR90 cells were infected using lentiviral particles. On the day prior to transfection, 293T cells were split 1:4 to achieve 85% cell confluency at the moment of transfection. On day 0, to co-transfect the required vectors into 293T cells, 2,5 μg of pCMV-VSVG, 7,5 μg of psPAX2 and 10 μg of the chosen plasmid were vortexed and incubated 10 min at room temperature in 0.5 mL of DMEM (Sigma, D5796) per each 10 cm dish to be transfected. Co-transfection of plasmids was performed as when producing retroviral particles, explained in section 2.3.1. On day 1, media was changed to all dishes and transfection efficiency was checked using a control dish transfected with a GFP-expressing plasmid. On day 1, IMR90s cells to be infected the following day were split 1:4.

On day 2, infections were performed. To perform infections, each viral supernatant was filtered using a 0,45 μm pore size filter (ThermoFisher, 15216869) into a 15 mL sterile Falcon tube. A separate mastermix was prepared containing standard media supplemented with polybrene (Sigma, H9268) at a final concentration of 4 μg/mL. Media on IMR90 was aspirated and 5 mL of polybrene-containing media were added to each dish. On top, 1 mL of filtered lentivirus-containing supernatant was added drop by drop carefully to each dish. After 3 h, media from IMR90 cells was aspirated and 10 mL of fresh standard media were added per dish. Infection efficiency and selection with puromycin were conducted as when performing retroviral infections (see section 2.3.2). Doxycyline was used for the inducible expression of pLVX-Tet-On vector constructs.

2.4 Short interfering RNA (siRNA)

2.4.1 siRNA sequences

siRNA technology was used to transiently knock-down the expression of a target gene. All siRNA reagents were ON-TARGETplus siRNA products (Dharmacon). Tubes containing siRNA were resuspended to 100 μM stocks following manufacturer's instructions. Stocks were further diluted to 10 μM and aliquoted in 50 μL tubes to avoid repeated thaw-freeze cycles. siRNA was resuspended and diluted in 1x siRNA buffer (5X

siRNA Buffer (Dharmacon, B-002000-UB-100) diluted in ultrapure DNase/RNase-free distilled water (ThermoFisher, 10977049). siRNA was stored at -20 ºC. Table 2.2 includes a list of the siRNA used to target the expression of human genes.

Name	Target sequence
CASP1-1	GGAAGACUCAUUGAACAUA
CASP1-2	GAUGGUAGAGCGCAGAUGC
CASP1-3	CCGCAAGGUUCGAUUUUCA
CASP1-4	GAGUGACUUUGACAAGAUG
CASP4-1	CAACGUAUGGCAGGACAAA
CASP4-2	UAACAUAGACCAAAUAUCC
CASP4-3	GGACUAUAGUGUAGAUGUA
CASP4-4	GAACUGUGCAUGAUGAGAA
GSDMD-1	CCACGUGUUGCAGGGUGA
GSDMD-2	GUCCUUCUCUUCCCGGAUA
GSDMD-3	GCACCUCAAUGAAUGUGUA
GSDMD-4	GGAACUCGCUAUCCCUGUU
Non-target control-1	UAGCGACUAAACACAUCAA
Non-target control-2	UAAGGCUAUGAAGAGAUAC
Non-target control-3	AUGUAUUGGCCUGUAUUAG
Non-target control-4	AUGAACGUGAAUUGCUCAA
P53-1	GAAAUUUGCGUGUGGAGUA
P53-2	GUGCAGCUGUGGGUUGAUU
P53-3	GCAGUCAGAUCCUAGCGUC
P53-4	GGAGAAUAUUUCACCCUUC
APAF1-1	AGAUAAUGAUUCCUACGUA
APAF1-2	AGUAAUGGGUCCUAAAUAU
APAF1-3	GUAUGAUGGAGCUGCAAAU
APAF1-4	UCAUGUAGGCAGAGUAUAA
DIABLO-1	CCGACAAUAUACAAGUUUA
DIABLO-2	GAUCAGGCCUCUAUAACCG
DIABLO-3	GAGCUGAGAUGACUUCAAA
DIABLO-4	GAUGAAGUGUGGCAGGUGA
CYCS-1	GCAUAUGCCUGAUGAAGUA
CYCS-2	GGACAAUUCUGGACUAAUG
CYCS -3	GAUUAGACUUCGUUAGUAA
CYCS -4	GGUGGUAGCUAGGGAUUUA
GBP1-1	CGAAAGGCAUGUACCAUAA
GBP1-2	UACAGGAUCUCCAGACGAA
GBP1-3	CAUACUCCCUGAAGCUGAA
GBP1-4	CCUAGUAUAUGUAGACUUU

Table 2.2 List of siRNA sequences

The name indicates the targeted gene followed by a number to uniquely identify the siRNA sequence.

2.4.2 siRNA transfection

siRNA was transfected into cells either by forward or reverse transfection, always using Dharmafect 1 (Dharmacon, T-2001) as the transfection agent and 30 nM final concentration of siRNA. A Dharmafect mix was obtained by diluting Dharmafect 1 in non-supplemented DMEM media (null media). 450 µL of 1x siRNA buffer were added to 50 µL of siRNA at 10 µM to obtain siRNA at 1 µM final concentration. Transfections were performed in 96-well or 6-well plates. IMR90 ER:STOP/ER:RAS cells were split 1:4 3 days before day 0. On day 0, senescence was induced by the addition of 4-hydroxytamoxifen and the first reverse transfection was performed. On day, 0 cells were also split and 200.000 cells / well were plated in 6-well plates. On day 3, cells were trypsinized, split 1:4 and reverse transfected. On day 5, cells were either harvest or fixed for downstream analysis, or forward transfected and kept in culture until day 8.

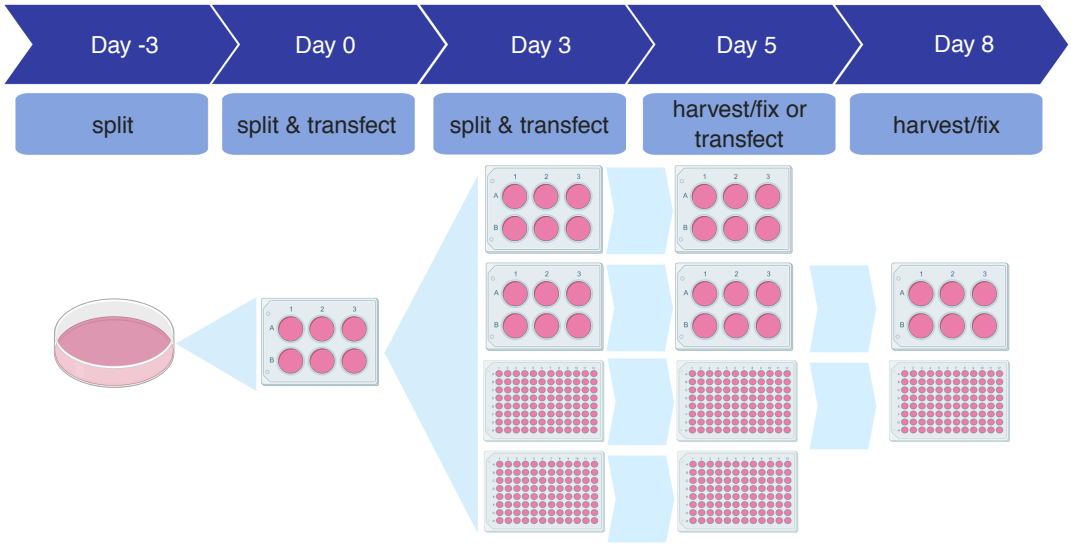

Figure 2.2 siRNA transfection protocol to transiently downregulate mRNA expression of target genes

Schematic timeline of the different steps of the siRNA transfection protocol. ER:STOP and ER:RAS cells were reverse transfected on day 0 and 3, and forward transfected on day 5.

To reverse transfect cells (day 0 and day 3), the specified amounts of siRNA in table 2.3 were added to each well. Next, the Dharmafect mix, prepared as specified in table 2.3, was added on top. Plates were incubated 1 h at room temperature. Meanwhile, cells were detached, counted and seeded, so that 100 μL or 2 mL final volume of cells were added to each siRNA:Dharmafect-containing well of a 96 or 6-well, respectively.

Well size	siRNA (1 μM)	Dharmafect 1 mix
96-well plate	3.6 μL	0.1 μL Dharmafect 1 + 17.4 μL null media
6-well plate	72 μL	2 μL Dharmafect 1 + 348 μL null media

Table 2.3 Reverse siRNA transfection specifications
Indicated shown amounts refer to one single well. A master Dharmafect 1 mix solution was prepared before distribution.

To forward transfect cells (day 5), solutions were prepared as indicated in table 2.4. siRNA and Dharmafect mix were incubated together for 20 min at room temperature. Then, standard media (when appropriate supplemented with 4-hydroxytamoxifen) was added and solutions were gently vortexed. Cell media was aspirated and substituted with the freshly prepared solutions as shown in table 2.4.

Well size	siRNA (1 μM)	Dharmafect 1 mix		Add standard media	Distribute / well
96-well plate	3.6 μL	0.1 μL Dharmafect 1 + 17.4 μL null media	20 min RT	100 μL	121.1 μL
6-well plate	72 μL	2 μL Dharmafect 1 + 348 μL null media		2 mL	2.4 mL

Table 2.4 Forward siRNA transfection specifications
Indicated shown amounts refer to one single well. A master Dharmafect 1 mix solution and master siRNA:Dharmafect solutions were prepared.

2.5 LPS transfection

2.5.1 Reagents

LPS (Invivogen, tlrl-3pelps) and MDP (Invivogen, tlrl-MDP) were reconstituted to 1 mg /mL following manufacturer's instructions and stored at -20 °C. LPS and MDP were aliquoted in several Eppendorf tubes to avoid multiple thaw-freeze cycles. LPS and MDP were reconstituted and further diluted in ultrapure DNase/RNase-free distilled water (ThermoFisher, 10977049).

2.5.2 Electroporation using the Neon Transfection System

To transfect LPS or MDP, the Neon Transfection System (Invitrogen, MPK5000) and the Neon Transfection System 100 µL Kit (MPK10025) were used. In each 100 µL tip, 5 x 10^5 cells were transfected with the indicated amount of PAMP (1, 0.1 or 0.01 µg).

Cells were detached and counted as explained in sections 2.2.1 and 2.2.2. After counting, 1,65 x 10^6 cells were washed once with PBS and resuspended in 315 µL of buffer R. 35 µL of 10x concentrated LPS or MDP were added to the cells. Electroporation parameters were set at as indicated in table 2.5.

Cell type	Pulse voltage (v)	Pulse width (ms)	Pulse number
293T	1100	20	2
IMR90	1500	30	1

Table 2.5 Selected parameters when using the Neon Transfection system

Once electroporated, the tip content was unloaded into a clean Eppendorf tube. Tubes were centrifuged on a bench-top centrifuge at 3000 rpm 3 min. Supernatant was removed to avoid any traces of MDP or LPS in the extracellular media. Cells were resuspended in 500 µL of media and plated in 6-well, 24-well and 96-well plates depending on further analysis.

Cell viability was determined as explained in section 2.2.2. For RNA extraction, SA-β-galactosidase and immunofluorescence assays, cell media was removed 24h after transfection and fresh media was added.

2.6 Senescence-associated β-galactosidase (SA-β-gal) activity assay

To perform an SA-β-gal assay, 5 x 10^4 cells were seeded in each well of a 6-well plate. Four days later, cells were fixed. To fix cells, wells were first washed once carefully with PBS 1x at room temperature before adding 0,5 mL of 0.5% glutaraldehyde (Sigma, G5882) in PBS / well and incubating 10 min. Fixed cells were washed three times with PBS/1 mM $MgCl_2$ pH 5.7, before incubating each well with 2 mLs of pre-warmed (37°C) X-Gal staining solution (2 mM $MgCl_2$, 5 mM $K_4Fe(CN)_6 \bullet 3H2O$, 5 mM $K_3Fe(CN)_6$, 1 mg/mL X-Gal solution ready to use (ThermoFisher, R0941) in PBS). Plates were covered in aluminium foil and incubated for 2-24 h at 37 °C.

2.7 Crystal-violet colony formation assay

To perform a crystal-violet colony formation assay, equal amounts of cells (either 5 x 10^4 or 1 x 10^5 cells) were seeded in 10 cm diameter dishes. Media was changed every three days and cells were fixed two weeks after initial seeding. To fix cells, dishes were first washed once carefully with PBS 1x at room temperature before adding 3 mL of 0.5% glutaraldehyde (Sigma, G5882) in PBS / dish for 20 min. Fixed dishes were washed two times with tap water and dried overnight. To stain the dishes, 4 mL 0.2% crystal violet staining solution were added to each dish and dishes were incubated on a rocker at room temperature. After 3 h, dishes were washed twice with tap water and dried.

To quantify cellular mass, cell bound crystal violet was dissolved in 10% acetic acid. Equal amounts were transferred to a spectrophotometer-compatible 96-well plate and absorbance was read at 595 nm.

2.8 Immunoblotting

2.8.1 Cell lysis

Cells were harvested as explained in section 2.2.4. Samples were lysed in Cell Lysis Buffer (to prepare 2.5 mL: 250 µL 10x Cell Lysis Buffer (Cell Signalling, 9803), 100 µL cOmplete EDTA-free Protease Inhibitor Cocktail (Roche, 04693159001) and 2150 dH_20). Cells were incubated on ice for 10 to 20 min and centrifuged 15 min at 10500 rpm at 4 °C. Supernatants were transferred to new Eppendorf tubes. Protein was store at -80 °C.

2.8.2 Determination of protein concentration

Protein concentration was determined using the Bradford assay. The 5x Bradford reagent (Biorad, 500-0006) was diluted 1:5 in dH_20. 2 µL of bovine serum albumin (BSA) pre-set standards (ThermoFisher, 23208) and samples were mixed with 198 µL of 1x Bradford reagent. Absorbance was measured at 595 nm using an iMark microplate reader (Biorad). BSA and unknown-concentrated samples were measured in triplicated. BSA samples were used to construct a standard curve and the derived regression formula was used to calculate the concentration of remaining samples.

2.8.3 SDS-PAGE electrophoresis

To prepare samples for sodium dodecyl sulfate polyacrylamide gel electrophoresis (SDS-PAGE), 15 µg of protein were mixed with 6 µL 6x Laemmli SDS sample buffer, reducing (Alfa Aesar, J61337) in a final volume of 36 µL. Samples were boiled 5 min at 95 °C. Samples were loaded in pre-cast Novex Tris-Glycine gels (Invitrogen). To determine protein size, a broad range colour pre-stained protein standard (NEB, P7712) was used. Different range or fix-concentrated gels were used depending on the molecular sizes of the proteins ot be detected. Pre-cast gels were run in am XCell SureLock™ Mini-Cell Electrophoresis tank (ThermoFisher). Tanks were filled with Novex Tris-Glycine SDS Running Buffer (10x) (ThermoFisher, LC2675) diluted 1:10 in dH_20. Electrophoresis conditions were 100 – 140 V, 1 – 2 h.

2.8.4 iBlot dry transfer

Samples were transferred into nitrocellulose membranes using the iBlot Gel Transfer Device (ThermoFisher) and nitrocellulose transfer stacks (Invitrogen, IB301002), following manufacturer's conditions. Transfer conditions were routinely set to 7 min at 20 V.

2.8.5 Antibody probing

After transferring, membranes were blocked in TBS supplemented with 5% non-fat milk (Marvel) (TBS-milk) 1 h at room temperature on a rocking shaker. Membranes were washed with TBS-T and primary antibodies were added. Used antibody concentrations are shown in table 2.6. All antibodies were diluted in TBS-milk. Membranes were incubated with primary antibodies overnight at 4 C. Membranes were then washed 10 times with TBS-T (x3 times) at room temperature on a rocking shaker.

Target	Host	Supplier	Dilution
Caspase-4	Mouse	Santa Cruz, 4B9	1:1000
Caspase-1	Mouse	Adipogen, Bally-1	1:1000
Gasdermin-D	Rabbit	Novus Biologicals, NBP2-33422	1:500
IL-1β	Mouse	R&D, MAB201	1:100 – 1:10000
IL-6	Goat	R&D, AF206NA	1:500
IL-8	Mouse	R&D MAB208	1:500
p53	Mouse	Santa Cruz, DO-1	1:1000
pRb	Mouse	BD Pharmigen, 554136	1:1000
p16	Mouse	Santa Cruz, JC-8	1:3000
β-Actin	Goat	Santa Cruz, I-19	1:5000

Table 2.6 Primary antibodies used for immunoblotting procedures

Next, membranes were incubated with secondary antibodies 1 h at room temperature on a rocking shaker. The secondary antibodies used are shown in table 2.7. Secondary antibodies were used at a range dilution of 1:10000 – 1:20000.

Target	Supplier
Mouse-HRP	Sigma, A2554
Rabbit-HRP	Sigma, A0545
Goat-HRP	Santa Cruz, 2020

Table 2.7 Secondary antibodies used for immunoblotting procedures

After incubation with the secondary antibody, membranes were washed 10 times with TBS-T (x3 times) at room temperature on a rocking shaker. Membranes were incubated during 2 min with 1:1 solution of A:B pre-mixed enhanced chemiluminescence solution (GE Healthcare, RPN2209). To visualize, bands, membranes were exposed to X-ray films (SLS, MOL7016 or GE Healthcare, 28906837). Films were developed using an X-ray processor.

2.9 Immunofluorescence

2.9.1 BrdU labelling

BrdU (Sigma, 858811) was added the day before cells were fixed. Briefly, a mastermix BrdU solution was prepared by adding 100 µL of 10 mM BrdU stock solution to 10 mL of null media. 10 µL of the mastermix BrdU solution were added to each well of a 96-well plate already containing 100 µL of media (50µM final BrdU concentration / well). Plates were placed back in the incubator for 16-18 h, after which, plates were fixed.

2.9.2 Staining protocol

To fix plates, plates were first washed once with 100 µL / well PBS, and then 30 µL of 4% paraformaldehyde in PBS (FD NeuroTech, PF101) were added to each well. Cells were fixed during 45 min at room temperature in a fume hood. Next, plates were washed with 100 µL / well PBS (x3 times). To permeabilise cells, 30 µL 0.2% Triton-X100 / PBS were added to each well and plates were incubated for 10 min on an orbital shaker at room temperature. Next, plates were washed with 100 µL / well PBS (x3 times). Cells were blocked with 30 µL /well immunofluorescence blocking buffer for 1 h on an orbital

shaker at room temperature. Next, the immunofluorescence blocking buffer was removed and 30 µL / well primary antibody were added. Plates were then incubated for 1h on an orbital shaker at room temperature. Primary antibodies were diluted in immunofluorescence blocking buffer and used as detailed in table 2.8. In addition, the anti-BrdU-containing solution was supplemented with 0.5 U / µL DNAse (SIGMA D4527) and 1 mM $MgCl_2$ to improve anti-BrdU access DNA-bound BrdU. Wells were incubated with anti-BrdU antibody 30 min on an orbital shaker at room temperature.

Target	Host	Supplier	Dilution
Caspase-4	Mouse	Santa Cruz, 4B9	1:100
BrdU	Mouse	BD Biosciences, 555627	1:2000
IL-1α	Mouse	R&D, MAB200	1:100
IL-1β	Mouse	R&D, MAB201	1:100
IL-6	Goat	R&D, AF206NA	1:100
IL-8	Mouse	R&D MAB208	1:100
p53	Mouse	Santa Cruz, DO-1	1:100
p21	Mouse	Sigma, P1484	1:200
p16	Rabbit	ProteinTech, 10883-1-AP	1:400

Table 2.8 Primary antibodies used for immunofluorescence procedures

After incubation with the primary antibody, plates were washed with 100 µL / well PBS (x3 times). Secondary antibodies, detailed in table 2.9, were diluted 1:1000 in immunofluorescence blocking buffer. Secondary antibodies were added (30 µL / well) and plates were immediately covered in aluminium foil and incubated for 45 min on an orbital shaker at room temperature.

Target	Supplier
Mouse-Alexa Fluor 488	ThermoFisher, A-11029
Rabbit-Alexa Fluor 594	ThermoFisher, A-11037
Goat-Alexa Fluor 594	ThermoFisher, A-11058

Table 2.9 Secondary antibodies used for immunofluorescence procedures

After incubation with the secondary antibody, plates were washed with 100 µL / well PBS (x3 times). Next, nuclei were stained with 4′,6-diamidino-2-phenylindole (DAPI) (Molecular Probes, D1306). To do so, 30 µL / well DAPI (1 µg/mL in PBS) were added and plates were incubated for 45 min on an orbital shaker at room temperature covered in aluminium foil. After incubation, plates were washed with 100 µL / well PBS (x3 times).

2.9.3 High-content microscopy

Immunofluorescence was visualized using the high-content microscopy ImageXpress Micro XLS High-Content Analysis System (Molecular devices), following manufacturer's instructions. Images were acquired at 10x magnification. Multi-wavelength cell scoring analysis on acquired data were performed using the MetaXpress High-Content Image Acquisition and Analysis software (Molecular devices). Thresholds were carefully manually set for positive scoring. DAPI detection was used to quantify total cell counts. Exported one-wavelength images of the same frame were merged using the software Fiji (ImageJ).

2.10 Enzyme-linked immunosorbent assay (ELISA)

2.10.1 Secreted IL-1β quantification

Detection of secreted IL-1β by ELISA was performed as previously described (321). Conditioned media was collected, centrifuged 10 min at 1000 rpm at 4 °C, transferred to a new tube and immediately stored at -80 °C. Detection of IL-1β was performed following the manufacturer's instructions of the Human IL-1 beta ELISA Ready-Set-Go! Kit (ThermoFisher, 15581087). GraphPad Prism software was used to generate a four-parameter logistic (4-PL) curve fit and create a standard curve using absorbance values of IL-1β standards. Concentrations of unknown samples were then deducted by interpolation of data from the standard curve.

2.11 Caspase-4 fluorometric activity assay

2.11.1 LEVD-AFC cleavage detection

To measure LEVD-AFC cleavage, the Caspase 4 Assay kit (Fluorometric) (Abcam, ab65658) was used following manufacturer's instructions. Briefly, cultured IMR90 ER:STOP and ER:RAS cells were counted and 2 x 10^6 cells were lysed in 50 µL cell lysis buffer and transferred to each well of a black sterile 96-well polystyrene plate (ThermoFisher, 137101). After a 10 min incubation on ice, 50 µL of DTT-containing reaction buffer was added to each well. 5 µl of 1 mM LEVD-AFC substrate were added to each well and the plate was covered with aluminium foil and incubated at 37 °C. Fluorescence was measured (excitation filter: 400 nm; emission filter: 505 nm) using the Infinite® 200 PRO (Tecan) plate reader. For the time-course experiments, induction with 4-hydroxytamoxifen was performed 8 and 4 days before LEVD-AFC cleavage detection so that all samples were subject to LEVD-AFC cleavage analysis using the same microplate on day 0.

2.12 Detection of caspase-4 oligomerization

2.12.1 Disuccinimidyl suberate (DSS) cross-linking

2 T-6 well / condition were pelleted as explained in section 2.2.4. Fresh pellets were resuspended in 0.5 ml of ice-cold buffer A (20 mM HEPES-KOH, pH 7.5; 10 mM KCl; 1.5 mM MgCl2; 1 mM EDTA; 1 mM EGTA; 320 mM sucrose) and lysed by shearing 10 times through a 25-gauge needle in microcentrifuge tubes. Lysates were centrifuged for 8 min at 1.800 g at 4 °C and supernatants were transferred to new tubes. At this step, 30 µL of lysates were kept as input controls. Remaining supernatants were diluted with 1 volume of CHAPS buffer (20 mM HEPES-KOH, pH 7.5; 5 mM MgCl2; 0.5 mM EGTA; 0.1 mM PMSF; 0.1% CHAPS) and centrifuged at 5,000 x g for 8 min. Supernatants were discarded and pellets resuspended in 50 µL of CHAPS buffer containing 4 mM of disuccinimidyl suberate and incubate for 30 min at room temperature to cross-link proteins. Next, samples were centrifuged at 5,000 x g for 8 min at 4 °C, supernatants

discarded and pellets resuspended in 60 µL of 2x protein loading buffer (2x loading buffer is prepared by diluting 4x protein loading buffer (50 mM Tris-HCl, pH 6.8; 2% SDS; 10% glycerol; 12.5 mM EDTA; 0.02% bromophenol blue) in dH_2O. Samples were then heated for 2 min at 90 °C. 18 µL of resuspended cross-linked pellets were loaded on 4-12% Tris-Glycine SDS-PAGE. Further immunodetection of caspase-4 in both cross-linked and input samples was performed following standard procedures as described in section 2.8.3 – 2.8.5.

2.13 Molecular cloning

2.13.1 Plasmid constructs

Retroviral vectors for gene overexpression were based on the (murine stem sell virus) (MSCV) retroviral expression system. The pMSCVpuro empty vector and pMSCVpuro-$HRAS^{G12V}$ were obtained from the laboratory stock plasmid collection. Human CASP1 and CASP4 coding sequences (CDS) were cloned into the pMSCVpuro empty vector plasmid as explained in section 2.13.2 to obtain MSCVpuro-CASP1 and MSCVpuro-CASp4 respectively. pMSCVpuro-CASP4 C258A for the overexpression of a mutant catalytic dead caspase-4 was generated using site-directed mutagenesis as explained in section 2.13.3.

Short-hairpin RNA (shRNA) expression was used to stable silence target genes. The retroviral vectors pSUPER.retro.puro (pRS) empty backbone vector and pRS-shP53 were obtained from the laboratory stock plasmid collection. pRS–shCASP4-1 and pRS-shCASP4-2 were generated by Dr Andrea Quintanilla by inserting the oligonucleotides (+) GATCCCCCAACGTATGGCAGGACAAATTCAAGAGATTTGTCCTGCCATACGTTGTTTTTG and GATCCCCTAACATAGACCAAATATCCTTCAAGAGAGGATATTTGGTCTATGTTATTTTTG into the pRS empty backgone to generate pRS–shCASP4-1 and pRS-shCASP4-2 respectively, and according to the pSuper RNAi System manual (OligoEngine) instructions.

To stably silence target genes through shRNA expression, lentiviral vectors belonging to the GIPZ microRNA-adapted shRNA collection (Dharmacon) were used. The pGIPZ

empty backbone, pGIPZ-shP53 and pGIPZ-shCASP1 (V3LHS_392179) were obtained from the laboratory stock plasmid collection. pGIPZ-shCASP4 (V3LHS_338745) was purchased from Dharmacon.

pCMV-VSVG, pUMVC3-gag-pol, psPAX2, pBABE-GFP and pULTRA were obtained from the laboratory stock plasmid and used during the generation of stable cell lines by retroviral and lentiviral infections either because necessary for viral packaging (pCMV-VSVG, pUMVC3-gag-pol and psPAX2) or for infection control due to lack of puromycin resistance (pBABE-GFP and pULTRA).

pLVX-Tet-On Advanced was obtained from the laboratory stock plasmid collection. pLVX-Tet-On-GSDMD-FL and pLVX-Tet-On-GSDMD-Nter were generated as explained in section 2.13.2.

pQXCIN-BirA-Myc-C and pQXCIN-Myc-BirA-N were obtained from the laboratory stock plasmid collection. pQXCIN-CASP4-BirA-Myc-C, pQXCIN-Myc-BirA-CASP4-N and pQXCIN-Myc-BirA-CASP1-N were generated as explained in section 2.13.2.

Plasmids were validated before use by Sanger sequencing using the in-house MRC HGU Technical Services.

2.13.2 Coding sequence (CDS) amplification by polymerase chain reaction (PCR)

Total RNA extracted from IMR90 cells was converted into cDNA generating a human coding sequence (CDS) library using standard retro-transcription procedures (see section 2.14.2). To clone into the pMSCVpuro empty vector, CASP1 and CASP4 CDS were amplified from the obtained CDS human library using customized primers with overhangs including recognition sites for selected restriction enzymes (table 2.10). The destination vector, pMSCVpuro, includes a modified multiple cloning site in which the polylinker BglII-EcoRI-AvrII-NotI-EcoRV-XhoI-MfeI has been cloned into the previous BglII-EcoRI site.

For the biotin identification (BioID) proximity-labelling system experiments, CASP1 and CASP4 CDS were cloned into the pQCXIN-BirA-Myc-C and pQCXIN-BirA-Myc-N. CASP1 and CASP4 CDS with customized overhangs (see table 2.x) were amplified from the pMSCVpuro-CASP1 and pMSCVpuro-CASP4 plasmids originally generated during this thesis and earlier mentioned.

Full-length and the fragment coding for the N-terminal domain of GSDMD were cloned into the pLVX-Tet-On vector. CDS fragments were obtained from the human CDS library obtained from IMR90 cells as explained previously.

Amplified DNA	Destination vector	Restriction enzymes	Forward primer (5' → 3')	Reverse primer (5' → 3')
Human CASP1 CDS	pMSCVpuro	AvrII - XhoI	ATAAACCTAGGATGGCC GACAAGGTCC	AATAACTCGAGTTAATGTCC TGGGAAGAGGTAG
Human CASP4 CDS	pMSCVpuro	AvrII - XhoI	ATAAACCTAGGATGGCA GAAGGCAACCA	AATAACTCGAGTCAATTGCC AGGAAAGAGGTAG
Human CASP1 CDS	pQCXIN-BirA-Myc-N	BsiWI-BamHI	ATAAACGTACGATGGCC GACAAGGTCCTGAAGGA	CGGGCGGATCCTTAATGTC CTGGGAAGAGGTAGA
Human CASP4 CDS	pQCXIN-BirA-Myc-N	BsiWI-BamHI	ATAAACGTACGATGGCA GAAGGCAACCA	CGGGCGGATCCTCAATTGC CAGGAAAGAGGTAG
Human CASP4 CDS	pQCXIN-BirA-Myc-C	NotI-BamHI	ATAAAGCGGCCGCATGG CAGAAGGCAACCA	CGGGCGGATCCATTGCCAG GAAAGAGGTAG
Human full-length GSDMD CDS	pLVX-Tet-On	EcoRI-BglII	ATTTAGAATTCATGGGGT CGGCCTTTGA	AACCAAGATCTCTAGTGGG GCTCCTGG
Human N-terminal GSDMD CDS	pLVX-Tet-On	EcoRI-BglII	ATTTAGAATTCATGGGGT CGGCCTTTGA	AACCAAGATCTCTAATCTGT CAGGAAGTTGTGGAGG

Table 2.10 Coding sequence (CDS) DNA fragments obtained by PCR

The table shows a list of the amplified CDS fragments, their destination vector and the restriction enzymes used to ligate the inserts into the destination vector.

PCR were performed using either Q5 high-fidelity DNA polymerase (New England Biolabs, M0491) or Phusion High-Fidelity PCR Master Mix with HF Buffer polymerase (New England Biolabs, M0531) using the SureCycler 8800 thermal cycler (Agilent); reaction conditions were optimized for each DNA target.

2.13.3 Site-directed mutagenesis by PCR

The catalytically dead caspase-4 overexpressing retroviral vector pMSCVpuro-CASP4 C258A was obtained through site-directed mutagenesis by PCR using the Q5 Site-Directed Mutagenesis Kit (New England Biolabs, E0554S) and following manufacturer's instructions. To perform the substitutional mutation (bases TGC to bases GCC at positions 772-774 of the 1134 bp CASP4CDS fragment), the NEBaseChanger online tool (New England Biolabs) was used and the following primers were picked: forward (5→3') TGTCCAGGCCgccAGAGGTGCAA; reverse (5→3') ATGATGACCTTGGGTTTG. The thermocycling conditions used to amplify the CDS fragment were: 30 s at 98 °C; 25 cycles of 10 s at 98 °C, 30 s at 60 °C and 4 min and 30 s at 72 °C; 2 min at 72 °C.

2.13.4 DNA digestion, ligation and bacterial methods

DNA sizes (kb) were checked by agarose gel electrophoresis before digestion with selected restriction enzymes. All restriction enzymes used were purchased from New England Biolabs. Vectors were also linearized using chosen restriction enzymes. When two different enzymes were used, sequential digestion was performed if enzyme activities were not compatible in the same digestion buffer.

Ligation was performed using the T4 DNA ligase (New England Biolabs, M0202S) following manufacturer's instructions. Broadly, 50 ng of vector DNA were mixed with the insert DNA in a 3:1 insert:vector DNA molar ratio, reagents added and the mix incubated overnight at 16 °C.

To transform bacteria, 5 µL of ligation product were added to 25 µl of 5-alpha competent *Escherichia coli* (New England Biolabs, C2987) and placed on ice for 15 min. Then, to heat-shock bacteria, tubes were incubated at 42 °C for 45 s and placed back on ice for 5 min. Next, 2-5 µL of bacteria were spread on L-Agar plates supplemented with the antibiotic of choice (ampicillin or kanamycin). Plates were incubated at 37 °C with agitation overnight.

The following day, isolated colonies were picked and further grown in 120 mL of L-Broth, supplemented with the antibiotic of choice, for 16 h. To generate glycerol plasmid stocks, the following day 10 mL of bacterial culture were centrifuged at 4.000 rpm 15 min at 4 °C. Supernatant was discarded and the pellet was resuspended in 1 mL of a 50% LB/glycerol sterile solution. Glycerol stocks were stored at -80 °C.

For plasmid extraction and purification, the the QIAGEN Plasmid Plus Midi Kit (Qiagen, 12945) was used following manufacturer's instructions. DNA was quantified using a Nanodrop 2000C (Thermo Scientific) spectrophotometer and stored at – 20 °C until further use.

2.14 Quantitative-reverse transcription polymerase chain reaction (qRT-PCR)

2.14.1 RNA extraction

Cells were harvested as explained in section 2.2.4. RNA was extracted using the RNeasy Plus Mini kit (Qiagen, 74134), following manufacturer's instructions. During RNA extraction, cell lysates were homogenized using QIAshredder (Qiagen, 79654). RNA was eluted in ultrapure DNase/RNase-free distilled water (ThermoFisher, 10977049), quantified using a a Nanodrop 2000C (Thermo Scientific) spectrophotometer and stored at – 80 °C.

2.14.2 Complementary DNA (cDNA) synthesis

RNA was transformed into cDNA using qSscript cDNA Supermix (Quanta Biosciences, 95048-100). Reactions were prepared in 0.2 mL 8-tube strips (Applied Biosystems, N8010580). 1 µg RNA was mixed with 4 µL of qScript cDNA SuperMix (5X) and topped to 20 µL final volume with ultrapure DNase/RNase-free distilled water (ThermoFisher, 10977049). Samples were incubated sequentially 5 min at 25 °C, 30 min at 42 °C and 5 min at 85ºC in a SureCycler 8800 thermal cycler (Agilent). cDNA was stored at -20 °C until further use.

2.14.3 Quantitative PCR

Primer sequences which were not already part of the laboratory primer stock collection were either retrieved from published data by others or newly designed. New primers were designed to have a length of 18-20 nucleotides and to amplify a DNA fragment between 120 and 180 nucleotides. Paired primers were designed to amplify a fragment containing an exon-exon junction to ensure only the CDS was amplified. Primer properties such as melting temperature or self-dimer and hetero-dimer tendencies were analysed using the online OligoAnalyzer Tool (Integrated DNA technologies). Primers were purchased from Sigma as dried DNA oligos in tubes. When received, primers were resuspended to 100 µM stock concentration. Intermediate 5 µM stocks were also prepared to avoid continuous thaw-freeze cycles of the 100 µM stocks. Primers were always resuspended and diluted in ultrapure DNase/RNase-free distilled water (ThermoFisher, 10977049). Primer sequences are shown in table 2.11.

Reaction samples were loaded in triplicate in 96-well PCR plates (Starlab, E1403-7700). Each well contained: 1 µL of cDNA, 200 nM forward primer, 200 nM reverse primer, 1x SYBR Select Master Mix (Applied Biosystems, 4472908S) and up to 20 µL of ultrapure DNase/RNase-free distilled water (ThermoFisher, 10977049), except for reactions targeting the housekeeping gene (ACTB), where primers were added at a 100 nM final concentration instead of 200 nM. Plates were loaded into the StepOnePlus Real-Time PCR System (ThermoFisher, 4376600). The following PCR cycling parameters were used: 10 min at 95 °C; 40 cycles of 15 s at 95 °C, 30 s at 60 °C and 15 s at 72 °C; 15 s at 95 °C. A ramp step (0.3 °C / 5 s) 60 °C to 95 °C was added immediately after the amplification stage to generate the melting curve. StepOnePlus Real-Time PCR System software was used to select PCR parameters and to analyse the quality of results once the qPCR was performed, including analysis of the melting curve and threshold cycle (Ct). Data was analysed using the double Delta Ct method (322). ACTB mRNA expression was used to normalize data.

Target	Forward primer (5' → 3')	Reverse primer (5' → 3')
ACTB	CATGTACGTTGCTATCCAGGC	CTCCTTAATGTCACGCACGAT
CASP1	CAACTACAGAAGAGTTTGAGG	AACATTATCTGGTGTGGAAG
CASP4	GAGAAGCAACGTATGGCAGG	GGAATTCTTCATGAGGACAAAGC
IL1B	TGCACGCTCCGGGACTCACA	CATGGAGAACACCACTTGTTGCTCC
IL1A	AGTGCTGCTGAAGGAGATGCCTGA	CCCCTGCCAAGCACACCCAGTA
IL6	CCAGGAGCCCAGCTATGAAC	CCCAGGGAGAAGGCAACTG
IL8	GAGTGGACCACACTGCGCCA	TCCACAACCCTCTGCACCCAGT
GSDMD	ATGGATGGGCAGATACAGGG	TGCTGCAGGACTTTGTGTTC
CDKN1A	CCTGTCACTGTCTTGTACCCT	GCGTTTGGAGTGGTAGAAATCT
CDKN2A	CGGTCGGAGGCCGATCCAG	GCGCCGTGGAGCAGCAGCAGCT
CDK1	CTTGGCTTCAAAGCTGGCTC	GGGTATGGTAGATCCCGGCT
BUB1	ACACCATTCCACAAGCTT	CGCCTGGGTACACTGTTT
CDC6	GTTCAATTCTGTGCCCGCAA	TAGCTCTCCTGCAAACATCCAG
CCNA2	AGGAAAACTTCAGCTTGTGGG	CACAAACTCTGCTACTTCTGGG
CCNB1	TGTGTCAGGCTTTCTCTGATG	TTGGTCTGACTGCTTGCTCT
MCM2	GTGGATAAGGCTCGTCAGAT	GTCGTGGCTGAACTTGTT
SAA1	GAGCACACCAAGGAGTGATTT	GAAGCTTCATGGTGCTCTCT
SAA2	GCTGCAGAAGTGATCAGCAAT	CAGCGAGTCCTCCGCAC
APAF1	CTCTCATTTGCTGATGTCGC	TCGAAATACCATGTTTGGTCA
DIABLO	AATGTGATTCCTGGCGGTTA	AGCTGGAAACCACTTGGATG
CYCS	GGCTGCAGTGTAGCTGTGAT	GATGGAGTTTCCTTTATCTGTTGC
GBP1	GGTCCAGTTGCTGAAAGAGC	CTTGGTTAGGGGTGACAGGA

Table 2.11 Primers used for qPCR

The table shows a list of primer pairs used to quantify human mRNA expression of target genes.

2.15 Transcriptomics

2.15.1 Ampliseq targeted RNA sequencing

For Ampliseq targeted RNA sequencing, RNA was extracted as explained in section 2.14.1. RNA quality control, reverse transcription, library preparation and sequencing were performed by the Wellcome Trust Clinical Research facility (WTCRF) as explained below.

RNA samples were assessed for quality on the Bioanalyser 2100 Electrophoresis Instrument (Agilent, G2939AA) with the RNA 6000 Nano Kit (Agilent, 5067-1511), providing an RNA Integrity Number (RIN). Samples were quantified using the Qubit 2.0 fluorometer (Q32866) and the Qubit RNA Broad Range assay (Q10210). 10 ng of RNA was reverse-transcribed to make cDNA, and then target genes were amplified for 12 cycles of PCR using the Ion AmpliSeq Human Gene Expression Core Panel (Thermofisher, A26325). This panel contains a pool of 20,802 amplicons (41,604 primers) of approximately 150 bases in length. Ion Torrent sequencing adapters and barcodes Ion XpressTM Barcode Adapters (Ion XpressTM Barcode Adapters, 4471250 and 4468802) were ligated to the amplicons and adapter-ligated libraries were purified using AMPure XP beads. Libraries were quantified by qPCR and diluted to 100 pM before being combined in equimolar pools of 8 per each chip (ThermoScientfic, Ion PI Chip Kit v3). Sequencing was performed using the Ion PI Hi-Q Sequencing 200 Kit (ThermoFisher, A26433) and the Ion Proton platform (ThermoFisher, 2456290-0449).

The WTCRF also conducted a first analysis of the Ion AmpliSeq Transcriptome libraries. Sequence reads were mapped to the hg19_AmpliSeq_Transcriptome_ERCC_v1.fasta reference. Next, matches per amplicon were quantified using defined amplicon regions from the hg19_AmpliSeq_Transcriptome_21K_v1.bed file. BAM files were generated using the Torrent Suite software v 5.2.0 (ThermoFisher). The ECRf provided the sequencing reports, including the unnormalized read counts and reads per million (RPM) gene counts.

2.15.2 Differentially expressed gene (DEG) analysis

DEG analysis was performed with the R Bioconductor package DESeq2 (323), using the matrix of read counts as input. Results tables with log2 fold changes, p values and adjusted p values were generated using the function *results*. Differential gene expression analysis results were explored using the *plotMA* function. Count data was transformed for clustering visualization using heatmaps and principal component analysis (PCA).

2.15.3 Gene set enrichment analysis (GSEA)

Gene Set Enrichment Analysis (GSEA) was performed using the Broad Institute GSEA software (324). The log2FC values obtained after the DEG analysis were used as inputs for the GSEA. Normalized Enrichment Scores (NES) were calculated for each of 50 hallmark gene sets; each hallmark gene set being a specific well-characterized group of genes related to a biological process. A GSEA was also performed using the same input against a collection of 615 gene sets; each set contains a number of genes that share upstream cis-regulatory motifs which can function as potential transcription factor binding sites (325).

2.16 Protein-protein interaction screening by proximity-labelling

2.16.1 *In situ* proximal biotinylation

Overexpression of the retroviral vectors encoding the fusion caspase-1/caspase-4-biotin ligase (BirA) proteins, as well as the BirA control, was performed as detailed in section 2.3.1. Three days after the addition of 4-hydroxy-tamoxifen, biotin was added at a final concentration of 25 μM per each 100 mm diameter round / condition.

2.16.2 Biotin-affinity capture

22h after the addition of biotin, cells were collected as explained in section 2.2.1. Each pellet was lysed in 400 µL of Cell Lysis Buffer (to prepare 2.5 mL: 250 µL 10x Cell Lysis Buffer (Cell Signalling, 9803), 100 µL cOmplete EDTA-free Protease Inhibitor Cocktail (Roche, 04693159001) and 2150 dH20). Cells were incubated on ice for 20 min and centrifuged 15 min at 14000 rpm at 4 °C. Supernatants were transferred to new Eppendorf tubes. 50 µl magnetic Myone Streptavidin Dynabeads (Thermo Fisher, 65601) conjugated were added to approximately 350 µl lysate and samples were incubated overnight at 4 °C on a tube rotator. The following day samples were washed twice in ice-cold PBS and transferred to the IGMM Mass Spectrometry facilities.

2.16.3 Mass spectrometry

Sample preparation of mass spectrometry (MS) and MS were performed by the IGMM Mass Spectrometry facilities as explained next. Beads were incubated in 50 µL for 30 minutes at 27°C with 0.3 µg trypsin in 2M urea, 50mM tris pH8, and the resulting supernatant transferred to a fresh tube. Beads were washed in a further 50 µL of the same buffer with Dithiothreitol (DTT) added to 10 mM. The wash was combined with the initial supernatant and incubated overnight at 37°C in a wet chamber. Iodoacetamide was added to 55 mM and after 30 minutes incubation at room temperature the solution was acidified by adding 8 µL of 10 % Trifluoroacetic acid (TFA). 50 µL of the resulting peptide solution was loaded onto an activated (20 µL methanol), equilibrated (50 µL 0.1% TFA) C18 Stage tip, and washed with 50 µL 0.1% TFA. The bound peptides were eluted into a 96-well PCR plate (Axymat) with 40 µL 80% Acetonitrile (ACN) 0.1% TFA and concentrated to less than 8 µL in a vacuum concentrator. The final volume was adjusted to 15 uL with 0.1% TFA. Online LC was performed using a Dionex RSLC Nano (Thermo Scientific). Following the C18 clean-up, 5 µL peptides (~ a fifth of the beads input) were injected onto a home-pulled, home-packed C18 analytical column over a gradient of 2%-40% ACN in 40 minutes, with 0.1% TFA throughout. Eluting peptides were ionised at +2kV before data-dependent analysis on a Thermo Q-Exactive Plus (Thermo Scientific). First stage of MS (MS1) was acquired with mz range 300-2000 and resolution 70,000, and top 10 ions were selected for

fragmentation with normalised collision energy of 30, and an exclusion window of 30 seconds. Second stage of MS (MS2) were collected with resolution 17,500. The AGC targets for MS1 and MS2 were 3e6 and 1e5 respectively, and all spectra were acquired without lockmass and 1 microscan. Finally, the data were analysed using MaxQuant (version MaxQuant_1.5.7.0). The IGMM Mass Spectrometry facilities provided logFC values for each protein in each sample.

2.16.4 Data analysis

Frequent contaminants in experiments using streptavidin pull-down approaches in *Homo sapiens* were discarded using data sets available at the contaminant repository for affinity purification website (www.crapome.org). A logFC value > 2.0 was estabishled as threshold for hit selection. To analyse subcellular localisation, a protein ID list of caspase-1 and caspase-4 interactor hits was used as input and submitted to gene ontology – cellular compartment analysis using the DAVID Bioinformatics Resources 6.8 online tool. To identify all CARD-containing proteins, the IPR001315 CARD domain *Homo sapiens* list from the EMBL-EBI Interpro classification containing 35 unique proteins was used.

2.17 Statistical methods

Experimental data were analysed as described in figure legends. Continuous variables were described as means and standard error of the mean (s.e.m). Categorical variables were described as frequencies and percentages. Normality of the residuals of the mixed models were assessed. In case of normal distribution, differences among study groups or times of assessments of continuous variables were analysed through one-way ANOVA. For each continuous variable, the overall F test was first assessed for significance. If it was significant, two-sided comparisons between each group and control were performed. Each pair-wise comparison was corrected using Bonferroni test, in order to control for the experiment-wise error rate. All statistical analyses were performed using GraphPad Prism version (version 7.0 for Mac GraphPad Software, La Jolla, CA, USA). Schematic diagrams were generated using BioRender.com.

Chapter 3 - Caspase-4 is required for a complete SASP in OIS

3.1 RAS^{G12V}-OIS as a model to study senescence

3.1.1 Constitutive RAS^{G12V} overexpression drives OIS in IMR90 cells

To model OIS, the overexpression of H-RAS^{G12V} (RAS^{G12V} from hereon) in IMR90 cells has been used throughout this thesis. To induce OIS by constitutive overexpression of RAS^{G12V}, IMR90 cells were infected with retroviral viruses carrying either a control or a RAS^{G12V}-encoding construct, as detailed in section 2.3.1 (Figure 3.1).

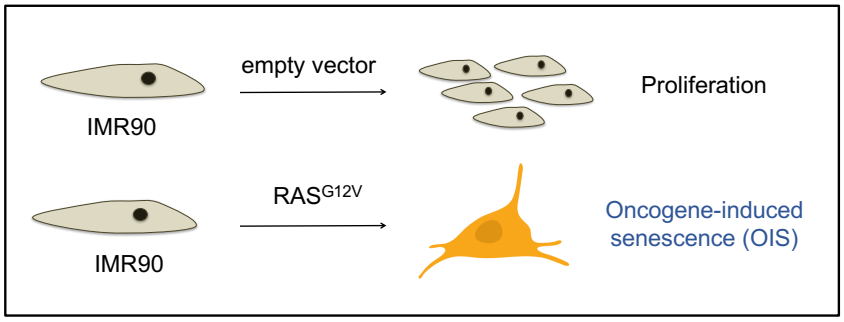

Figure 3.1 Constitutive overexpression of RAS^{G12V} model
Schematic representation of constitutively overexpressed RAS^{G12V}-driven OIS model in IMR90 cells.

Stably transfected cells were seeded at equal numbers prior to the assessment of senescence markers. RAS^{G12V}-overexpressing cells showed clear senescent features such as decreased BrdU incorporation or increased SA-β-galactosidase positive staining (Figure 3.2).

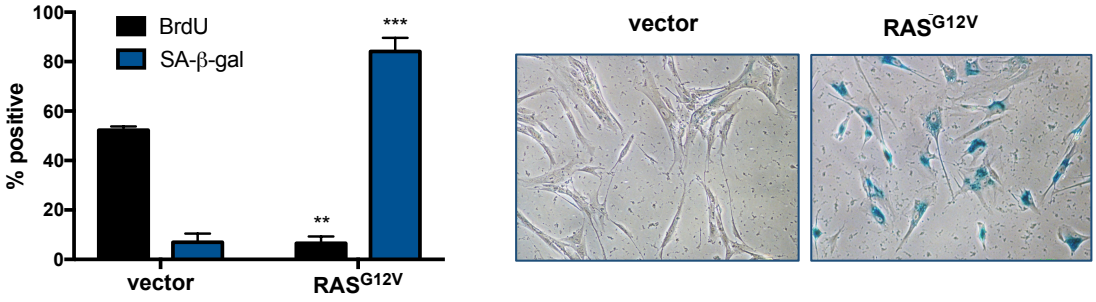

Figure 3.2 Constitutive overexpression of RAS^{G12V} drives OIS in IMR90 cells

Once IMR90 human fibroblasts infected with either the empty or the RAS^{G12V} overexpression vector were selected, cells were counted and equal numbers of cells were seeded. Quantification of BrdU incorporation and SA-β-galactosidase activity was performed four days after equal cell numbers were seeded. Representative pictures of the SA-β-galactosidase staining of one experiment are also shown. Data shown as mean ± s.e.m of n=3 experiments, paired t test, **=p<0.01, ***=p<0.001.

3.1.2 Inducible model of OIS in IMR90 cells: the ER:RAS system

To exert a tight control on the onset of senescence, an inducible system extensively used to generate conditional forms of transcription factors and protein kinases (326) was used. This system is based on the use of a construct consisting of a mutant form of the estrogen receptor (ER) ligand-binding domain fused to the protein of interest, RAS, in cis (327). If no synthetic ER ligand 4-hydroxytamoxifen (4OHT) is added, the fused protein of interest remains complexed to inhibitory proteins. In contrast, addition of 4-hydroxytamoxifen releases the fusion protein from the inhibitory proteins, allowing activation of the protein of interest (328). Using this system to generate an inducible OIS model, IMR90 human fibroblasts are stably modified to either express a control construct (the modified ER coupled to a stop codon, i.e. ER:STOP) or the ER fused to H-RAS^{G12V} (ER:RAS) (126, 320, 329). After addition of 4OHT, ER:RAS cells undergo OIS (Figure 3.3).

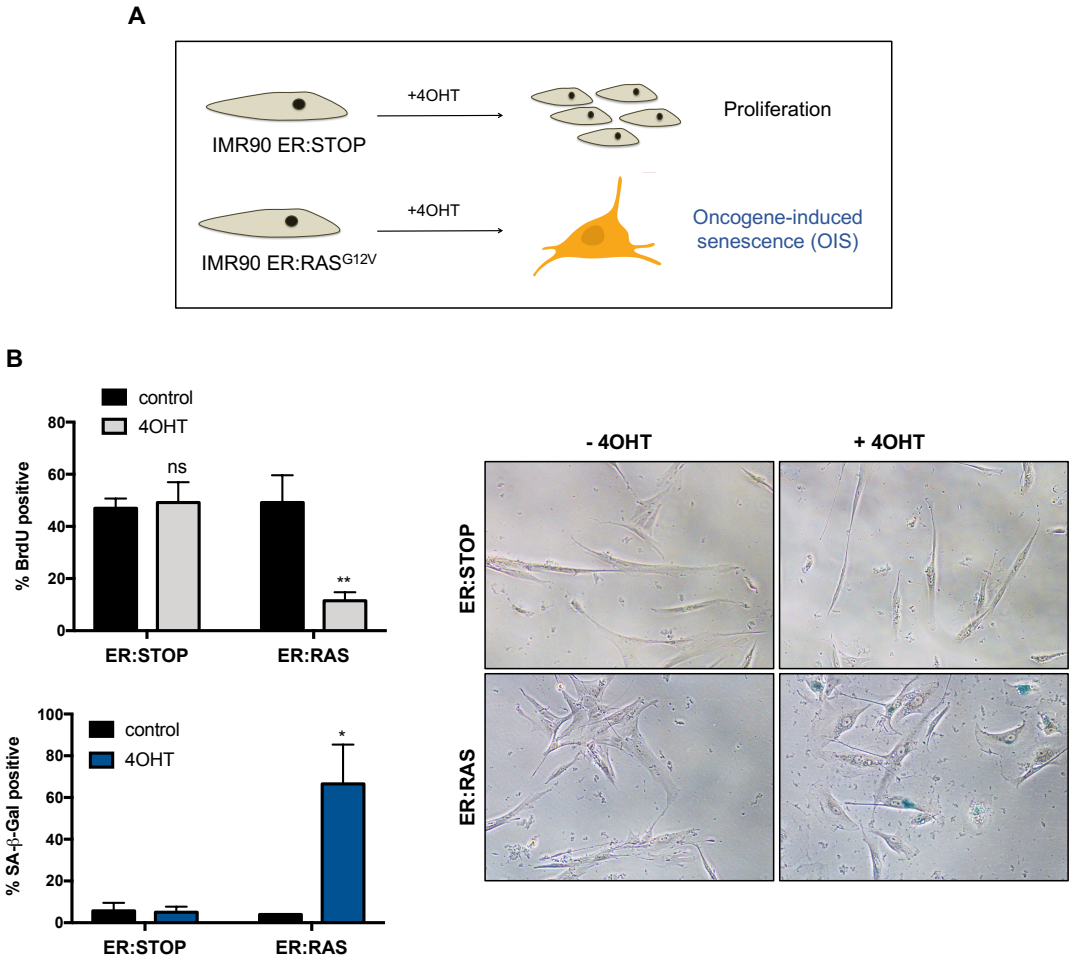

Figure 3.3 Inducible activation of RAS^{G12V} drives OIS in IMR90 cells

A. Schematic representation of the inducible ER:RAS OIS model in IMR90 cells. **B.** Equal amounts of cells were seeded; BrdU was quantified five days after the addition of 4OHT (*upper left*) and SA-β-galactosidase activity was quantified one week after the addition of 4OHT (*lower left*). Representative pictures of the SA-β-galactosidase staining are shown on the right.

Data shown as mean ± s.e.m of n=3 experiments, paired t test of each condition treated with 4-hydroxytamoxifen compared to its non-treated counterpart, *=p<0.05, **=p<0.01, ns = non-significant. 4OHT = 4-hydroxytamoxifen.

3.2 Caspase-4 expression is increased in OIS

A first approach towards investigating inflammatory caspases in senescence was conducted by studying the levels of caspase-1 and caspase-4 expression in RAS^{G12V}-driven OIS. Furthermore, the proteolytic activity of caspase-4 in OIS was also investigated using a fluorometric assay based on cleavage specificity. Finally, the oligomeric state of caspase-4 was interrogated.

3.2.1 Caspase-4 levels are increased in RAS^{G12V}-induced senescence

To induce OIS, RAS^{G12V} was constitutively overexpressed in IMR90 fibroblasts. Cells infected with either a control empty vector or the RAS^{G12V} construct were analysed by RT-qPCR and immunofluorescence to study the levels of endogenous inflammatory caspases. In contrast to CASP1, CASP4 transcription was increased in OIS (Figure 3.4) and, concomitantly, so was caspase-4 protein expression (Figure 3.5).

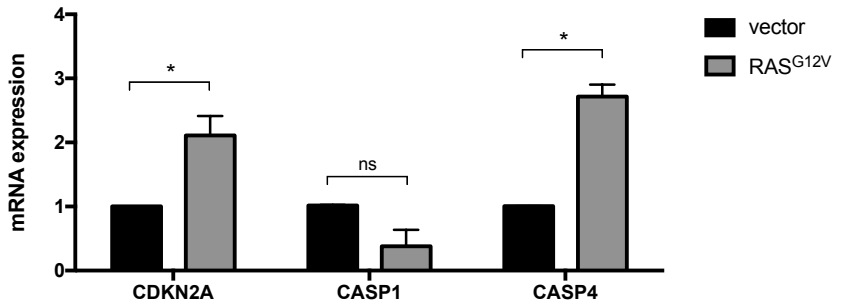

Figure 3.4 CASP4 mRNA expression but not CASP1 is increased in RAS^{G12V}-OIS
CDKN2A, CASP1 and CASP4 relative mRNA levels were quantified by RT-qPCR analysis after RNA extraction of control (empty vector) and RAS^{G12V} overexpressing IMR90 cells. Data shown as mean ± s.e.m of n=3 experiments, paired t test, *=$p<0.05$, ns = non-significant.

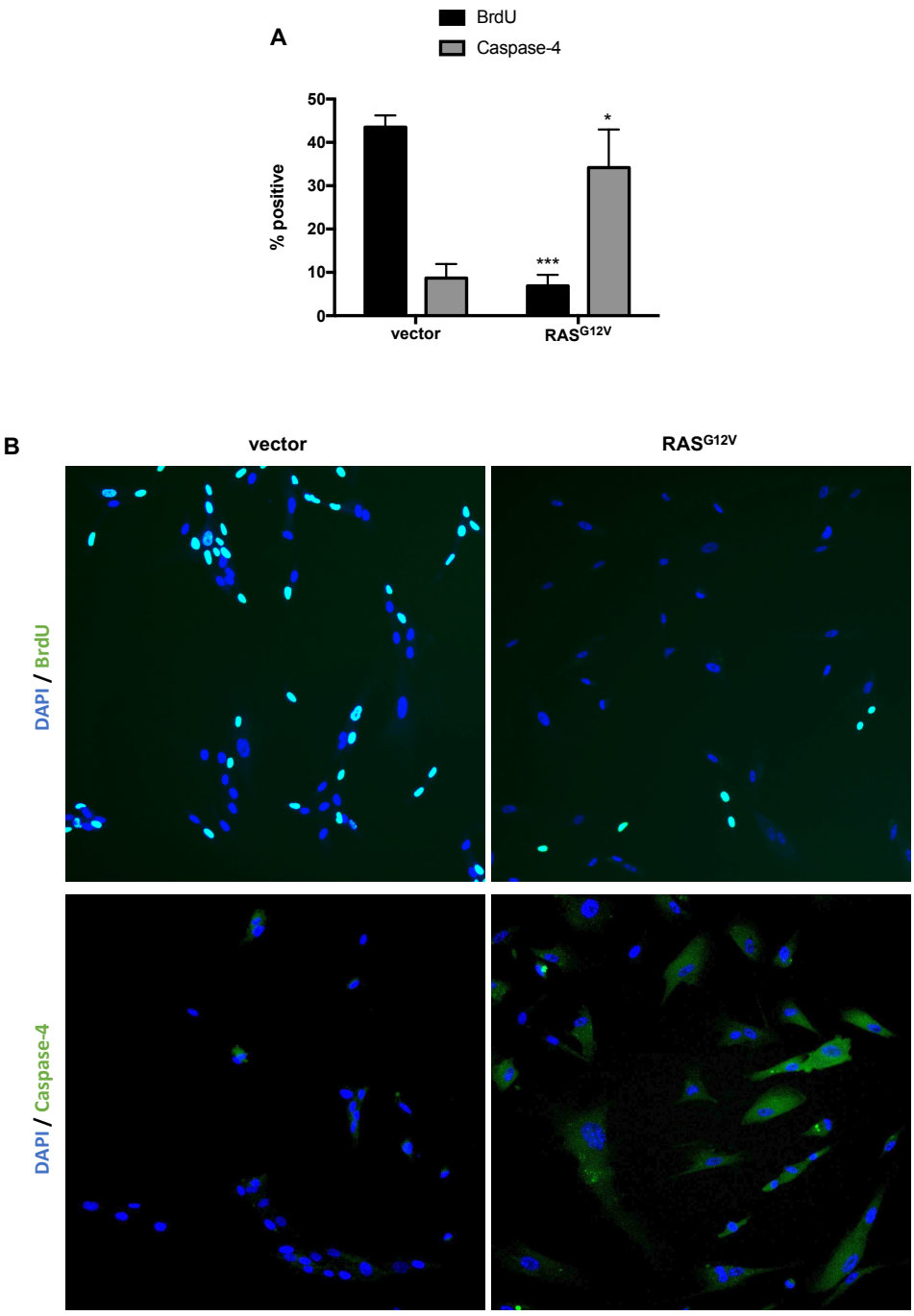

Figure 3.5 Caspase-4 protein levels are increased in RAS^{G12V}-OIS

A. Quantification of BrdU incorporation and endogenous caspase-4 protein in IMR90 cells overexpressing the empty vector control or RAS^{G12V} using high-content analysis. B. Representative images of IMR90 cells stained for caspase-4 (FITC) and DAPI used for the quantification. Data shown as mean ± s.e.m of n=4 experiments, paired t test, *=p<0.05, ***=p<0.01.

Next, CASP-1 and -4 expression was further analysed using the inducible RAS^{G12V} model. A time-course analysis of CASP1 and CASP4 mRNA expression every 48h until 8 days after the addition of 4-hydroxytamoxifen was performed. Interestingly, CASP4 but not CASP1 mRNA expression increased from the early stages after the induction of OIS, in parallel to the exponential increase of IL1B mRNA expression (Figure 3.6).

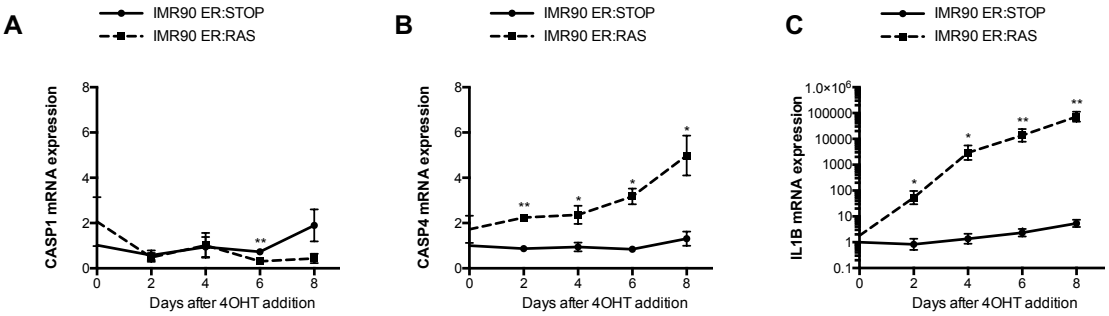

Figure 3.6 CASP4 expression increases over time in an inducible model of RAS^{G12V}-OIS
(A) CASP1, (B) CASP4 and (C) IL1B relative mRNA levels were quantified by RT-qPCR analysis after RNA extraction of ER:STOP and ER:RAS cells 0, 2, 4, 6 and 8 days after 4-hydroxytamoxifen addition.
All data shown as mean ± s.e.m of n=3 experiments, paired t test, *=p<0.05, **=p<0.01. 4OHT = 4-hydroxytamoxifen.

3.2.2 LEVD-AFC cleavage is increased in OIS

Over the last 20 years, the substrate specificity of caspases has been investigated using different biochemical *in vitro* assays of varying complexity. Although there is some controversy regarding these studies (see section *1.2.1.1 Classification and function of caspases*), researchers concluded that caspase-4 has preferential cleavage activity after the LEVD amino acid sequence. Consequently, specific probes have been designed for colorimetric and fluorometric detection of cleavage after the LEVD amino acid sequence. These probes are synthetic substrates containing the peptide sequence and a reporter. For instance, in a fluorometric assay, a fluorophore is used as a reporter

because its emitted fluorescence at a particular wavelength can be detected and quantified.

To examine caspase-4 activity in senescence, the LEVD-AFC fluorogenic substrate was used as a readout for caspase-4 proteolytic activity. In this assay, upon protease cleavage of the substrate (LEVD-AFC), the fluorophore (AFC) is released and its emission spectra shifts, namely LEVD-bound AFC emits blue light whereas free AFC emits yellow-green fluorescence.

LEVD-AFC cleavage was examined after 4 days of 4-hydroxytamoxifen in IMR90 ER:STOP/ER:RAS cells cultured in two different serum percentages of cell media, 0.5% and 10% (Figure 3.7). Fluorescence values were recorded every 10 minutes during the incubation of the cell lysates with the fluorogenic substrates. To avoid a confounding factor due to potential different autofluorescence in control and senescent cells, absolute values of fluorescence intensity were corrected by autofluorescence values (fluorescence of cell lysates without substrate). An increase in fluorescence intensity in senescent cells was observed independent of the serum conditions in which cells were grown. Moreover, LEVD-AFC cleavage analysis in a RAS^{G12V}-OIS time-course revealed that senescent cells display approximately twice cleavage activity than proliferating cells 4 and 8 after 4-hydroxytamoxifen addition. In all, these experiments show an increased LEVD-AFC cleavage activity in RAS^{G12V}-OIS.

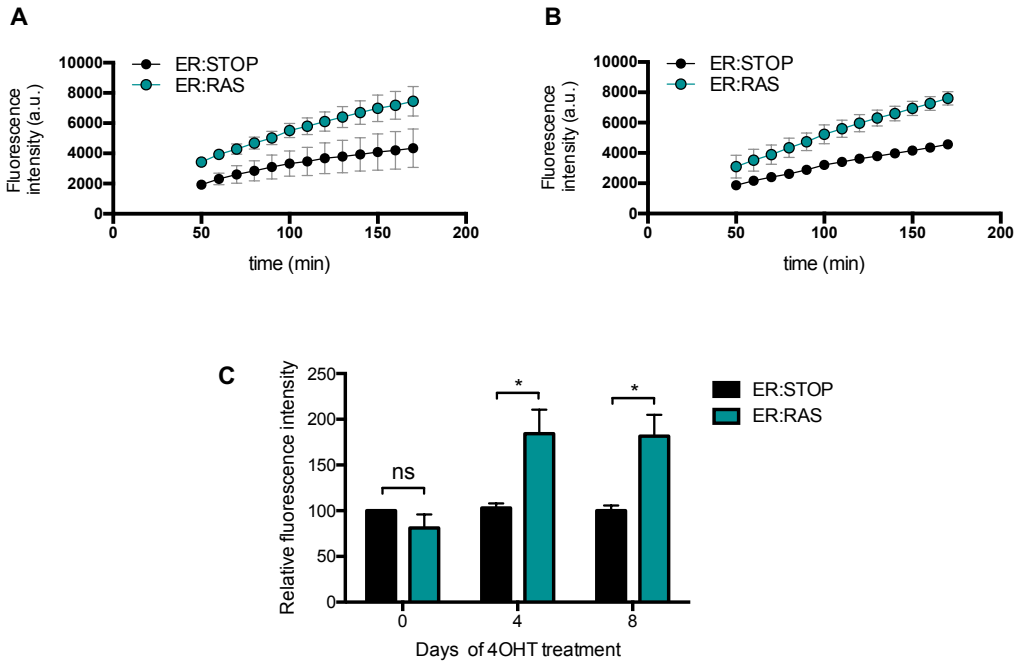

Figure 3.7 LEVD-AFC cleavage is increased in RAS^{G12V}-OIS

LEVD-AFC cleavage was measured in IMR90 ER:STOP/ER:RAS cells cultured either in (A) low-serum (0.5% FBS) or (B) normal serum (10% FBS) 4 days after 4-hydroxytamoxifen addition. Cell lysates were incubated with the fluorogenic substrate and fluorescence was measured every 10 minutes. C. LEVD-AFC cleavage was measured in low serum (0.5% FBS) in a time-course experiment 4 and 8 days after 4-hydroxytamoxifen addition. Fluorescence was measured after 100 min of incubation of the cell lysates with the fluorogenic substrate. To calculate relative fluorescence intensity values, all corrected absolute fluorescence intensity values were made relative to ER:STOP cells at 0 days of 4-hydroxytamoxifen addition.

All data shown as mean ± s.e.m of n=3 experiments, multiple t tests, *=p<0.05. 4OHT = 4-hydroxytamoxifen; a.u. = arbitrary units.

3.2.3 Caspase-4 activity is increased in OIS

Oligomerization of caspase-4 is essential for its activity (193). To further explore caspase-4 activation in senescence, an assay was performed to investigate whether caspase-4 is found in an oligomeric state in senescence. Disuccinimidyl suberate (DSS) was used to crosslink the samples previous to SDS-PAGE resolution. High molecular size bands appeared 3 days after 4-hydroxytamoxifen addition in senescent (ER:RAS) but not control (ER:STOP) samples (Figure 3.8).

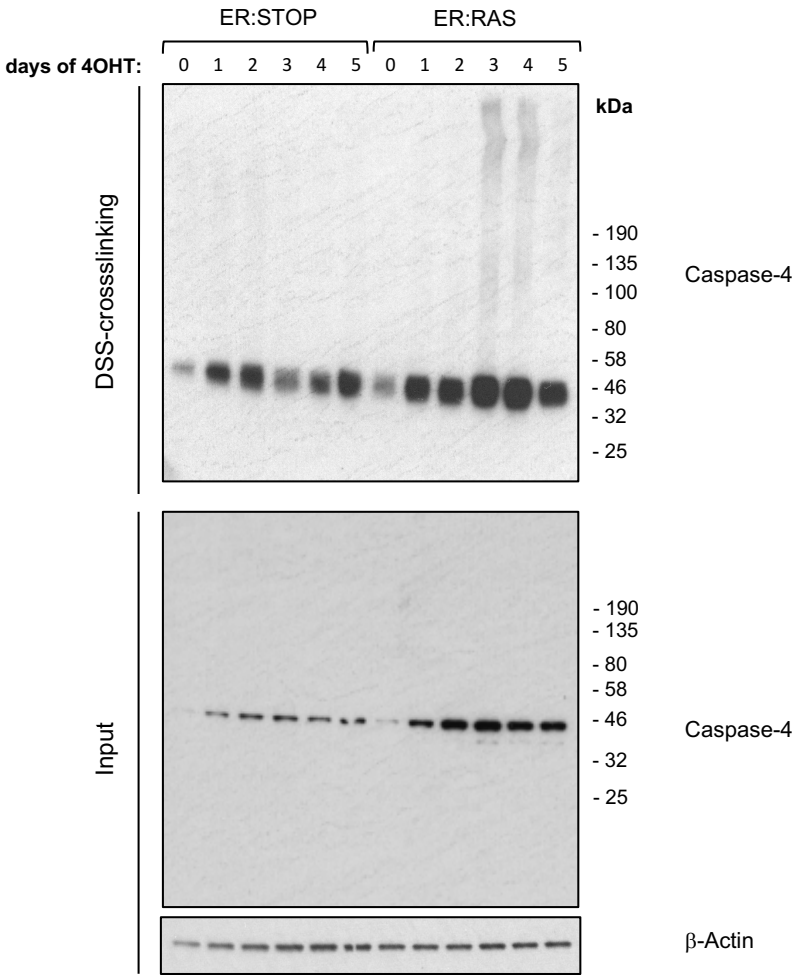

Figure 3.8 Caspase-4 oligomerizes during OIS

DSS-crosslinked samples were eluted in 2x loading buffer and loaded on a 10-20% gradient Tris-Glycine gel. After SDS-PAGE separation, both DSS-crosslinked samples and inputs (2.5%) were transferred to nitrocellulose membranes and probed for caspase-4 following regular western blot procedures. Blots belong to one representative experiment. DSS = disuccinimidyl suberate; 4OHT = 4-hydroxytamoxifen.

3.3 Transcriptomic analysis

To further investigate the potential role of caspase-4 in RAS^{G12V}-OIS, whether global changes in mRNA expression would occur upon caspase-4 depletion was interrogated. Data mining of the transcriptomic results was conducted through differentially expressed gene (DEG) analysis and gene set enrichment analysis (GSEA).

3.3.1 Experimental design and quality control

siRNA technology was used to knock-down the target gene (CASP4). First, a pilot experiment was conducted to explore the efficiency of the knock-down. Targeting CASP4 with a pool of four different siRNA sequences (siCASP4) significantly reduced CASP4 mRNA expression, thus validating the use of these reagents for further experiments (Figure 3.9).

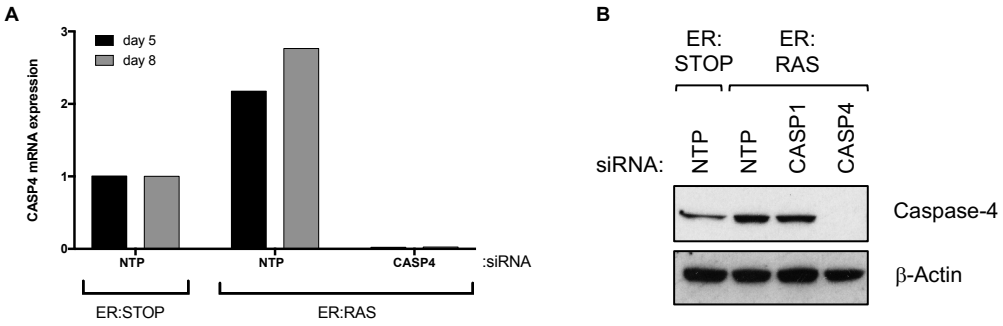

Figure 3.9 SiRNA-mediated targeting of CASP4 effectively reduces the levels of CASP4 mRNA

ER:STOP and ER:RAS cells were transfected 0, 3 and 5 days after 4-hydroxytamoxifen addition with a pool of 4 control siRNAs with no target (non-target pool, NTP) or targeting CASP4. A. CASP4 mRNA expression 5 and 8 days after 4-hydroxytamoxifen addition was quantified by RT-qPCR. B. Caspase-4 protein expression was analysed by western blotting 5 days after 4-hydroxytamoxifen addition.

Data belong to one representative experiment. 4OHT = 4-hydroxytamoxifen; NTP = non-targeting pool.

Next, a transcriptomics experiment was performed to assess the effect of CASP4 knock-down in OIS. ER:RAS cells were transfected with either a control non-targeting pool siRNA (siNTP) or a CASP4-targeting pool(siCASP4). ER:STOP cells were also transfected with siNTP and used as a proliferating control (Figure 3.10).

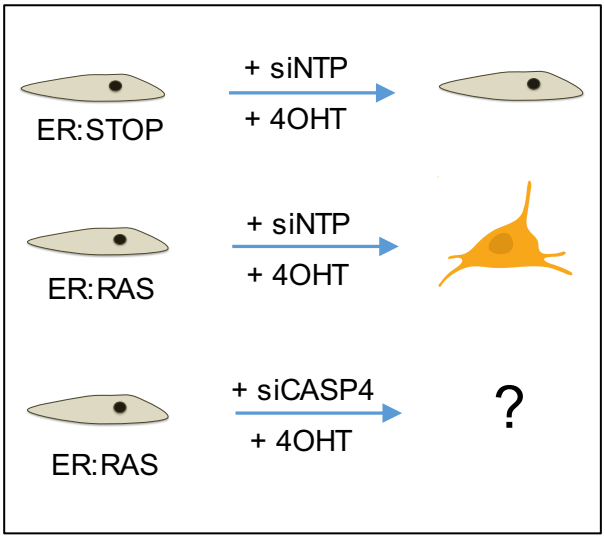

Figure 3.10 Experimental design for the combined approach of transcriptomic analysis following siRNA-mediated targeting of CASP4 in RAS^{G12V}-OIS

The diagram depicts the rationale and strategy supporting the transcriptomics experiment. 4OHT = 4-hydroxytamoxifen; NTP = non-targeting pool.

Because of the transient nature of siRNA, cells were transfected several times (day 0, 3 and 5 after 4-hydroxytamoxifen addition) to maintain the knockdown effect. RNA was extracted 5 and 8 days after 4-hydroxytamoxifen addition. Three biological replicates of this experiment were performed. RNA quality control (QC), library preparation and sequencing using Ampliseq transcriptome technology were conducted by the WTCRF facilities at the Western General Hospital. RNA QC results showed optimal RNA quality, with all samples having and RNA Integrity number (RIN) > 9.0. Each library generated more than 11 x 10^6 reads and 95% valid reads per sample (above the expected for this sequencing technology). The WTCRF facilities conducted raw data processing, generating gene counts per each sample (Figure 3.11).

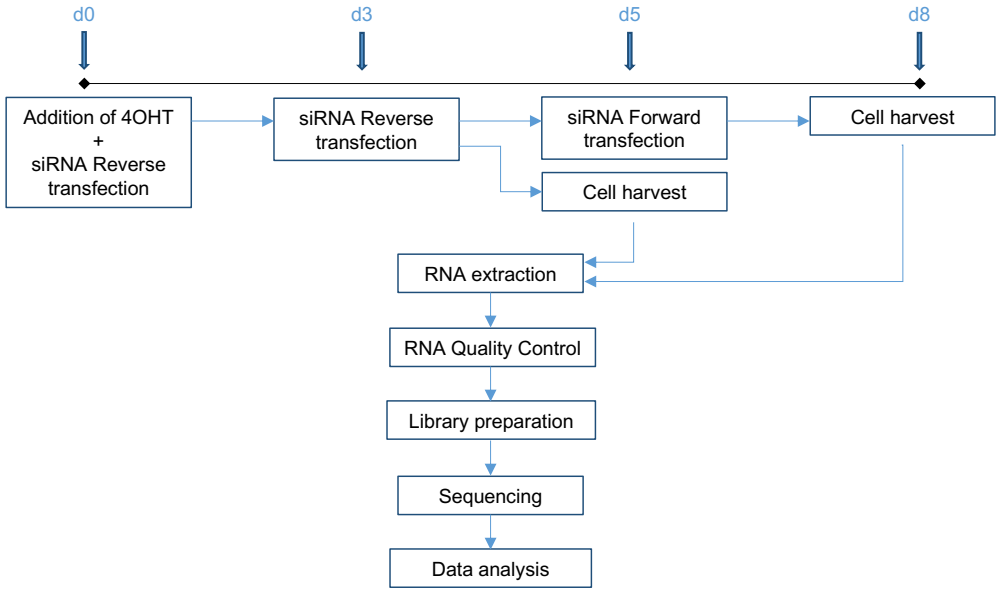

Figure 3.11 Schematic diagram of the experimental setup and sequencing pipeline
ER:STOP and ER:RAS cells were transfected with siRNA 0 and 3 days after 4-hydroxytamoxifen addition for day 5 cell harvest, or on day 0, 3 and 5 for day 8 cell harvest. Extracted RNA was submitted to Ampliseq sequencing. 4OHT = 4-hydroxytamoxifen.

3.3.2 DEG analysis: exploration of results

Differentially expressed gene (DEG) analysis was conducted using the DESeq2 package. Similarities between replicates and differential behaviour between conditions where confirmed by principal component analysis (PCA) visualization and heatmap sample clustering (Figure 3.12 and 3.13).

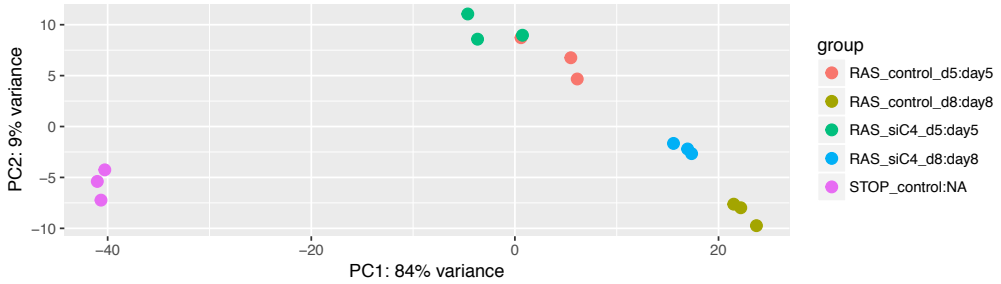

Figure 3.12 PCA visualization of DEG analysis results
PCA of variance stabilized transformed data using a parametric fit for the dispersion. Each dot corresponds to a sample replicate.

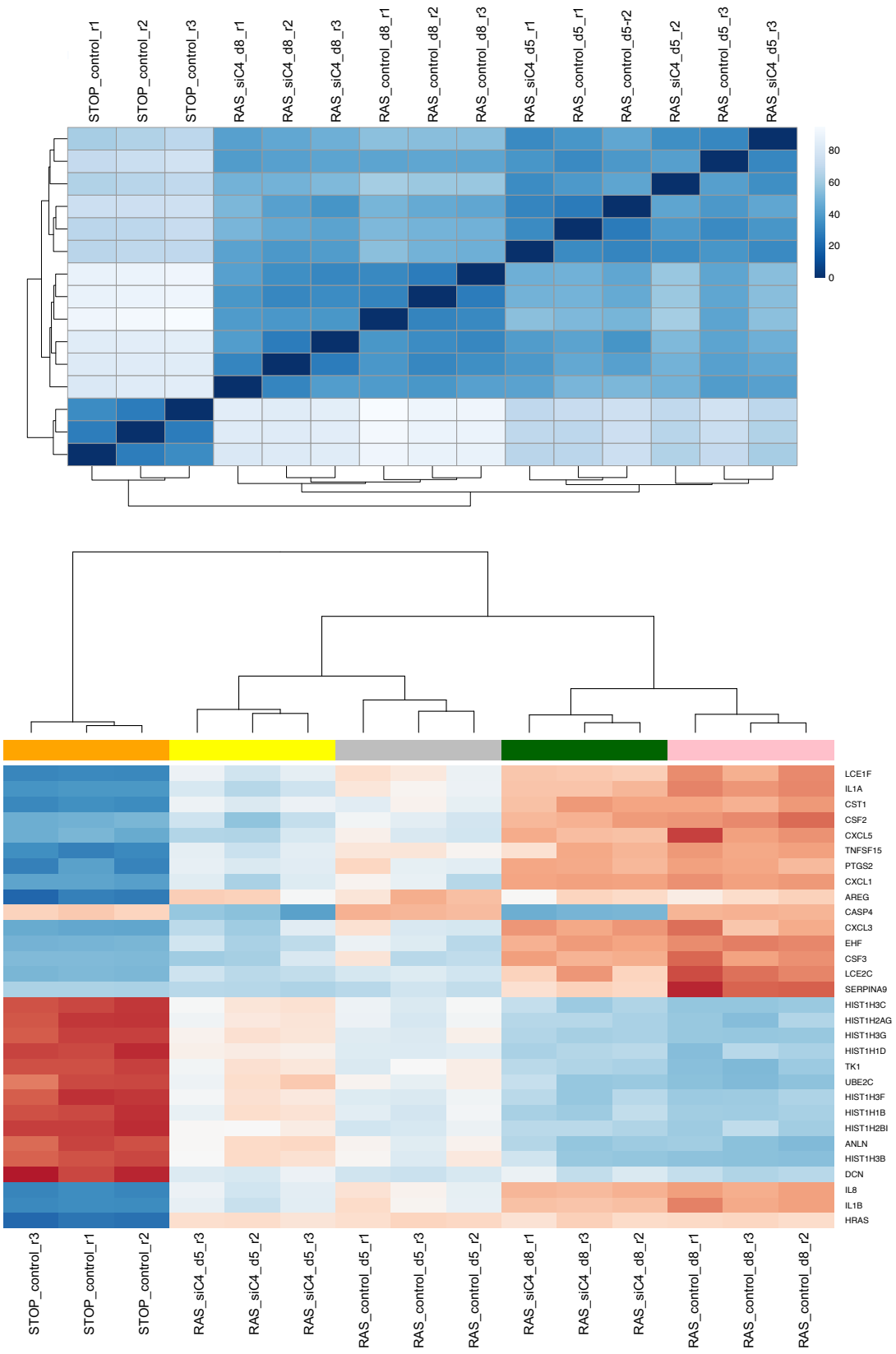

Figure 3.13 DEG analysis quality assessment by heatmaps and hierarchical clustering

(See previous page). *Top*: heatmap and hierarchical clustering of the sample-to-sample distances. *Bottom*: heatmap of the 30 genes with highest variance across all samples based on the total transformed data. Control = transfected with non-targeting siRNA; siC4 = transfected with CASP4-targeting siRNA; r1 = replicate 1; r2 = replicate 2; r3 = replicate 3.

The DEG analysis identified 557 and 478 genes significantly differentially expressed (p-adjusted <0.01) upon CASP4 targeting 5 and 8 days after 4-hydroxytamoxifen addition, respectively (Figure 3.14).

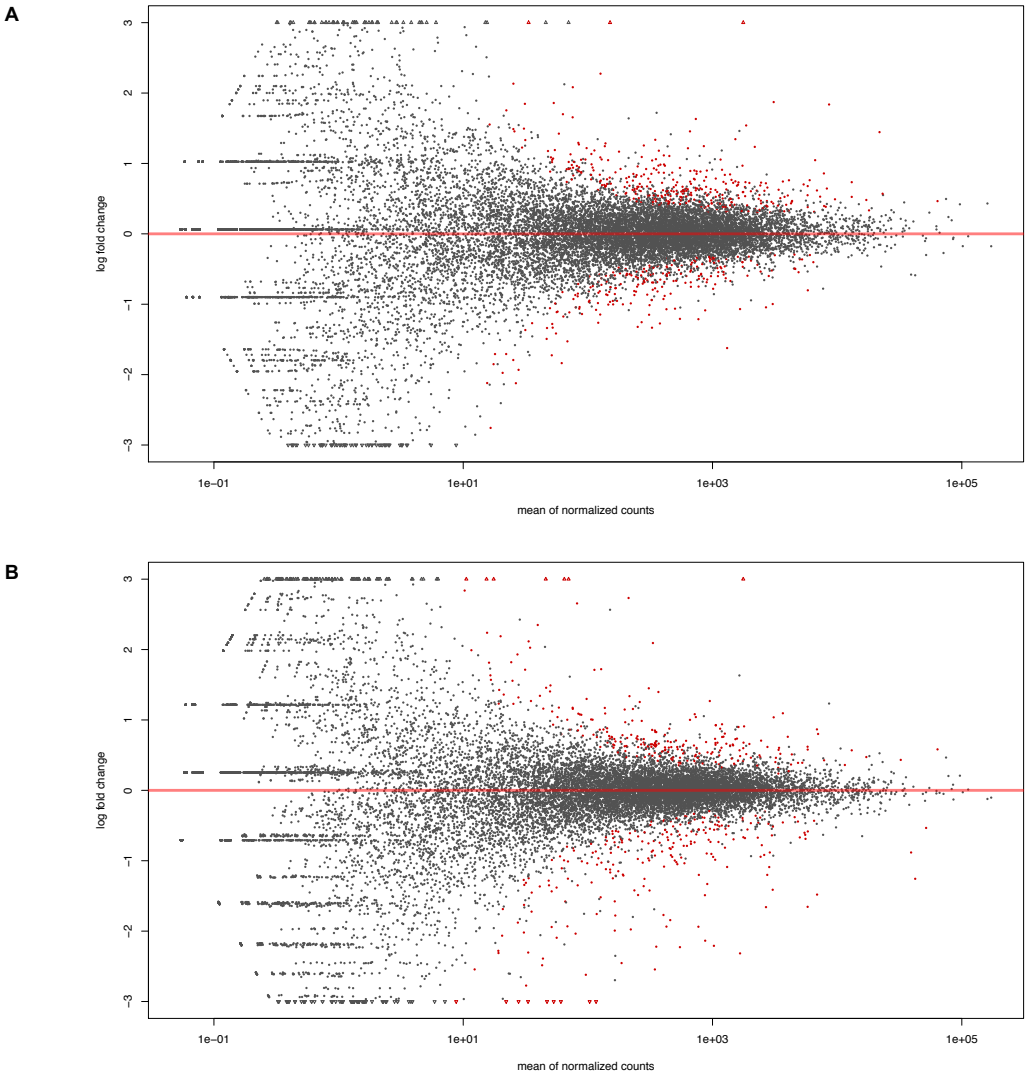

Figure 3.14 DEG analysis after CASP4-targeting in ER:RAS

Log_2 fold expression changes over the mean of normalized gene counts of CASP4-knockdown ER:RAS samples compared to control ER:RAS samples after 5 days (A) or 8 days (B) of 4-hydroxytamoxifen treatment. Each point represents a gene, which appears red-coloured when its adjusted *p* value is less than 0.01. Points which fall out of the window are plotted as triangles.

The top downregulated gene at day 5 and day 8 was CASP4, validating an efficient siRNA knockdown (Table 3.1).

Day 5		Day 8	
Gene	**p-adj**	**Gene**	**p-adj**
CASP4	2.84E-126	CASP4	7.03E-144
GREM1	1.55E-12	CNN1	9.23E-19
LARP1	6.66E-08	ACTG2	1.29E-18
IL1A	1.31E-07	SERPINA9	2.61E-18
VASN	6.34E-07	ANO4	1.14E-14

Table 3.1 Top differentially expressed genes upon CASP4 targeting
List of the top five differentially expressed genes upon between CASP4-knockdown ER:RAS and control ER:RAS five and eight days after 4-hydroxytamoxifen. p-adj = adjusted p-value.

3.3.3 Gene Set Enrichment Analysis (GSEA)

Next, a GSEA was performed and the Normalized Enriched Scores (NES), p-values and False Discovery Rate (FDR) q-values of different gene sets were examined. These statistics are defined as (324):

- NES: the enrichment score for the gene set after it has been normalized across analysed genes sets
- p-value: the statistical significance of the enrichment score
- FDR q-value: the estimated probability that the normalized enrichment score represents a positive finding

Importantly, whereas the FDR q-value is adjusted for gene size and multiple hypotheses testing, the p-value is not. Therefore, if a gene set has a small p-value but a high FDR q-value, it generally means that it is not as significant when compared with other gene sets in an empirical null distribution.

NES obtained through GSEA of 50 hallmark gene sets showed a positive regulation of CASP4 in RAS^{G12V}-OIS of gene signatures related to inflammatory processes, including TNF-α signalling and interferon responses both 5 and 8 days after the addition of 4-hydroxytamoxifen (Table 3.2).

Gene set:	Day 5			Day 8		
	NES	p-value	FDR q-val	NES	p-value	FDR q-val
TNFA SIGNALING VIA NFKB	1.845	<0.001	0.001	1.571	<0.001	0.054
INTERFERON GAMMA RESPONSE	1.574	<0.001	0.046	0.973	0.480	0.683
UV RESPONSE UP	1.439	0.004	0.132	1.041	0.354	0.562
APOPTOSIS	1.407	0.013	0.136	1.520	<0.001	0.055
CHOLESTEROL HOMEOSTASIS	1.354	0.029	0.188	0.985	0.467	0.709
INFLAMMATORY RESPONSE	1.336	0.023	0.184	1.607	<0.001	0.069
P53 PATHWAY	1.307	0.015	0.212	0.983	0.558	0.681
COMPLEMENT	1.300	0.022	0.198	1.250	0.077	0.312
PI3K AKT MTOR SIGNALING	1.268	0.074	0.234	-0.955	0.554	1.000
REACTIVE OXIGEN SPECIES PATHWAY	1.234	0.136	0.276	1.019	0.400	0.608
ESTROGEN RESPONSE LATE	1.231	0.040	0.259	-1.197	0.093	0.521
INTERFERON ALPHA RESPONSE	1.214	0.135	0.273	1.065	0.327	0.543
FATTY ACID METABOLISM	1.195	0.107	0.294	-0.787	0.949	1.000
IL6 JAK STAT3 SIGNALING	1.180	0.164	0.309	1.238	0.094	0.267
KRAS SIGNALING UP	1.173	0.125	0.305	-1.037	0.378	0.866
XENOBIOTIC METABOLISM	1.161	0.128	0.311	1.113	0.190	0.449
OXIDATIVE PHOSPHORYLATION	1.108	0.175	0.421	0.530	1.000	0.999
COAGULATION	1.086	0.245	0.467	1.103	0.247	0.452
HYPOXIA	1.080	0.262	0.458	1.044	0.329	0.583
NOTCH SIGNALING	1.074	0.334	0.455	1.178	0.212	0.390
ESTROGEN RESPONSE EARLY	0.950	0.571	0.875	-1.099	0.249	0.883
MTORC1 SIGNALING	0.886	0.809	1.000	-0.559	1.000	1.000
HEME METABOLISM	0.883	0.829	1.000	1.177	0.090	0.357
GLYCOLYSIS	0.863	0.860	1.000	0.744	0.998	1.000
APICAL SURFACE	0.854	0.727	1.000	0.933	0.568	0.796
ADIPOGENESIS	0.793	0.975	1.000	-0.596	1.000	1.000
TGF BETA SIGNALING	0.786	0.850	1.000	0.720	0.933	1.000
UNFOLDED PROTEIN RESPONSE	0.776	0.952	1.000	0.642	1.000	1.000
DNA REPAIR	0.722	0.998	1.000	0.823	0.913	1.000
MYC TARGETS V2	0.686	0.970	1.000	-0.631	0.992	1.000
ANDROGEN RESPONSE	0.665	0.998	1.000	1.122	0.223	0.453
MYC TARGETS V1	0.419	1.000	1.000	-0.326	1.000	1.000
UV RESPONSE DN	-0.725	0.992	0.978	-0.797	0.930	1.000
WNT BETA CATENIN SIGNALING	-0.739	0.916	1.000	1.144	0.254	0.419
PROTEIN SECRETION	-0.789	0.930	1.000	-0.859	0.772	1.000
ANGIOGENESIS	-0.869	0.688	0.948	-1.222	0.167	0.709
PEROXISOME	-0.883	0.722	0.975	-0.772	0.923	1.000
IL2 STAT5 SIGNALING	-0.957	0.586	0.768	1.257	0.060	0.341
PANCREAS BETA CELLS	-1.022	0.428	0.590	1.435	0.061	0.097
ALLOGRAFT REJECTION	-1.034	0.340	0.599	1.328	0.027	0.217
APICAL JUNCTION	-1.036	0.352	0.652	-0.863	0.816	1.000
MITOTIC SPINDLE	-1.074	0.270	0.577	-1.214	0.089	0.567
BILE ACID METABOLISM	-1.094	0.262	0.566	0.736	0.948	1.000
MYOGENESIS	-1.118	0.193	0.555	-0.847	0.863	1.000
KRAS SIGNALING	-1.135	0.172	0.577	1.247	0.039	0.280
EPITHELIAL MESENCHYMAL TRANSITION	-1.139	0.139	0.674	-0.873	0.811	1.000
SPERMATOGENESIS	-1.166	0.180	0.694	-1.052	0.359	0.892
HEDGEHOG SIGNALING	-1.303	0.114	0.298	-1.075	0.345	0.884
E2F TARGETS	-1.513	0.002	0.050	-1.701	<0.001	0.010
G2M CHECKPOINT	-1.534	<0.001	0.076	-1.460	<0.001	0.105

Table 3.2 GSEA identifies pathways regulated by CASP4 in RAS^{G12V}-OIS

Normalized Enriched Scores (NES) of curated hallmark gene signatures were calculated based on the DEG analysis performed between control ER:RAS and CASP4-knockdown ER:RAS samples after 5 days or 8 days of 4-hydroxytamoxifen treatment. Gene sets with positive NES are positively regulated by CASP4 whereas gene sets with negative NES are negatively regulated by CASP4. FDR q-val = false discovery rate q-value.

Moreover, analysis of the enrichment of specific transcription factor target signatures suggests that CASP4 positively regulates the expression of NF-kB target genes (Table 3.3).

Gene set	NES	p-value	FDR q-val
EVI1_06	1.540	0.032	0.707
AP2REP_01	1.432	0.002	1.000
GGGNNTTTCC_NFKB_Q6_01	1.418	0.013	0.967
TAAWWATAG_RSRFC4_Q2	1.388	0.002	0.999
MEF2_01	1.365	0.021	1.000
NFKAPPAB_01	1.360	0.006	0.888
NFKAPPAB65_01	1.280	0.024	1.000
LEF1_Q6	1.277	0.031	1.000
GATA1_04	1.270	0.035	1.000
NFKB_Q6_01	1.240	0.048	1.000
AML_Q6	1.234	0.049	1.000
HNF1_01	-1.253	0.049	1.000
MEIS1BHOXA9_01	-1.335	0.033	1.000
E2F_01	-1.361	0.043	1.000
KRCTCNNNNMANAGC_UNKNOWN	-1.567	0.004	0.451

Table 3.3 GSEA identifies specific transcription factor target signatures regulated by CASP4 in RAS^{G12V}-OIS

Normalized Enriched Scores (NES) of transcription factor target signatures were calculated based on the DEG analysis performed between control ER:RAS and CASP4-knockdown ER:RAS samples after 5 days of 4-hydroxytamoxifen treatment. Gene sets with positive NES are positively regulated by CASP4 whereas gene sets with negative NES are negatively regulated by CASP4. For simplicity, this table only shows gene signatures with p-value <0.05. FDR q-val = false discovery rate q-value.

A deeper exploration of the gene signature hallmark "INFLAMMATORY RESPONSE", that showed both a small p-value and FDR q-value, (Table 3.2), was performed by plotting a heatmap of the log_2FC values of control ER:STOP and CASP4-knockdown ER:RAS vs control ER:RAS of all genes included in this gene set (Figure 3.15). This analysis revealed a pattern by which the increased expression of inflammatory-related genes in senescence is abrogated if CASP4 is targeted, including SASP factors. Although transcriptomic data will be again gathered and discussed in subsequent chapters, the following subheadings of this chapter focus on the validation of the role of CASP4 in regulating the positive expression of inflammatory genes in OIS, including SASP factors.

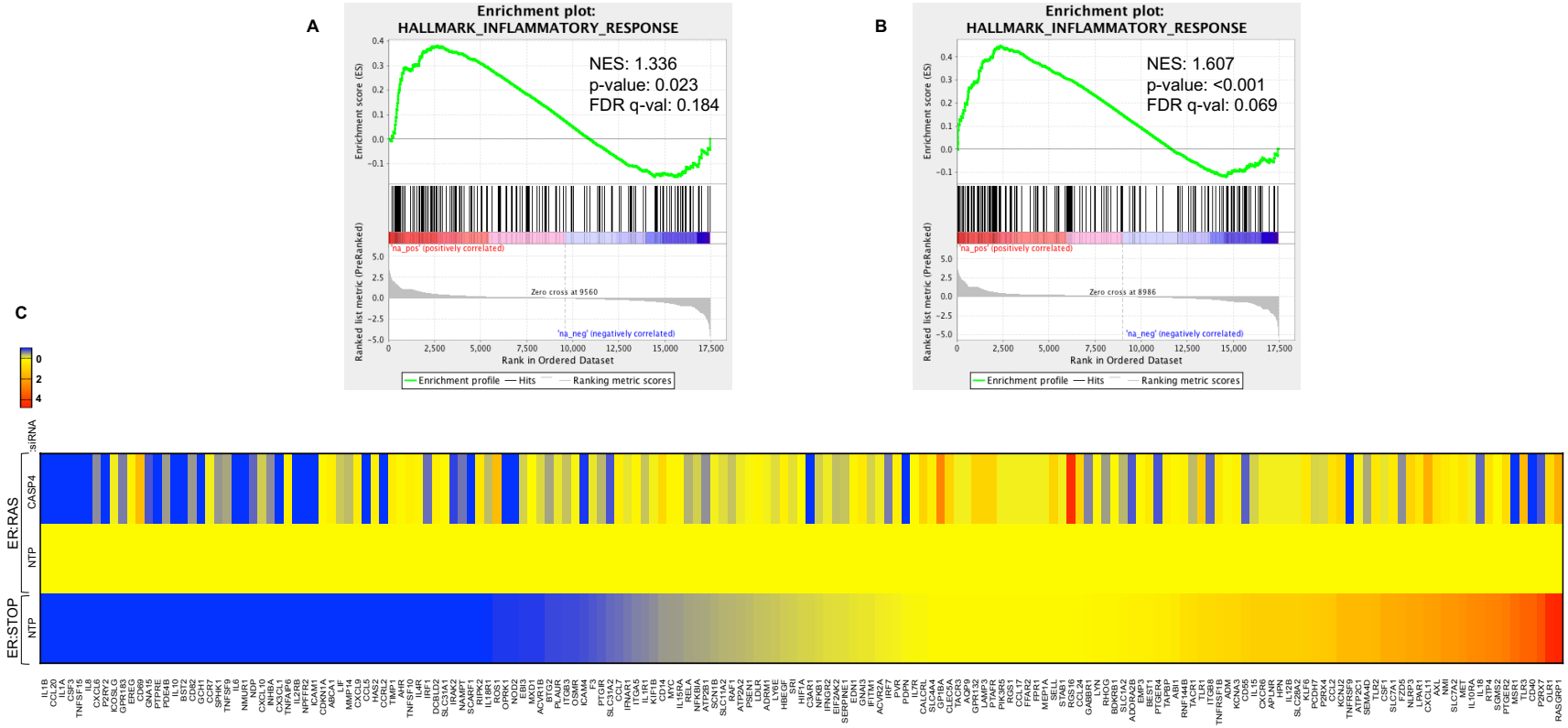

Figure 3.15 Gene expression of SASP factors is regulated by CASP4 in RAS^{G12V}-OIS

Enrichment plot of the signature "INFLAMMATORY RESPONSE" upon CASP4 silencing in RAS^{G12V} –OIS 5 (A) and 8 days (B) after 4-hydroxytamoxifen addition. Each vertical black line below the enrichment plot corresponds to one specific gene, and its position –left to right- depends on whether its expression increases or decreases upon CASP4 targeting. C. Heatmap of the log_2FC values of all genes included in the "INFLAMMATORY RESPONSE" GSEA gene set of control ER:STOP and CASP4–targeted ER:RAS compared to control ER:RAS after 5 days of 4-hydroxytamoxifen addition. A log_2FC values colour legend has also been plotted. FDR q-val = false discovery rate q-value; NTP = non-targeting pool.

3.4 IL-1 signalling is impacted by caspase-4 targeting

Analysis of transcriptomic data had revealed a role for CASP4 in regulating an inflammatory signature in OIS that included SASP factors. Next, mRNA expression changes were validated by RT-qPCR and the effect of CASP4 on IL-1 signalling was further investigated.

3.4.1 Caspase-4 regulates the SASP

Gene expression analysis by RT-qPCR confirmed the on-target effect of 2 individual CASP4-knockdown siRNA sequences (siCASP4-1 and siCASP4-2) and a pool of 4 different CASP4-targeting sequences (siCASP4-p) (Figure 3.16A). CASP4 targeting did not affect CASP1 mRNA levels (Figure 3.16B).

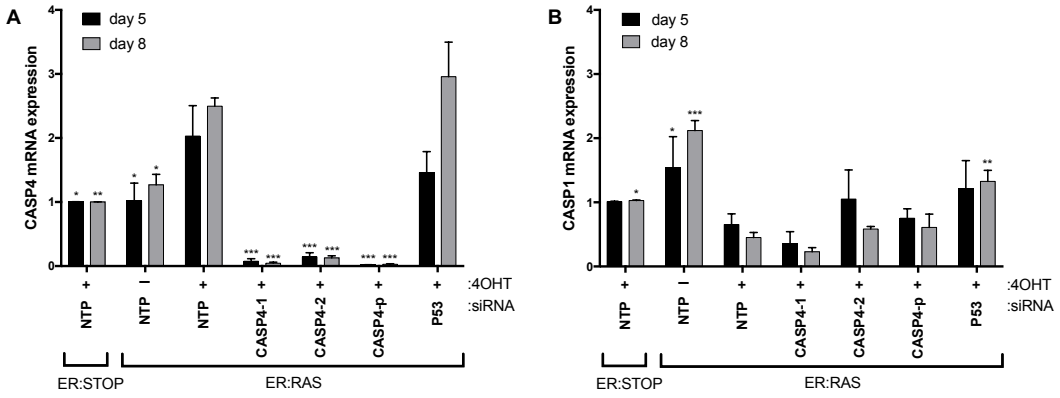

Figure 3.16 CASP1 and CASP4 mRNA expression after CASP4 siRNA-mediated targeting
IMR90 ER:STOP/ER:RAS cells were transfected with control (NTP), CASP4-targeting or p53-targeting siRNA. CASP4 was targeted by two individual siRNAs (CASP4-1 and CASP4-2) and a pool of four different siRNA sequences (CASP4-p). Senescence was induced by addition of 4-hydroxytamoxifen. CASP1 (A) and CASP4 (B) mRNA expression was measured 5 and 8 days after the induction of senescence by RT-qPCR.
All data shown as mean ± s.e.m of n=3 experiments, one-way ANOVA and post-hoc Bonferroni´s multiple comparisons comparing all conditions to ER:RAS +4OHT NTP, *=p<0.05, **=p<0.01, ***=p<0.001, where unstated non-significant. 4OHT = 4-hydroxytamoxifen; NTP = non-targeting pool.

CASP4 knockdown in RAS^{G12V}-OIS resulted in reduced mRNA expression levels of SASP factors, such as IL1A, IL1B, IL8, IL6, SAA1 and SAA2 (330), compared to control senescence cells, in consonance with the transcriptomic data analysis (Figure 3.17). High-content analysis following immunofluorescence staining further confirmed that, upon CASP4 knockdown, the intracellular protein levels of IL1-α, IL-1β, IL-6 and IL-8 are decreased compared to those in control senescent cells (Figure 3.18).

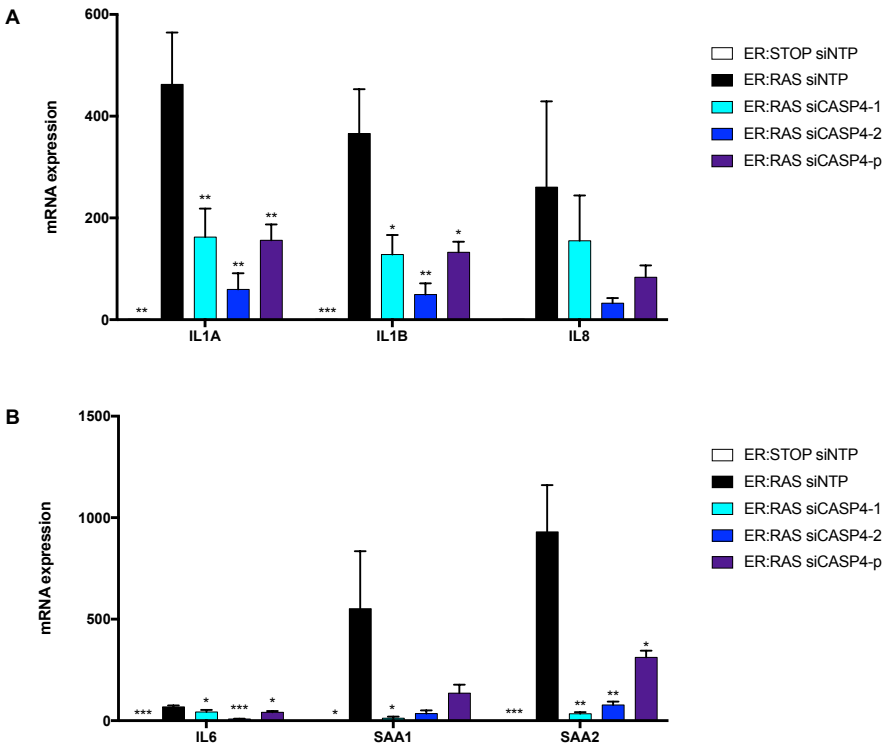

Figure 3.17 mRNA expression of SASP factors is regulated by CASP4

IMR90 ER:STOP/ER:RAS cells were transfected with control (NTP) or CASP4-targeting. CASP4 was targeted by two individual siRNAs (CASP4-1 and CASP4-2) and a pool of four different siRNA sequences (CASP4-p). Senescence was induced by addition of 4-hydroxytamoxifen. All samples were treated with 4-hydroxytamoxifen. A. IL1A, IL1B and IL8 mRNA expression was measured 5 days after the induction of senescence by RT-qPCR. B. IL6, SAA1 and SAA2 mRNA expression was measured 8 days after the induction of senescence by RT-qPCR.

All data are shown as mean ± s.e.m of n=3 experiments, one-way ANOVA and post-hoc Bonferroni´s multiple comparisons comparing all conditions to ER:RAS siNTP, *=p<0.05, **=p<0.01, ***=p<0.001, where unstated non-significant.

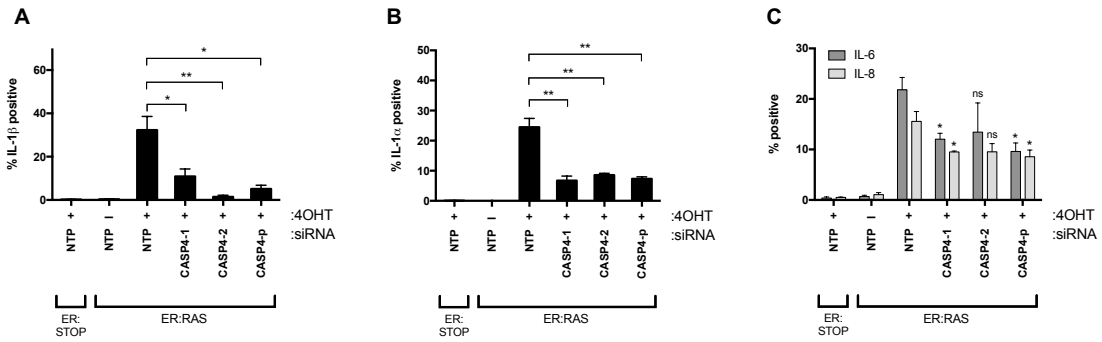

Figure 3.18 Immunofluorescence detection of IL-1α, IL-1β, IL-6 and IL-8 confirms requirement of CASP1 and CASP4 for a full SASP activation in OIS

IMR90 ER:STOP/ ER:RAS cells were transfected with control (NTP) siRNA or CASP4-targeting siRNA (either two individual sequences (siCASP4-1/siCASP4-2) or a pool of four different sequences (siCASP4-p). Cells were fixed 8 days after 4-hydroxytamoxifen addition and quantification of (A) IL-1α, (B) IL-1β and (C) IL-8 and IL-6 was performed using high-content analysis.

All data are shown as mean ± s.e.m of n=3 experiments, t tests were performed comparing each CASP4-knockdown ER:RAS sample to the respective control senescent sample, *=p<0.05, **=p<0.01, ns=non-significant. NTP = non-targeting pool; 4OHT = 4-hydroxytamoxifen.

Figure 3.19 Immunofluorescence detection of IL-1α, IL-1β, IL-6 and IL-8 confirms requirement of CASP1 and CASP4 for a full SASP activation in OIS

See following page. IMR90 ER:STOP/ ER:RAS cells were transfected with control (NTP), CASP4-targeting or CASP1-targeting siRNA. All samples were treated with 4-hydroxytamoxifen. IL-1α, IL-1β, IL-6 and IL-8 were quantified by high-content analysis 8 days after 4-hydroxytamoxifen addition. Representative images of the immunofluorescence staining are shown on the left side of each graph (*top*: IL-1α: FITC; *middle*: IL-1β: FITC, *bottom*: co-staining IL-6 and IL-8, TxRed and FITC respectively).

All data are shown as mean ± s.e.m of n=3 experiments, t tests were performed comparing each CASP1- or CASP4-knockdown ER:RAS sample to the respective control senescent sample, *=p<0.05, **=p<0.01, ***=p<0.001, ns=non-significant. NTP = non-targeting pool.

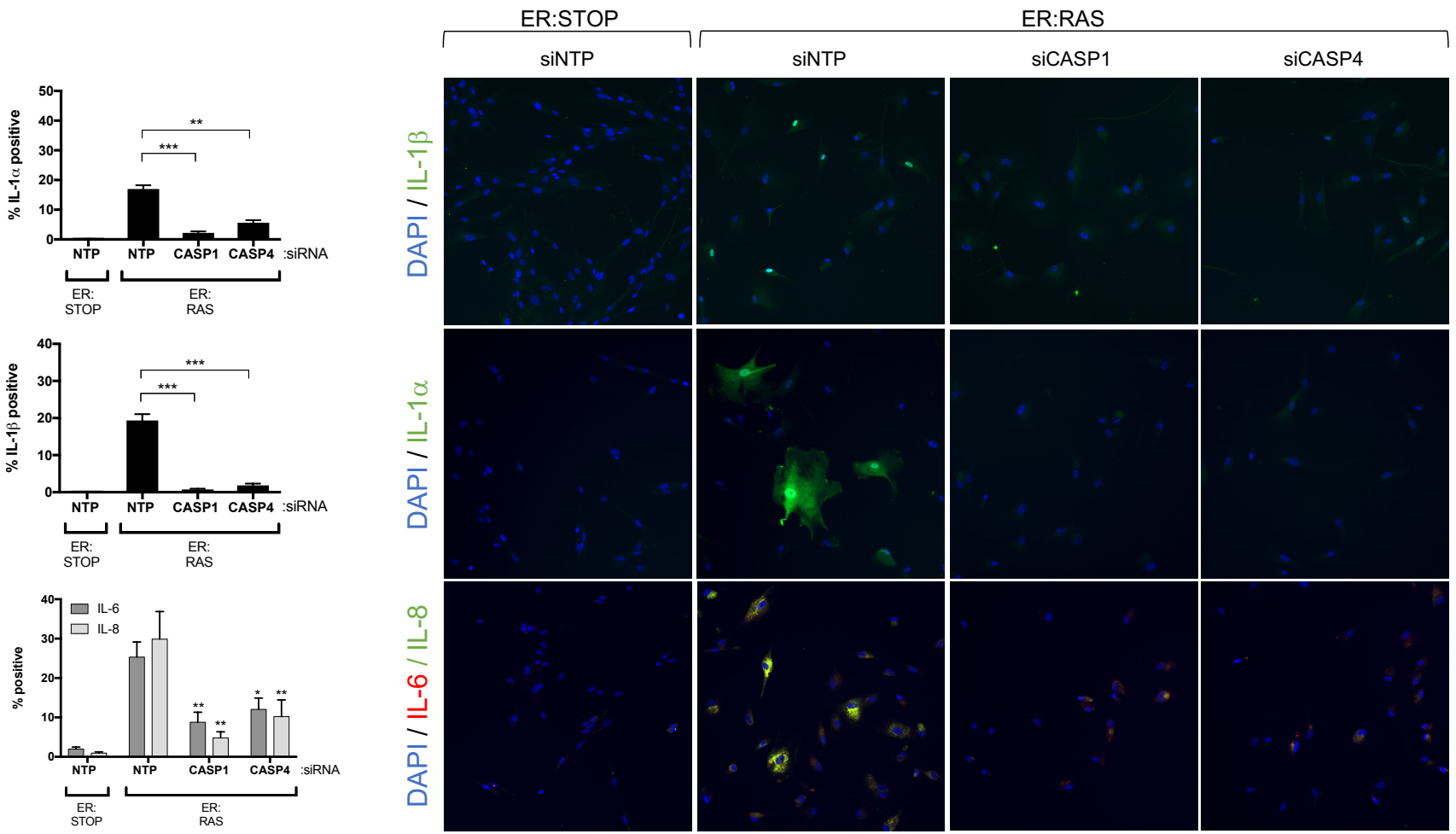
ER:STOP
ER:RAS
siNTP
siNTP
siCASP1
siCASP4
DAPI / IL-1β
DAPI / IL-1α
DAPI / IL-6 / IL-8
% IL-1α positive
% IL-1β positive
% positive
IL-6
IL-8
NTP
NTP
CASP1
CASP4
:siRNA
ER: STOP
ER: RAS

3.4.2 Mature IL-1β levels in RAS^{G12V}-OIS are impaired upon caspase-4 targeting

Because IL-1 signalling is a key component of the SASP and caspase-4 has been reported to modulate caspase-1 activity in other contexts (175), the role of caspase-4 in IL-1 signalling in OIS was further explored. Analysis of IL-1β expression by western blotting allows the detection of both the full-length (31 kDa) and the mature active fragment (17 KDa) which results from caspase-1 cleavage. CASP1 or CASP4 knockdown in RAS^{G12V}-OIS resulted in decreased levels of full-length IL-1β (proIL-1β) and a reduction to a similar extent of the amount of mature IL-1β (Figure 3.20).

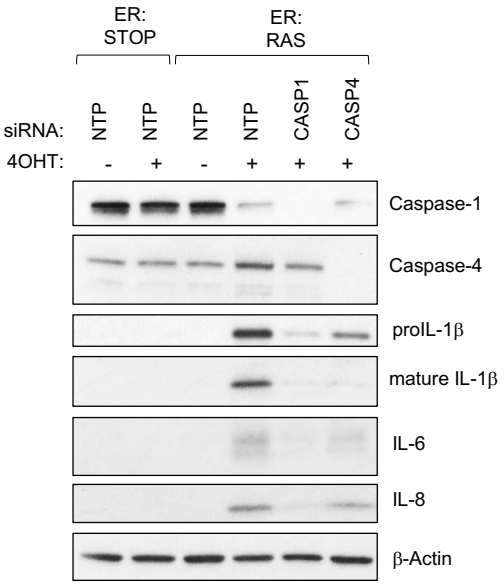

Figure 3.20 CASP4 targeting decreases the levels of intracellular mature IL-1β
IMR90 ER:STOP/ER:RAS cells were transfected with control (NTP), CASP1- or CASP4-targeting pool siRNA. Cells were collected 8 days after addition of 4-hydroxytamoxifen, lysed and analysed by western blotting using the indicated antibodies. Data belong to one representative experiment. NTP = non-targeting pool; 4OHT = 4-hydroxytamoxifen.

3.4.3 IL-1β secretion in RAS^{G12V}-OIS is controlled by caspase-4

IL-1β is released from senescent cells into the extracellular space, where it can bind to membrane IL1-receptor (IL-1R), contributing to the SASP cascade amplification and paracrine senescence. Quantification of extracellular IL-1β by ELISA in CASP4-targeted RAS^{G12V}-OIS cells decreased the amount of IL-1β released (Figure 3.21).

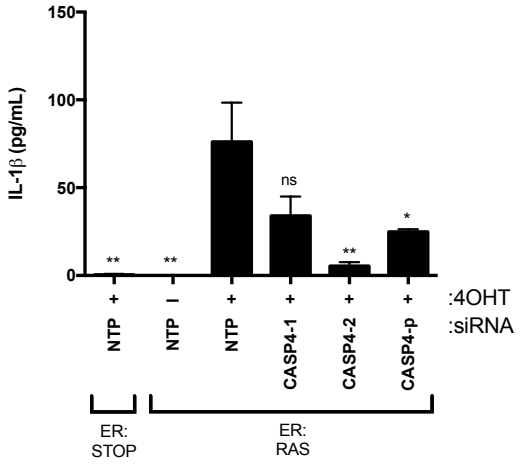

Figure 3.21 IL-1β release is impaired upon CASP4 targeting in RAS^{G12V}-OIS
IMR90 ER:STOP/ER:RAS cells were transfected with control (NTP) siRNA or CASP4-targeting siRNA (either two individual sequences (siCASP4-1/siCASP4-2) or a pool of four different sequences (siCASP4-p)). Eight days after 4-hydroxytamoxifen addition, conditioned media was collected and IL-1β was quantified by ELISA. Data are shown as mean ± s.e.m of n=3 experiments, one-way ANOVA and post-hoc Bonferroni´s multiple comparisons comparing all conditions to ER:RAS +4OHT NTP, *=p<0.05, **=p<0.01, ns=non-significant. NTP = non-targeting pool; 4OHT = 4-hydroxytamoxifen.

3.4.4 Induction of paracrine SASP is regulated by caspase-4

Senescent cells can induce senescence in neighbouring non-senescent cells, a phenomenon termed paracrine senescence and that is mediated by soluble secreted factors by senescent cells among others (80). CASP4 knockdown in growing fibroblasts diminished the inflammatory response upon the induction of senescence by addition of senescent conditioned media (Figure 3.22). Remarkably, the paracrine upregulation of SASP factors such as IL1A, IL1B, Il6 or IL8 was independent of CASP1.

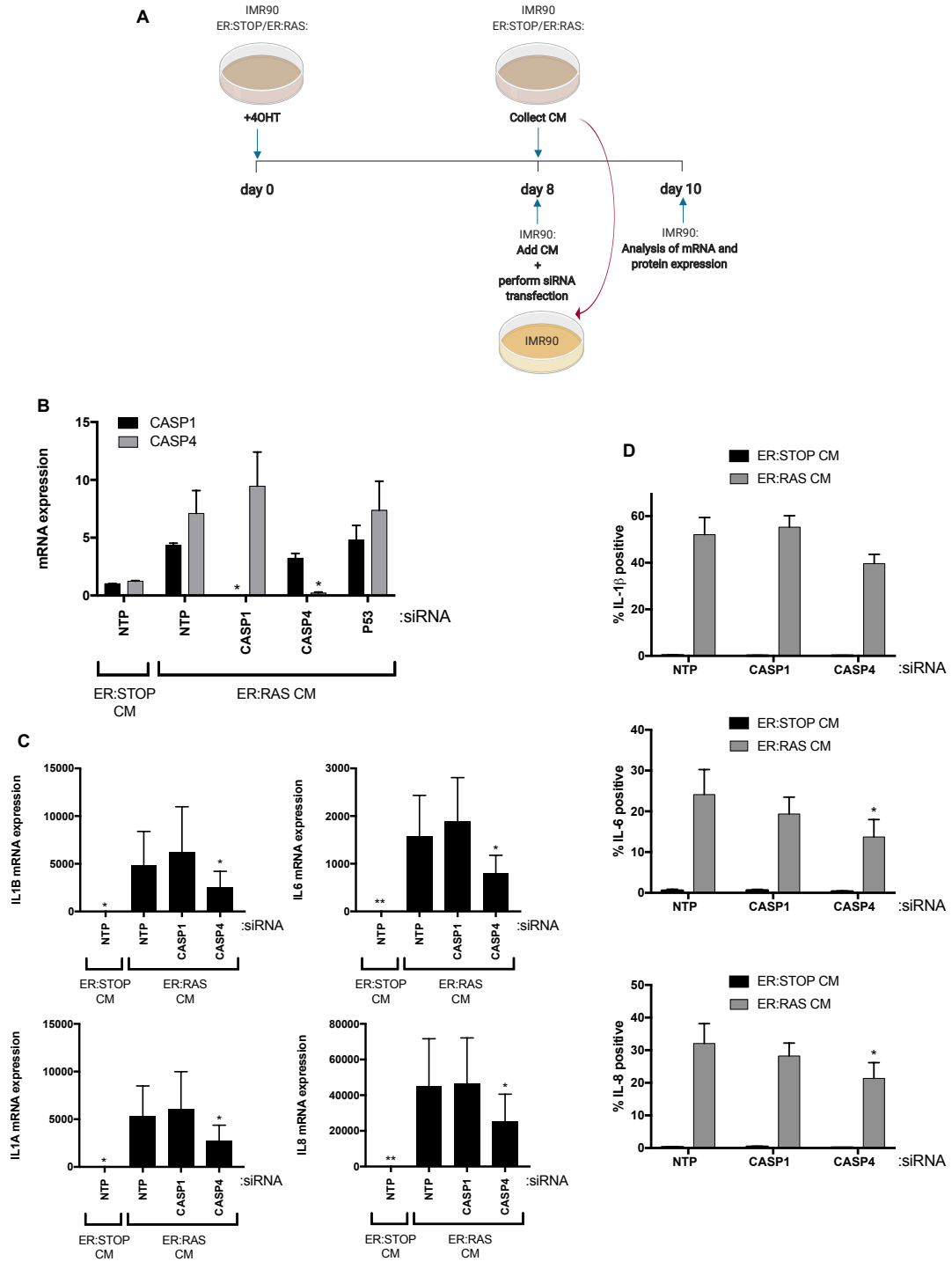

Figure 3.22 Regulation of paracrine SASP induction upon CASP4 knockdown

Paracrine senescence experiments showed in this figure were performed by Dr Núria Tarrats. After 8 days of 4-hydroxytamoxifen treatment, conditioned media from ER:STOP or ER:RAS cells was collected an added on growing IMR90 cells. Concomitantly, IMR90 cells were

transfected with the indicated siRNAs. A. Schematic diagram illustrating the experimental procedure. B. CASP1 and CASP4 mRNA expression was measured by RT-qPCR two days after the addition of conditioned media. C. IL1A, IL1B, IL8 and IL6 mRNA expression was measured by RT-qPCR two days after the addition of conditioned media. D. IL-1β, IL-6 and IL-8 were quantified using high-content analysis two days after the addition of conditioned media.

All data are shown as mean ± s.e.m of n=3 experiments, t tests were performed comparing each CASP1- or CASP4-knockdown ER:RAS sample to the respective control senescent sample, *=p<0.05, **=p<0.01, where unstated non-significant. 4OHT = 4-hydroxytamoxifen; NTP = non-targeting pool, CM = conditioned media.

3.5 Exploring the role of gasdermin-D in OIS

In recent years, gasdermin-D has gained major relevance as a target of inflammatory caspases in pyroptosis and it is currently the most well-characterized substrate of caspase-4. Therefore, gasdermin-D was studied as a potential downstream mechanism of inflammatory caspases in OIS.

3.5.1 Gasdermin-D is cleaved in RAS^{G12V}-OIS

Analysis of GSDMD mRNA relative expression in a RAS^{G12V}-OIS time-course did not show transcriptional regulation (Fig 3.23A). However, a key regulatory element of gasdermin-D activity is its cleavage (284, 285). Interestingly, gasdermin-D cleavage was observed in RAS^{G12V}-OIS (Figure 3.23B, C).

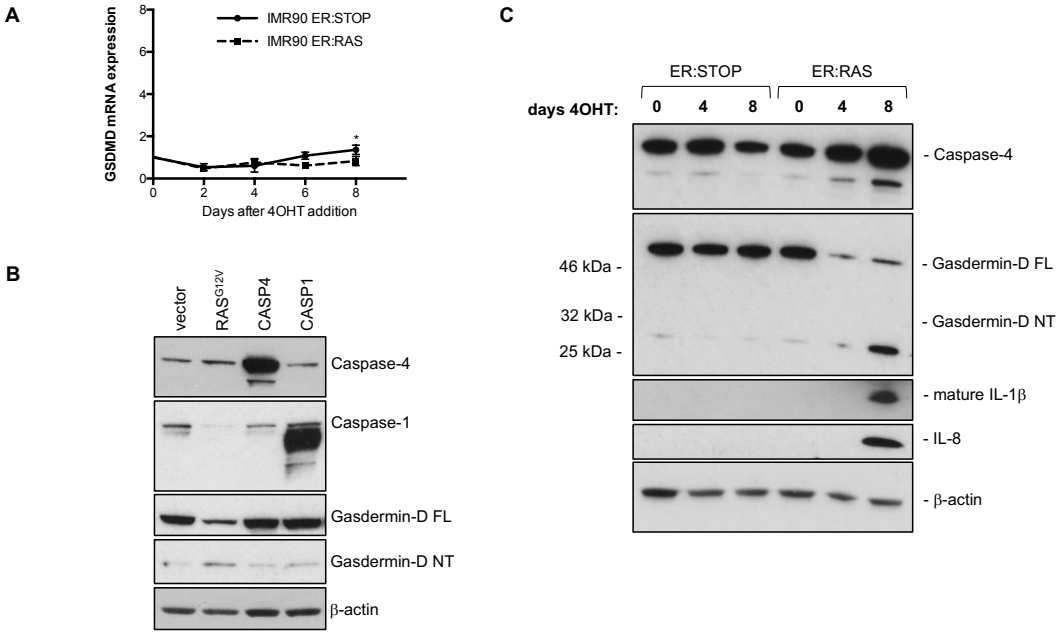

Figure 3.23 Gasdermin-D cleavage in RAS^{G12V}-OIS

A. GSDMD relative mRNA levels were quantified in a RAS^{G12V}-OIS time-course. Data are shown as mean ± s.e.m of n=3 experiments, paired t test, *=p<0.05. B. RAS^{G12V}, caspase-4 and caspase-1 were overexpressed by retroviral infection in IMR90 cells and cell lysates were probed with the indicated antibodies following western blotting procedures. Infection with the empty retroviral MSCV vector was used as a negative control. C. Protein expression was analysed by western

blotting in a time-course of ER:STOP and ER:RAS cell lysates 0, 4 and 8 days after addition of 4-hydroxytamoxifen. 4OHT = 4-hydroxytamoxifen; FL = full-length; NT = N-terminal domain.

3.5.2 GSDMD knockdown has a limited impact on the SASP

Because gasdermin-D is the key effector of inflammasome activation during pyroptosis, whether gasdermin-D is the downstream mediator of caspase-1/caspase-4-mediated SASP regulation in OIS was investigated.

RT-qPCR confirmed the on–target effect of GSDMD targeting by siRNA (Figure 3.24A). GSDMD downregulation did not halt transcriptional activation of IL1A, IL1B and IL8 in OIS (Figure 3.24B). In line with the lack of transcriptional IL1B regulation, the amount of full-length IL-1β was not regulated by GSDMD siRNA-mediated targeting, although decreased levels of intracellular mature IL-1β were detected (Figure 3.24C, D). Importantly, recent studies have described that pores formed by gasdermin-D are essential for IL-1β release in some cell types (292). However, gasdermin-D downregulation in RAS^{G12V}-OIS did not affect secreted IL-1β, which was impaired when caspase-1 or caspase-4 was targeted (Figure 3.24E).

These results show that downregulation of GSDMD has a limited effect on the transcription, translation or secretion of IL-1β compared to knockdown of CASP1 or CASP4, suggesting that inflammatory caspases regulate the SASP independently of gasdermin-D

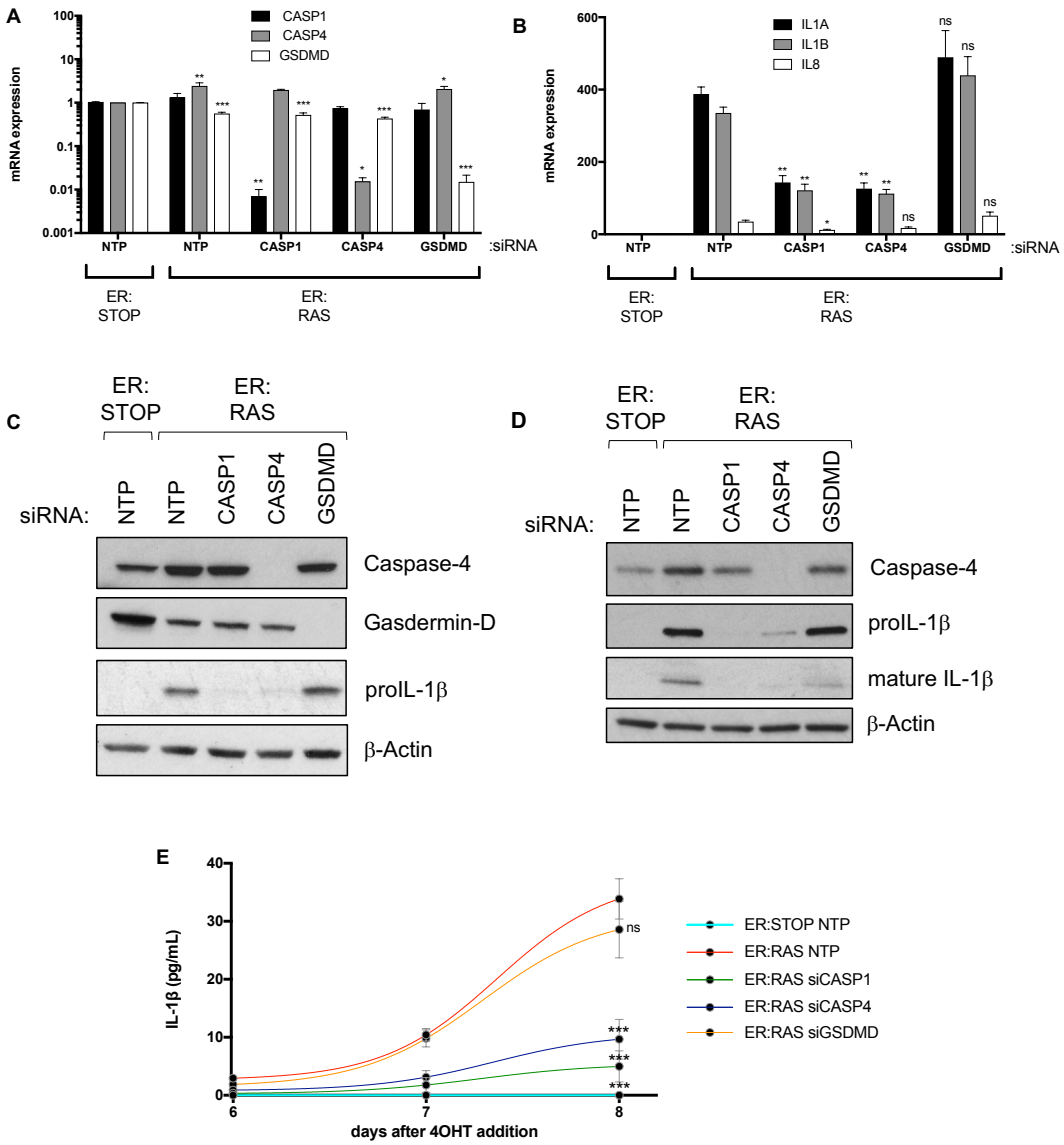

Figure 3.24 GSDMD knockdown does not impact IL-1 signalling in RAS^{G12V}-OIS

IMR90 ER:STOP/ER:RAS cells were transfected with the indicated pool siRNAs at day 0, 3 and 5 after 4-hydroxytamoxifen addition. A. CASP1, CASP4 and GSDMD relative mRNA expression was quantified using RT-qPCR in cells treated 5 days with 4-hydroxytamoxifen. B. IL1A, IL1B and IL8 relative mRNA expression were quantified using RT-qPCR in cells treated 5 days with 4-hydroxytamoxifen. C. and D. Protein expression in cell lysates was detected by western blotting using the indicated antibodies 5 and 8 days after 4-hydroxytamoxifen addition respectively. E. Released IL-1β was detected by ELISA 6, 7 and 8 days after 4-hydroxytamoxifen addition.

Data in A, B and E are shown as mean ± s.e.m, n=3, one-way ANOVA and post-hoc Bonferroni's multiple comparisons test, all samples compared to control cells, *=p<0.05, **=p<0.01, ***=p<0.001, where unstated non-significant. NTP = non-target pool; 4OHT = 4-hydroxytamoxifen.

3.6 Summary

In this chapter the expression of caspase-4 has been shown to increase 2-3 fold both at the mRNA and protein level in a well-characterized model of RAS^{G12V}-OIS. Simultaneously, during OIS caspase-4 oligomerizes and its cleavage activity is enhanced.

CASP4 targeting by siRNA in RAS^{G12V}-OIS followed by transcriptomic analysis revealed that CASP4 regulates a subset of genes involved in inflammatory processes, including the SASP. A pattern could be identified for most of the genes of this specific inflammatory gene set: upregulated expression in RAS^{G12V}-OIS, compared to non-senescent control, is halted upon CASP4 targeting. Changes in the mRNA expression of some of these genes were validated by RT-qPCR.

Specifically, IL-1 signalling was further investigated, and, importantly, depletion of caspase-4 does not only affect overall levels of proIL-1β but also decreases the pool of intracellular cleaved mature IL-1β, as well as its release. Moreover, caspase-4 also mediates paracrine SASP signalling.

Cleavage of endogenous gasdermin-D, an endogenous substrate of inflammatory caspases, was observed in RAS^{G12V}-OIS. However, GSDMD siRNA-mediated targeting did not impact the SASP at the same extent than CASP1 or CASP4, suggesting that IL-1 regulation by inflammatory caspases is independent of gasdermin-D, and that IL-1β is released from senescent cells in a gasdermin-D independent manner.

In all, these results demonstrate that both the canonical and non-canonical inflammasome regulate the SASP in OIS and reveal that caspase-4 is necessary for a full SASP activation in senescence (Figure 3.25).

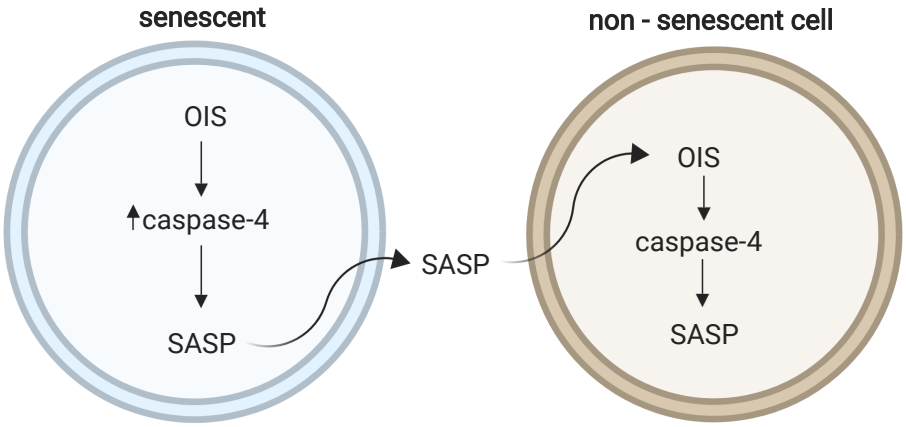

Figure 3.25 Caspase-4 regulates the SASP in OIS

Senescent cells display increased proteins levels of caspase-4. In senescent cells, caspase-4 is necessary for a complete induction of the SASP and the secretion of IL-1β. Nonetheless, caspase-4 is also necessary for a full SASP induction in paracrine senescence. Altogether, caspase-4 plays a key role in the maintenance and amplification of SASP signalling.

Chapter 4 - Activation of caspase-4 induces a senescent phenotype

4.1 Caspase-1 and caspase-4 overexpression induces a phenotype with senescence features

In the previous chapter, results regarding the role of caspase-4 regulating inflammatory features of OIS were presented. This chapter focuses on the potential role of inflammatory caspases regarding cellular proliferation. A first approach was conducted by overexpressing caspase-1 and caspase-4 in IMR90 cells.

4.1.1 Overexpression of caspase-1 and caspase-4 reduces cell proliferation and increases SA-β-galactosidase activity

Human CASP1 and CASP4 CDS were cloned into the retroviral MSCV vector and efficient caspase-1 and caspase-4 overexpression in IMR0 cells was confirmed by western blotting (Figure 4.1A). Phenotypical outcome of the overexpression of caspase-1 and caspase-4 in IMR90 cells was then assessed, using the overexpression of the empty MSCV retroviral vector as negative control and the overexpression of RAS^{G12V} as a positive control for the induction of senescence.

Both the overexpression of caspase-1 or caspase-4 reduced cell proliferation, measured by colony formation assay and 5-bromo-2-deoxyuridine (BrdU) incorporation (Figure 4.1B, C). Senescence-associated β-galactosidase activity (SA-β-galactosidase activity) was also increased upon caspase-1 or caspase-4 overexpression, although only statistically significant in the later (Figure 4.1D).

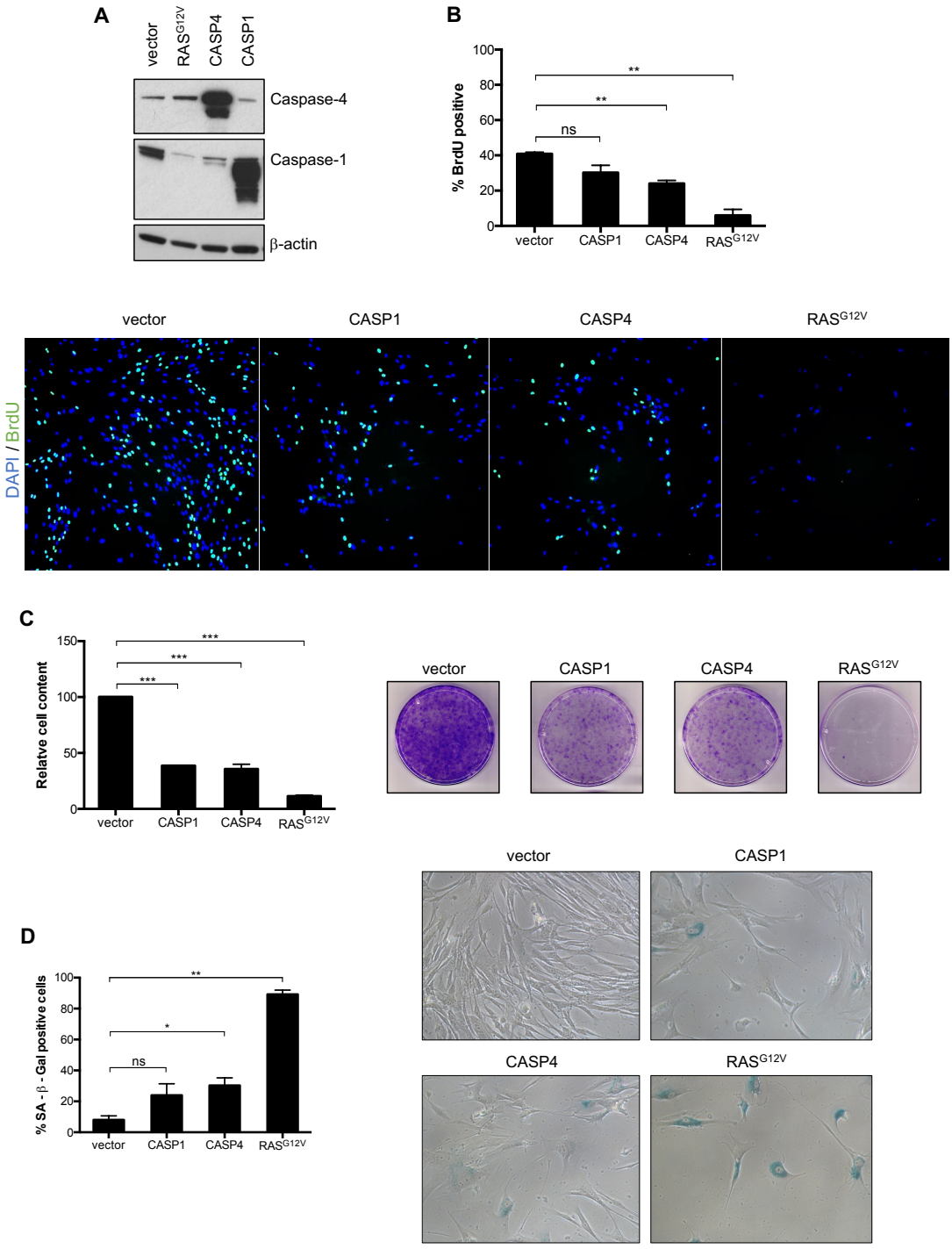

Figure 4.1 Caspase-1 and caspase-4 overexpression in human fibroblasts induce a senescent phenotype

CASP1, CASP4 and RAS^{G12V} were overexpressed in IMR90 cells. IMR90 cells were also infected with the empty vector and used as negative control. A. Caspase-1 and caspase-4 detection in IMR90 lysates by western blotting four days after equal numbers of cells were seeded. B. BrdU incorporation was measured by high-content analysis four days after equal number of cells were

plated. Representative images of BrdU staining as detected by immunofluorescence and used for high-content analysis are shown below. C. Relative cell content quantification after performing a colony formation assay; representative images of crystal violet stained plates from one experiment are shown on the right. D. SA-β-galactosidase activity was quantified four days after equal number of cells were plated. Images of SA-β-galactosidase stained cells from one representative experiment are shown on the right.
Data in A belongs to one representative experiment. Data in B, C and D are shown as mean ± s.e.m of n=3 experiments, paired t test, *=p<0.05, **=p<0.01, ***=p<0.001. ns = non-significant.

4.1.2 Inflammasome priming is required to activate IL1B transcription

Because depletion of either caspase-1 or caspase-4 impacted on IL-1 signalling in RAS^{G12V}-OIS (see section 3.4), whether the overexpression of caspase-1 or caspase-4 *per se* had an effect on endogenous levels of IL1A or IL1B was analysed. IL1A and IL1B mRNA expression were not increased upon caspase-1 or caspase-4 overexpression (Figure 4.2A).

Previous studies have described a two-step model for inflammasome activation in which a priming signal is followed by an activating stimulus (see Figure 1.9). Accordingly, addition of the synthetic lipopeptides Pam2CSK4 and Pam3CSK4 (TLR2/6 and TLR1/2 agonists respectively) to IMR90 cells highly increased IL1B transcription (Figure 4.2B). Interestingly, addition of Pam2CSK4 also increased the levels of caspase-4 in IMR90 cells (Figure 4.2C). When Pam2CSK4 or Pam3CSK4 were added on cells overexpressing caspase-1 or caspase-4, IL1B transcription was increased in a similar fashion to control cells. (Figure 4.2D).

In all, these results suggest that the sole overexpression of an inflammatory caspase is not enough for transcriptional activation of IL1 genes, which depends on an external stimulus able to prime the inflammasome.

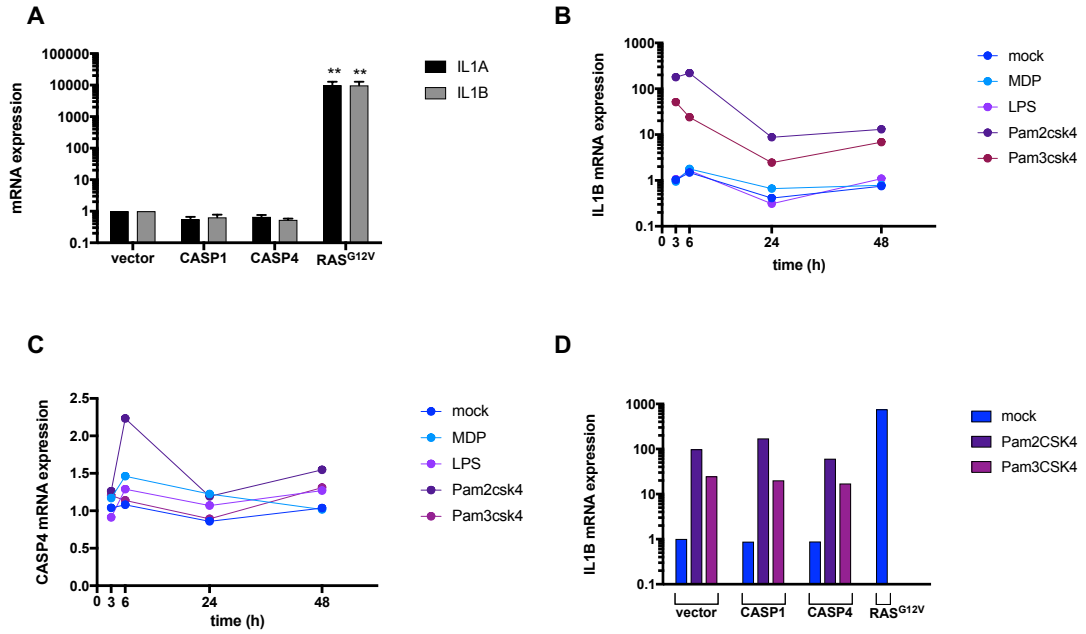

Figure 4.2 Activation of IL1B transcription requires inflammasome priming independently of caspase-1/caspase-4 overexpression

A. IL1A and IL1B relative mRNA expression were quantified using RT-qPCR in control or CASP1-, CASP4- or RAS^{G12V}-overexpressing IMR90 cells. (B) IL1B and (C) CASP4 mRNA relative expression were quantified by RT-qPCR in IMR90 cells treated with MDP, LPS, Pam2CSK4 or Pam3CSK4 as indicated. In B and C all data are relative to gene expression at t = 3 h in control (mock) cells. D. IL1B relative mRNA expression was quantified by RT-qPCR in control or CASP1-, CASP4- or RAS^{G12V}-overexpressing IMR90 cells with the indicated TLR agonists for 3h; overexpression of RAS^{G12V} was used as a positive control for IL1B mRNA expression. In D all data are relative to IL1B mRNA relative expression in mock-treated empty vector overexpressing IMR90.

Data in A are mean ± s.e.m, n=3, one-way ANOVA and post-hoc Bonferroni´s multiple comparisons test comparing all samples to control cells transfected with the empty vector (vector), **=p<0.01, where unstated non-significant. B, C and D show data of one representative experiment. Data in A, B and D are plotted in a logarithmic scale Y axis. MDP = muramyl dipeptide; LPS = lipopolysaccharide.

4.2 LPS-driven non-canonical inflammasome activation induces a caspase-4-dependent senescence response

Because overexpression of caspase-4 and caspase-1 suggested a potential role for inflammatory caspases in cell proliferation, whether the non-canonical inflammasome is involved in cell proliferation was explored by targeting endogenous caspase-4. Elegant studies have thoroughly described the activation of the non-canonical inflammasome by intracellular LPS (193, 280) (see section *1.2.3 The non-canonical inflammasome*). Therefore, this well-characterized non-canonical inflammasome activation system was used to investigate the potential effect of caspase-4 activation on cell proliferation in human fibroblasts.

4.2.1 Intracellular LPS causes cell death in IMR90 cells

To transfect LPS into IMR90 cells, the transfection protocol described by Shi *et al.* (193) was adapted. In their research, the authors described that the 293T cell line is resistant to cell death by LPS transfection due to lack of caspase-4 expression and this result was confirmed (Figure 4.3A). In contrast to 293T cells, IMR90 were sensitive to intracellular LPS (Figure 4.3A), like other human cells that express caspase-4 (193). Addition of LPS without electroporation did not result in cell death, confirming the requirement of intracellular location to elicit pyroptosis. Moreover, transfection with muramyl dipeptide (MDP), a bacterial cell wall component that activates the cytoplasmic receptor NOD2 generating a proinflammatory response (331), did not cause cell death, supporting the specificity of LPS in triggering pyroptosis (Figure 4.3B, C). Nonetheless, LPS also induced cell death in a dose-dependent manner (Figure 4.3B, C).

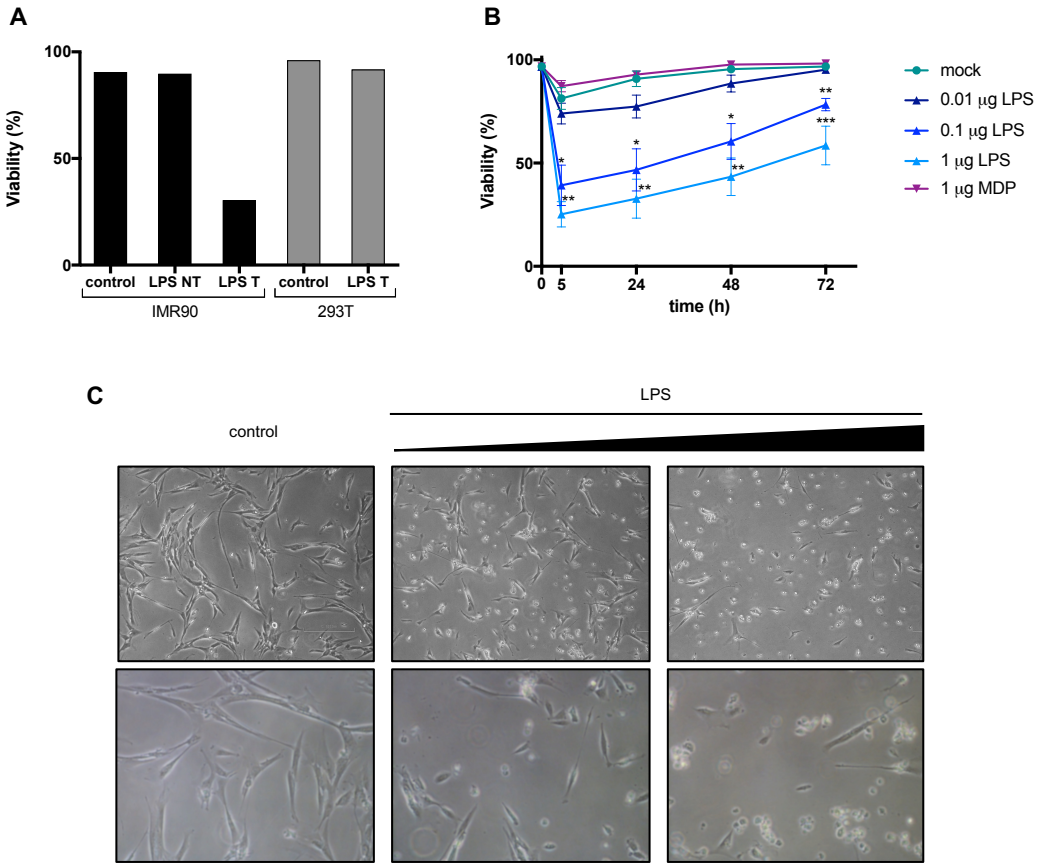

Figure 4.3 Intracellular LPS elicits cell death in IMR90 in a dose-dependent manner

A. IMR90 or 293T were untransfected (control) or transfected with 1 µg LPS / 5 x 10^5 cells (LPS T). For further control, IMR90 were also treated with 1 µg LPS / 5 x 10^5 cells without subsequent transfection (LPS NT). Cell viability was measured 2.5 h after transfection. B. IMR90 cells were transfected with 1 µg MDP / 5 x 10^5 cells or with three different doses of LPS (0.01; 0.1 or 1 µg LPS / 5 x 10^5 cells). Cell viability was measured at different times after transfection. C. Representative images of IMR90 cells mock-transfected (*left*) or transfected with 0.1 µg LPS / 5 x 10^5 cells (*middle*) or 1 µg LPS / 5 x 10^5 cells (*right*) under brightfield microscopy 4x (*upper row*) or 10x magnification (*lower row*) 24h after transfection.

Data in A belong to one representative experiment. Data in B are shown as mean ± s.e.m, n=3, t-tests were performed at each time-point comparing each condition to control cells (mock), *=p<0.05, **=p<0.01, where unstated non-significant. MDP = muramyl dipeptide; LPS = lipopolysaccharide.

Stable GSDMD knockdown in IMR90 cells before LPS transfection confirmed that LPS-driven cell death was GSDMD-dependent (Figure 4.4A). Moreover, full-length and the N-terminal fragment of gasdermin-D were overexpressed using an inducible doxycycline-dependant system. Overexpression of the N-terminal gasdermin-D fragment but not the full-length protein resulted in cell death in IMR90 cells (Figure 4.4B, C).

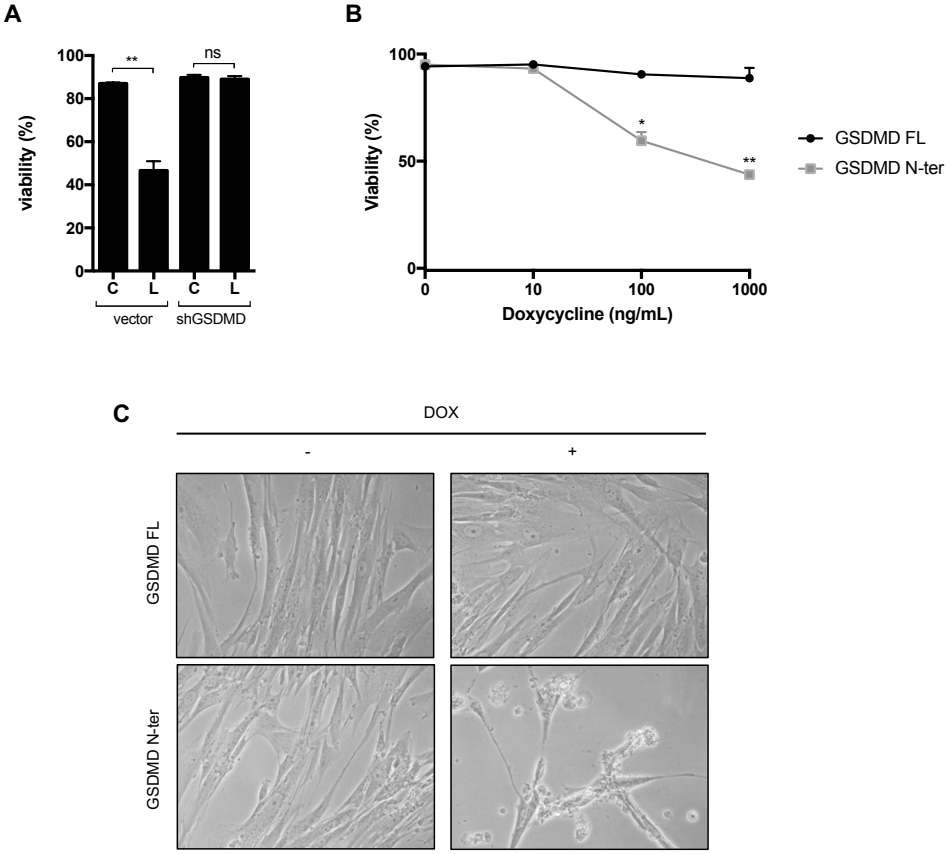

Figure 4.4 Intracellular LPS elicits cell death in IMR90 in a GSDMD-dependent manner
A. Stable GSDMD knockdown in IMR90 cells by lentiviral shRNA was followed by LPS transfection (0.1 μg LPS/transfection), and cell viability was measured 24 h after transfection B. Overexpression of full-length (FL) and the N-terminal (N-ter) fragment of gasdermin-D (GSDMD) in IMR90 cells was induced by addition of doxycycline after stable transfection with lentiviral vectors, and viability was measured 24 h after addition of doxycycline. Representative images of cells in culture 24 after doxycycline (DOX) addition (100 ng / mL) are shown in C. Data shown in A as mean ± s.e.m of n =3, paired t test, **=p<0.01, ns=non-significant. Data shown in B are mean ± s.e.m of n =3, one-way ANOVA and post-hoc Bonferroni´s multiple comparisons test comparing all samples to 0 ng/mL doxycycline, *=p<0.1, **=p<0.01, where unstated non-significant.

4.2.2 Intracellular LPS promotes a caspase-4 dependent senescence phenotype

Cell death was detectable within the first hours after LPS transfection. However, the fraction of cells surviving cell death after these hours remained viable and this subpopulation was further studied. This subset of cells displayed decreased cell proliferation (measured by BrdU incorporation) in an LPS dose-dependent manner (Figure 4.5A) 48 h after transfection. Moreover, the reduction in cell proliferation was accompanied by an increase in the protein levels of caspase-4 as well as the cell cycle regulators p21 and p16 (Figure 4.5B, C, E). Quantification of SA-β-galactosidase positive cells 4 days after LPS transfection revealed an increase in SA-β-galactosidase activity in LPS transfected cells compared to control or MDP-transfected cells (Figure 4.5D, F). These results indicate that the portion of cells surviving cell death display senescent features, including reduced cell proliferation, increased levels of cell cycle regulators and enhanced SA-β-galactosidase activity.

Next, we investigated the requirement of caspase-1 or/and caspase-4 for the acquisition of senescent features after LPS transfection. To stably knockdown CASP1 or CASP4, IMR90 cells were infected with lentiviral shRNAs targeting either CASP1 or CASP4. CASP4 knockdown but not CASP1 knockdown abrogated cell death following LPS transfection (Figure 4.6A). Interestingly, the decrease in cell proliferation after transfection with LPS was also rescued when CASP4 but not CASP1 was targeted (Figure 4.6B). Both CASP1 and CASP4 knockdown were validated by RT-qPCR and immunofluorescence staining, respectively (Figure 4.6C, D). Concomitant to the decrease in BrdU incorporation, CASP4-dependent increase in the levels of the cell cycle regulators p53, p21 and p16 after LPS transfection was observed (Figure 4.6E, F). CASP4 knockdown did also prevent an increase in SA-β-galactosidase activity following LPS transfection (Figure 4.6G).

Overall, these results suggest that the acquisition of a senescent phenotype following LPS transfection is caspase-4 dependent but caspase-1 independent.

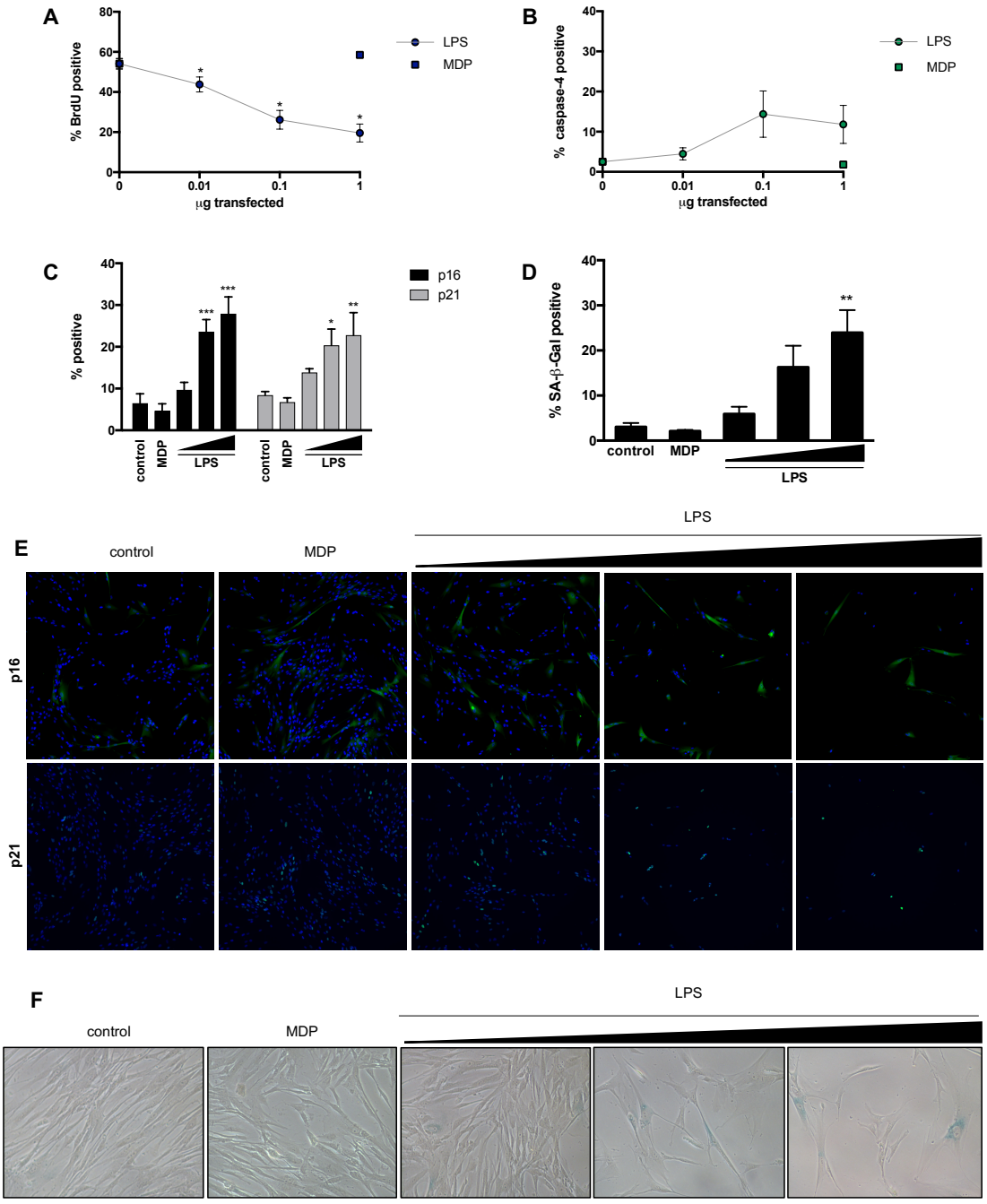

Figure 4.5 LPS transfection causes cell proliferation arrest

IMR90 cells were transfected with 1 μg MDP / 5 x 10^5 cells or with increasing doses of LPS (0.01/0.1/1 μg / 5 x 10^5 cells). BrdU incorporation (A) and caspase-4 (B), p21 and p16 (C) protein levels were quantified by high content analysis 48 h after LPS transfection. D. Quantification of SA-β-galactosidase activity 4 days after transfection. E. Representative images used for p21 and p16 quantification (C). F. Representative images used for the SA-β-gal quantification (D).

All data are shown as mean ± s.e.m, n=3, one-way ANOVA and post-hoc Bonferroni´s multiple comparisons test, all samples compared to control cells, *=p<0.05, **=p<0.01, ***=p<0.001, where unstated non-significant.

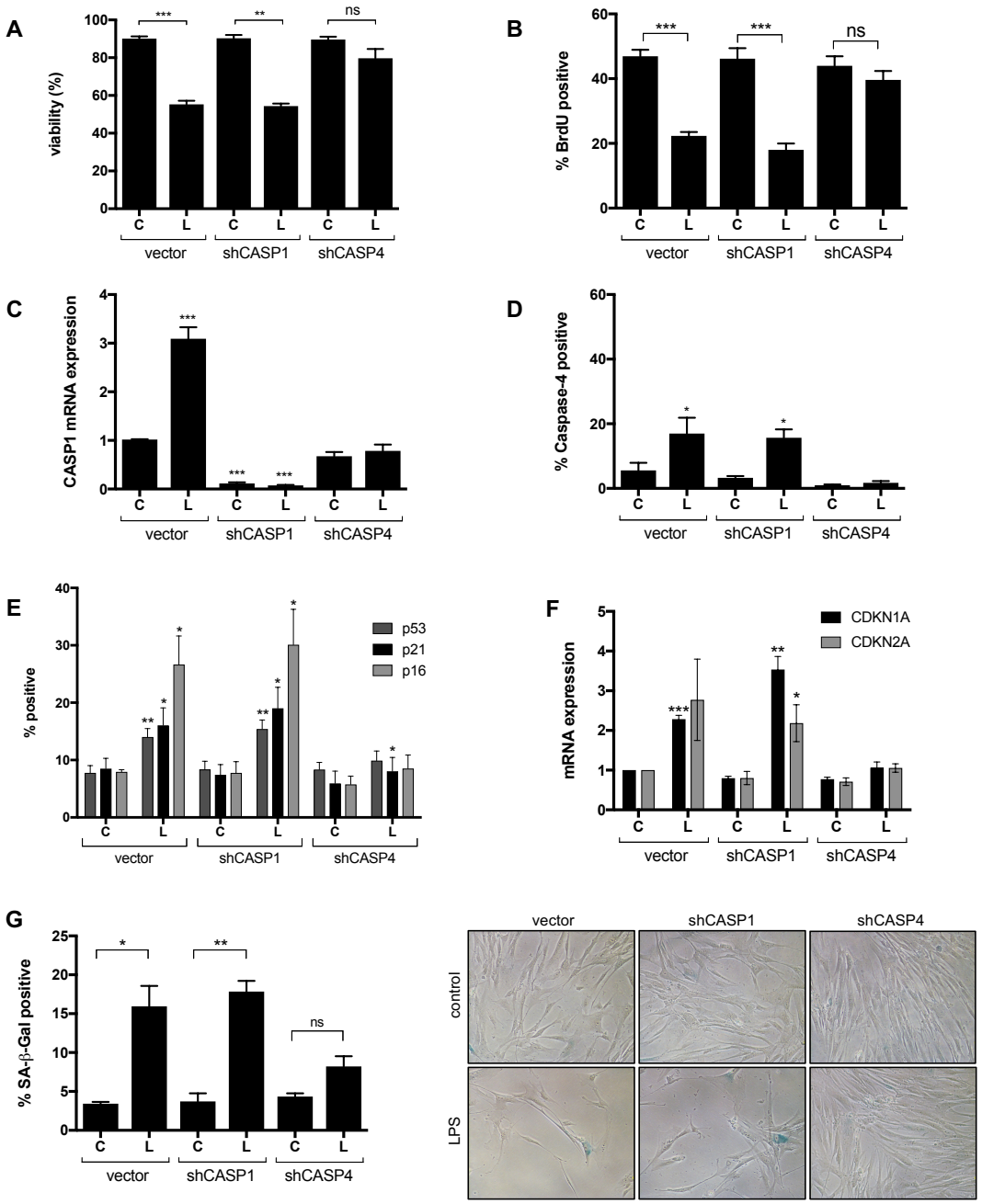

Figure 4.6 Acquisition of a senescent phenotype following LPS transfection is caspase-4-dependent but caspase-1-independent

Stable CASP1 and CASP4 knockdown in IMR90 cells by lentiviral shRNA was followed by LPS transfection (0.1 μg LPS/transfection). A. Cell viability was measured 24 h after transfection (n=3, mean ± s.e.m, paired t test, **=p<0.01, ***p<0.001, ns=non-significant). B. BrdU incorporation was quantified 48 h after transfection (n=4, mean ± s.e.m, paired t test, ***p<0.001, ns=non-significant). C. CASP1 mRNA expression was analysed 48 h after LPS transfection was performed by RT-qPCR (n=3, mean ± s.e.m, one-way ANOVA and post-hoc

Bonferroni´s multiple comparisons test comparing all samples to control cells, ***p<0.001, where unstated non-significant) D. Caspase-4 protein levels were quantified 48 h after LPS transfection by high-content analysis (n=3, mean ± s.e.m, one-way ANOVA and post-hoc Bonferroni´s multiple comparisons test comparing all samples to control cells, *p<0.05, where unstated non-significant). E. p53, p21 and p16 levels were quantified by high-content analysis 48h after LPS transfection (n= 4, mean ± s.e.m, paired t test comparing each transfected samples to the respective control, *p<0.05, **p<0.01, where unstated non-significant). F. CDKN1A and CDKN1B mRNA expression analysis 48 h after LPS transfection was performed by RT-qPCR (n=3, mean ± s.e.m, unpaired t test comparing each transfected sample to the respective control, *p<0.05, **p<0.01, ***p<0.001, where unstated non-significant). G. Quantification of SA-β-galactosidase activity 4 days after transfection (n=4, mean ± s.e.m, paired t test, **=p<0.01, **=p<0.01, ns=non-significant,); representative images of cells stained for SA-β-galactosidase activity are shown on the right. C = control; L = LPS.

Next, LPS was transfected into IMR90 cells constitutively overexpressing caspase-4. Transfection of LPS into caspase-4 overexpressing cells increased cell proliferation arrest compared to overexpression of caspase-4 alone (Figure 4.7A). Moreover, when transfected, overexpressing caspase-4 IMR90 cells incorporated less BrdU than control cells with endogenous caspase-4 levels. Interestingly, LPS-transfected caspase-4 overexpressing cells proliferated at a similar rate than cells undergoing RASG12V-OIS. The levels of p21 and p16, which are not induced by caspase-4 overexpression alone, were increased after LPS transfection (Figure 4.7B, C). High levels of caspase-4 were still detectable in caspase-4-overexpressing cells surviving pyroptosis (Figure 4.7C). SA-β-galactosidase activity was also enhanced in a dose-dependent manner when LPS was transfected into cells overexpressing caspase-4 (Figure 4.7D).

These results suggest that the overexpression of caspase-4 enhances the acquisition of a senescent phenotype following transfection with LPS.

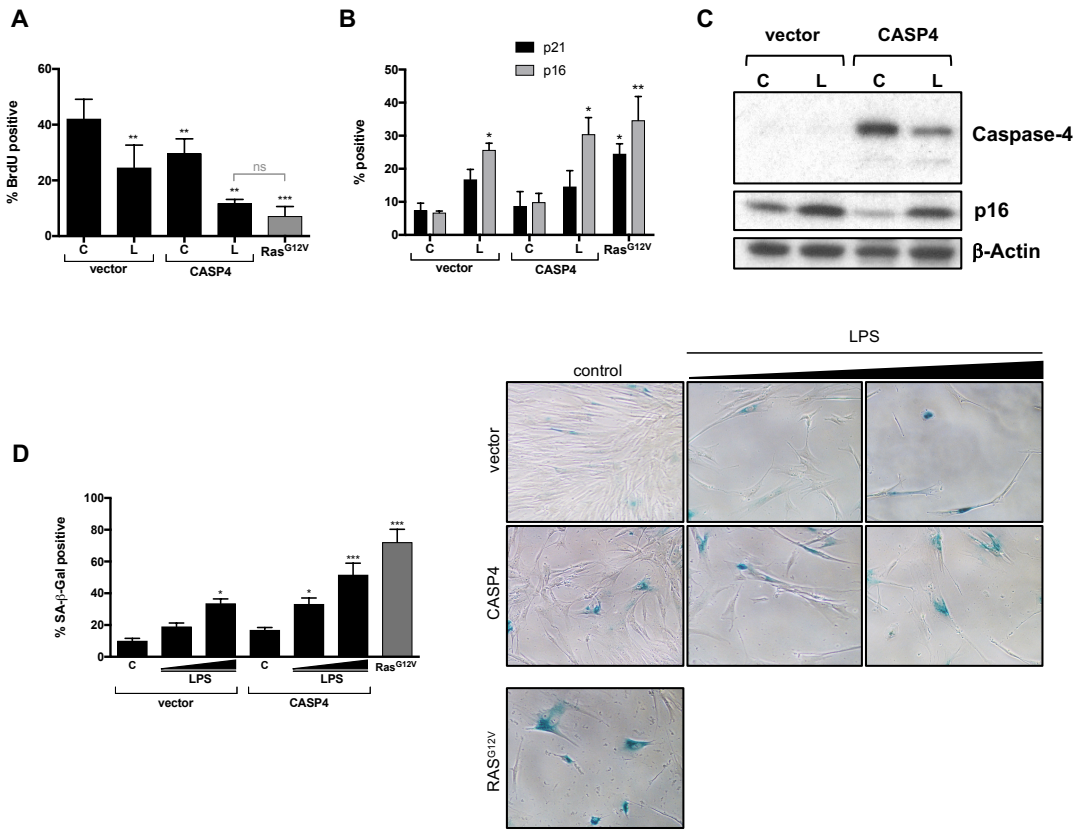

Figure 4.7 Overexpression of caspase-4 in IMR90 exacerbates the acquisition of a senescent phenotype following LPS transfection

Caspase-4 was stably overexpressed in IMR90 cells previously to LPS transfection. Cells infected with the empty vector (vector) were used as negative control whereas overexpression of RAS^{G12V} was used as a positive control for the induction of senescence. A. BrdU incorporation was quantified 48 h after LPS transfection. B. p21 and p16 were quantified 48h after LPS transfection using high-content analysis. C. Caspase-4 and p16 protein levels were analysed by western blotting 48 h after LPS transfection. D. Quantification of SA-β-galactosidase activity 4 days after transfection with 0, 0.1 or 1 μg LPS/transfection; representative images of the SA-β-galactosidase staining are also shown on the right.

Data in A, B and D are shown as mean ± s.e.m of n=3, one-way ANOVA and post-hoc Bonferroni´s multiple comparisons test comparing all samples to control cells, *=p<0.05, **p<0.01, ***p<0.01, where unstated non-significant. In A, an additional paired t-test was performed comparing LPS transfected caspase-4 overexpression and Ras^{G12V}-overexpression, Data in C show one representative blot. C = control, L = LPS, ns = non-significant.

4.2.3 Role of p53 in the acquisition of a senescence phenotype following LPS transfection

The tumour suppressor p53 has been shown to be a key mediator of senescence induction after telomere dysfunction and oncogene activation among others (4). To investigate whether the acquisition of senescent features following LPS transfection depends on p53, LPS was transfected into IMR90 cells where p53 expression is stably downregulated by shRNA targeting.

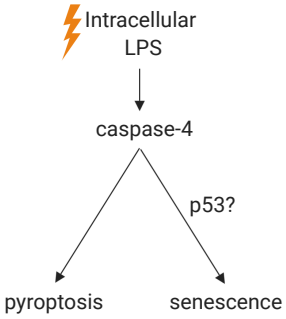

Cell death was not abrogated by P53 targeting, indicating that P53-knockdown cells are as sensitive to pyroptosis as control cells (Figure 4.8A). P53-knockdown in IMR90 cells without further treatment increased cellular proliferation compared to control cells as expected (Figure 4.8B). However, LPS transfection into P53-knockdown cells reduced cellular proliferation by approximately 50% compared to mock-transfected P53-knockdown cells, proportionally similar to the decrease observed in control cells (Figure 48B). Furthermore, LPS-transfected P53-knockdown cells showed increased levels of caspase-4 and p16 (Figure 4.8C). On the other hand, LPS-transfected P53-knockdown cells showed no activation of p21 (Figure 4.8C) and a mild increase in SA-β-galactosidase activity (Figure 4.8D). Taken together, these results suggest that although p53 contributes to the acquisition of senescent features after LPS transfection together with p16 activation, activation of caspase-4 by intracellular LPS induces cellular proliferation arrest through p53-independent mechanism(s).

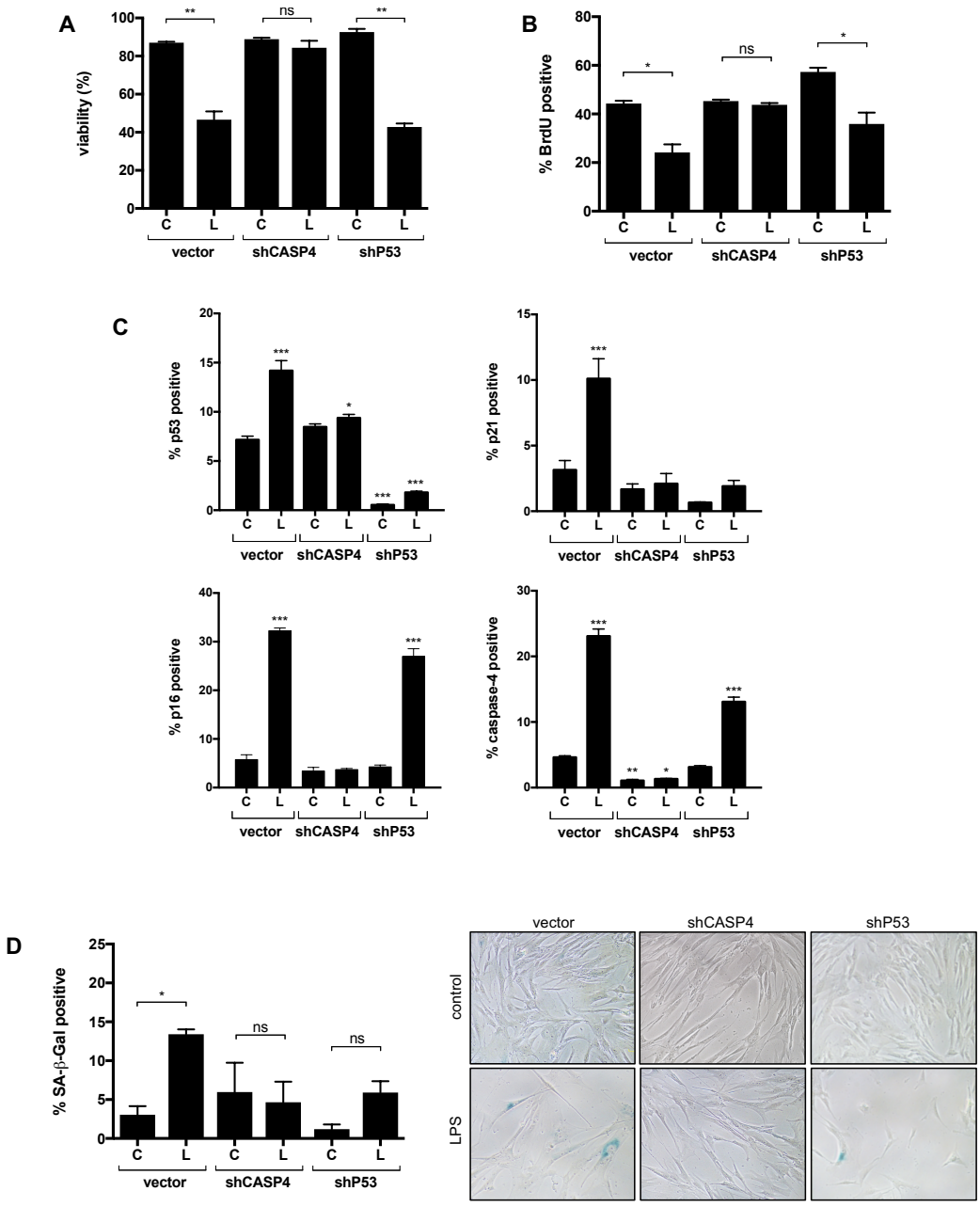

Figure 4.8 p53 contributes to the acquisition of an LPS-driven senescence phenotype

Stable CASP4 and p53 knockdown in IMR90 cells by lentiviral shRNA was followed by LPS transfection (0.1 µg LPS/transfection). IMR90 cells were transfected with the empty vector for control (vector). A. Cell viability was measured 24 h after transfection. BrdU incorporation (B) and p53, p21, p16 and caspase-4 protein levels (C) were quantified by high-content analysis 48 h after LPS transfection. D. SA-β-galactosidase activity was quantified 4 days after transfection and representative pictures of cells stained for SA-β-galactosidase activity are shown in the right. Data in A and B are shown as mean ± s.e.m, of n=3, paired t-test, each transfected sample was compared to its respective mock control., *=p<0.05, **p<0.01, ns=non-significant. Data in C and

D are shown as mean ± s.e.m of n=3, one-way ANOVA and post-hoc Bonferroni´s multiple comparisons test comparing all samples to empty vector control cells, *=p<0.05, **p<0.01, ***p<0.01, where unstated non-significant. C = control; L = LPS.

4.2.4 Inflammasome priming is not involved in LPS-driven cell proliferation arrest

To investigate whether inflammasome priming is required for the acquisition of a senescent phenotype following transfection with LPS, cells were primed with Pam2csk4 for 3 h. This stimulus was chosen because Pam2CSK4 had induced the highest IL1B transcription activation when added to IMR90 cells among the ones tested (Figure 4.2). Addition of Pam2CSK4 alone or followed by LPS transfection did not reduce cellular proliferation (Figure 4.9A) or alter SA-β-galactosidase activity (Figure 4.9B, C). Similarly, Pam2CSK4 did not enhance the acquisition of a senescent phenotype in cells overexpressing caspase-4, irrespectively of whether these were transfected with LPS (Figure 4.9B, C).

Next, whether the acquisition of senescent features following LPS transfection was accompanied by an activation of IL-1 signalling was investigated. LPS transfection increased IL1B mRNA levels in a CASP4-dependent CASP1-independent manner (Figure 4.9E). Addition of Pam2CSK4 prior to LPS transfection further increased IL1B transcription (Figure 4.9D). Thus, although inflammasome priming can reinforce the transcriptional activation of IL1B, it is not involved in the acquisition of senescent features such as decreased cell proliferation and increased SA-β-galactosidase observed after activation of the non-canonical inflammasome activation by LPS transfection.

Altogether, these results suggest that, in contrast to RAS^{G12V}-OIS, cell proliferation halt following LPS transfection is uncoupled from a strong IL-1 signalling transcriptional activation. Moreover, inflammasome priming does not impact on the acquisition of senescent features, such as cell proliferation arrest or enhanced SA-β-activity, following LPS transfection. In contrast, these results suggest that inflammasome priming is indispensable to activate an IL-1 signalling response in a senescent context.

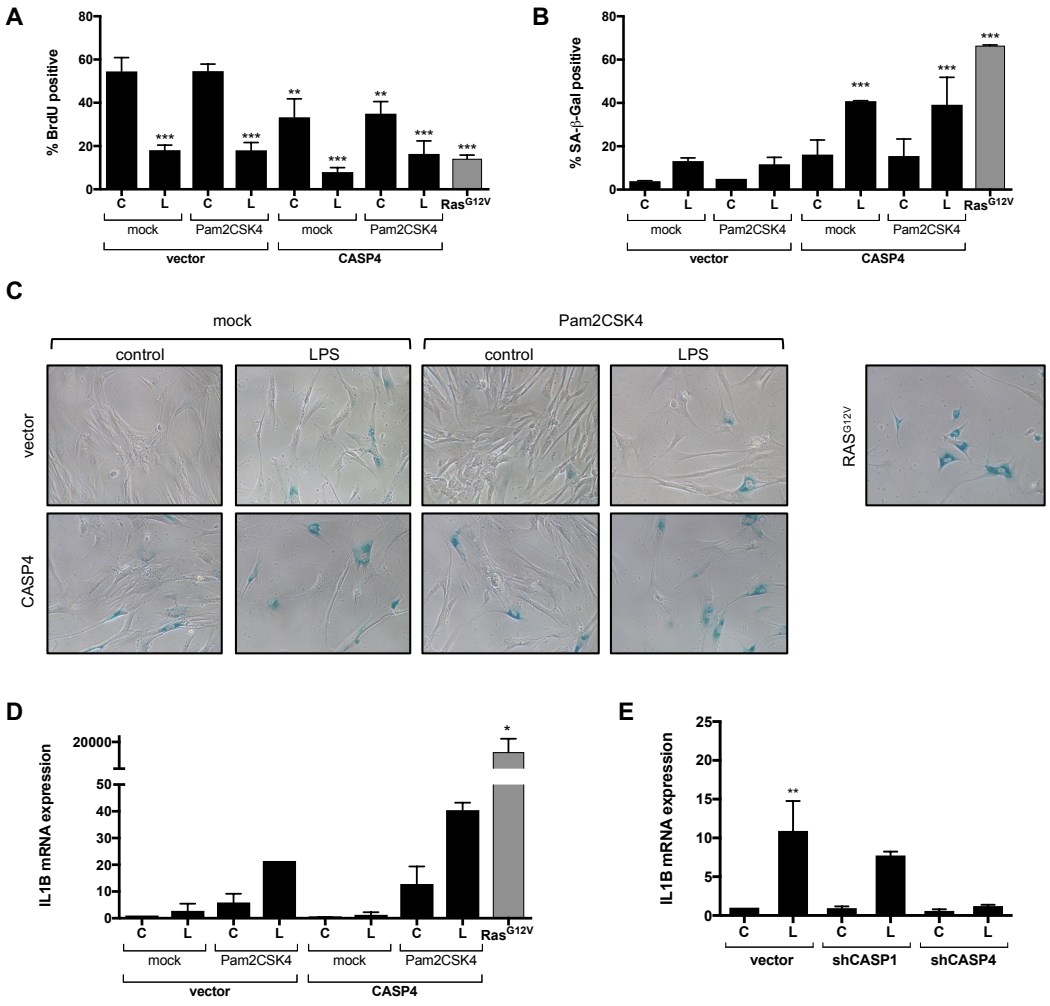

Figure 4.9 Inflammasome priming did not alter proliferation halt after LPS transfection

For data shown in A-D, IMR90 cells were infected to constitutively overexpress caspase-4. Cells infected with the empty vector (vector) were used for negative control, whereas cells overexpressing RAS^{G12V} were used as a positive control for senescence induction. Control and caspase-4 overexpressing cells were treated for 3 h with Pam3CSK4 prior to LPS transfection (0.1 μg/transfection). A. BrdU incorporation was quantified 48 h after LPS transfection. B. Quantification of SA-β-galactosidase activity 4 days after transfection C. Representative images of SA-β-galactosidase quantification (B). D. IL1B relative mRNA expression was quantified using RT-qPCR 48 h after LPS transfection. E. Cells were treated as explained in Figure 4.5. IL1B relative mRNA expression was quantified by RT-qPCR 48 h after LPS transfection.

In A, B and D, data are shown as mean ± s.d, n=2, one-way ANOVA and post-hoc Bonferroni´s multiple comparisons test comparing all samples to control cells, *=p<0.05, **=p<0.01, ***=p<0.001, where unstated non-significant. Data in E are shown as mean ± s.e.m, n=3, one-way ANOVA and post-hoc Bonferroni´s multiple comparisons test comparing all samples to control cell, **=p<0.01, s. C = control, L = LPS.

4.3 CASP4 knockdown partially bypasses cell proliferation arrest in RAS^{G12V}-OIS

Data presented in the previous section show that activation of the non-canonical inflammasome by intracellular LPS results in the acquisition of senescent features, including cell proliferation arrest, in the fraction of cells surviving pyroptosis. Next, whether caspase-4 is involved in cellular proliferation in OIS was investigated.

4.3.1 siRNA and shRNA-mediated CASP4 targeting results in a partial cell proliferation arrest bypass in RAS^{G12V}-OIS

CASP4 knockdown by siRNA in RAS^{G12V}-OIS partially bypassed cell proliferation arrest; of note, this effect was not observed when CASP1 or GSDMD were targeted (Figure 4.10).

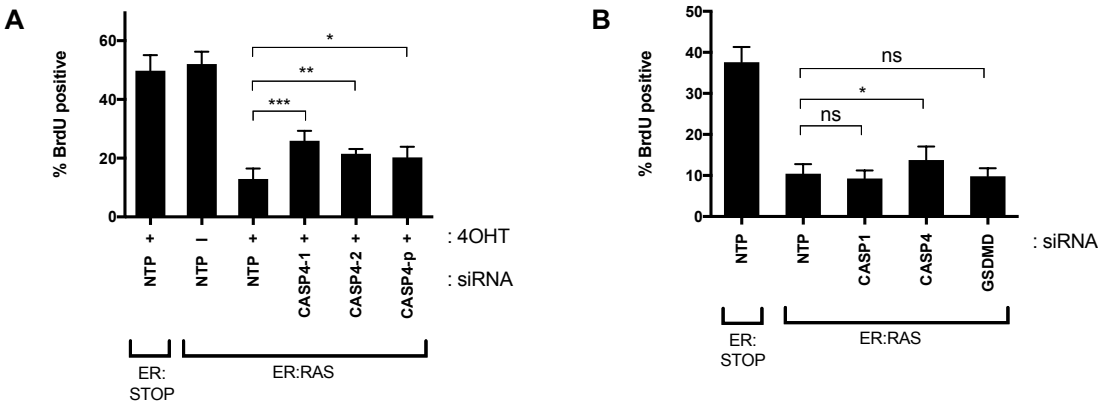

Figure 4.10 siRNA-targeted CASP4-knockdown causes partial cell proliferation arrest bypass in RAS^{G12V}-OIS

IMR90 ER:STOP/ER:RAS cells were transfected with siRNA 0 and 3 days after 4-hydroxytamoxifen addition and BrdU incorporation was measured 5 days after 4-hydroxytamoxifen addition. In A, CASP4 expression was targeted with two individual sequences and a pool of 4 different siRNA sequences. In B, CASP1, CASP4 or GSDMD were targeted with a pool of 4 different siRNAs sequences/gene; all samples were treated with 4-hydroxytamoxifen. In A, data are shown as mean ± s.e.m, n=3, one-way ANOVA and post-hoc Bonferroni´s multiple comparisons test comparing the indicated samples, *p<0.05, **p<0.01, ***p<0.01). In B, data are

shown as mean ± s.e.m, n=4, one-way ANOVA and post-hoc Bonferroni´s multiple comparisons test comparing the indicated samples, *p<0.1, ns = non-significant. NTP = non-targeting pool; 4OHT = 4-hydroxytamoxifen.

Moreover, targeting CASP4, but not CASP1, decreased SA-β-galactosidase activity in RAS^{G12V}-OIS (Figure 4.11).

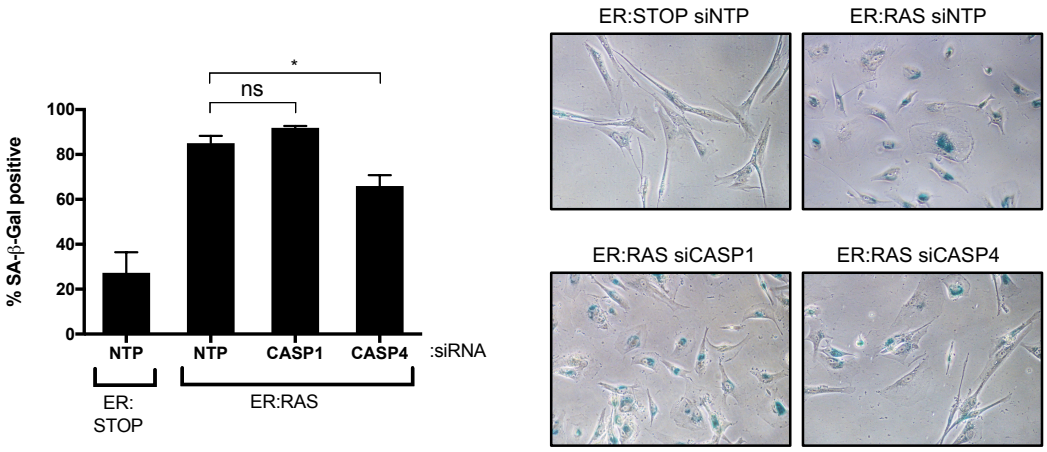

Figure 4.11 CASP4 downregulation reduces SA-β-galactosidase activity in RAS^{G12V}-OIS
IMR90 ER:STOP/ER:RAS cells were transfected with the indicated siRNAs 0, 3 and 5 days after 4-hydroxytamoxifen addition. Quantification of SA-β-galactosidase activity was performed 8 days after 4-hydroxytamoxifen addition. Data are shown as mean ± s.e.m, n=3, one-way ANOVA and post-hoc Bonferroni´s multiple comparisons test comparing the indicated samples, *p<0.05, ns = non-significant). Representative images of SA-β-galactosidase stained cells are also shown on the right. NTP = non-targeting pool; 4OHT = 4-hydroxytamoxifen.

To confirm the aforementioned results, CASP4 was stably targeted by retroviral shRNAs. A colony formation assay confirmed that CASP4 knockdown by shRNA-mediated targeting also resulted in a partial bypass of proliferation arrest in RAS^{GI2V}-OIS (Figure 4.12).

Altogether these results suggest that caspase-4 contributes to cellular proliferation arrest and enhanced SA-β-galactosidase in RAS^{GI2V}-OIS.

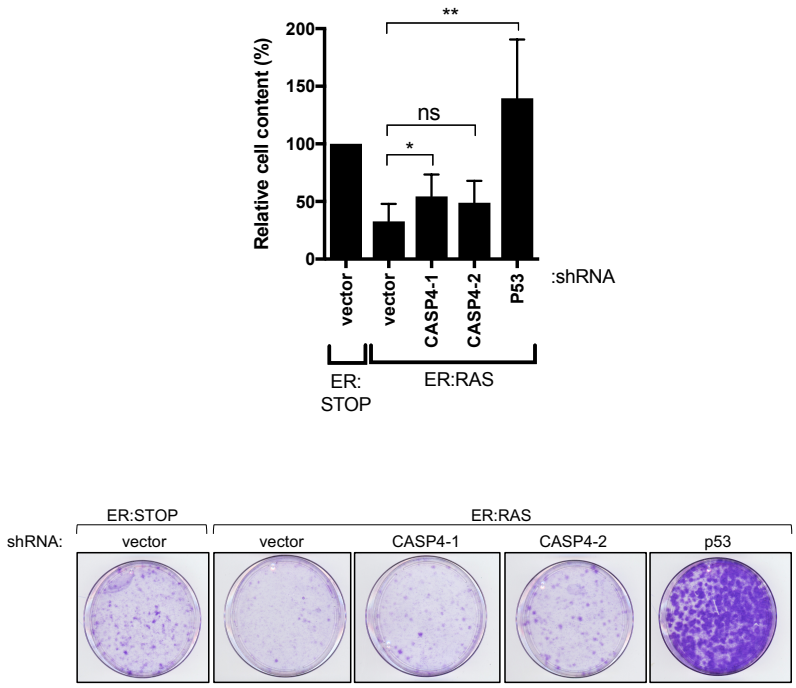

Figure 4.12 shRNA-mediated CASP4-knockdown causes partial cell proliferation arrest bypass in RAS^{G12V}-OIS

IMR90 ER:STOP/ERRAS cells were stably transfected using retroviral shRNA vectors. Infection with the empty vector was used as negative control and an shRNA targeting p53 was used as a positive control for bypass of cellular proliferation arrest. All conditions were treated with 4-hydroxytamoxifen. IMR90 ER:RAS cells were infected with two different retroviral vectors targeting CASP4 and one targeting P53. After selection, equal number of cells were plated on day 0 and 4-hydroxytamoxifen was added to all conditions. 15 days after 4-hydroxytamoxifen addition, plates were fixed and stained with crystal violet. Crystal violet was extracted and used to quantify the cell content in each plate (n=3, ratio paired t test as indicated, *p<0.1, **p<0.01, ns = non-significant) Representative crystal violet stained plates of one experiment are also shown below.

4.3.2 Caspase-4 regulates cell proliferation in RAS^{G12V}-OIS through pRb

Interestingly, among those hallmark gene sets analysed by GSEA in the transcriptomic analysis, the gene sets "G2M_CHECKPOINT" and "E2F_TARGETS" had the lowest Normalized Enriched Score (NES) when CASP4 was targeted by siRNA in RAS^{G12V}-OIS (Figure 4.13, Table 3.2). Moreover, the transcription factor E2F was also amongst the most highly regulated transcription factors by CASP4 (Table 3.3).

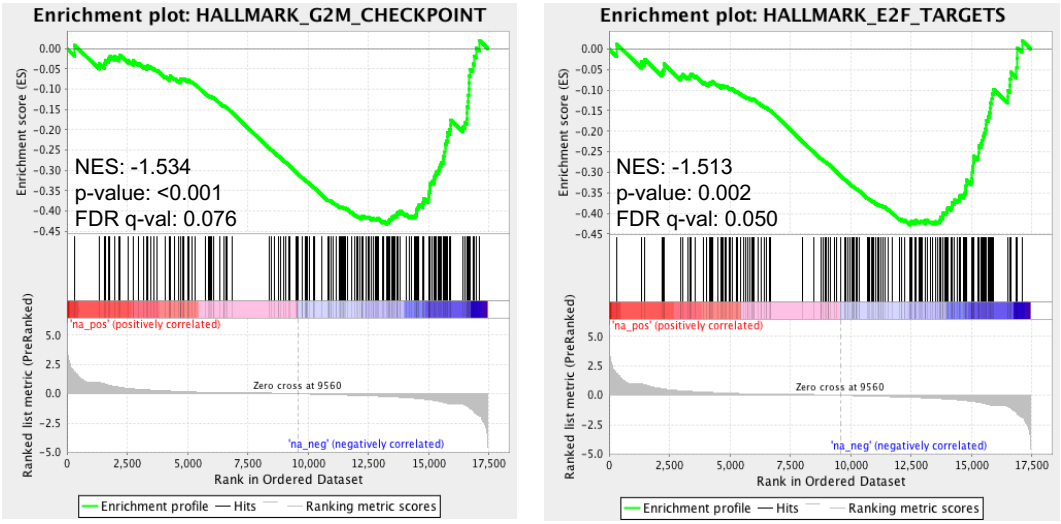

Figure 4.13 GSEA identifies "G2M Checkpoint" and "E2F targets" as gene sets regulated by CASP4

Enrichment plots for "G2M CHECKPOINT" and "E2F TARGETS" hallmark gene sets comparing control ER:RAS and CASP4 knockdown ER:RAS 5 days after addition of 4-hydroxytamoxifen.

The key mediator event leading to the irreversible implementation of cell senescence is the hypophosphorylation of pRb and subsequent silencing of E2F target genes (5, 332). CASP4 knockdown in RAS^{G12V}-OIS resulted in impaired hypophosphorylation of pRb, (Figure 4.14A). In line with this finding, the reduced expression of E2F target genes in RAS^{G12V}-OIS was partially rescued upon CASP4 knockdown (Fig 4.14B). In this same context, CASP4 knockdown did not alter the levels of p53 and p21, (Fig. 4.15A, B), suggesting that caspase-4 regulates pRb phosphorylation state downstream p53 and p21.

Nonetheless, there were no significant changes on p16 mRNA and proteins levels or CDKN2B mRNA levels upon caspase-4 targeting (Fig, 4.14A, 4.15A, 1.15B). Altogether, these results suggest that caspase-4, through a mechanism which is independent of p21 and p16 mRNA and protein levels, regulates the phosphorylation state of pRb and, consequently, the transcription of E2F target genes and thus cell proliferation.

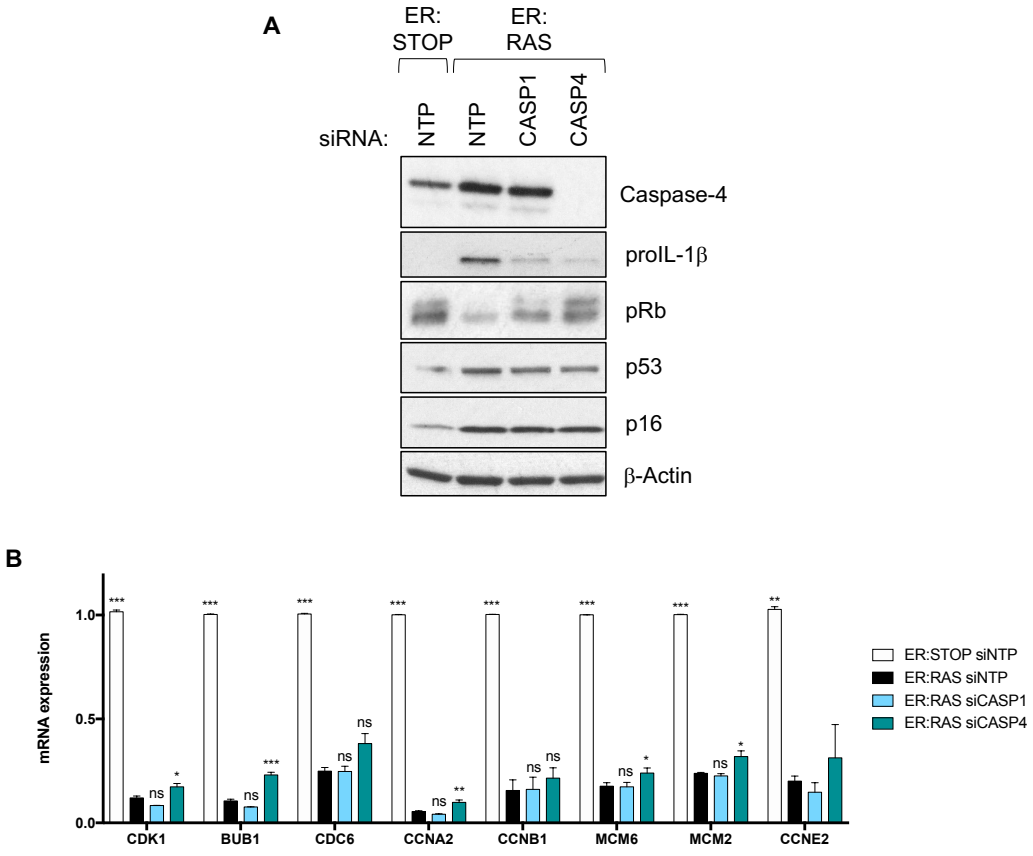

Figure 4.14 CASP4 knockdown in RAS^{G12V}-OIS regulates phosphorylation of pRb

IMR90 ER:STOP/ER:RAS cells were transfected with the indicated siRNAs at day 0 and 3 after 4-hydroxytamoxifen addition (where unspecified, a pool of 4 different siRNA sequences was used). All samples were treated with 4-hydroxytamoxifen. A. Cells were pelleted on day 5 after 4-hydroxytamoxifen addition and subjected to western blotting procedures using the indicated antibodies. An antibody that detects the different phosphorylated states of pRb was used. B. Relative mRNA expression of the indicated genes 5 days after 4-hydroxytamoxifen addition. Data in B are shown as mean ± s.e.m, n=3, one-way ANOVA and post-hoc Bonferroni's multiple comparisons test comparing all samples to ER:RAS siNTP, *p<0.05, **p<0.01, ***p<0.001, ns = non-significant. NTP = non-targeting pool; 4OHT = 4-hydroxytamoxifen.

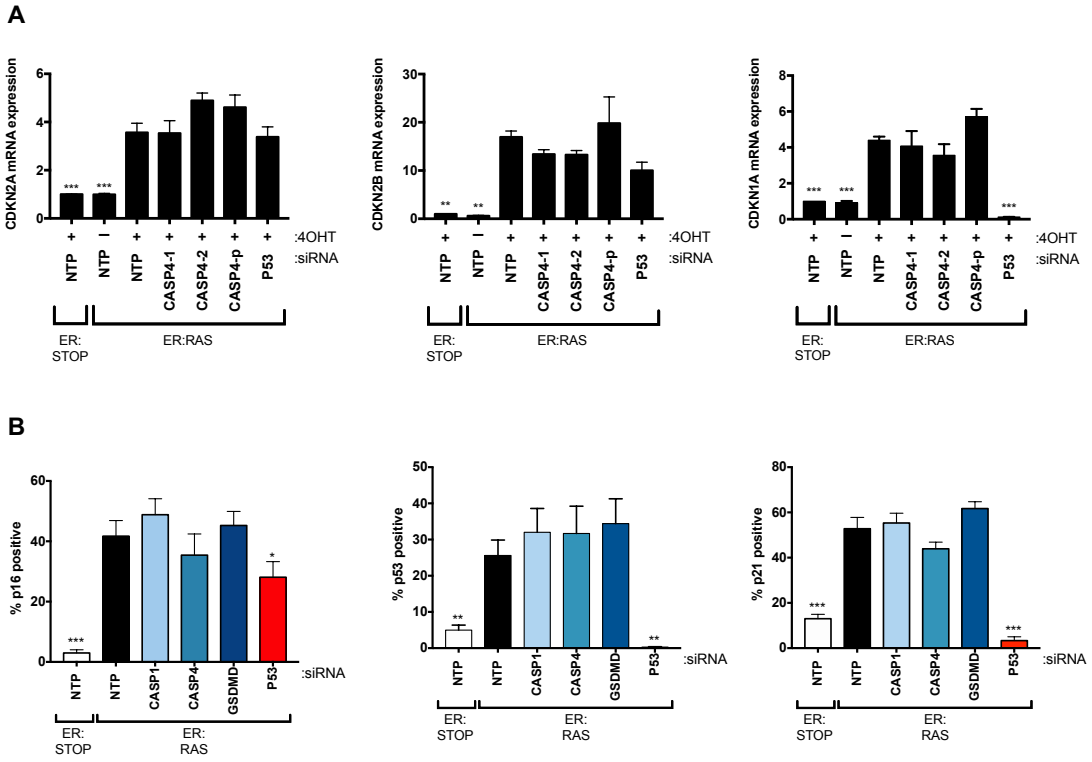

Figure 4.15 CASP4 knockdown regulation of proliferation in RAS^{G12V}-OIS is independent of CDK2A, CDKN2B and CDKN1A and p53 levels

IMR90 ER:STOP/ER:RAS cells were transfected with the indicated siRNAs at day 0 and 3 after 4-hydroxytamoxifen addition (where unspecified, a pool of 4 different siRNA sequences was used). A. CDKN1A and CDKN2A mRNA expression levels were analysed 5 days after addition of 4-hydroxytamoxifen B. Quantification of p16, p53 and p21 5 days after 4-hydroxytamoxifen addition by high-content analysis. In B, all samples were treated with 4-hydroxytamoxifen.

All data are shown as mean ± s.e.m, n=3, one-way ANOVA and post-hoc Bonferroni′s multiple comparisons test comparing all samples to ER:RAS siNTP, *p<0.05, **p<0.01, ***p<0.001, where unstated non-significant. NTP = non-targeting pool; 4OHT = 4-hydroxytamoxifen.

4.4 Caspase-4 regulation of cell proliferation is independent of its catalytic activity

4.4.1 Overexpression of a catalytic dead mutant caspase-4 induces senescence to a similar extent than wild-type caspase-4 overexpression

Caspases are cysteine-dependent proteases; hence their catalytic activity depends on a conserved cysteine residue. The active site of human caspase-4 has been well characterized and associated to residue C258 (Cysteine 258) and point mutations of this amino acid render the protein catalytically inactive (Figure 4.16).

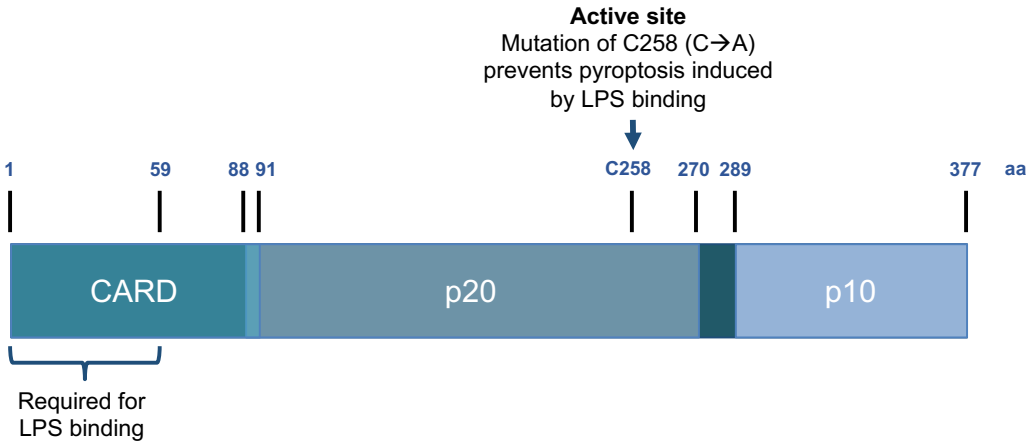

Figure 4.16 Schematic representation of caspase-4

A schematic representation of caspase-4 is shown. C = cysteine; A =alanine; aa = amino acid.

Catalytic dead CASP4 CDS (CASP4 C258A) was cloned into the retroviral MSCV vector using site-directed mutagenesis. Both wild-type (WT) and catalytic dead (C258A) caspase-4 were overexpressed in IMR90 cells and the phenotypical outcome was assessed. The overexpression of either construct induced similar levels of caspase-4 expression (Figure 5.2A). Interestingly, the overexpression of caspase-4 C258A reduced cell proliferation and increased the levels of SA-β-galactosidase activity to a similar extent than caspase-4 WT overexpression (Figure 4.17).

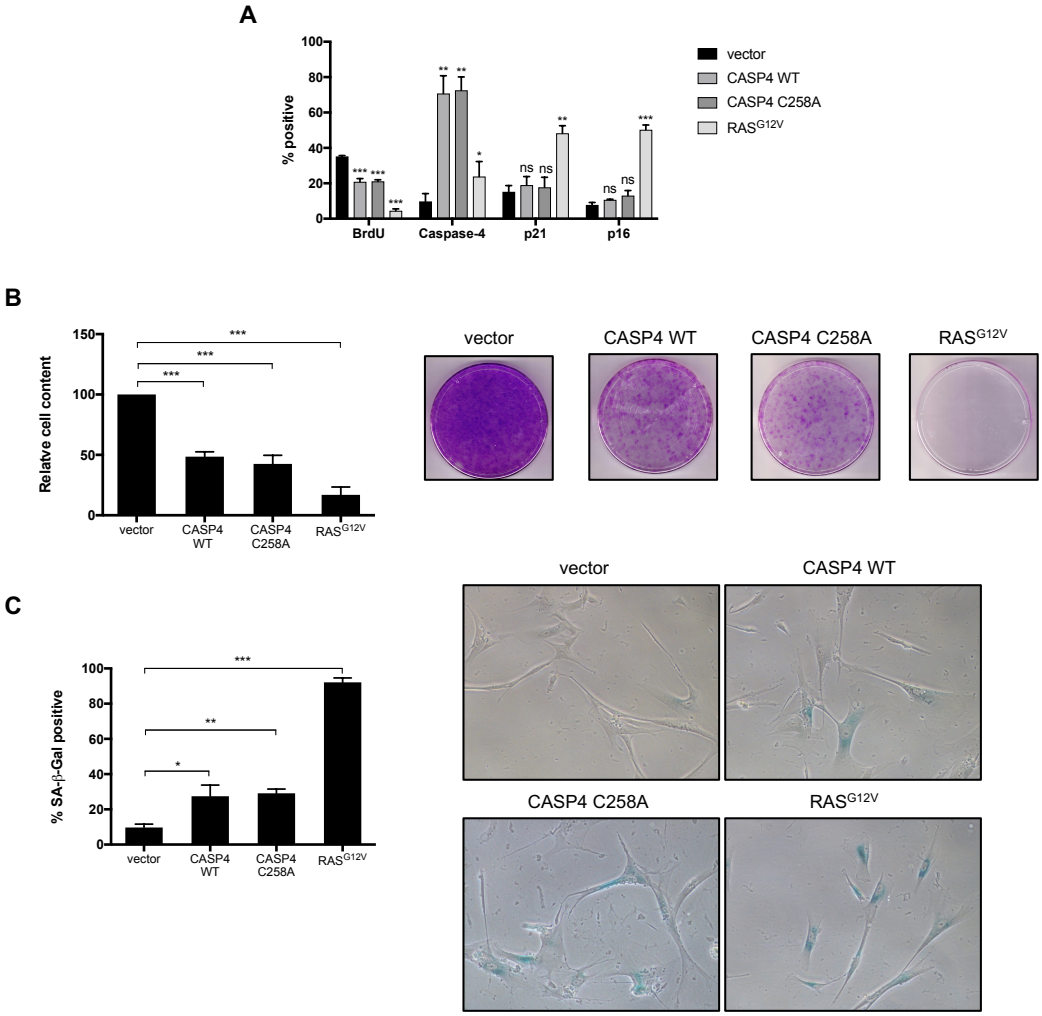

Figure 4.17 Overexpression of C258A caspase-4 induces cell proliferation arrest and SA-β-galactosidase activity

WT or C258A caspase-4 were overexpressed in IMR90 cells. Overexpression of the empty MSCV retroviral vector was used as negative control, whereas overexpression of RAS^{G12V} was used as a positive control for the induction of senescence. A. BrdU incorporation, caspase-4, p21 and p16 levels were quantified using high-content analysis 4 days after equal amounts of cells were plated. B. A colony formation assay was performed and crystal violet was extracted and used to quantify the cell content in each plate; representative images of stained plates of one experiment are also shown on the right. C. Quantification of SA-β-galactosidase activity 4 days after equal amounts of cells were plated; representative images of SA-β-galactosidase stained are also shown on the right.

All data are shown as mean ± s.e.m, n=3, one-way ANOVA and post-hoc Bonferroni´s multiple comparisons test comparing to empty vector control, *p<0.05, **p<0.01, ***p<0.001, ns = non-significant.

4.4.2 Overexpression of a catalytic dead mutant caspase-4 prior to LPS transfection rescues cell death but not acquisition of a senescence phenotype

Assessment of the phenotypical outcome of the overexpression of caspase-4 C258A suggested that caspase-4's regulation of cellular proliferation could be independent of its catalytic activity. To further investigate this hypothesis, LPS was transfected into IMR90 cells overexpressing either WT or C258A caspase-4.

As expected, overexpression of caspase-4 C258A preceding LPS transfection prevented cell death (Figure 4.18A, B). However, caspase-4 C258A overexpression did not rescue the acquisition of senescent features such as reduced cell proliferation and increased SA-β-galactosidase (Figure 4.18C, D). Interestingly, pRb was majorly detected in its hypophosphorylated state in CASP4 C258A overexpressing IMR90 following LPS transfection compared to untransfected cells (Figure 4.18E).

These results suggest that, although the catalytic activity is essential for pyroptosis, the role of caspase-4 in regulating cell cycle during senescence is independent of its proteolytic activity.

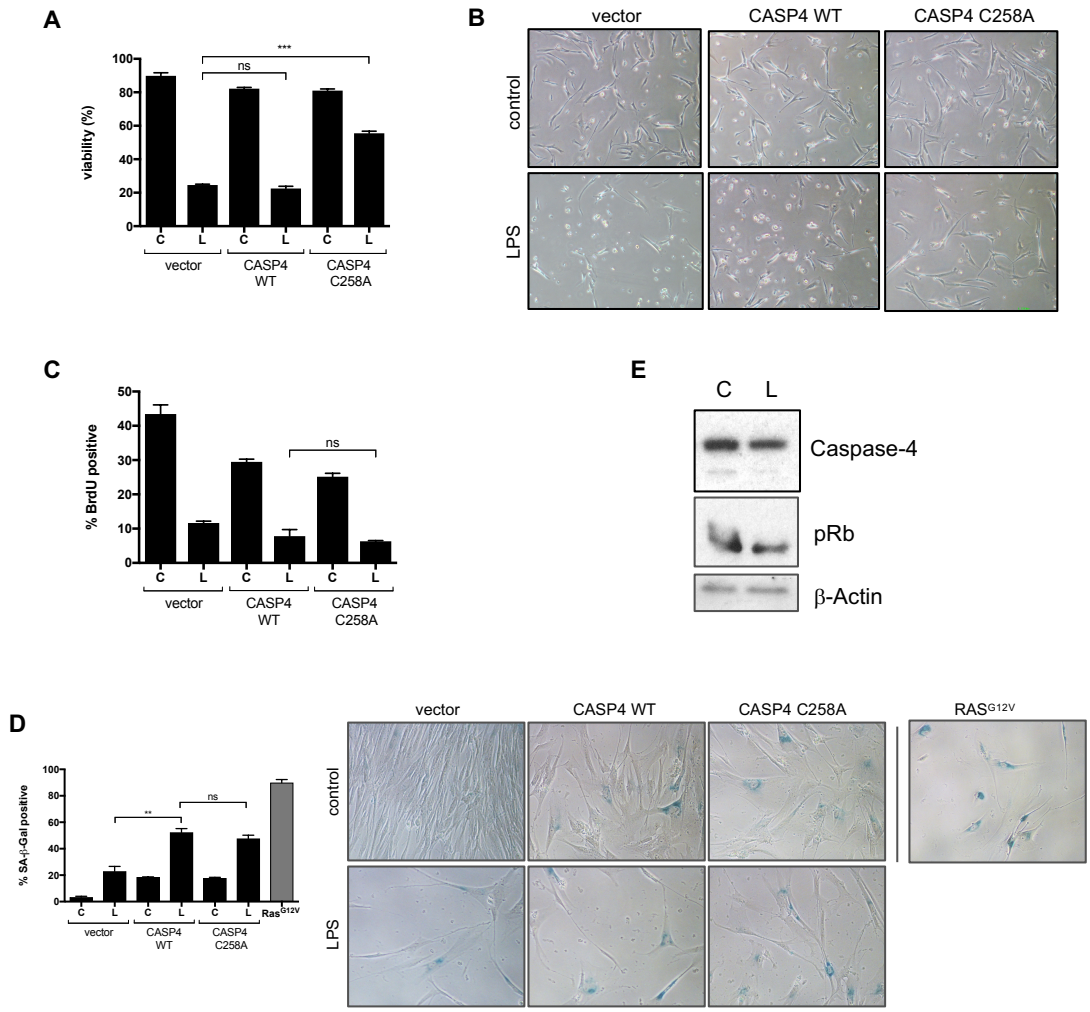

Figure 4.18 Overexpression of a catalytic dead mutant caspase-4 before LPS transfection prevents cell death but not the acquisition of a senescence phenotype

WT and a C258A caspase-4 were stably overexpressed in IMR90 cells and these were subjected to LPS transfection. Infection with the empty vector was used as a negative control whereas overexpression of RAS^{G12V} was used as positive control for the induction of senescence. A. Cell viability was measured 24 h after transfection (1 μg LPS transfected/ 5 x 10^5 cells). B. Representative bright-field pictures of cells in culture 24 h after LPS transfection (0.1 μg LPS transfected/ 5 x 10^5 cells). C. BrdU incorporation was quantified 48 h after LPS transfection (1 μg LPS transfected/ 5 x 10^5 cells). D. SA-β-galactosidase activity was quantified 4 days after LPS transfection (1 μg LPS transfected/ 5 x 10^5 cells); representative pictures are also shown (*right*). E. Caspase-4 and pRb were analysed by western blotting 48 h after LPS transfection in cells overexpressing the catalytic dead caspase-4 (C258A caspase-4).

Data in A, C, and D are shown as mean ± s.e.m, n=3, one-way ANOVA and post-hoc Bonferroni´s multiple comparisons comparing the indicated conditions, **p<0.01, ***p<0.001, ns = non-significant). C = control; L = LPS.

4.5 Summary

Overexpression of caspase-4 and caspase-1 in IMR90 cells resulted in cell proliferation arrest. Moreover, activation of the non-canonical inflammasome by intracellular LPS induced a senescence phenotype in the fraction of cells surviving pyroptosis (Figure 4.19). shRNA-mediated endogenous CASP4 downregulation abrogated LPS-driven senescence features whereas overexpression of caspase-4 enhanced them, confirming that caspase-4 is the key mediator of the senescence phenotype acquisition following LPS transfection. In contrast, CASP1 knockdown prior to LPS transfection did not have the same effect, indicating that the acquisition of senescence features following LPS transfection is caspase-1 independent. P53 knockdown prior to LPS transfection mildly affected the acquisition of senescence features, suggesting that the p53-p21 axis contributes but is not solely responsible for the senescence response following caspase-4 activation.

Inflammasome priming by addition of Pam2CSK4 did not alter cell proliferation arrest. However, cell proliferation arrest after LPS transfection was accompanied by a mild activation of IL-1β mRNA expression, which was enhanced upon addition of Pam2CSK4. These results suggest that inflammasome priming is necessary to activate inflammatory components such as IL-1 signalling within a senescence response.

CASP4 knockdown by siRNA or shRNA targeting partially bypassed cell proliferation arrest in RAS^{G12V}-OIS, suggesting caspase-4 regulates cell proliferation in OIS. Moreover, further exploration of the transcriptomic data earlier presented, suggested that caspase-4 regulates proliferation in RAS^{G12V}-OIS by controlling the phosphorylation state of pRb. Caspase-4 knockdown in RAS^{G12V}-OIS did not affect the levels of p53 or p21, suggesting that caspase-4 regulates pRb phosphorylation state downstream the p53-p21 axis, as in LPS-driven senescence. Nonetheless, CDKN2A and CDKN2B mRNA levels were unaffected by CASP4 targeting in RAS^{G12V}-OIS.

Finally, overexpression of a catalytic dead mutant caspase-4 induced a similar phenotype to the overexpression of wild-type caspase-4, including decreased cell proliferation and an increase in SA-β-galactosidase activity. Moreover, overexpression of the catalytic dead mutant caspase-4 prior to LPS transfection significantly abrogated cell death, suggesting a dominant negative effect. In contrast, analysis of senescence markers did not show differences between WT or C258 caspase-4 overexpression prior to LPS-driven activation of the non-canonical inflammasome. Altogether these results suggest that the catalytic activity of caspase-4 is dispensable for the acquisition of senescent features following LPS transfection.

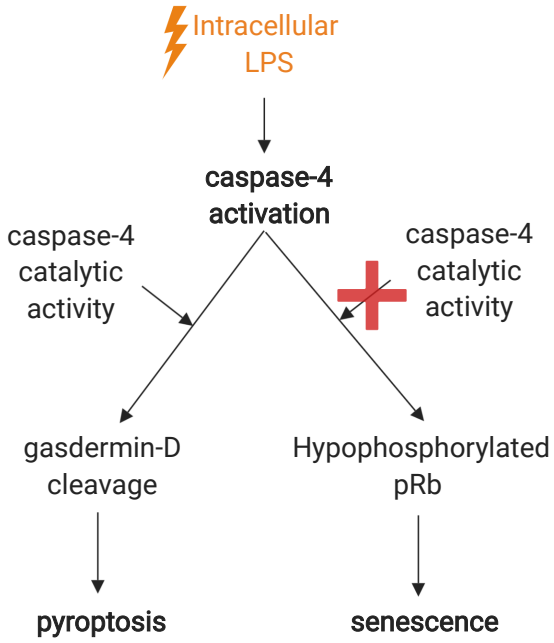

Figure 4.19 Caspase-4 activation by intracellular LPS induces the acquisition of a senescent phenotype

Intracellular LPS activates caspase-4 and elicits a rapid pyroptotic response. Cells surviving pyroptosis present senescence features such as reduced cellular proliferation and increased SA-β-galactosidase staining. Whereas pyroptosis depends on caspase-4 cleavage of gasdermin-D, the experimental results presented in this chapter suggest that the acquisition of a senescence phenotype following LPS transfection is independent of caspase-4 catalytic activity.

Chapter 5 - Identification of novel interactors of inflammatory caspases in OIS

In this chapter, a protein-protein interaction screening was performed to identify novel interactors of inflammatory caspases in OIS. Selected candidate proteins were then targeted by siRNA in OIS, and their phenotypical impact was assessed in terms of cell proliferation and IL-1 signalling.

5.1 Characterization of the inflammatory caspase interactome in OIS

5.1.1 BioID: protein interactome discovery by proximity biotinylation

The results presented in the previous chapter suggest a role for caspase-4 in regulating cell proliferation independent of its catalytic activity. With the aim of targeting potential non-proteolytic functions of inflammatory caspases, the BioID technique, which allows identification of protein-protein interactions *in vivo* by proximity biotinylation, was used. Briefly, in a BioID proteomic screening, the protein of interest is fused to a promiscuous biotin ligase (BirA) and overexpressed *in vivo*. After addition of the substrate (biotin), the ligase will biotinylate endogenous proteins in the proximity, which can then be pulled-down by biotin-affinity capture (333).

With the aim of applying this technique to identify potential interactors of caspase-1 and caspase-4 in OIS, caspase-4 or caspase-1 were fused to the biotin ligase (Figure 5.1A). For further control, two caspase-4 expression constructs were generated, one with the biotin ligase located prior to caspase-4 N-terminus and another with the biotin ligase placed after caspase-4 C-terminus. Additionally, each construct was also fused to a MYC tag. Expression of the constructs in 293T cells validated the correct expression

of the constructs, with fusion proteins having an approximate size of 80 kDa, in accordance with their predicted sizes (Figure 5.1B, C).

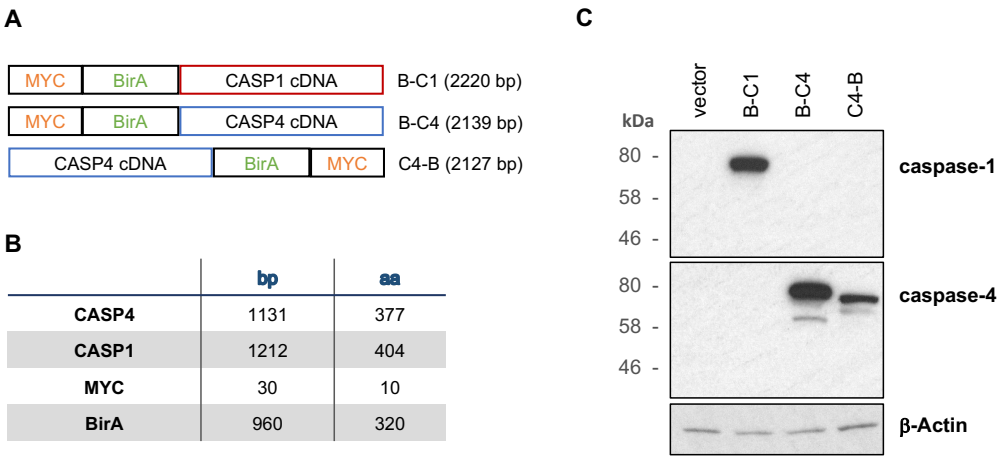

	bp	aa
CASP4	1131	377
CASP1	1212	404
MYC	30	10
BirA	960	320

Figure 5.1 Caspase-1-BirA and caspase-4-BirA fusion constructs generated to identify interacting proteins by proximity biotinylation

A. Schematic representation of the three generated constructs: CASP1 CDS fused to the biotin ligase (BirA) (B-C1), CASP4 cDNA fused to the biotin ligase in its N-terminus (B-C4) and Casp4 CDS fused to the biotin ligase in its C-terminus (C4-B). B. Table indicating the reference number of base pairs (bp) and amino acids (aa) relative to each component of the fusion proteins. C. Western blotting analysis using the indicated antibodies for caspase-1 and caspase-4 detection in 293T cell lysates 48 h after transfection with the indicated constructs.

5.1.2 BioID screening results

IMR90 ER:STOP and ER:RAS cells were transfected with each of the three constructs described in the previous subheading and the empty vector control by retroviral infection. Three days after the addition of 4-hydroxytamoxifen, biotin was added. The following day, biotinylated proteins were pulled-down using streptavidin-coupled beads. Attached proteins were sent to the Mass Spectrometry IGMM Facility where identification of the biotinylated proteins was performed using mass spectrometry (Fig 5.2). Downstream analysis was performed with the label-free quantification (LFQ) intensity values for all detected proteins provided by the Mass Spectrometry IGMM Facility.

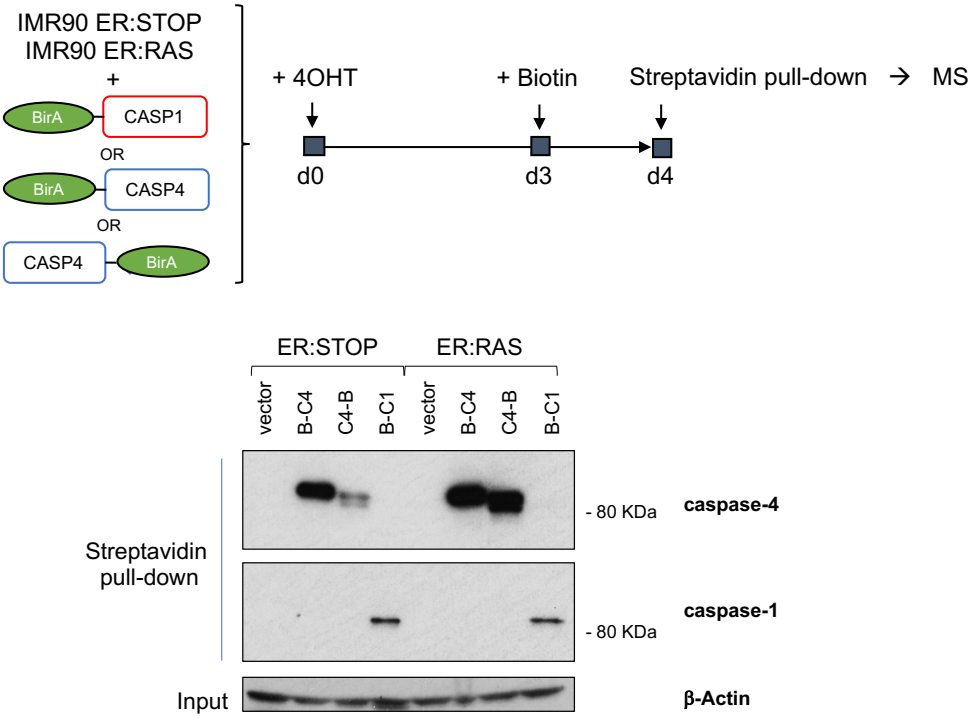

Figure 5.2 Schematic diagram of the streptavidin pull-down followed by MS analysis approach to detect potential inflammatory caspase interactors in OIS

On top, a schematic representation of the screening performed to identify potential interactors of caspase-1 and caspase-4 in OIS. Below, IMR90 ER:STOP/ER:RAS cells had been infected with the indicated vectors. 4 days after the addition of 4-hydroxytamoxifen and 22 h after biotin addition, cells were lysed and biotinylated proteins were pull-down with streptavidin beads. Western blotting was performed using the indicated antibodies for caspase-1 and caspase-4 detection in streptavidin-pulldown samples.

MS = Mass Spectrometry; 4OHT = 4-hydroxytamoxifen.

To identify candidate interactors in OIS, we calculated logFC values using LFQ intensity values of ER:RAS + caspase-1-BirA or ER:RAS + caspase-4-BirA samples relative to ER:RAS + empty vector control. The same analysis was performed in non-senescent (ER:STOP) samples. Potential interactors for each caspase were considered as those with logFC>2 in senescent but logFC<2 in non-senescent cells. For a more stringent analysis, only proteins that were enriched in both caspase-4-BirA samples were selected as potential caspase-4 interactors.

Using this approach, 83 and 72 proteins were identified as potential interactors of caspase-4 and caspase-1 respectively in OIS (Figure 5.3). Interestingly, there was a significant overlap among caspase-1 and caspase-4 potential interactors in OIS (41 identified proteins were common candidates). For further exploration, potential caspase-1 and caspase-4 interactors in OIS were classified into categorical cellular component terms using the DAVID Bioinformatics Resources 6.8 (334). (Table 5.1). Both caspase-1 and caspase-4 potential interactors were mostly found in the cytosol.

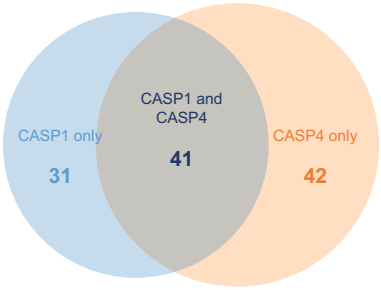

Figure 5.3 Potential interactors of caspase-1 and/or caspase-4 in OIS

Above, a Venn diagram of the identified potential interactors of caspase-1, caspase-4 or both in OIS is shown. A heatmap of the logFC values of the potential candidate interactors of caspase-1 and caspase-4 is shown in the following page.

Cellular component enrichment analysis of caspase-4 candidate interactors in OIS:					
Term	**Count**	**p-value**	**Bonferroni**	**Benjamini**	**FDR**
GO:0005829~cytosol	45	3.0E-11	4.13E-09	4.13E-09	3.54E-08
GO:0070062~extracellular exosome	38	3.9E-09	5.30E-07	2.65E-07	4.55E-06
GO:0045335~phagocytic vesicle	4	9.4E-04	0.12	0.04	1.10
GO:0042470~melanosome	5	1.6E-03	0.19	0.05	1.84
GO:0005737~cytoplasm	39	4.0E-03	0.42	0.10	4.57
GO:0035145~exon-exon junction complex	3	5.2E-03	0.51	0.11	5.97
GO:0005739~mitochondrion	15	5.5E-03	0.53	0.10	6.31
Cellular component enrichment analysis of caspase-1 candidate interactors in OIS:					
Term	**Count**	**p-value**	**Bonferroni**	**Benjamini**	**FDR**
GO:0005829~cytosol	23	1.47E-03	0.15	0.15	1.65
GO:0035145~exon-exon junction complex	3	2.68E-03	0.26	0.14	3.00

Table 5.1 Cellular component enrichment analysis of potential interactors of caspase-1 or caspase-4 in OIS

The 83 and 72 respectively identified caspase-1 or caspase-4 interactor candidates in OIS were interrogated for cellular component enrichment using DAVID Bioinformatics Resources 6.8.

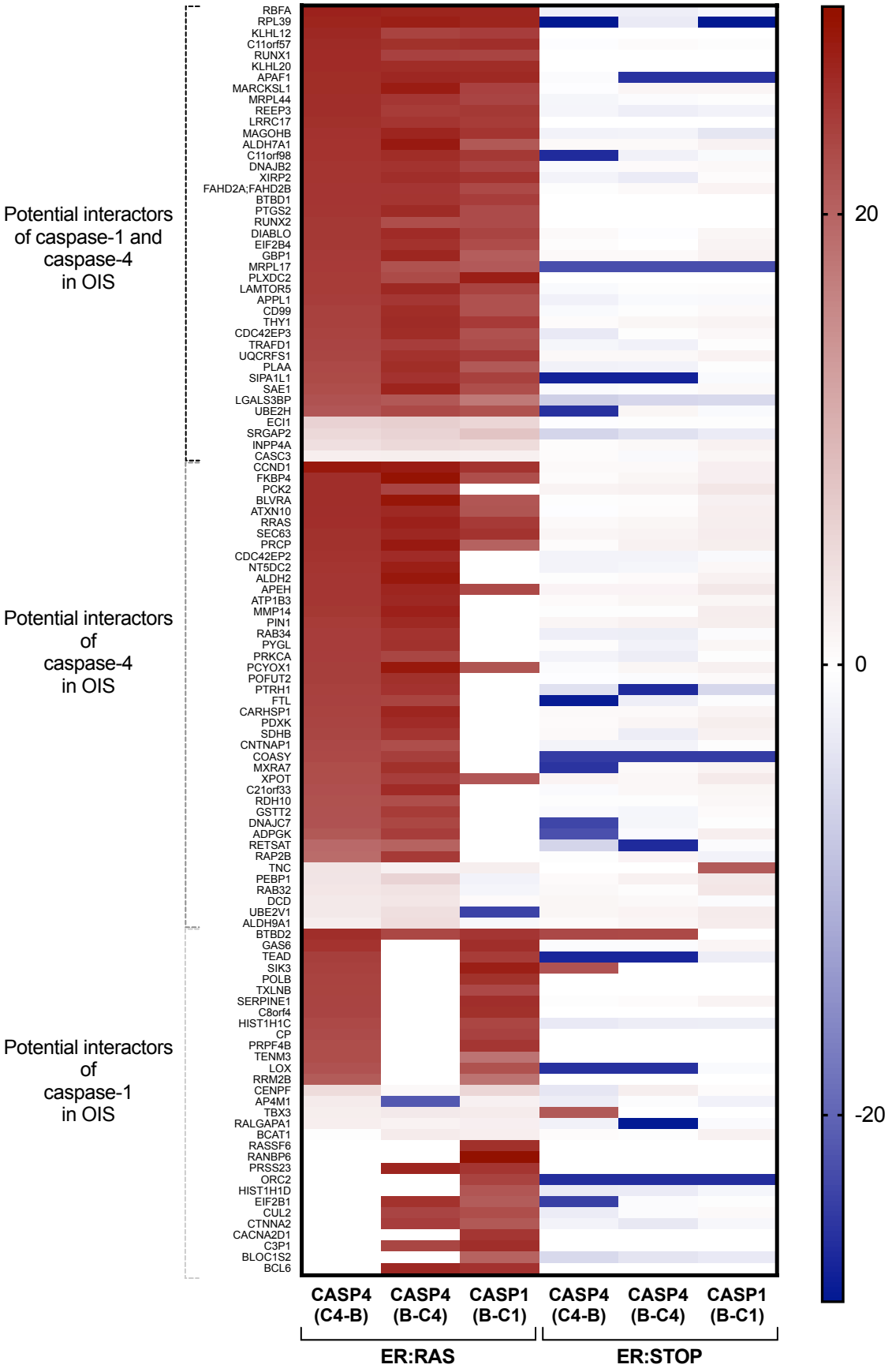
Potential interactors of caspase-1 and caspase-4 in OIS
Potential interactors of caspase-4 in OIS
Potential interactors of caspase-1 in OIS
RBFA
RPL39
KLHL12
C11orf57
RUNX1
KLHL20
APAF1
MARCKSL1
MRPL44
REEP3
LRRC17
MAGOHB
ALDH7A1
C11orf98
DNAJB2
XIRP2
FAHD2A;FAHD2B
BTBD1
PTGS2
RUNX2
DIABLO
EIF2B4
GBP1
MRPL17
PLXDC2
LAMTOR5
APPL1
CD99
THY1
CDC42EP3
TRAFD1
UQCRFS1
PLAA
SIPA1L1
SAE1
LGALS3BP
UBE2H
ECI1
SRGAP2
INPP4A
CASC3
CCND1
FKBP4
PCK2
BLVRA
ATXN10
RRAS
SEC63
PRCP
CDC42EP2
NT5DC2
ALDH2
APEH
ATP1B3
MMP14
PIN1
RAB34
PYGL
PRKCA
PCYOX1
POFUT2
PTRH1
FTL
CARHSP1
PDXK
SDHB
CNTNAP1
COASY
MXRA7
XPOT
C21orf33
RDH10
GSTT2
DNAJC7
ADPGK
RETSAT
RAP2B
TNC
PEBP1
RAB32
DCD
UBE2V1
ALDH9A1
BTBD2
GAS6
TEAD
SIK3
POLB
TXLNB
SERPINE1
C8orf4
HIST1H1C
CP
PRPF4B
TENM3
LOX
RRM2B
CENPF
AP4M1
TBX3
RALGAPA1
BCAT1
RASSF6
RANBP6
PRSS23
ORC2
HIST1H1D
EIF2B1
CUL2
CTNNA2
CACNA2D1
C3P1
BLOC1S2
BCL6
CASP4 (C4-B)
CASP4 (B-C4)
CASP1 (B-C1)
CASP4 (C4-B)
CASP4 (B-C4)
CASP1 (B-C1)
ER:RAS
ER:STOP
20
0
-20

5.2 siRNA targeting of selected BioID candidates in OIS

5.2.1 Selection of candidates from the BioID screening results

In the process of canonical inflammasome activation, a key upstream signalling event is the interaction of caspase-1 with other proteins through the caspase recruitment domain (CARD) (see section 1.2.1.1). These CARD-CARD interactions occur between the CARD motif of caspase-1 and the CARD motif of the binding protein.

Seven proteins with a CARD domain were identified in the mass spectrometry results generated from the BioID screening. Strikingly, the only CARD-containing protein identified as a potential interactor of both caspase-1 and caspase-4 in OIS was the apoptotic peptidase activating factor 1 (Apaf-1) (Figure 5.4).

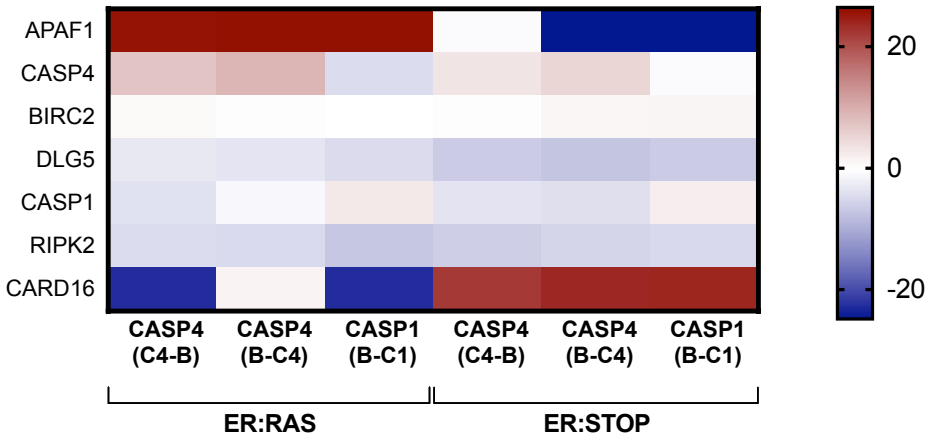

Figure 5.4 CARD-containing proteins identified in the BioID screening results analysis
Heatmap of the logFC values of the potential candidate interactors of caspase-1 and caspase-4 containing a CARD domain. All proteins identified by mass spectrometry were screened for human proteins containing a CARD domain (IPR001315; list accessible at: http://www.ebi.ac.uk/interpro/entry/IPR001315/taxonomy). C4-B, B-C4 and B-C1 refer to the overexpressed constructs.

Apaf-1 is a master signalling protein of apoptosis: after detecting cytochrome C released from mitochondria, it forms a multimeric protein cytosolic complex called the apoptosome, which recruits and activates caspase-9 through CARD domain homotypic interactions between Apaf-1 and caspase-9 (335). Caspase-9 then activates the effector caspase-3, which cleaves many substrates, ultimately leading to apoptotic cell death.

Interestingly, analysis of the BioID screening data also revealed significant potential interaction of cytochrome C with caspase-1 in proliferating cells and with caspase-4 in both proliferating and senescent cells (see Appendix). Moreover, Smac/DIABLO (hereafter referred as DIABLO), which promotes apoptosis by blocking the inhibitors of apoptosis (IAPs) proteins (336), was also detected in the screen as a candidate interactor protein with both caspases in OIS (Figure 5.3).

Of note, CARD16 was enriched in caspase-1 and caspase-4 pull-down samples in ER:STOP samples but not in ER:RAS samples (Figure 5.4), suggesting that a potential interaction between CARD16 and inflammatory caspases is lost in OIS. Interestingly, CARD16 is a CARD-only protein (COP) that acts a negative regulator of caspase-1 and caspase-4 activity and inhibits IL-1β release from LPS-stimulated monocytes as well as prevents inflammatory caspase-mediated cell death in non-immune cells (337-339).

The guanylate-binding protein 1 (GBP1), a protein involved in host defence, was another candidate interactor protein of both caspase-1 and caspase-4 identified in the BioID screening (Figure 5.3). Of note, GBP1 can be cleaved by caspase-1 and secreted in a caspase-1 dependent manner (340), is necessary for caspase-11 LPS-driven pyroptosis in some infection models (341) and causes mitochondrial dysfunction and senescence in macrophages (342).

In light of their previously described functions, a targeted approach was conducted towards the potential role of Apaf-1, DIABLO, cytochrome C and GBP1 in OIS using siRNA. The effect of the knockdown of these genes was assessed in terms of proliferation as well as regulation of the SASP.

5.2.2 APAF-1 regulates IL-1 signalling in OIS

Efficiency of the siRNA-mediated knockdown targeting of candidates was validated by mRNA expression. All siRNA significantly decreased the mRNA levels of their target genes (Figure 5.5A).

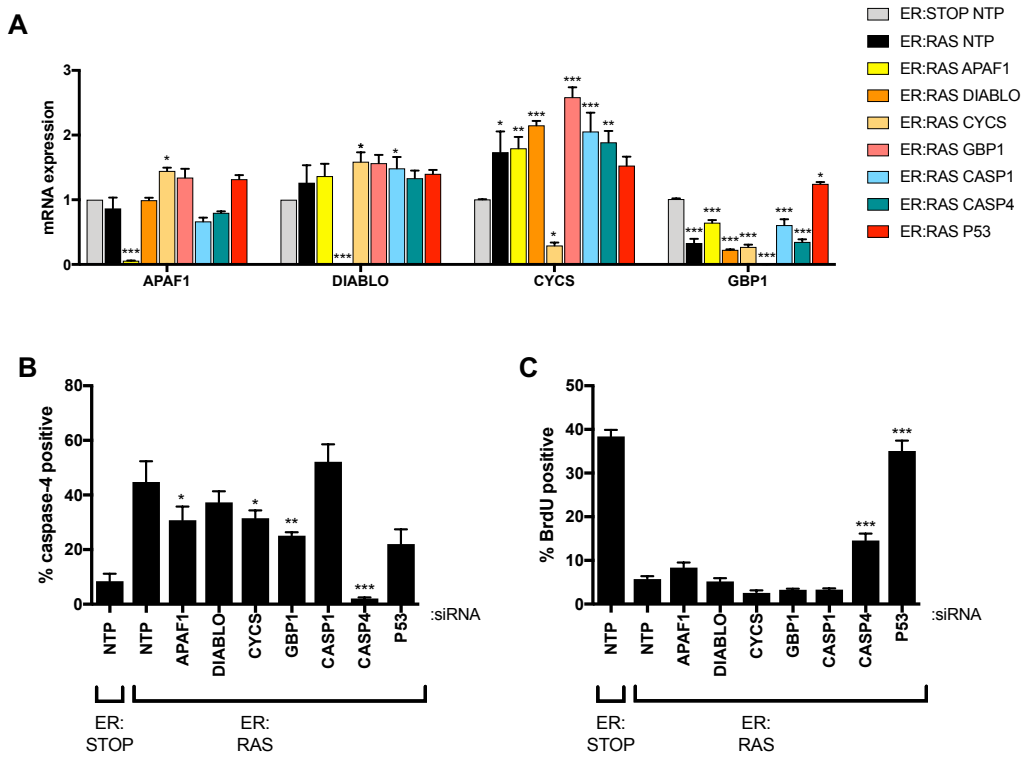

Figure 5.5 siRNA-targeting of APAF1, DIABLO, CYCS and GBP1 does not bypass proliferation arrest in OIS

IMR90 ER:STOP/ER:RAS cells were transfected with the indicated siRNAs 0 and 3 days after 4-hydroxytamoxifen addition. All samples were treated with 4-hydroxytamoxifen. A. APAF1, DIABLO, CYCS and GBP1 mRNA expression was quantified 5 days after addition of 4-hydroxytamoxifen. Dara are shown as mean ± s.e.m, n=3, one-way ANOVA and post-hoc Bonferroni´s multiple comparisons test comparing to ER:STOP NTP, *p<0.05, **p<0.01, ***p<0.01, where unstated non-significant. Data obtained in collaboration with Dr Fraser Millar. B. Caspase-4 was quantified 5 days after the addition of 4-hydroxytamoxifen by high-content analysis. Data are shown as mean ± s.e.m, n=3, one-way ANOVA and post-hoc Bonferroni´s multiple comparisons comparing senescent samples to ER:RAS NTP, *p<0.05, **p<0.01, ***p<0.01, where unstated non-significant. C. BrdU incorporation was quantified 5 days after

the addition of 4-hydroxytamoxifen. Data are shown as mean ± s.e.m, n=3, one-way ANOVA and post-hoc Bonferroni´s multiple comparisons comparing senescent samples to ER:RAS NTP, ***p<0.01, where unstated non-significant,.

NTP = non-targeting pool. Where asterisks are not shown, comparisons are non-significant.

APAF1, DIABLO, CYCS and GBP1 knockdown slightly decreased the levels of caspase-4 in senescence (Figure 5.5B). Measurement of BrdU incorporation five days after the addition of 4-hydroxytamoxifen showed only a marginal increase in cellular proliferation when targeting APAF1 and no difference when targeting the other candidates. (Figure 5.5C).

Notably, downregulation of APAF1 (but not CYCS or DIABLO) significantly decreased the levels of IL1A, IL1B, IL8 and IL6 mRNA expression compared to control senescent cells (Figure 5.6A). These substantial changes were also observed by immunofluorescence staining of IL-1α and IL-1β (Figure 5.7).

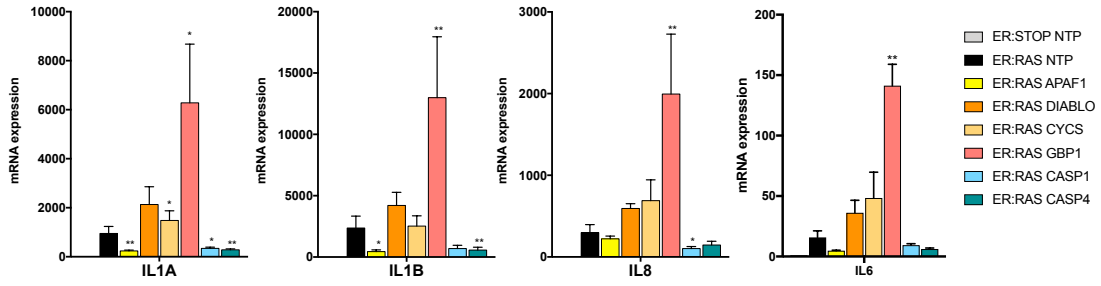

Figure 5.6 IL-1 signalling is controlled by APAF1 in RAS^{G12V}-induced senescence in human fibroblasts

IMR90 ER:STOP/ER:RAS cells were transfected with the indicated siRNAs 0 and 3 days after 4-hydroxytamoxifen addition. All samples were treated with 4-hydroxytamoxifen. **A**. IL1A, IL1B, IL8 and IL6 mRNA expression was quantified 5 days after addition of 4-hydroxytamoxifen. Dar are shown as mean ± s.e.m, ratio paired t tests were performed comparing ER:RAS samples to ER:RAS NTP control, n=3, *p<0.1, **p<0.05, where unstated non-significant, Data obtained in collaboration with Dr Fraser Millar.

NTP = non-targeting pool.

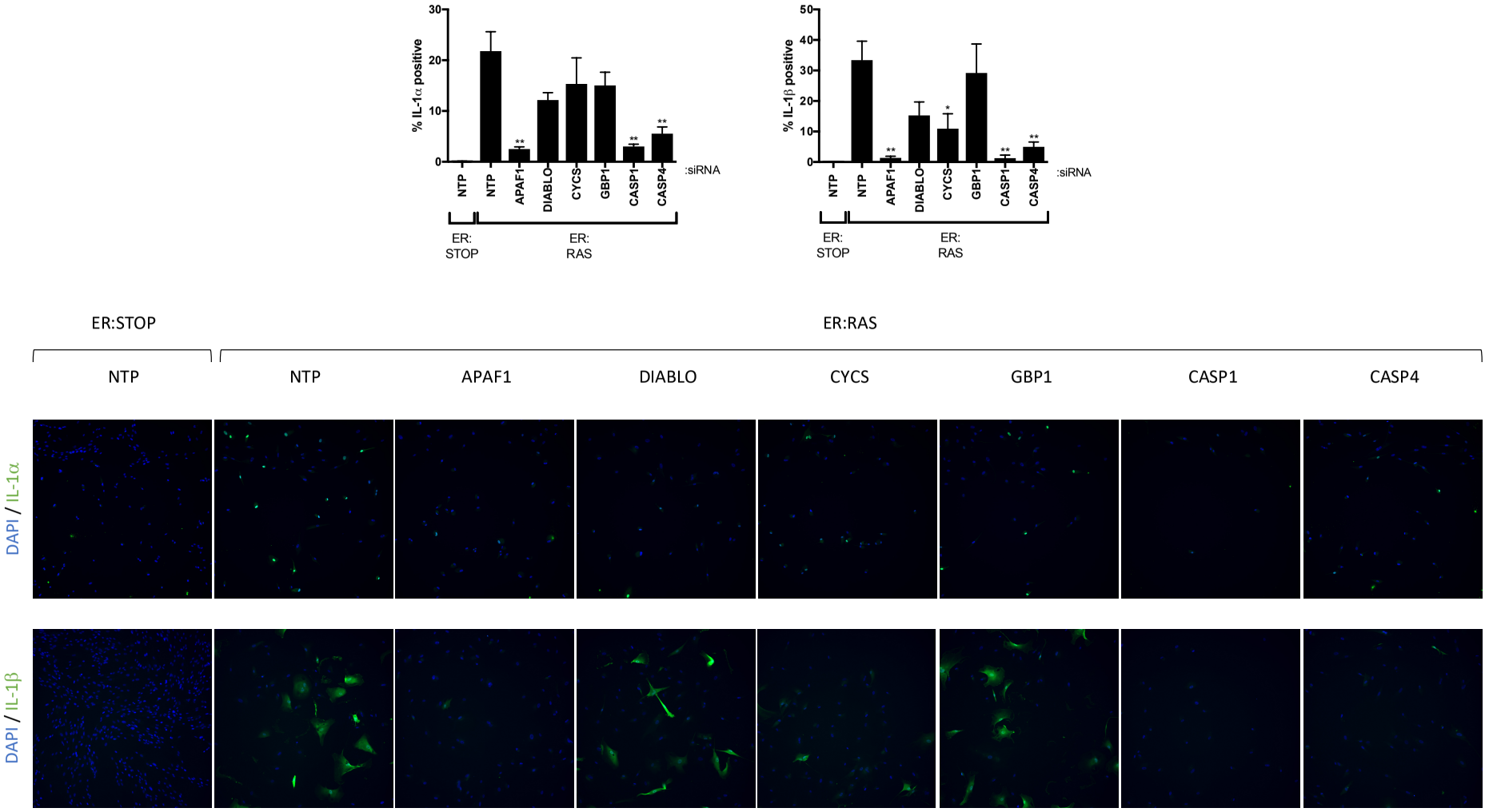
% IL-1α positive
30
20
10
0
NTP
NTP
APAF1
DIABLO
CYCS
GBP1
CASP1
CASP4
:siRNA
ER: STOP
ER: RAS
% IL-1β positive
50
40
30
20
10
0
ER:STOP
ER:RAS
NTP
NTP
APAF1
DIABLO
CYCS
GBP1
CASP1
CASP4
DAPI / IL-1α
DAPI / IL-1β

Figure 5.7 IL-1α and IL-1β protein levels are significantly decreased after APAF1-targeting in RAS^{G12V}-OIS

See previous page. IL-1α and IL-1β proteins levels were quantified 8 days after 4-hydroxytamoxifen addition by high-content analysis. Data are shown as mean ± s.e.m, n=3, one-way ANOVA and post-hoc Bonferroni´s multiple comparisons test comparing all senescent samples to ER:RAS NTP, *p<0.05, **p<0.01, where unstated non-significant. NTP = non-target pool.

Importantly, the secretion of IL-1β was also impaired to a similar extent when knocking down either APAF1 of CASP1 (Figure 5.8). In all, these results suggest a prominent role for Apaf-1 in mediating SASP signalling independently of cytochrome C or Diablo.

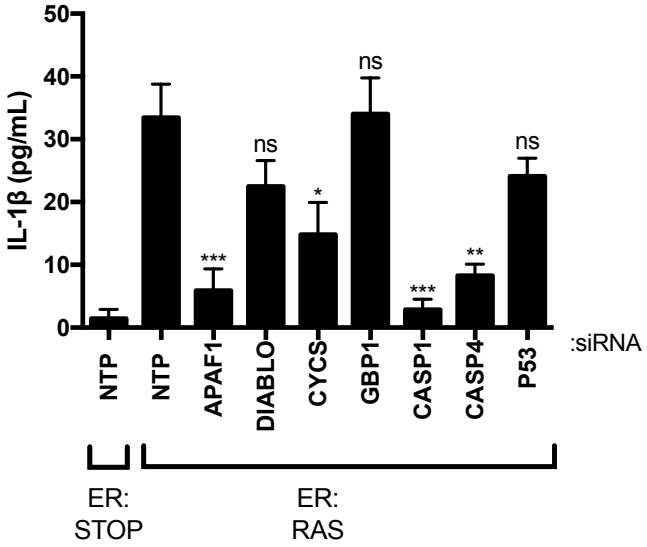

Figure 5.8 IL-1β secretion is significantly impaired after APAF1-targeting in RAS^{G12V}-OIS

Released IL-1β was detected by ELISA 8 days after 4-hydroxytamoxifen addition. Data are shown as mean ± s.e.m, n=3, one-way ANOVA and post-hoc Bonferroni's multiple comparisons comparing senescent samples to ER:RAS NTP, *p<0.05, **p<0.01, ***p<0.01, where unstated non-significant.

In contrast to APAF1, GBP1 knockdown increased the mRNA levels of IL1A, IL1B, IL8 and IL6 in OIS, suggesting that GBP1 may be a negative regulator of IL-1 signalling in OIS (Figure 5.6). However, the effect of the increased translation of these genes was not observed at the protein level, as there were no significant changes in the protein levels of IL-1α and IL-1β or IL-1β secretion when depleting GBP1 (Figure 5.7, 5.8).

5.3 Summary

Using a BioID proteomic approach coupled to mass spectrometry downstream analysis, a screening for potential interacting proteins with caspase-1 and caspase-4 in OIS was performed. 41 proteins were identified as potential interactors of both caspase-1 and caspase-4 in OIS. Moreover, 31 and 42 proteins were identified as candidate interactors of caspase-1 or caspase-4 respectively. Of note, there was a significant overlap among the identified candidate interactors of both inflammatory caspases.

A functional validation of selected hits was conducted. SiRNA-mediated knockdown in OIS of selected candidates from the BioID screening results (APAF1, DIABLO, CYCS and GBP1) was performed and BrdU incorporation as well as SASP quantification were used as readouts. Although none of the targeted genes had a remarkable effect on the bypass of cell proliferation, strikingly, APAF1 downregulation significantly decreased the mRNA levels of some key SASP factors to a similar extent than CASP1 knockdown. Moreover, APAF1 targeting did also reduce the levels of intracellular IL-1α and IL-1β as well as significantly impair IL-1β release. Importantly, Apaf-1 was the only protein containing a CARD domain identified as a potential interactor of caspase-1 and caspase-4 in OIS.

In all, these results suggest a potential interaction between inflammatory caspases and Apaf-1 in OIS which controls IL-1 signalling.

Chapter 6 - Discussion

6.1 Caspase-4 and IL-1 signalling in OIS

IL-1 proinflammatory cytokines (IL-1α and IL-1β) are key apical SASP components and master regulators of inflammation in senescent cells (80, 100). A previous study had shown that IL-1 signalling and the SASP are controlled by caspase-1 in OIS (80). However, in this thesis, the role of caspase-4 in senescence has been investigated for the first time.

The results here presented have unveiled a new role for caspase-4 in regulating IL-1 signalling in a sterile context. First, a transcriptomic approach was conducted to interrogate the role of caspase-4 in OIS. Downstream analysis of the obtained transcriptomic data revealed that downregulation of caspase-4 in OIS attenuates the inflammatory response. A deeper exploration of these results showed that caspase-4 targeting directly impacted on the mRNA and protein levels of different SASP components and, in particular, the exponential increase of IL-1β in OIS was halted. Nonetheless, both mature intracellular IL-1β and released IL-1β were reduced to a similar extent when targeting either caspase-1 or caspase-4. Altogether, these results suggest that the roles of the canonical and non-canonical inflammasome in regulating IL-1 signalling in OIS are critical and non-redundant (Figure 6.1).

Caspase-4 limited the induction of the SASP in non-senescent cells to which conditioned media was added to a greater extent than caspase-1. This suggests differential roles for caspase-1 and caspase-4 in regulating the SASP. However, the addition of conditioned media to simulate paracrine senescence has two important limitations: [1] SASP content changes over time and conditioned media collected at day 8 does not reflect earlier stage of senescence (82) and [2] addition of concentrated conditioned media at a certain point might overstimulate proliferating cells. To better understand the role of caspase-4 in paracrine senescence, it would be convenient to

perform true co-culture experiments, in which senescent and non-senescent cells are cultured together, either by using trans-well chambers that prevent direct contact between cells or fluorescent markers that allow to distinguish different cellular populations in co-culture (80).

Noteworthy, a key mediator for the maintenance of SASP signalling is IL-1R (80), which recognizes both IL-1β and IL-1α. In contrast to IL-1β, IL-1α secretion has been described to be caspase-1 independent (273). Of note, in a model of *Francisella novicida* infected human macrophages, IL-1α release was shown to be caspase-4 dependent and caspase-1 independent (217). It would be interesting to investigate whether caspase-4 and caspase-1 have a similar effect on the amount of IL-1α released from senescent cells. Moreover, because the SASP is a highly heterogenous phenotype (24), hypothetically, caspase-4 may be regulating a partially different SASP subset. In this sense, comparing the proteome of conditioned media of caspase-1 and caspase-4 depleted senescent cells could be informative.

In contrast to caspase-1, caspase-4 does not cleave IL-1β directly (270). How caspase-4 regulates IL-1β post-translationally is still under debate. It has been suggested that caspase-4 is an upstream regulator of caspase-1 and that direct interaction between caspase-1 and caspase-4 is involved in the regulatory mechanism (229, 271, 272). However, the results of the BioID experimental approach suggest no robust interaction between caspase-1 and caspase-4 in senescence (Figure 5.4), suggesting that inflammasome platforms that contain caspase-1 do not recruit caspase-4 and vice versa.

To date, the better characterized caspase-4 downstream mechanisms involve the direct cleavage of a substrate. However, the absence of highly specific caspase inhibitors is a substantial limitation when investigating the role of a caspase catalytic activity, specially, when trying to depict the effect of a particular caspase (see section 1.2.1.1). One way to circumvent this obstacle involves direct targeting of the identified substrates. In particular, because recent discoveries have brought to light an indisputable key role for gasdermin-D downstream inflammatory caspases in pyroptosis (283-285), gasdermin-D was investigated as a potential downstream effector of inflammasome activation in senescence. Experimental data originated during this

thesis shows that inflammatory caspase activity in OIS is accompanied by the cleavage of gasdermin-D; however, pyroptosis is not present during OIS. Taking into account that apoptosis resistance is one of the hallmarks of senescence, could there also exist mechanisms that prevent pyroptosis during senescence? Exploiting apoptosis resistance has been key in the development of senolytics. Therefore, it is possible that understanding a potential pyroptotic resistance mechanism could contribute to the development of new senolytic strategies. Furthermore, downregulation of gasdermin-D in OIS marginally decreased IL-1β secretion, suggesting that IL-1β is not released from senescent cells through gasdermin-D-formed membrane pores, but by gasdermin-D independent mechanisms.

Besides gasdermin-D, the other key caspase-4 substrate with a well-described role is the cGMP-AMP (cGAMP) synthase (cGAS). Inflammatory caspases cleave cGAS in response to viral DNA and dampen cGAS-STING IFN production (209). Recently, a key role has also been describe for the innate immune DNA sensor cGAS in senescence: cGAS detects cytosolic DNA fragments in senescent cells and activates the production of SASP factors through the cGAS-STING pathway (97-99). Noteworthy, cGAS has been described to activate the non-canonical inflammasome in age-related macular degeneration (343). Further research on the role of cGAS both upstream and downstream caspase-4 activation might provide insights into non-canonical inflammasome signalling in senescence.

Activation of caspase-1 occurs upon recruitment to a cytosolic multiprotein complex through CARD-CARD domain homotypic interactions (175). In contrast, caspase-4 is activated in the cytosol by specific lipid species (193). During this thesis research, a proteomic screening was conducted to identify potential inflammatory caspase interactors in OIS by proximity biotinylation. None of the previously described CARD-containing caspase-1 recruiters in canonical inflammasome assembly were identified when analysing the list of hits of potential interactors of inflammatory caspases in OIS. However, one CARD-containing protein, Apaf-1, was found to be a potential interactor of both caspase-1 and caspase-4 specifically in OIS. Intriguingly, resembling inflammasome formation, Apaf-1 also forms a cytoplasmic oligomeric complex and recruits caspase-9 through homotypic CARD-CARD domain interactions (335).

Downregulation of endogenous APAF-1 in OIS resulted in a strong inhibition of the expression of some SASP factors and, in particular, of IL-1β levels and cellular release. Altogether, these results suggest that Apaf-1 interacts with caspase-1 and caspase-4 in OIS and activates their respective inflammasomes, thus regulating IL-1 signalling. How Apaf-1 is activated in OIS should be further investigated. Apoptosome formation is initiated by cytochrome C release from mitochondria (335); however, cytochrome C targeting in RAS^{G12V} did not recapitulate the regulation of IL-1 signalling observed upon Apaf-1 targeting. Moreover, the role of Apaf-1 in non-cell autonomous signalling has not been investigated in this thesis. Co-culture experiments targeting Apaf-1 could provide insights into whether Apaf-1 mediates non-cell autonomous senescence.

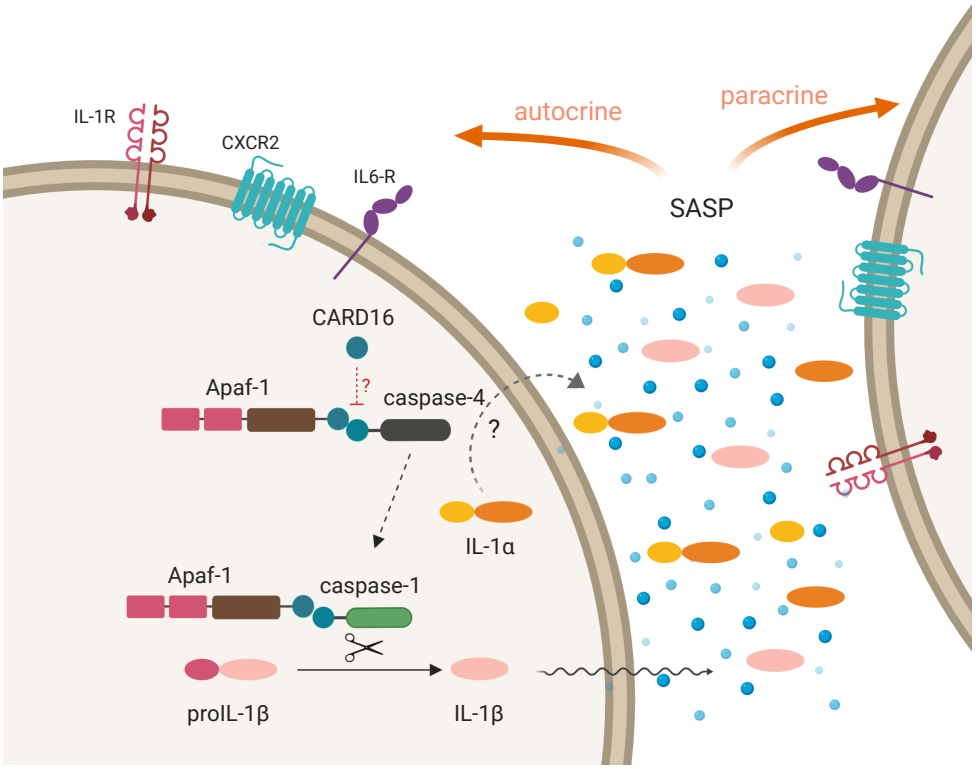

Figure 6.1 Model for the mechanism by which inflammatory caspases regulate IL-1 signalling in OIS

In this hypothetical model, Apaf-1 binds either caspase-1 or caspase-4 through the homotypic interaction of their CARD domains. Consequently, caspase-1 and caspase-4 are activated and proIL-1β cleaved and released from senescent cells, together with other SASP factors that induce autocrine and paracrine effects. A potential role for caspase-4 in the release of IL-1α is also discussed in the text.

A limitation of this study is that the potential interaction between caspase-1 or caspase-4 and Apaf-1 in OIS has not been validated. It would be very interesting to validate the physical Apaf-1+caspase-1 or Apaf-1+caspase-4 interaction by means of an appropriate technique, for instance, a co-immunoprecipitation assay. Nonetheless, two independent strategies conducted in this thesis (interactome analysis by BioID + APAF-1 siRNA-mediated targeting) support a role for Apaf-1 in regulating IL-1 signalling in OIS. Moreover, caspase-1, caspase-4 and Apaf-1 bear CARD domains, and these have been strongly linked to their interaction with other proteins and functional role in all cases. Finally, caspase-4 and Apaf-1 interaction has been described once previously. Hu et al. co-transfected 293T with different plasmids to overexpress Apaf-1 and other CARD-containing proteins; interestingly, caspase-4 and caspase-9 were co-immunoprecipitated with Apaf-1, in contrast to caspase-3 (344).

From a more conceptual point of view, these results suggest that an Apaf-1 – inflammatory caspase axis regulates an inflammatory process, and hence the classic apoptotic vs inflammatory functional division does not only misrepresent caspase functions but also other proteins in their signalling pathways. Indeed, it would be intriguing to explore the role of Apaf-1 in other inflammatory settings. Noteworthy, the apoptotic caspase-8, which has a key described role in apoptosis, can also be recruited to canonical inflammasomes, regulate caspase-1 activity and even, in some scenarios, directly cleave proIL-1β (175). Therefore caspase-4 might, in a similar way to caspase-8, be involved in both inflammatory and cell death processes.

Two potential novel negative regulators of the SASP can be proposed from the data presented in Chapter 5. On the one hand, the CARD-containing protein CARD16 was identified as a potential interactor of caspase-1 and caspase-4 only in proliferating but not the counterpart senescent samples and, interestingly, several studies have described an inhibitory caspase-1 function for CARD16 (337, 338). On the other hand, GBP1, which has also been functionally linked to inflammatory caspases by others (340-342), was identified as a potential interactor of both caspase-1 and caspase-4 only in senescent cells. Further GBP1 siRNA-mediated targeting in OIS resulted in increased transcriptional levels of IL1A, IL1B, IL6 and IL8. Further research on the roles of CARD16

and GBP1 might provide more insights into the complexity of the SASP machinery and regulation.

6.2 The role of caspase-4 in senescence beyond IL-1 signalling

Importantly, activation of the non-canonical inflammasome by intracellular LPS challenge resulted in reduced cellular proliferation whereas caspase-4 targeting in OIS partially bypassed cell proliferation arrest. Hence, several questions arise from the fact that caspase-4 regulates cell proliferation. Which is the upstream stimulus that induces caspase-4-dependent cell proliferation arrest? The results presented in this thesis suggest, that, in contrast to IL-1 signalling, APAF-1 and caspase-1 do not regulate cellular proliferation. Intracellular LPS in itself, which directly binds caspase-4, causes caspase-4-dependent proliferation arrest. Noteworthy, senescent cells present an altered lipidome (44). An exciting hypothesis is that the change in lipid content propitiates specific contacts between certain endogenous lipid species and caspase-4, activating the non-canonical inflammasome towards proliferation regulation in OIS (Figure 6.3). It will be interesting to see whether in the near future novel functional interactions between lipids, specially of endogenous origin, and inflammatory caspases are described.

The experimental data included in this thesis suggests that caspase-4 catalytic activity is not involve in the regulation of cell proliferation and its effect may be limited (if any) to the regulation of the SASP. Mechanistically, the data presented in this thesis shows that caspase-4 can partially control cell proliferation in senescence through the regulation of the phosphorylation state of pRb and hence the transcription of E2F target genes, necessary for cell cycle progression. In senescence, hypophosphorylation of pRb has been classically described as a downstream signalling event of the stabilization of p53, following DDR activation, or p16 upregulation due to INK4-ARF locus de-repression. However, the results here presented suggest that caspase-4 regulation of pRb phosphorylation state is independent of the mRNA and protein levels of p53, p21 and p16.

How caspase-4 contributes to pRb hypophosphorylation requires further research. The activity of CDK–cyclin complexes is necessary to phosphorylate and inactivate pRb (345). In senescence, a number of CDKi have been described to inhibit the activity of CDK-cyclin complexes (24). TGF-β has been suggested to both upregulate the mRNA levels of CDKN2B and promote protein stabilization of the cell cycle inhibitor p15, consequently preventing CDK4-cyclin D association in senescence (346). Although caspase-4 targeting in RAS^{G12V}-OIS did not affect the mRNA levels of CDKN2A, the levels of p15 protein were not analysed. Therefore, it is not possible to rule out the implication of p15 downstream caspase-4 (Figure 6.2).

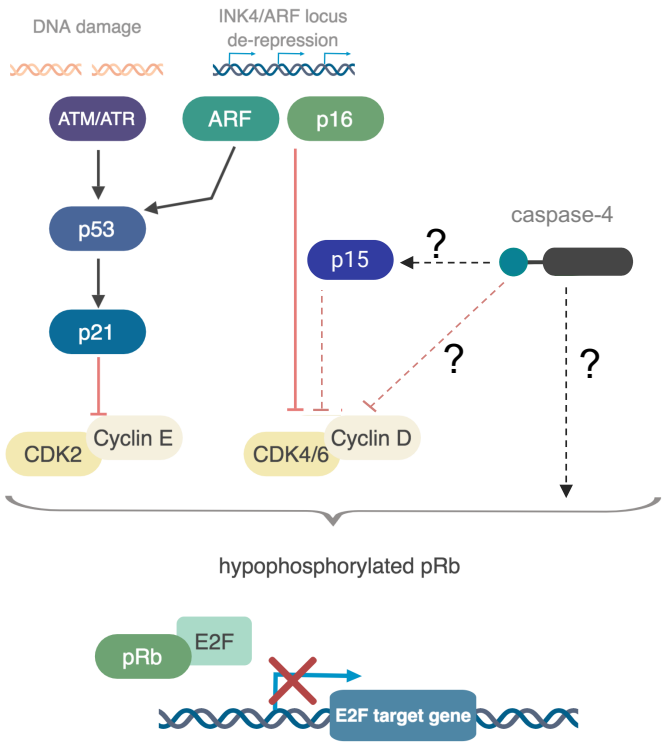

Figure 6.2 Potential mechanisms by which caspase-4 regulates pRb phosphorylation in senescence

Caspase-4 regulates proliferation downstream p53, p21, p16 protein levels. Of note, cyclin D was identified as a potential interactor of caspase-4 exclusively in senescence. Therefore, one hypothesis is that, caspase-4 might function as a CDKi itself preventing CDK4/6-cyclin D association/activity. Nonetheless, caspase-4 might be regulating pRb phosphorylation by other potential mechanisms such as p15 protein stabilization.

Whereas p21 binds CDK-cyclin complexes, p16 prevents the association of CDK4/6 and cyclin D by binding exclusively to CDK4/6 (347). Interestingly, G1/S-specific cyclin D1 was identified as a potential interactor of caspase-4 specifically in OIS (Figure 5.3). Therefore, one hypothetical mechanism could be that, similarly to p16 binding to CDK4/6, caspase-4 sequesters cyclin-D and therefore prevents its binding to CDK4/CDK6 (Figure 6.2). Further studies that confirm the potential interaction of caspase-4 and cyclin D in senescence could provide insights into the validity of this hypothesis. Alternatively, the non-canonical inflammasome might regulate phosphorylation of pRb through an unexplored pathway during this thesis' research such as defective ribosomal biogenesis signalling (348).

6.3 Concluding remarks

In summary, the results described throughout this thesis suggest that caspase-4 is at the crossroads of cellular inflammation and cellular proliferation in senescence. Inflammatory caspases, potentially activated through the homotypic interaction of their CARD domains with Apaf-1, regulate IL-1 signalling in OIS. Nonetheless, intracellular LPS alone is able to elicit a senescence response through the activation of caspase-4. Remarkably, in both LPS-driven senescence and OIS models, caspase-4 mediates cellular proliferation arrest through the regulation of the phosphorylation of pRb (Figure 6.3).

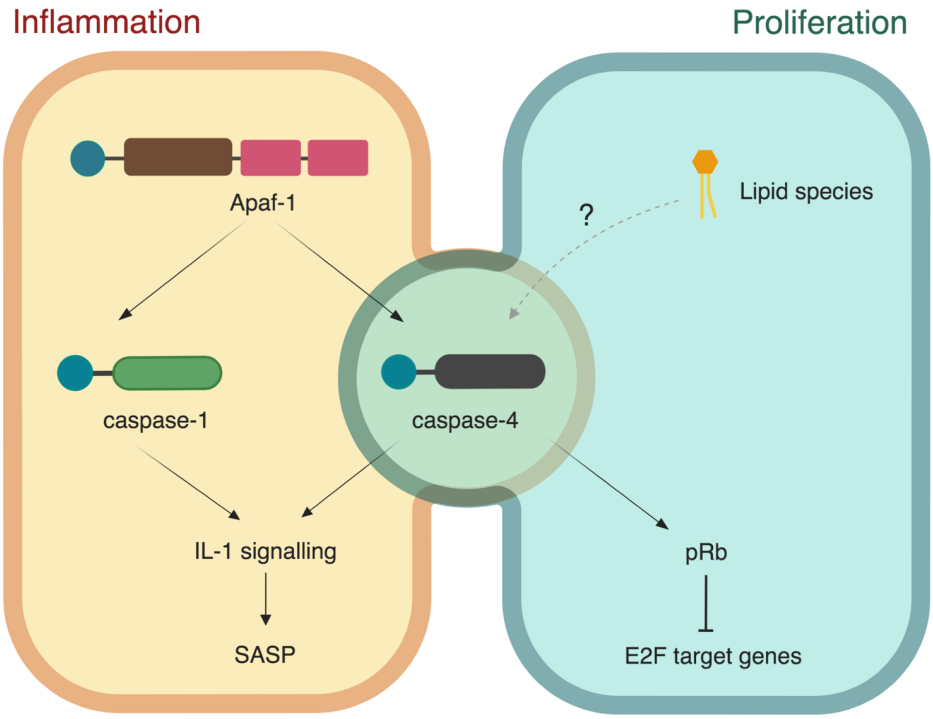

Figure 6.3 The dual role of caspase-4 in OIS

Schematic diagram of the model proposed for caspase-4 in senescence in regulating both IL-1 signalling (together with caspase-1) as well as cellular proliferation through pRb regulation.

Given the current excitement in therapeutic strategies based on senescence targeting, a better understanding of the complexity entailed in senescence might contribute to the development of therapies. In particular, elucidating the mechanisms that govern the SASP might be critical to the development of therapeutic strategies focused on the selective depletion of the SASP (161). At present, SASP targeting remains elusive because of the off-target effects of current SASP-targeting approaches (142, 162). Here, not only new insights are provided into inflammasome signalling in senescence but also novel SASP regulators, such as Apaf-1 have been identified.

Nonetheless, recent insights into the role of caspase-4 in various cellular processes, including now senescence, reveal an indisputable role for this protein in numerous contexts that might have previously been overlooked or unexplored. The results here presented contribute to expand our knowledge of the non-canonical inflammasome and provide new insights into the biology of inflammasomes which might be relevant to senescence and beyond.

Bibliography

1. Hayflick L, Moorhead PS. The serial cultivation of human diploid cell strains. Exp Cell Res. 1961;25:585-621.
2. Hernandez-Segura A, Nehme J, Demaria M. Hallmarks of Cellular Senescence. Trends Cell Biol. 2018.
3. Salama R, Sadaie M, Hoare M, Narita M. Cellular senescence and its effector programs. Genes Dev. 2014;28(2):99-114.
4. Kuilman T, Michaloglou C, Mooi WJ, Peeper DS. The essence of senescence. Genes Dev. 2010;24(22):2463-79.
5. Munoz-Espin D, Serrano M. Cellular senescence: from physiology to pathology. Nat Rev Mol Cell Biol. 2014;15(7):482-96.
6. Dimri GP, Lee XH, Basile G, Acosta M, Scott C, Roskelley C, et al. A Biomarker That Identifies Senescent Human-Cells in Culture and in Aging Skin in-Vivo. P Natl Acad Sci USA. 1995;92(20):9363-7.
7. Kurz DJ, Decary S, Hong Y, Erusalimsky JD. Senescence-associated beta-galactosidase reflects an increase in lysosomal mass during replicative ageing of human endothelial cells. Journal of Cell Science. 2000;113(20):3613-22.
8. Severino J, Allen RG, Balin S, Balin A, Cristofalo VJ. Is beta-galactosidase staining a marker of senescence in vitro and in vivo? Experimental Cell Research. 2000;257(1):162-71.
9. Kee N, Sivalingam S, Boonstra R, Wojtowicz JM. The utility of Ki-67 and BrdU as proliferative markers of adult neurogenesis. J Neurosci Meth. 2002;115(1):97-105.
10. Gratzner HG. Monoclonal-Antibody to 5-Bromodeoxyuridine and 5-Iododeoxyuridine - a New Reagent for Detection of DNA-Replication. Science. 1982;218(4571):474-5.
11. Scholzen T, Gerdes J. The Ki-67 protein: From the known and the unknown. Journal of Cellular Physiology. 2000;182(3):311-22.
12. de Jesus BB, Blasco MA. Assessing Cell and Organ Senescence Biomarkers. Circulation Research. 2012;111(1):97-109.
13. Wiley CD, Flynn JM, Morrissey C, Lebofsky R, Shuga J, Dong X, et al. Analysis of individual cells identifies cell-to-cell variability following induction of cellular senescence. Aging Cell. 2017;16(5):1043-50.
14. Narita M, Nunez S, Heard E, Narita M, Lin AW, Hearn SA, et al. Rb-mediated heterochromatin formation and silencing of E2F target genes during cellular senescence. Cell. 2003;113(6):703-16.
15. Shimi T, Butin-Israeli V, Adam SA, Hamanaka RB, Goldman AE, Lucas CA, et al. The role of nuclear lamin B1 in cell proliferation and senescence. Gene Dev. 2011;25(24):2579-93.
16. Ferbeyre G, de Stanchina E, Querido E, Baptiste N, Prives C, Lowe SW. PML is induced by oncogenic ras and promotes premature senescence. Gene Dev. 2000;14(16):2015-27.
17. Pearson M, Carbone R, Sebastiani C, Cioce M, Fagioli M, Saito S, et al. PML regulates p53 acetylation and premature senescence induced by oncogenic Ras. Nature. 2000;406(6792):207-10.
18. Rodier F, Munoz DP, Teachenor R, Chu V, Le O, Bhaumik D, et al. DNA-SCARS: distinct nuclear structures that sustain damage-induced senescence growth arrest and inflammatory cytokine secretion. Journal of Cell Science. 2011;124(1):68-81.
19. Coppe JP, Desprez PY, Krtolica A, Campisi J. The senescence-associated secretory phenotype: the dark side of tumor suppression. Annu Rev Pathol. 2010;5:99-118.
20. Kuilman T, Peeper DS. Senescence-messaging secretome: SMS-ing cellular stress. Nat Rev Cancer. 2009;9(2):81-94.

21. Matjusaitis M, Chin G, Sarnoski EA, Stolzing A. Biomarkers to identify and isolate senescent cells. Ageing Research Reviews. 2016;29:1-12.
22. Coppe JP, Rodier F, Patil CK, Freund A, Desprez PY, Campisi J. Tumor Suppressor and Aging Biomarker p16(INK4a) Induces Cellular Senescence without the Associated Inflammatory Secretory Phenotype. Journal of Biological Chemistry. 2011;286(42):36396-403.
23. Childs BG, Baker DJ, Kirkland JL, Campisi J, van Deursen JM. Senescence and apoptosis: dueling or complementary cell fates? EMBO Rep. 2014;15(11):1139-53.
24. Herranz N, Gil J. Mechanisms and functions of cellular senescence. J Clin Invest. 2018;128(4):1238-46.
25. Ryu SJ, Oh YS, Park SC. Failure of stress-induced downregulation of Bcl-2 contributes to apoptosis resistance in senescent human diploid fibroblasts. Cell Death Differ. 2007;14(5):1020-8.
26. Yosef R, Pilpel N, Tokarsky-Amiel R, Biran A, Ovadya Y, Cohen S, et al. Directed elimination of senescent cells by inhibition of BCL-W and BCL-XL. Nat Commun. 2016;7:11190.
27. Wiley CD, Campisi J. From Ancient Pathways to Aging Cells-Connecting Metabolism and Cellular Senescence. Cell Metab. 2016;23(6):1013-21.
28. Jones RG, Plas DR, Kubek S, Buzzai M, Mu J, Xu Y, et al. AMP-activated protein kinase induces a p53-dependent metabolic checkpoint. Mol Cell. 2005;18(3):283-93.
29. Wang WG, Yang XL, de Silanes IL, Carling D, Gorospe M. Increased AMP : ATP ratio and AMP-activated protein kinase activity during cellular senescence linked to reduced HuR function. Journal of Biological Chemistry. 2003;278(29):27016-23.
30. Passos JF, Saretzki G, Ahmed S, Nelson G, Richter T, Peters H, et al. Mitochondrial dysfunction accounts for the stochastic heterogeneity in telomere-dependent senescence. Plos Biology. 2007;5(5):1138-51.
31. Moiseeva O, Bourdeau V, Roux A, Deschenes-Simard X, Ferbeyre G. Mitochondrial Dysfunction Contributes to Oncogene-Induced Senescence. Molecular and Cellular Biology. 2009;29(16):4495-507.
32. Korolchuk VI, Miwa S, Carroll B, von Zglinicki T. Mitochondria in Cell Senescence: Is Mitophagy the Weakest Link? EBioMedicine. 2017;21:7-13.
33. Correia-Melo C, Passos JF. Mitochondria: Are they causal players in cellular senescence? Biochim Biophys Acta. 2015;1847(11):1373-9.
34. Correia-Melo C, Marques FD, Anderson R, Hewitt G, Hewitt R, Cole J, et al. Mitochondria are required for pro-ageing features of the senescent phenotype. EMBO J. 2016;35(7):724-42.
35. Kang HT, Lee KB, Kim SY, Choi HR, Park SC. Autophagy impairment induces premature senescence in primary human fibroblasts. PL0S One. 2011;6(8):e23367.
36. Tai HR, Wang Z, Gong H, Han XJ, Zhou J, Wang XB, et al. Autophagy impairment with lysosomal and mitochondrial dysfunction is an important characteristic of oxidative stress-induced senescence. Autophagy. 2017;13(1):99-113.
37. Kang C, Xu Q, Martin TD, Li MZ, Demaria M, Aron L, et al. The DNA damage response induces inflammation and senescence by inhibiting autophagy of GATA4. Science. 2015;349(6255):aaa5612.
38. Kang C, Elledge SJ. How autophagy both activates and inhibits cellular senescence. Autophagy. 2016;12(5):898-9.
39. Garcia-Prat L, Martinez-Vicente M, Perdiguero E, Ortet L, Rodriguez-Ubreva J, Rebollo E, et al. Autophagy maintains stemness by preventing senescence. Nature. 2016;529(7584):37-42.
40. von Zglinicki T, Nilsson E, Docke WD, Brunk UT. Lipofuscin accumulation and ageing of fibroblasts. Gerontology. 1995;41 Suppl 2:95-108.
41. Salmonowicz H, Passos JF. Detecting senescence: a new method for an old pigment. Aging Cell. 2017;16(3):432-4.
42. Ademowo OS, Dias HKI, Burton DGA, Griffiths HR. Lipid (per) oxidation in mitochondria: an emerging target in the ageing process? Biogerontology. 2017;18(6):859-79.
43. Venable ME, Lee JY, Smyth MJ, Bielawska A, Obeid LM. Role of ceramide in cellular senescence. J Biol Chem. 1995;270(51):30701-8.

44. Quijano C, Cao L, Fergusson MM, Romero H, Liu J, Gutkind S, et al. Oncogene-induced senescence results in marked metabolic and bioenergetic alterations. Cell Cycle. 2012;11(7):1383-92.
45. Shay JW, Wright WE. Hayflick, his limit, and cellular ageing. Nat Rev Mol Cell Bio. 2000;1(1):72-6.
46. McClintock B. The Stability of Broken Ends of Chromosomes in Zea Mays. Genetics. 1941;26(2):234-82.
47. Cooke HJ, Smith BA. Variability at the Telomeres of the Human X/Y Pseudoautosomal Region. Cold Spring Harb Sym. 1986;51:213-9.
48. Harley CB, Futcher AB, Greider CW. Telomeres Shorten during Aging of Human Fibroblasts. Nature. 1990;345(6274):458-60.
49. Bodnar AG, Ouellette M, Frolkis M, Holt SE, Chiu CP, Morin GB, et al. Extension of life-span by introduction of telomerase into normal human cells. Science. 1998;279(5349):349-52.
50. Campisi J. Aging, cellular senescence, and cancer. Annu Rev Physiol. 2013;75:685-705.
51. Di Leonardo A, Linke SP, Clarkin K, Wahl GM. DNA-Damage Triggers a Prolonged P53-Dependent G(1) Arrest and Long-Term Induction of Cip1 in Normal Human Fibroblasts. Gene Dev. 1994;8(21):2540-51.
52. Debacq-Chainiaux F, Leduc C, Verbeke A, Toussaint O. UV, stress and aging. Dermatoendocrinol. 2012;4(3):236-40.
53. Petrova NV, Velichko AK, Razin SV, Kantidze OL. Small molecule compounds that induce cellular senescence. Aging Cell. 2016.
54. Parrinello S, Samper E, Krtolica A, Goldstein J, Melov S, Campisi J. Oxygen sensitivity severely limits the replicative lifespan of murine fibroblasts. Nat Cell Biol. 2003;5(8):741-7.
55. Lu T, Finkel T. Free radicals and senescence. Exp Cell Res. 2008;314(9):1918-22.
56. Passos JF, Nelson G, Wang CF, Richter T, Simillion C, Proctor CJ, et al. Feedback between p21 and reactive oxygen production is necessary for cell senescence. Mol Syst Biol. 2010;6.
57. Lee AC, Fenster BE, Ito H, Takeda K, Bae NS, Hirai T, et al. Ras proteins induce senescence by altering the intracellular levels of reactive oxygen species. Journal of Biological Chemistry. 1999;274(12):7936-40.
58. Chen Q, Fischer A, Reagan JD, Yan LJ, Ames BN. Oxidative DNA damage and senescence of human diploid fibroblast cells. Proc Natl Acad Sci U S A. 1995;92(10):4337-41.
59. Macip S, Igarashi M, Fang L, Chen A, Pan ZQ, Lee SW, et al. Inhibition of p21-mediated ROS accumulation can rescue p21-induced senescence. EMBO J. 2002;21(9):2180-8.
60. Davalli P, Mitic T, Caporali A, Lauriola A, D'Arca D. ROS, Cell Senescence, and Novel Molecular Mechanisms in Aging and Age-Related Diseases. Oxid Med Cell Longev. 2016;2016:3565127.
61. Wang Z, Wei DD, Xiao HY. Methods of Cellular Senescence Induction Using Oxidative Stress. Biological Aging: Methods and Protocols, 2nd Edition. 2013;1048:135-44.
62. Gorgoulis VG, Halazonetis TD. Oncogene-induced senescence: the bright and dark side of the response. Curr Opin Cell Biol. 2010;22(6):816-27.
63. Serrano M, Lin AW, McCurrach ME, Beach D, Lowe SW. Oncogenic ras provokes premature cell senescence associated with accumulation of p53 and p16INK4a. Cell. 1997;88(5):593-602.
64. Wei S, Wei WY, Sedivy JM. Expression of catalytically active telomerase does not prevent premature senescence caused by overexpression of oncogenic Ha-Ras in normal human fibroblasts. Cancer Research. 1999;59(7):1539-43.
65. Courtois-Cox S, Jones SL, Cichowski K. Many roads lead to oncogene-induced senescence. Oncogene. 2008;27(20):2801-9.
66. Bartkova J, Rezaei N, Liontos M, Karakaidos P, Kletsas D, Issaeva N, et al. Oncogene-induced senescence is part of the tumorigenesis barrier imposed by DNA damage checkpoints. Nature. 2006;444(7119):633-7.
67. Di Micco R, Fumagalli M, Cicalese A, Piccinin S, Gasparini P, Luise C, et al. Oncogene-induced senescence is a DNA damage response triggered by DNA hyper-replication. Nature. 2006;444(7119):638-42.

68. Kaplon J, Zheng L, Meissl K, Chaneton B, Selivanov VA, Mackay G, et al. A key role for mitochondrial gatekeeper pyruvate dehydrogenase in oncogene-induced senescence. Nature. 2013;498(7452):109-+.
69. Liu X-l, Ding J, Meng L-h. Oncogene-induced senescence: a double edged sword in cancer. Acta Pharmacologica Sinica. 2018.
70. Gupta R, Wajapeyee N. Induction of Cellular Senescence by Oncogenic RAS. Biological Aging: Methods and Protocols, 2nd Edition. 2013;1048:127-33.
71. Fernandez-Medarde A, Santos E. Ras in cancer and developmental diseases. Genes Cancer. 2011;2(3):344-58.
72. Prior IA, Lewis PD, Mattos C. A comprehensive survey of Ras mutations in cancer. Cancer Res. 2012;72(10):2457-67.
73. Nardella C, Clohessy JG, Alimonti A, Pandolfi PP. Pro-senescence therapy for cancer treatment. Nat Rev Cancer. 2011;11(7):503-11.
74. Chen Z, Trotman LC, Shaffer D, Lin HK, Dotan ZA, Niki M, et al. Crucial role of p53-dependent cellular senescence in suppression of Pten-deficient tumorigenesis. Nature. 2005;436(7051):725-30.
75. Alimonti A, Nardella C, Chen ZB, Clohessy JG, Carracedo A, Trotman LC, et al. A novel type of cellular senescence that can be enhanced in mouse models and human tumor xenografts to suppress prostate tumorigenesis. Journal of Clinical Investigation. 2010;120(3):681-93.
76. Wiley CD, Velarde MC, Lecot P, Liu S, Sarnoski EA, Freund A, et al. Mitochondrial Dysfunction Induces Senescence with a Distinct Secretory Phenotype. Cell Metab. 2016;23(2):303-14.
77. Acosta JC, O'Loghlen A, Banito A, Guijarro MV, Augert A, Raguz S, et al. Chemokine signaling via the CXCR2 receptor reinforces senescence. Cell. 2008;133(6):1006-18.
78. Kuilman T, Michaloglou C, Vredeveld LC, Douma S, van Doorn R, Desmet CJ, et al. Oncogene-induced senescence relayed by an interleukin-dependent inflammatory network. Cell. 2008;133(6):1019-31.
79. Wajapeyee N, Serra RW, Zhu X, Mahalingam M, Green MR. Oncogenic BRAF induces senescence and apoptosis through pathways mediated by the secreted protein IGFBP7. Cell. 2008;132(3):363-74.
80. Acosta JC, Banito A, Wuestefeld T, Georgilis A, Janich P, Morton JP, et al. A complex secretory program orchestrated by the inflammasome controls paracrine senescence. Nat Cell Biol. 2013;15(8):978-90.
81. Hubackova S, Krejcikova K, Bartek J, Hodny Z. IL1- and TGFbeta-Nox4 signaling, oxidative stress and DNA damage response are shared features of replicative, oncogene-induced, and drug-induced paracrine 'bystander senescence'. Aging (Albany NY). 2012;4(12):932-51.
82. Hoare M, Ito Y, Kang TW, Weekes MP, Matheson NJ, Patten DA, et al. NOTCH1 mediates a switch between two distinct secretomes during senescence. Nat Cell Biol. 2016;18(9):979-92.
83. Nelson G, Wordsworth J, Wang C, Jurk D, Lawless C, Martin-Ruiz C, et al. A senescent cell bystander effect: senescence-induced senescence. Aging Cell. 2012;11(2):345-9.
84. Biran A, Perelmutter M, Gal H, Burton DG, Ovadya Y, Vadai E, et al. Senescent cells communicate via intercellular protein transfer. Genes Dev. 2015;29(8):791-802.
85. Lehmann BD, Paine MS, Brooks AM, McCubrey JA, Renegar RH, Wang R, et al. Senescence-associated exosome release from human prostate cancer cells. Cancer Res. 2008;68(19):7864-71.
86. di Fagagna FD. Living on a break: cellular senescence as a DNA-damage response. Nature Reviews Cancer. 2008;8(7):512-22.
87. Bartek J, Lukas J. Chk1 and Chk2 kinases in checkpoint control and cancer. Cancer Cell. 2003;3(5):421-9.
88. Gil J, Peters G. Regulation of the INK4b-ARF-INK4a tumour suppressor locus: all for one or one for all. Nat Rev Mol Cell Bio. 2006;7(9):667-77.
89. Kim WY, Sharpless NE. The regulation of INK4/ARF in cancer and aging. Cell. 2006;127(2):265-75.

90. el-Deiry WS, Tokino T, Velculescu VE, Levy DB, Parsons R, Trent JM, et al. WAF1, a potential mediator of p53 tumor suppression. Cell. 1993;75(4):817-25.
91. Beausejour CM, Krtolica A, Galimi F, Narita M, Lowe SW, Yaswen P, et al. Reversal of human cellular senescence: roles of the p53 and p16 pathways. EMBO J. 2003;22(16):4212-22.
92. Ben-Porath I, Weinberg RA. The signals and pathways activating cellular senescence. Int J Biochem Cell B. 2005;37(5):961-76.
93. Freund A, Orjalo AV, Desprez PY, Campisi J. Inflammatory networks during cellular senescence: causes and consequences. Trends Mol Med. 2010;16(5):238-46.
94. Coppe JP, Patil CK, Rodier F, Sun Y, Munoz DP, Goldstein J, et al. Senescence-associated secretory phenotypes reveal cell-nonautonomous functions of oncogenic RAS and the p53 tumor suppressor. PLoS Biol. 2008;6(12):2853-68.
95. Rodier F, Coppe JP, Patil CK, Hoeijmakers WA, Munoz DP, Raza SR, et al. Persistent DNA damage signalling triggers senescence-associated inflammatory cytokine secretion. Nat Cell Biol. 2009;11(8):973-9.
96. Freund A, Patil CK, Campisi J. p38MAPK is a novel DNA damage response-independent regulator of the senescence-associated secretory phenotype. Embo Journal. 2011;30(8):1536-48.
97. Dou Z, Ghosh K, Vizioli MG, Zhu J, Sen P, Wangensteen KJ, et al. Cytoplasmic chromatin triggers inflammation in senescence and cancer. Nature. 2017;550(7676):402-6.
98. Gluck S, Guey B, Gulen MF, Wolter K, Kang TW, Schmacke NA, et al. Innate immune sensing of cytosolic chromatin fragments through cGAS promotes senescence. Nat Cell Biol. 2017;19(9):1061-70.
99. Yang H, Wang H, Ren J, Chen Q, Chen ZJ. cGAS is essential for cellular senescence. Proc Natl Acad Sci U S A. 2017;114(23):E4612-E20.
100. Orjalo AV, Bhaumik D, Gengler BK, Scott GK, Campisi J. Cell surface-bound IL-1alpha is an upstream regulator of the senescence-associated IL-6/IL-8 cytokine network. Proc Natl Acad Sci U S A. 2009;106(40):17031-6.
101. Kim YH, Choi YW, Lee J, Soh EY, Kim JH, Park TJ. Senescent tumor cells lead the collective invasion in thyroid cancer. Nat Commun. 2017;8:15208.
102. Parrinello S, Coppe JP, Krtolica A, Campisi J. Stromal-epithelial interactions in aging and cancer: senescent fibroblasts alter epithelial cell differentiation. J Cell Sci. 2005;118(Pt 3):485-96.
103. Krtolica A, Parrinello S, Lockett S, Desprez PY, Campisi J. Senescent fibroblasts promote epithelial cell growth and tumorigenesis: a link between cancer and aging. Proc Natl Acad Sci U S A. 2001;98(21):12072-7.
104. Yoshimoto S, Loo TM, Atarashi K, Kanda H, Sato S, Oyadomari S, et al. Obesity-induced gut microbial metabolite promotes liver cancer through senescence secretome. Nature. 2013;499(7456):97-101.
105. Xue W, Zender L, Miething C, Dickins RA, Hernando E, Krizhanovsky V, et al. Senescence and tumour clearance is triggered by p53 restoration in murine liver carcinomas. Nature. 2007;445(7128):656-60.
106. Kang TW, Yevsa T, Woller N, Hoenicke L, Wuestefeld T, Dauch D, et al. Senescence surveillance of pre-malignant hepatocytes limits liver cancer development. Nature. 2011;479(7374):547-51.
107. Sagiv A, Krizhanovsky V. Immunosurveillance of senescent cells: the bright side of the senescence program. Biogerontology. 2013;14(6):617-28.
108. Toso A, Revandkar A, Di Mitri D, Guccini I, Proietti M, Sarti M, et al. Enhancing chemotherapy efficacy in Pten-deficient prostate tumors by activating the senescence-associated antitumor immunity. Cell Rep. 2014;9(1):75-89.
109. Di Mitri D, Toso A, Chen JJ, Sarti M, Pinton S, Jost TR, et al. Tumour-infiltrating Gr-1+ myeloid cells antagonize senescence in cancer. Nature. 2014;515(7525):134-7.
110. Eggert T, Wolter K, Ji J, Ma C, Yevsa T, Klotz S, et al. Distinct Functions of Senescence-Associated Immune Responses in Liver Tumor Surveillance and Tumor Progression. Cancer Cell. 2016;30(4):533-47.

111. Coppe JP, Kauser K, Campisi J, Beausejour CM. Secretion of vascular endothelial growth factor by primary human fibroblasts at senescence. Journal of Biological Chemistry. 2006;281(40):29568-74.
112. Sparmann A, Bar-Sagi D. Ras-induced interleukin-8 expression plays a critical role in tumor growth and angiogenesis. Cancer Cell. 2004;6(5):447-58.
113. Oubaha M, Miloudi K, Dejda A, Guber V, Mawambo G, Germain MA, et al. Senescence-associated secretory phenotype contributes to pathological angiogenesis in retinopathy. Science Translational Medicine. 2016;8(362).
114. Jun JI, Lau LF. The matricellular protein CCN1 induces fibroblast senescence and restricts fibrosis in cutaneous wound healing. Nat Cell Biol. 2010;12(7):676-85.
115. Demaria M, Ohtani N, Youssef SA, Rodier F, Toussaint W, Mitchell JR, et al. An essential role for senescent cells in optimal wound healing through secretion of PDGF-AA. Dev Cell. 2014;31(6):722-33.
116. Lujambio A, Akkari L, Simon J, Grace D, Tschaharganeh DF, Bolden JE, et al. Non-cell-autonomous tumor suppression by p53. Cell. 2013;153(2):449-60.
117. Krizhanovsky V, Yon M, Dickins RA, Hearn S, Simon J, Miething C, et al. Senescence of activated stellate cells limits liver fibrosis. Cell. 2008;134(4):657-67.
118. Mosteiro L, Pantoja C, Alcazar N, Marion RM, Chondronasiou D, Rovira M, et al. Tissue damage and senescence provide critical signals for cellular reprogramming in vivo. Science. 2016;354(6315).
119. Ritschka B, Storer M, Mas A, Heinzmann F, Ortells MC, Morton JP, et al. The senescence-associated secretory phenotype induces cellular plasticity and tissue regeneration. Genes Dev. 2017;31(2):172-83.
120. Childs BG, Baker DJ, Wijshake T, Conover CA, Campisi J, van Deursen JM. Senescent intimal foam cells are deleterious at all stages of atherosclerosis. Science. 2016;354(6311):472-7.
121. Jeon OH, Kim C, Laberge RM, Demaria M, Rathod S, Vasserot AP, et al. Local clearance of senescent cells attenuates the development of post-traumatic osteoarthritis and creates a pro-regenerative environment. Nat Med. 2017;23(6):775-81.
122. Franceschi C, Campisi J. Chronic inflammation (inflammaging) and its potential contribution to age-associated diseases. J Gerontol A Biol Sci Med Sci. 2014;69 Suppl 1:S4-9.
123. Ohanna M, Giuliano S, Bonet C, Imbert V, Hofman V, Zangari J, et al. Senescent cells develop a PARP-1 and nuclear factor-{kappa}B-associated secretome (PNAS). Genes Dev. 2011;25(12):1245-61.
124. Georgilis A, Klotz S, Hanley CJ, Herranz N, Weirich B, Morancho B, et al. PTBP1-Mediated Alternative Splicing Regulates the Inflammatory Secretome and the Pro-tumorigenic Effects of Senescent Cells. Cancer Cell. 2018;34(1):85-102 e9.
125. Laberge RM, Sun Y, Orjalo AV, Patil CK, Freund A, Zhou L, et al. MTOR regulates the pro-tumorigenic senescence-associated secretory phenotype by promoting IL1A translation. Nat Cell Biol. 2015;17(8):1049-61.
126. Herranz N, Gallage S, Mellone M, Wuestefeld T, Klotz S, Hanley CJ, et al. mTOR regulates MAPKAPK2 translation to control the senescence-associated secretory phenotype. Nat Cell Biol. 2015;17(9):1205-17.
127. Narita M, Young AR, Arakawa S, Samarajiwa SA, Nakashima T, Yoshida S, et al. Spatial coupling of mTOR and autophagy augments secretory phenotypes. Science. 2011;332(6032):966-70.
128. Morancho B, Martinez-Barriocanal A, Villanueva J, Arribas J. Role of ADAM17 in the non-cell autonomous effects of oncogene-induced senescence. Eur J Cancer. 2016;61:S4-S.
129. Effenberger T, von der Heyde J, Bartsch K, Garbers C, Schulze-Osthoff K, Chalaris A, et al. Senescence-associated release of transmembrane proteins involves proteolytic processing by ADAM17 and microvesicle shedding. Faseb Journal. 2014;28(11):4847-56.
130. Takasugi M, Okada R, Takahashi A, Chen DV, Watanabe S, Hara E. Small extracellular vesicles secreted from senescent cells promote cancer cell proliferation through EphA2. Nature Communications. 2017;8.
131. Collado M, Serrano M. Senescence in tumours: evidence from mice and humans. Nature reviews Cancer. 2010;10(1):51-7.

132. Collado M, Gil J, Efeyan A, Guerra C, Schuhmacher AJ, Barradas M, et al. Tumour biology: senescence in premalignant tumours. Nature. 2005;436(7051):642.
133. Michaloglou C, Vredeveld LC, Soengas MS, Denoyelle C, Kuilman T, van der Horst CM, et al. BRAFE600-associated senescence-like cell cycle arrest of human naevi. Nature. 2005;436(7051):720-4.
134. Braig M, Lee S, Loddenkemper C, Rudolph C, Peters AHFM, Schlegelberger B, et al. Oncogene-induced senescence as an initial barrier in lymphoma development. Nature. 2005;436(7051):660-5.
135. Adams PD. Healing and hurting: molecular mechanisms, functions, and pathologies of cellular senescence. Mol Cell. 2009;36(1):2-14.
136. Ventura A, Kirsch DG, McLaughlin ME, Tuveson DA, Grimm J, Lintault L, et al. Restoration of p53 function leads to tumour regression in vivo. Nature. 2007;445(7128):661-5.
137. He S, Sharpless NE. Senescence in Health and Disease. Cell. 2017;169(6):1000-11.
138. Wellenstein MD, de Visser KE. Cancer-Cell-Intrinsic Mechanisms Shaping the Tumor Immune Landscape. Immunity. 2018;48(3):399-416.
139. Rodier F, Campisi J. Four faces of cellular senescence. J Cell Biol. 2011;192(4):547-56.
140. Bavik C, Coleman I, Dean JP, Knudsen B, Plymate S, Nelson PS. The gene expression program of prostate fibroblast senescence modulates neoplastic epithelial cell proliferation through paracrine mechanisms. Cancer Research. 2006;66(2):794-802.
141. Liu D, Hornsby PJ. Senescent human fibroblasts increase the early growth of xenograft tumors via matrix metalloproteinase secretion. Cancer Research. 2007;67(7):3117-26.
142. Watanabe S, Kawamoto S, Ohtani N, Hara E. Impact of senescence-associated secretory phenotype and its potential as a therapeutic target for senescence-associated diseases. Cancer Science. 2017;108(4):563-9.
143. Sharpless NE, Sherr CJ. Forging a signature of in vivo senescence. Nat Rev Cancer. 2015;15(7):397-408.
144. Lopez-Otin C, Blasco MA, Partridge L, Serrano M, Kroemer G. The Hallmarks of Aging. Cell. 2013;153(6):1194-217.
145. Wang C, Jurk D, Maddick M, Nelson G, Martin-Ruiz C, von Zglinicki T. DNA damage response and cellular senescence in tissues of aging mice. Aging Cell. 2009;8(3):311-23.
146. McHugh D, Gil J. Senescence and aging: Causes, consequences, and therapeutic avenues. J Cell Biol. 2018;217(1):65-77.
147. Baker DJ, Wijshake T, Tchkonia T, LeBrasseur NK, Childs BG, van de Sluis B, et al. Clearance of p16(Ink4a)-positive senescent cells delays ageing-associated disorders. Nature. 2011;479(7372):232-U112.
148. Baker DJ, Childs BG, Durik M, Wijers ME, Sieben CJ, Zhong J, et al. Naturally occurring p16(Ink4a)-positive cells shorten healthy lifespan. Nature. 2016;530(7589):184-+.
149. Matheu A, Maraver A, Klatt P, Flores I, Garcia-Cao I, Borras C, et al. Delayed ageing through damage protection by the Arf/p53 pathway. Nature. 2007;448(7151):375-U14.
150. Matheu A, Maraver A, Collado M, Garcia-Cao I, Canamero M, Borras C, et al. Anti-aging activity of the Ink4/Arf locus. Aging Cell. 2009;8(2):152-61.
151. Campisi J. Aging, tumor suppression and cancer: high wire-act! Mechanisms of Ageing and Development. 2005;126(1):51-8.
152. Baar MP, Brandt RM, Putavet DA, Klein JD, Derks KW, Bourgeois BR, et al. Targeted Apoptosis of Senescent Cells Restores Tissue Homeostasis in Response to Chemotoxicity and Aging. Cell. 2017;169(1):132-47 e16.
153. Harrison DE, Strong R, Sharp ZD, Nelson JF, Astle CM, Flurkey K, et al. Rapamycin fed late in life extends lifespan in genetically heterogeneous mice. Nature. 2009;460(7253):392-5.
154. Ewald JA, Desotelle JA, Wilding G, Jarrard DF. Therapy-induced senescence in cancer. J Natl Cancer Inst. 2010;102(20):1536-46.
155. Dickson MA. Molecular pathways: CDK4 inhibitors for cancer therapy. Clin Cancer Res. 2014;20(13):3379-83.
156. Miettinen TP, Peltier J, Hartlova A, Gierlinski M, Jansen VM, Trost M, et al. Thermal proteome profiling of breast cancer cells reveals proteasomal activation by CDK4/6 inhibitor palbociclib. EMBO J. 2018;37(10).

157. Sherr CJ, Beach D, Shapiro GI. Targeting CDK4 and CDK6: From Discovery to Therapy. Cancer Discov. 2016;6(4):353-67.
158. Chien Y, Scuoppo C, Wang X, Fang X, Balgley B, Bolden JE, et al. Control of the senescence-associated secretory phenotype by NF-kappaB promotes senescence and enhances chemosensitivity. Genes Dev. 2011;25(20):2125-36.
159. Demaria M, O'Leary MN, Chang J, Shao L, Liu S, Alimirah F, et al. Cellular Senescence Promotes Adverse Effects of Chemotherapy and Cancer Relapse. Cancer Discov. 2017;7(2):165-76.
160. Milanovic M, Fan DNY, Belenki D, Dabritz JHM, Zhao Z, Yu Y, et al. Senescence-associated reprogramming promotes cancer stemness. Nature. 2018;553(7686):96-100.
161. Schmitt CA. UnSASPing Senescence: Unmasking Tumor Suppression? Cancer Cell. 2018;34(1):6-8.
162. Soto-Gamez A, Demaria M. Therapeutic interventions for aging: the case of cellular senescence. Drug Discov Today. 2017;22(5):786-95.
163. Kirkland JL, Tchkonia T. Cellular Senescence: A Translational Perspective. EBioMedicine. 2017;21:21-8.
164. Laberge RM, Zhou LL, Sarantos MR, Rodier F, Freund A, de Keizer PLJ, et al. Glucocorticoids suppress selected components of the senescence-associated secretory phenotype. Aging Cell. 2012;11(4):569-78.
165. Moiseeva O, Deschenes-Simard X, St-Germain E, Igelmann S, Huot G, Cadar AE, et al. Metformin inhibits the senescence-associated secretory phenotype by interfering with IKK/NF-B activation. Aging Cell. 2013;12(3):489-98.
166. Childs BG, Gluscevic M, Baker DJ, Laberge RM, Marquess D, Dananberg J, et al. Senescent cells: an emerging target for diseases of ageing. Nat Rev Drug Discov. 2017;16(10):718-35.
167. Zhu Y, Tchkonia T, Pirtskhalava T, Gower AC, Ding H, Giorgadze N, et al. The Achilles' heel of senescent cells: from transcriptome to senolytic drugs. Aging Cell. 2015;14(4):644-58.
168. Chang J, Wang Y, Shao L, Laberge RM, Demaria M, Campisi J, et al. Clearance of senescent cells by ABT263 rejuvenates aged hematopoietic stem cells in mice. Nat Med. 2016;22(1):78-83.
169. Dorr JR, Yu Y, Milanovic M, Beuster G, Zasada C, Dabritz JH, et al. Synthetic lethal metabolic targeting of cellular senescence in cancer therapy. Nature. 2013;501(7467):421-5.
170. Sieben CJ, Sturmlechner I, van de Sluis B, van Deursen JM. Two-Step Senescence-Focused Cancer Therapies. Trends Cell Biol. 2018.
171. Xu M, Pirtskhalava T, Farr JN, Weigand BM, Palmer AK, Weivoda MM, et al. Senolytics improve physical function and increase lifespan in old age. Nat Med. 2018;24(8):1246-56.
172. Munoz-Espin D, Rovira M, Galiana I, Gimenez C, Lozano-Torres B, Paez-Ribes M, et al. A versatile drug delivery system targeting senescent cells. EMBO Mol Med. 2018.
173. Alnemri ES, Livingston DJ, Nicholson DW, Salvesen G, Thornberry NA, Wong WW, et al. Human ICE/CED-3 protease nomenclature. Cell. 1996;87(2):171.
174. McIlwain DR, Berger T, Mak TW. Caspase functions in cell death and disease. Cold Spring Harb Perspect Biol. 2013;5(4):a008656.
175. Man SM, Kanneganti TD. Converging roles of caspases in inflammasome activation, cell death and innate immunity. Nat Rev Immunol. 2016;16(1):7-21.
176. Li J, Yuan J. Caspases in apoptosis and beyond. Oncogene. 2008;27(48):6194-206.
177. Galluzzi L, Vitale I, Aaronson SA, Abrams JM, Adam D, Agostinis P, et al. Molecular mechanisms of cell death: recommendations of the Nomenclature Committee on Cell Death 2018. Cell Death Differ. 2018;25(3):486-541.
178. Denecker G, Ovaere P, Vandenabeele P, Declercq W. Caspase-14 reveals its secrets. J Cell Biol. 2008;180(3):451-8.
179. Creagh EM. Caspase crosstalk: integration of apoptotic and innate immune signalling pathways. Trends Immunol. 2014;35(12):631-40.
180. McArthur K, Kile BT. Apoptotic Caspases: Multiple or Mistaken Identities? Trends Cell Biol. 2018;28(6):475-93.

181. Siegel RM. Caspases at the crossroads of immune-cell life and death. Nat Rev Immunol. 2006;6(4):308-17.
182. Denes A, Lopez-Castejon G, Brough D. Caspase-1: is IL-1 just the tip of the ICEberg? Cell Death Dis. 2012;3:e338.
183. Bouchier-Hayes L, Martin SJ. CARD games in apoptosis and immunity. EMBO Rep. 2002;3(7):616-21.
184. Kostura MJ, Tocci MJ, Limjuco G, Chin J, Cameron P, Hillman AG, et al. Identification of a monocyte specific pre-interleukin 1 beta convertase activity. Proc Natl Acad Sci U S A. 1989;86(14):5227-31.
185. Black RA, Kronheim SR, Merriam JE, March CJ, Hopp TP. A Pre-Aspartate-Specific Protease from Human-Leukocytes That Cleaves Pro-Interleukin-1-Beta. Journal of Biological Chemistry. 1989;264(10):5323-6.
186. Pop C, Salvesen GS. Human caspases: activation, specificity, and regulation. J Biol Chem. 2009;284(33):21777-81.
187. Boatright KM, Salvesen GS. Mechanisms of caspase activation. Curr Opin Cell Biol. 2003;15(6):725-31.
188. Thornberry NA, Bull HG, Calaycay JR, Chapman KT, Howard AD, Kostura MJ, et al. A Novel Heterodimeric Cysteine Protease Is Required for Interleukin-1-Beta Processing in Monocytes. Nature. 1992;356(6372):768-74.
189. Chang HY, Yang X. Proteases for cell suicide: functions and regulation of caspases. Microbiol Mol Biol Rev. 2000;64(4):821-46.
190. Motani K, Kushiyama H, Imamura R, Kinoshita T, Nishiuchi T, Suda T. Caspase-1 protein induces apoptosis-associated speck-like protein containing a caspase recruitment domain (ASC)-mediated necrosis independently of its catalytic activity. J Biol Chem. 2011;286(39):33963-72.
191. Kang S, Fernandes-Alnemri T, Rogers C, Mayes L, Wang Y, Dillon C, et al. Caspase-8 scaffolding function and MLKL regulate NLRP3 inflammasome activation downstream of TLR3. Nat Commun. 2015;6:7515.
192. Boucher D, Monteleone M, Coll RC, Chen KW, Ross CM, Teo JL, et al. Caspase-1 self-cleavage is an intrinsic mechanism to terminate inflammasome activity. J Exp Med. 2018;215(3):827-40.
193. Shi J, Zhao Y, Wang Y, Gao W, Ding J, Li P, et al. Inflammatory caspases are innate immune receptors for intracellular LPS. Nature. 2014;514(7521):187-92.
194. Boatright KM, Renatus M, Scott FL, Sperandio S, Shin H, Pedersen IM, et al. A unified model for apical caspase activation. Molecular Cell. 2003;11(2):529-41.
195. Donepudi M, Mac Sweeney A, Briand C, Grutter MG. Insights into the regulatory mechanism for caspase-8 activation. Molecular Cell. 2003;11(2):543-9.
196. Conos SA, Lawlor KE, Vaux DL, Vince JE, Lindqvist LM. Cell death is not essential for caspase-1-mediated interleukin-1 beta activation and secretion. Cell Death and Differentiation. 2016;23(11):1827-38.
197. Crawford ED, Wells JA. Caspase Substrates and Cellular Remodeling. Annual Review of Biochemistry, Vol 80. 2011;80:1055-87.
198. Rano TA, Timkey T, Peterson EP, Rotonda J, Nicholson DW, Becker JW, et al. A combinatorial approach for determining protease specificities: application to interleukin-1beta converting enzyme (ICE). Chem Biol. 1997;4(2):149-55.
199. Thornberry NA, Ranon TA, Pieterson EP, Rasper DM, Timkey T, GarciaCalvo M, et al. A combinatorial approach defines specificities of members of the caspase family and granzyme B - Functional, relationships established for key mediators of apoptosis. Journal of Biological Chemistry. 1997;272(29):17907-11.
200. McStay GP, Salvesen GS, Green DR. Overlapping cleavage motif selectivity of caspases: implications for analysis of apoptotic pathways. Cell Death Differ. 2008;15(2):322-31.
201. Julien O, Wells JA. Caspases and their substrates. Cell Death and Differentiation. 2017;24(8):1380-9.

202. Julien O, Zhuang M, Wiita AP, O'Donoghue AJ, Knudsen GM, Craik CS, et al. Quantitative MS-based enzymology of caspases reveals distinct protein substrate specificities, hierarchies, and cellular roles. Proc Natl Acad Sci U S A. 2016;113(14):E2001-10.
203. Talanian RV, Quinlan C, Trautz S, Hackett MC, Mankovich JA, Banach D, et al. Substrate specificities of caspase family proteases. J Biol Chem. 1997;272(15):9677-82.
204. Afonina IS, Muller C, Martin SJ, Beyaert R. Proteolytic Processing of Interleukin-1 Family Cytokines: Variations on a Common Theme. Immunity. 2015;42(6):991-1004.
205. Agard NJ, Maltby D, Wells JA. Inflammatory stimuli regulate caspase substrate profiles. Mol Cell Proteomics. 2010;9(5):880-93.
206. Pop C, Salvesen GS, Scott FL. Caspase assays: identifying caspase activity and substrates in vitro and in vivo. Methods Enzymol. 2008;446:351-67.
207. McStay GP, Green DR. Measuring apoptosis: caspase inhibitors and activity assays. Cold Spring Harb Protoc. 2014;2014(8):799-806.
208. Ramirez MLG, Poreba M, Snipas SJ, Groborz K, Drag M, Salvesen GS. Extensive peptide and natural protein substrate screens reveal that mouse caspase-11 has much narrower substrate specificity than caspase-1. J Biol Chem. 2018;293(18):7058-67.
209. Wang Y, Ning X, Gao P, Wu S, Sha M, Lv M, et al. Inflammasome Activation Triggers Caspase-1-Mediated Cleavage of cGAS to Regulate Responses to DNA Virus Infection. Immunity. 2017;46(3):393-404.
210. Martinon F, Tschopp J. Inflammatory caspases and inflammasomes: master switches of inflammation. Cell Death Differ. 2007;14(1):10-22.
211. Kuida K, Lippke JA, Ku G, Harding MW, Livingston DJ, Su MS, et al. Altered cytokine export and apoptosis in mice deficient in interleukin-1 beta converting enzyme. Science. 1995;267(5206):2000-3.
212. Li P, Allen H, Banerjee S, Franklin S, Herzog L, Johnston C, et al. Mice deficient in IL-1 beta-converting enzyme are defective in production of mature IL-1 beta and resistant to endotoxic shock. Cell. 1995;80(3):401-11.
213. Kayagaki N, Warming S, Lamkanfi M, Vande Walle L, Louie S, Dong J, et al. Non-canonical inflammasome activation targets caspase-11. Nature. 2011;479(7371):117-21.
214. Ng TM, Monack DM. Revisiting caspase-11 function in host defense. Cell Host Microbe. 2013;14(1):9-14.
215. Man SM, Karki R, Briard B, Burton A, Gingras S, Pelletier S, et al. Differential roles of caspase-1 and caspase-11 in infection and inflammation. Sci Rep. 2017;7:45126.
216. Lin XY, Choi MS, Porter AG. Expression analysis of the human caspase-1 subfamily reveals specific regulation of the CASP5 gene by lipopolysaccharide and interferon-gamma. J Biol Chem. 2000;275(51):39920-6.
217. Lagrange B, Benaoudia S, Wallet P, Magnotti F, Provost A, Michal F, et al. Human caspase-4 detects tetra-acylated LPS and cytosolic Francisella and functions differently from murine caspase-11. Nat Commun. 2018;9(1):242.
218. Vigano E, Diamond CE, Spreafico R, Balachander A, Sobota RM, Mortellaro A. Human caspase-4 and caspase-5 regulate the one-step non-canonical inflammasome activation in monocytes. Nat Commun. 2015;6:8761.
219. Zerbino DR, Johnson N, Juetteman T, Sheppard D, Wilder SP, Lavidas I, et al. Ensembl regulation resources. Database (Oxford). 2016;2016.
220. Roy S, Sharom JR, Houde C, Loisel TP, Vaillancourt JP, Shao W, et al. Confinement of caspase-12 proteolytic activity to autoprocessing. Proc Natl Acad Sci U S A. 2008;105(11):4133-8.
221. Vande Walle L, Jimenez Fernandez D, Demon D, Van Laethem N, Van Hauwermeiren F, Van Gorp H, et al. Does caspase-12 suppress inflammasome activation? Nature. 2016;534(7605):E1-4.
222. Salvamoser R, Brinkmann K, O'Reilly LA, Whitehead L, Strasser A, Herold MJ. Characterisation of mice lacking the inflammatory caspases-1/11/12 reveals no contribution of caspase-12 to cell death and sepsis. Cell Death Differ. 2018.
223. Fischer H, Koenig U, Eckhart L, Tschachler E. Human caspase 12 has acquired deleterious mutations. Biochem Bioph Res Co. 2002;293(2):722-6.

224. Lamkanfi M, Kalai M, Vandenabeele P. Caspase-12: an overview. Cell Death Differ. 2004;11(4):365-8.
225. Skeldon AM, Morizot A, Douglas T, Santoro N, Kursawe R, Kozlitina J, et al. Caspase-12, but Not Caspase-11, Inhibits Obesity and Insulin Resistance. J Immunol. 2016;196(1):437-47.
226. Fuchs T, Kelly JA, Simon E, Sivils KL, Hermel E. The anti-inflammatory CASPASE-12 gene does not influence SLE phenotype in African-Americans. Immunol Lett. 2016;173:21-5.
227. Marshall L, Obaidullah M, Fuchs T, Fineberg NS, Brinkley G, Mikuls TR, et al. CASPASE-12 and rheumatoid arthritis in African-Americans. Immunogenetics. 2014;66(4):281-5.
228. Chen J, Wilson ES, Dahmer MK, Quasney MW, Waterer GW, Feldman C, et al. Lack of association of the caspase-12 long allele with community-acquired pneumonia in people of African descent. PLoS One. 2014;9(2):e89194.
229. Martinon F, Burns K, Tschopp J. The inflammasome: a molecular platform triggering activation of inflammatory caspases and processing of proIL-beta. Mol Cell. 2002;10(2):417-26.
230. Schroder K, Tschopp J. The inflammasomes. Cell. 2010;140(6):821-32.
231. Lamkanfi M, Dixit VM. Mechanisms and functions of inflammasomes. Cell. 2014;157(5):1013-22.
232. Chen GY, Nunez G. Sterile inflammation: sensing and reacting to damage. Nature Reviews Immunology. 2010;10(12):826-37.
233. Liston A, Masters SL. Homeostasis-altering molecular processes as mechanisms of inflammasome activation. Nat Rev Immunol. 2017;17(3):208-14.
234. Mathur A, Hayward JA, Man SM. Molecular mechanisms of inflammasome signaling. J Leukoc Biol. 2018;103(2):233-57.
235. Broz P, Dixit VM. Inflammasomes: mechanism of assembly, regulation and signalling. Nat Rev Immunol. 2016;16(7):407-20.
236. Franklin BS, Latz E, Schmidt FI. The intra- and extracellular functions of ASC specks. Immunol Rev. 2018;281(1):74-87.
237. Datta D, McClendon CL, Jacobson MP, Wells JA. Substrate and Inhibitor-induced Dimerization and Cooperativity in Caspase-1 but Not Caspase-3. Journal of Biological Chemistry. 2013;288(14):9971-81.
238. Monteleone M, Stow JL, Schroder K. Mechanisms of unconventional secretion of IL-1 family cytokines. Cytokine. 2015;74(2):213-8.
239. March CJ, Mosley B, Larsen A, Cerretti DP, Braedt G, Price V, et al. Cloning, sequence and expression of two distinct human interleukin-1 complementary DNAs. Nature. 1985;315(6021):641-7.
240. Dinarello CA. Overview of the IL-1 family in innate inflammation and acquired immunity. Immunol Rev. 2018;281(1):8-27.
241. Di Paolo NC, Shayakhmetov DM. Interleukin 1alpha and the inflammatory process. Nat Immunol. 2016;17(8):906-13.
242. Garlanda C, Dinarello CA, Mantovani A. The interleukin-1 family: back to the future. Immunity. 2013;39(6):1003-18.
243. Palazon-Riquelme P, Lopez-Castejon G. The inflammasomes, immune guardians at defence barriers. Immunology. 2018.
244. Dinarello CA. Immunological and inflammatory functions of the interleukin-1 family. Annu Rev Immunol. 2009;27:519-50.
245. Schett G, Dayer JM, Manger B. Interleukin-1 function and role in rheumatic disease. Nat Rev Rheumatol. 2016;12(1):14-24.
246. Netea MG, Balkwill F, Chonchol M, Cominelli F, Donath MY, Giamarellos-Bourboulis EJ, et al. A guiding map for inflammation. Nat Immunol. 2017;18(8):826-31.
247. Takahama M, Akira S, Saitoh T. Autophagy limits activation of the inflammasomes. Immunol Rev. 2018;281(1):62-73.
248. Indramohan M, Stehlik C, Dorfleutner A. COPs and POPs Patrol Inflammasome Activation. J Mol Biol. 2018;430(2):153-73.
249. Kanneganti TD. The inflammasome starts rolling. Nat Rev Immunol. 2018;18(8):483.

250. de Torre-Minguela C, Mesa Del Castillo P, Pelegrin P. The NLRP3 and Pyrin Inflammasomes: Implications in the Pathophysiology of Autoinflammatory Diseases. Front Immunol. 2017;8:43.
251. Masters SL, Simon A, Aksentijevich I, Kastner DL. Horror autoinflammaticus: the molecular pathophysiology of autoinflammatory disease (*). Annu Rev Immunol. 2009;27:621-68.
252. Zhong FL, Mamai O, Sborgi L, Boussofara L, Hopkins R, Robinson K, et al. Germline NLRP1 Mutations Cause Skin Inflammatory and Cancer Susceptibility Syndromes via Inflammasome Activation. Cell. 2016;167(1):187-202 e17.
253. Jesus AA, Goldbach-Mansky R. IL-1 blockade in autoinflammatory syndromes. Annu Rev Med. 2014;65:223-44.
254. Dinarello CA, Simon A, van der Meer JW. Treating inflammation by blocking interleukin-1 in a broad spectrum of diseases. Nat Rev Drug Discov. 2012;11(8):633-52.
255. Arranz L, Arriero MD, Villatoro A. Interleukin-1 beta as emerging therapeutic target in hematological malignancies and potentially in their complications. Blood Rev. 2017;31(5):306-17.
256. Dinarello CA. Interleukin-1 in the pathogenesis and treatment of inflammatory diseases. Blood. 2011;117(14):3720-32.
257. Guo H, Callaway JB, Ting JP. Inflammasomes: mechanism of action, role in disease, and therapeutics. Nat Med. 2015;21(7):677-87.
258. Mistry A, Savic S, van der Hilst JCH. Interleukin-1 Blockade: An Update on Emerging Indications. BioDrugs. 2017;31(3):207-21.
259. Bent R, Moll L, Grabbe S, Bros M. Interleukin-1 Beta-A Friend or Foe in Malignancies? Int J Mol Sci. 2018;19(8).
260. Mantovani A, Barajon I, Garlanda C. IL-1 and IL-1 regulatory pathways in cancer progression and therapy. Immunol Rev. 2018;281(1):57-61.
261. Zitvogel L, Kepp O, Galluzzi L, Kroemer G. Inflammasomes in carcinogenesis and anticancer immune responses. Nat Immunol. 2012;13(4):343-51.
262. Karki R, Man SM, Kanneganti TD. Inflammasomes and Cancer. Cancer Immunol Res. 2017;5(2):94-9.
263. Kantono M, Guo B. Inflammasomes and Cancer: The Dynamic Role of the Inflammasome in Tumor Development. Front Immunol. 2017;8:1132.
264. Man SM, Zhu QF, Zhu LQ, Liu ZP, Karki R, Malik A, et al. Critical Role for the DNA Sensor AIM2 in Stem Cell Proliferation and Cancer. Cell. 2015;162(1):45-58.
265. He Q, Fu Y, Tian D, Yan W. The contrasting roles of inflammasomes in cancer. Am J Cancer Res. 2018;8(4):566-83.
266. Ridker PM, MacFadyen JG, Thuren T, Everett BM, Libby P, Glynn RJ, et al. Effect of interleukin-1 beta inhibition with canakinumab on incident lung cancer in patients with atherosclerosis: exploratory results from a randomised, double-blind, placebo-controlled trial. Lancet. 2017;390(10105):1833-42.
267. Gottschlich A, Endres S, Kobold S. Can we use interleukin-1 beta blockade for lung cancer treatment? Transl Lung Cancer R. 2018;7:S160-S4.
268. Hickish T, Andre T, Wyrwicz L, Saunders M, Sarosiek T, Kocsis J, et al. MABp1 as a novel antibody treatment for advanced colorectal cancer: a randomised, double-blind, placebo-controlled, phase 3 study. Lancet Oncol. 2017;18(2):192-201.
269. Rooney C, Sauer T. Modeling cytokine release syndrome. Nat Med. 2018;24(6):705-6.
270. Fassy F, Krebs O, Rey H, Komara B, Gillard C, Capdevila C, et al. Enzymatic activity of two caspases related to interleukin-1beta-converting enzyme. Eur J Biochem. 1998;253(1):76-83.
271. Sollberger G, Strittmatter GE, Kistowska M, French LE, Beer HD. Caspase-4 is required for activation of inflammasomes. J Immunol. 2012;188(4):1992-2000.
272. Kajiwara Y, Schiff T, Voloudakis G, Gama Sosa MA, Elder G, Bozdagi O, et al. A critical role for human caspase-4 in endotoxin sensitivity. J Immunol. 2014;193(1):335-43.
273. Casson CN, Yu J, Reyes VM, Taschuk FO, Yadav A, Copenhaver AM, et al. Human caspase-4 mediates noncanonical inflammasome activation against gram-negative bacterial pathogens. Proc Natl Acad Sci U S A. 2015;112(21):6688-93.

274. Baker PJ, Boucher D, Bierschenk D, Tebartz C, Whitney PG, D'Silva DB, et al. NLRP3 inflammasome activation downstream of cytoplasmic LPS recognition by both caspase-4 and caspase-5. Eur J Immunol. 2015;45(10):2918-26.
275. Schmid-Burgk JL, Gaidt MM, Schmidt T, Ebert TS, Bartok E, Hornung V. Caspase-4 mediates non-canonical activation of the NLRP3 inflammasome in human myeloid cells. Eur J Immunol. 2015;45(10):2911-7.
276. Wang S, Miura M, Jung Y, Zhu H, Gagliardini V, Shi L, et al. Identification and characterization of Ich-3, a member of the interleukin-1beta converting enzyme (ICE)/Ced-3 family and an upstream regulator of ICE. J Biol Chem. 1996;271(34):20580-7.
277. Wang SY, Miura M, Jung YK, Zhu H, Li E, Yuan JY. Murine caspase-11, an ICE-interacting protease, is essential for the activation of ICE. Cell. 1998;92(4):501-9.
278. Cookson BT, Brennan MA. Pro-inflammatory programmed cell death. Trends Microbiol. 2001;9(3):113-4.
279. Hagar JA, Powell DA, Aachoui Y, Ernst RK, Miao EA. Cytoplasmic LPS activates caspase-11: implications in TLR4-independent endotoxic shock. Science. 2013;341(6151):1250-3.
280. Kayagaki N, Wong MT, Stowe IB, Ramani SR, Gonzalez LC, Akashi-Takamura S, et al. Noncanonical inflammasome activation by intracellular LPS independent of TLR4. Science. 2013;341(6151):1246-9.
281. Aglietti RA, Dueber EC. Recent Insights into the Molecular Mechanisms Underlying Pyroptosis and Gasdermin Family Functions. Trends Immunol. 2017;38(4):261-71.
282. Man SM, Karki R, Kanneganti TD. Molecular mechanisms and functions of pyroptosis, inflammatory caspases and inflammasomes in infectious diseases. Immunol Rev. 2017;277(1):61-75.
283. He WT, Wan H, Hu L, Chen P, Wang X, Huang Z, et al. Gasdermin D is an executor of pyroptosis and required for interleukin-1beta secretion. Cell Res. 2015;25(12):1285-98.
284. Kayagaki N, Stowe IB, Lee BL, O'Rourke K, Anderson K, Warming S, et al. Caspase-11 cleaves gasdermin D for non-canonical inflammasome signalling. Nature. 2015;526(7575):666-71.
285. Shi J, Zhao Y, Wang K, Shi X, Wang Y, Huang H, et al. Cleavage of GSDMD by inflammatory caspases determines pyroptotic cell death. Nature. 2015;526(7575):660-5.
286. Liu X, Zhang Z, Ruan J, Pan Y, Magupalli VG, Wu H, et al. Inflammasome-activated gasdermin D causes pyroptosis by forming membrane pores. Nature. 2016;535(7610):153-8.
287. Ding J, Wang K, Liu W, She Y, Sun Q, Shi J, et al. Pore-forming activity and structural autoinhibition of the gasdermin family. Nature. 2016;535(7610):111-6.
288. Aglietti RA, Estevez A, Gupta A, Ramirez MG, Liu PS, Kayagaki N, et al. GsdmD p30 elicited by caspase-11 during pyroptosis forms pores in membranes. Proc Natl Acad Sci U S A. 2016;113(28):7858-63.
289. Sborgi L, Ruhl S, Mulvihill E, Pipercevic J, Heilig R, Stahlberg H, et al. GSDMD membrane pore formation constitutes the mechanism of pyroptotic cell death. EMBO J. 2016;35(16):1766-78.
290. Chen X, He WT, Hu LC, Li JX, Fang Y, Wang X, et al. Pyroptosis is driven by non-selective gasdermin-D pore and its morphology is different from MLKL channel-mediated necroptosis. Cell Research. 2016;26(9):1007-20.
291. Shi J, Gao W, Shao F. Pyroptosis: Gasdermin-Mediated Programmed Necrotic Cell Death. Trends Biochem Sci. 2017;42(4):245-54.
292. Evavold CL, Ruan J, Tan Y, Xia S, Wu H, Kagan JC. The Pore-Forming Protein Gasdermin D Regulates Interleukin-1 Secretion from Living Macrophages. Immunity. 2017.
293. Heilig R, Dick MS, Sborgi L, Meunier E, Hiller S, Broz P. The Gasdermin-D pore acts as a conduit for IL-1 secretion in mice. European Journal of Immunology. 2018;48(4):584-92.
294. Martin-Sanchez F, Diamond C, Zeitler M, Gomez AI, Baroja-Mazo A, Bagnall J, et al. Inflammasome-dependent IL-1beta release depends upon membrane permeabilisation. Cell Death Differ. 2016;23(7):1219-31.
295. Brough D, Rothwell NJ. Caspase-1-dependent processing of pro-interleukin-1 beta is cytosolic and precedes cell death. Journal of Cell Science. 2007;120(5):772-81.

296. Russo HM, Rathkey J, Boyd-Tressler A, Katsnelson MA, Abbott DW, Dubyak GR. Active Caspase-1 Induces Plasma Membrane Pores That Precede Pyroptotic Lysis and Are Blocked by Lanthanides. Journal of Immunology. 2016;197(4):1353-67.
297. Chen KW, Gross CJ, Sotomayor FV, Stacey KJ, Tschopp J, Sweet MJ, et al. The neutrophil NLRC4 inflammasome selectively promotes IL-1beta maturation without pyroptosis during acute Salmonella challenge. Cell Rep. 2014;8(2):570-82.
298. Gaidt M, Ebert T, Chauhan D, Schmidt T, Schmid-Burgk J, Rapino F, et al. Human monocytes engage an alternative inflammasome pathway. European Journal of Immunology. 2016;46:568-9.
299. Kovacs SB, Miao EA. Gasdermins: Effectors of Pyroptosis. Trends Cell Biol. 2017;27(9):673-84.
300. Zanoni I, Tan Y, Di Gioia M, Broggi A, Ruan J, Shi J, et al. An endogenous caspase-11 ligand elicits interleukin-1 release from living dendritic cells. Science. 2016;352(6290):1232-6.
301. Chu LH, Indramohan M, Ratsimandresey RA, Gangopadhyay A, Morris EP, Monack DM, et al. The oxidized phospholipid oxPAPC protects from septic shock by targeting the non-canonical inflammasome in macrophages. Nat Commun. 2018;9(1):996.
302. Li J, Brieher WM, Scimone ML, Kang SJ, Zhu H, Yin H, et al. Caspase-11 regulates cell migration by promoting Aip1-Cofilin-mediated actin depolymerization. Nat Cell Biol. 2007;9(3):276-86.
303. Hitomi J, Katayama T, Eguchi Y, Kudo T, Taniguchi M, Koyama Y, et al. Involvement of caspase-4 in endoplasmic reticulum stress-induced apoptosis and Abeta-induced cell death. J Cell Biol. 2004;165(3):347-56.
304. Li C, Wei J, Li Y, He X, Zhou Q, Yan J, et al. Transmembrane Protein 214 (TMEM214) mediates endoplasmic reticulum stress-induced caspase 4 enzyme activation and apoptosis. J Biol Chem. 2013;288(24):17908-17.
305. Stowe I, Lee B, Kayagaki N. Caspase-11: arming the guards against bacterial infection. Immunol Rev. 2015;265(1):75-84.
306. Jorgensen I, Rayamajhi M, Miao EA. Programmed cell death as a defence against infection. Nature Reviews Immunology. 2017;17(3):151-64.
307. Rathkey JK, Zhao J, Liu Z, Chen Y, Yang J, Kondolf HC, et al. Chemical disruption of the pyroptotic pore-forming protein gasdermin D inhibits inflammatory cell death and sepsis. Sci Immunol. 2018;3(26).
308. Sollberger G, Choidas A, Burn GL, Habenberger P, Di Lucrezia R, Kordes S, et al. Gasdermin D plays a vital role in the generation of neutrophil extracellular traps. Sci Immunol. 2018;3(26).
309. Kajiwara Y, McKenzie A, Dorr N, Gama Sosa MA, Elder G, Schmeidler J, et al. The human-specific CASP4 gene product contributes to Alzheimer-related synaptic and behavioural deficits. Hum Mol Genet. 2016;25(19):4315-27.
310. Hisahara S, Yuan J, Momoi T, Okano H, Miura M. Caspase-11 mediates oligodendrocyte cell death and pathogenesis of autoimmune-mediated demyelination. J Exp Med. 2001;193(1):111-22.
311. Oficjalska K, Raverdeau M, Aviello G, Wade SC, Hickey A, Sheehan KM, et al. Protective role for caspase-11 during acute experimental murine colitis. J Immunol. 2015;194(3):1252-60.
312. Demon D, Kuchmiy A, Fossoul A, Zhu Q, Kanneganti TD, Lamkanfi M. Caspase-11 is expressed in the colonic mucosa and protects against dextran sodium sulfate-induced colitis. Mucosal Immunol. 2014;7(6):1480-91.
313. Soung YH, Jeong EG, Ahn CH, Kim SS, Song SY, Yoo NJ, et al. Mutational analysis of caspase 1, 4, and 5 genes in common human cancers. Hum Pathol. 2008;39(6):895-900.
314. Shibamoto M, Hirata H, Eguchi H, Sawada G, Sakai N, Kajiyama Y, et al. The loss of CASP4 expression is associated with poor prognosis in esophageal squamous cell carcinoma. Oncology Letters. 2017;13(3):1761-6.
315. Flood B, Oficjalska K, Laukens D, Fay J, O'Grady A, Caiazza F, et al. Altered expression of caspases-4 and -5 during inflammatory bowel disease and colorectal cancer: Diagnostic and therapeutic potential. Clin Exp Immunol. 2015;181(1):39-50.

316. Terlizzi M, Colarusso C, De Rosa I, De Rosa N, Somma P, Curcio C, et al. Circulating and tumor-associated caspase-4: a novel diagnostic and prognostic biomarker for non-small cell lung cancer. Oncotarget. 2018;9(27):19356-67.
317. Okondo MC, Johnson DC, Sridharan R, Go EB, Chui AJ, Wang MS, et al. DPP8 and DPP9 inhibition induces pro-caspase-1-dependent monocyte and macrophage pyroptosis. Nat Chem Biol. 2017;13(1):46-53.
318. Okondo MC, Rao SD, Taabazuing CY, Chui AJ, Poplawski SE, Johnson DC, et al. Inhibition of Dpp8/9 Activates the Nlrp1b Inflammasome. Cell Chem Biol. 2018;25(3):262-7 e5.
319. Wang Y, Gao W, Shi X, Ding J, Liu W, He H, et al. Chemotherapy drugs induce pyroptosis through caspase-3 cleavage of a gasdermin. Nature. 2017;547(7661):99-103.
320. Innes AJ, Gil J. IMR90 ER:RAS: A Cell Model of Oncogene-Induced Senescence. Methods Mol Biol. 2019;1896:83-92.
321. Fernandez-Duran I, Tarrats N, Hari P, Acosta JC. Measuring the Inflammasome in Oncogene-Induced Senescence. Methods Mol Biol. 2019;1896:57-70.
322. Livak KJ, Schmittgen TD. Analysis of relative gene expression data using real-time quantitative PCR and the 2(-Delta Delta C(T)) Method. Methods. 2001;25(4):402-8.
323. Love MI, Huber W, Anders S. Moderated estimation of fold change and dispersion for RNA-seq data with DESeq2. Genome Biol. 2014;15(12):550.
324. Subramanian A, Tamayo P, Mootha VK, Mukherjee S, Ebert BL, Gillette MA, et al. Gene set enrichment analysis: a knowledge-based approach for interpreting genome-wide expression profiles. Proc Natl Acad Sci U S A. 2005;102(43):15545-50.
325. Xie X, Lu J, Kulbokas EJ, Golub TR, Mootha V, Lindblad-Toh K, et al. Systematic discovery of regulatory motifs in human promoters and 3' UTRs by comparison of several mammals. Nature. 2005;434(7031):338-45.
326. Whitfield J, Littlewood T, Evan GI, Soucek L. The estrogen receptor fusion system in mouse models: a reversible switch. Cold Spring Harb Protoc. 2015;2015(3):227-34.
327. Dajee M, Tarutani M, Deng H, Cai T, Khavari PA. Epidermal Ras blockade demonstrates spatially localized Ras promotion of proliferation and inhibition of differentiation. Oncogene. 2002;21(10):1527-38.
328. Mattioni T, Louvion JF, Picard D. Regulation of protein activities by fusion to steroid binding domains. Methods Cell Biol. 1994;43 Pt A:335-52.
329. Barradas M, Anderton E, Acosta JC, Li S, Banito A, Rodriguez-Niedenfuhr M, et al. Histone demethylase JMJD3 contributes to epigenetic control of INK4a/ARF by oncogenic RAS. Genes Dev. 2009;23(10):1177-82.
330. Hari P, Millar FR, Tarrats N, Birch J, Quintanilla A, Rink CJ, et al. The innate immune sensor Toll-like receptor 2 controls the senescence-associated secretory phenotype. Sci Adv. 2019;5(6):eaaw0254.
331. Boyle JP, Parkhouse R, Monie TP. Insights into the molecular basis of the NOD2 signalling pathway. Open Biol. 2014;4(12).
332. Chicas A, Wang X, Zhang C, McCurrach M, Zhao Z, Mert O, et al. Dissecting the unique role of the retinoblastoma tumor suppressor during cellular senescence. Cancer Cell. 2010;17(4):376-87.
333. Roux KJ, Kim DI, Burke B, May DG. BioID: A Screen for Protein-Protein Interactions. Curr Protoc Protein Sci. 2018;91:19 23 1-19 23 15.
334. Huang da W, Sherman BT, Lempicki RA. Bioinformatics enrichment tools: paths toward the comprehensive functional analysis of large gene lists. Nucleic Acids Res. 2009;37(1):1-13.
335. Shakeri R, Kheirollahi A, Davoodi J. Apaf-1: Regulation and function in cell death. Biochimie. 2017;135:111-25.
336. Vasudevan D, Ryoo HD. Regulation of Cell Death by IAPs and Their Antagonists. Curr Top Dev Biol. 2015;114:185-208.
337. Druilhe A, Srinivasula SM, Razmara M, Ahmad M, Alnemri ES. Regulation of IL-1beta generation by Pseudo-ICE and ICEBERG, two dominant negative caspase recruitment domain proteins. Cell Death Differ. 2001;8(6):649-57.

338. Lee SH, Stehlik C, Reed JC. Cop, a caspase recruitment domain-containing protein and inhibitor of caspase-1 activation processing. J Biol Chem. 2001;276(37):34495-500.
339. Wang X, Narayanan M, Bruey JM, Rigamonti D, Cattaneo E, Reed JC, et al. Protective role of Cop in Rip2/caspase-1/caspase-4-mediated HeLa cell death. Biochim Biophys Acta. 2006;1762(8):742-54.
340. Naschberger E, Geissdorfer W, Bogdan C, Tripal P, Kremmer E, Sturzl M, et al. Processing and secretion of guanylate binding protein-1 depend on inflammatory caspase activity. J Cell Mol Med. 2017;21(9):1954-66.
341. Pilla DM, Hagar JA, Haldar AK, Mason AK, Degrandi D, Pfeffer K, et al. Guanylate binding proteins promote caspase-11-dependent pyroptosis in response to cytoplasmic LPS. Proc Natl Acad Sci U S A. 2014;111(16):6046-51.
342. Qiu X, Guo H, Yang J, Ji Y, Wu CS, Chen X. Down-regulation of guanylate binding protein 1 causes mitochondrial dysfunction and cellular senescence in macrophages. Sci Rep. 2018;8(1):1679.
343. Kerur N, Fukuda S, Banerjee D, Kim Y, Fu D, Apicella I, et al. cGAS drives noncanonical-inflammasome activation in age-related macular degeneration. Nat Med. 2018;24(1):50-61.
344. Hu Y, Benedict MA, Wu D, Inohara N, Nunez G. Bcl-XL interacts with Apaf-1 and inhibits Apaf-1-dependent caspase-9 activation. Proc Natl Acad Sci U S A. 1998;95(8):4386-91.
345. Campisi J, d'Adda di Fagagna F. Cellular senescence: when bad things happen to good cells. Nat Rev Mol Cell Biol. 2007;8(9):729-40.
346. Sandhu C, Garbe J, Bhattacharya N, Daksis J, Pan CH, Yaswen P, et al. Transforming growth factor beta stabilizes p15INK4B protein, increases p15INK4B-cdk4 complexes, and inhibits cyclin D1-cdk4 association in human mammary epithelial cells. Mol Cell Biol. 1997;17(5):2458-67.
347. Serrano M, Hannon GJ, Beach D. A new regulatory motif in cell-cycle control causing specific inhibition of cyclin D/CDK4. Nature. 1993;366(6456):704-7.
348. Lessard F, Igelmann S, Trahan C, Huot G, Saint-Germain E, Mignacca L, et al. Senescence-associated ribosome biogenesis defects contributes to cell cycle arrest through the Rb pathway. Nat Cell Biol. 2018;20(7):789-99.

Appendix – BioID interactome analysis supplemental data

Heatmap of the identified potential interactors of caspase-1 and/or caspase 4 irrespective of RAS^{G12V}. The last two columns show cells which are coloured in green if a protein is considered a potential interactor of caspase-4 or caspase-1, respectively, in this analysis.


GLTP
UQCRB
FLG
PDHX
DLAT
PDHA1
DLD
OGDH
DLST
AKAP8
BCKDHA
CCND1
FKBP4
BLVRA
ATXN10
RRAS
SEC63
PRCP
APEH
PCYOX1
XPOT
TNC
KRT16
LRWD1
FBL;FBLL1
ACAA2
MRPL38
GABRR1
SRI
DHRS7
DERL2
ALB
MRPL50
RAB6C
JAGN1
KRT14
CIR1
PTBP3
ENOPH1
DYRK4
CYB5B
CASP1
BTBD2
ENO2
ARMT1
IARS2
CTSZ
IMPA1
CPOX
ALDH1L2
CHMP1A
TP53I3
CYCS
HEXA
PGRMC1
HSP90AB4P
M6PR
DSG1
PAFAH1B3

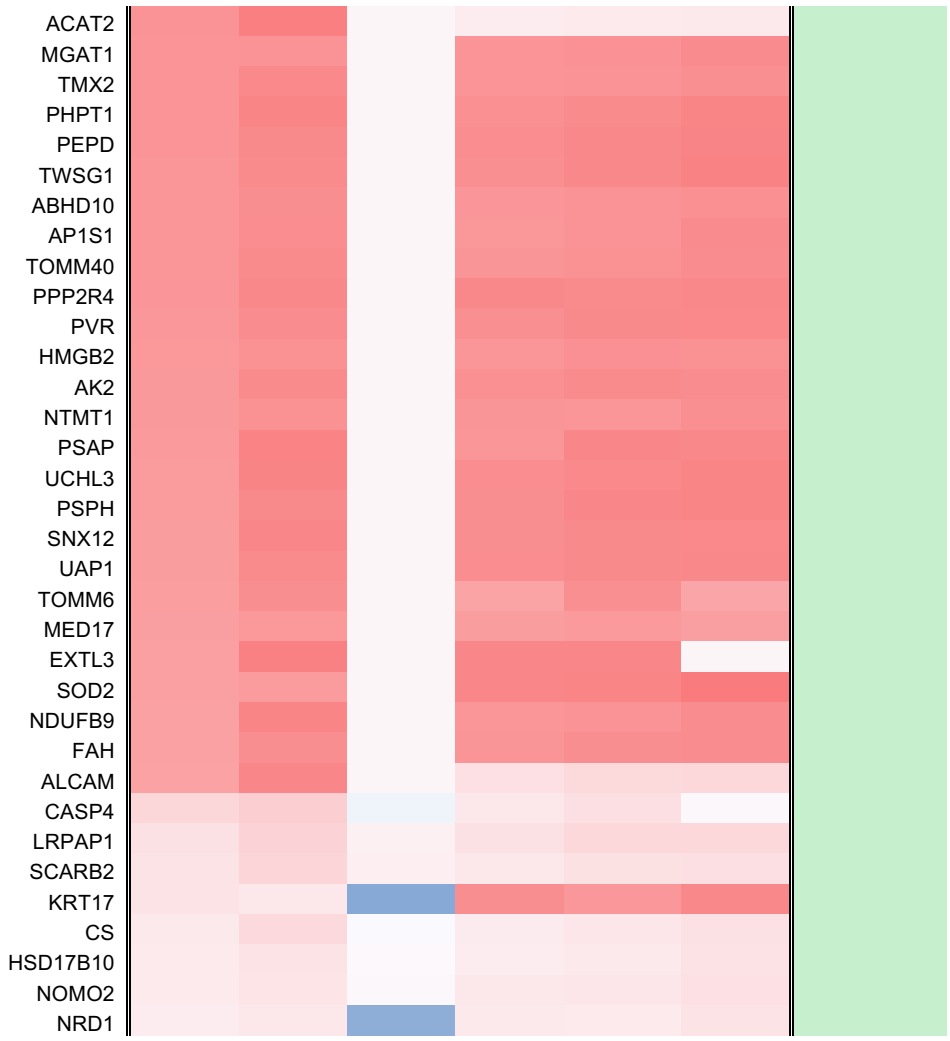
ACAT2
MGAT1
TMX2
PHPT1
PEPD
TWSG1
ABHD10
AP1S1
TOMM40
PPP2R4
PVR
HMGB2
AK2
NTMT1
PSAP
UCHL3
PSPH
SNX12
UAP1
TOMM6
MED17
EXTL3
SOD2
NDUFB9
FAH
ALCAM
CASP4
LRPAP1
SCARB2
KRT17
CS
HSD17B10
NOMO2
NRD1